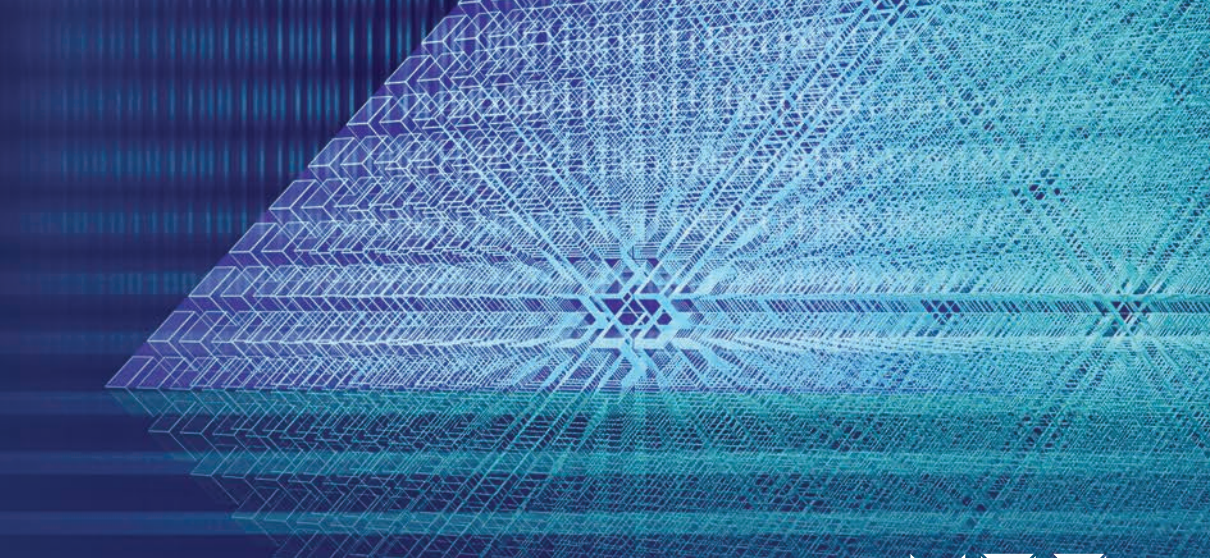

TECHNICAL REPORTS SERIES NO. 483

Dosimetry of Small Static Fields Used in External Beam Radiotherapy

An International Code of Practice for Reference and Relative Dose Determination

Sponsored by the IAEA and AAPM

IAEA

International Atomic Energy Agency

IAEA SAFETY STANDARDS AND RELATED PUBLICATIONS

IAEA SAFETY STANDARDS

Under the terms of Article III of its Statute, the IAEA is authorized to establish or adopt standards of safety for protection of health and minimization of danger to life and property, and to provide for the application of these standards.

The publications by means of which the IAEA establishes standards are issued in the **IAEA Safety Standards Series**. This series covers nuclear safety, radiation safety, transport safety and waste safety. The publication categories in the series are **Safety Fundamentals**, **Safety Requirements** and **Safety Guides**.

Information on the IAEA's safety standards programme is available on the IAEA Internet site

http://www-ns.iaea.org/standards/

The site provides the texts in English of published and draft safety standards. The texts of safety standards issued in Arabic, Chinese, French, Russian and Spanish, the IAEA Safety Glossary and a status report for safety standards under development are also available. For further information, please contact the IAEA at: Vienna International Centre, PO Box 100, 1400 Vienna, Austria.

All users of IAEA safety standards are invited to inform the IAEA of experience in their use (e.g. as a basis for national regulations, for safety reviews and for training courses) for the purpose of ensuring that they continue to meet users' needs. Information may be provided via the IAEA Internet site or by post, as above, or by email to Official.Mail@iaea.org.

RELATED PUBLICATIONS

The IAEA provides for the application of the standards and, under the terms of Articles III and VIII.C of its Statute, makes available and fosters the exchange of information relating to peaceful nuclear activities and serves as an intermediary among its Member States for this purpose.

Reports on safety in nuclear activities are issued as **Safety Reports**, which provide practical examples and detailed methods that can be used in support of the safety standards.

Other safety related IAEA publications are issued as **Emergency Preparedness and Response** publications, **Radiological Assessment Reports**, the International Nuclear Safety Group's **INSAG Reports**, **Technical Reports** and **TECDOCs**. The IAEA also issues reports on radiological accidents, training manuals and practical manuals, and other special safety related publications.

Security related publications are issued in the **IAEA Nuclear Security Series**.

The **IAEA Nuclear Energy Series** comprises informational publications to encourage and assist research on, and the development and practical application of, nuclear energy for peaceful purposes. It includes reports and guides on the status of and advances in technology, and on experience, good practices and practical examples in the areas of nuclear power, the nuclear fuel cycle, radioactive waste management and decommissioning.

DOSIMETRY OF SMALL STATIC FIELDS USED IN EXTERNAL BEAM RADIOTHERAPY

The Agency's Statute was approved on 23 October 1956 by the Conference on the Statute of the IAEA held at United Nations Headquarters, New York; it entered into force on 29 July 1957. The Headquarters of the Agency are situated in Vienna. Its principal objective is "to accelerate and enlarge the contribution of atomic energy to peace, health and prosperity throughout the world''.

TECHNICAL REPORTS SERIES No. 483

DOSIMETRY OF SMALL STATIC FIELDS USED IN EXTERNAL BEAM RADIOTHERAPY

AN INTERNATIONAL CODE OF PRACTICE FOR REFERENCE AND RELATIVE DOSE DETERMINATION

INTERNATIONAL ATOMIC ENERGY AGENCY
VIENNA, 2017

COPYRIGHT NOTICE

All IAEA scientific and technical publications are protected by the terms of the Universal Copyright Convention as adopted in 1952 (Berne) and as revised in 1972 (Paris). The copyright has since been extended by the World Intellectual Property Organization (Geneva) to include electronic and virtual intellectual property. Permission to use whole or parts of texts contained in IAEA publications in printed or electronic form must be obtained and is usually subject to royalty agreements. Proposals for non-commercial reproductions and translations are welcomed and considered on a case-by-case basis. Enquiries should be addressed to the IAEA Publishing Section at:

Marketing and Sales Unit, Publishing Section
International Atomic Energy Agency
Vienna International Centre
PO Box 100
1400 Vienna, Austria
fax: +43 1 2600 29302
tel.: +43 1 2600 22417
email: sales.publications@iaea.org
http://www.iaea.org/books

© IAEA, 2017

Printed by the IAEA in Austria
November 2017
STI/DOC/010/483

IAEA Library Cataloguing in Publication Data

Names: International Atomic Energy Agency.
Title: Dosimetry of small static fields used in external beam radiotherapy: an IAEA-AAPM International Code of Practice for reference and relative dose determination / International Atomic Energy Agency.
Description: Vienna : International Atomic Energy Agency, 2017. | Series: Technical reports series (International Atomic Energy Agency), ISSN 0074–1914 ; no. 483 | Includes bibliographical references.
Identifiers: IAEAL 17-01121 | ISBN 978–92–0–105916–1 (paperback : alk. paper)
Subjects: LCSH: Radiation dosimetry. | Radiotherapy. | Radiotherapy — Safety measures.
Classification: UDC 615.849.5 | STI/DOC/010/483

FOREWORD

In radiotherapy it is essential that the dose delivered to the patient be known accurately so that patients receive the correct amount of radiation to kill the cancer cells while at the same time sparing healthy tissue. Consistent reference dosimetry traceable to metrological primary standards is key to the radiotherapy process and enables common procedures to be followed within a country. For conventional radiotherapy this has been achieved by universally adopted codes of practice such as the IAEA publication titled Absorbed Dose Determination in External Beam Radiotherapy: An International Code of Practice for Dosimetry Based on Standards of Absorbed Dose to Water (Technical Reports Series No. 398) and the American Association of Physicists in Medicine (AAPM) publication titled AAPM's TG-51 Protocol for Clinical Reference Dosimetry of High-Energy Photon and Electron Beams. However, recent developments in radiotherapy have resulted in an upsurge in the use of small static photon beams such as those used in various forms of stereotactic radiotherapy, stereotactic body radiotherapy, stereotactic radiosurgery and intensity modulated radiotherapy. These radiotherapy treatments are performed not only with specialized, dedicated machines such as TomoTherapy®, CyberKnife® or Gamma Knife®, but also with conventional, non-dedicated accelerators equipped with high resolution multileaf collimators. These developments have increased the uncertainty of clinical dosimetry and weakened its traceability to reference dosimetry based on codes of practice for conventional radiotherapy. Accidents have occurred in some radiotherapy centres owing to the use of methods and procedures recommended in conventional codes of practice that are not applicable to small fields.

This publication has been written in collaboration with the AAPM. It is the first Code of Practice dedicated to the dosimetry of small static fields used in radiotherapy and fulfils the need for a systematic and internationally unified approach to the dosimetry of small static fields.

This Code of Practice is addressed to clinical medical physicists using small static photon fields with energies less than 10 MV, provided with ionization chambers calibrated in terms of absorbed dose to water traceable to a primary standards dosimetry laboratory.

The IAEA wishes to express its gratitude to the authors and reviewers of this publication, in particular H. Palmans (Belgium), P. Andreo (Sweden), M. Saiful Huq (United States of America) and J. Seuntjens (Canada).

The IAEA officers responsible for this publication were S. Vatnitsky, A. Meghzifene and K. Christaki of the Division of Human Health.

ACKNOWLEDGEMENTS

The IAEA and the AAPM wish to acknowledge the following people for their valuable suggestions:

M. Aspradakis (Switzerland), H. Bouchard (Canada), G. Bruggmoser (Germany), S. Derreumaux (France), G. Ding (United States of America), D. Followill (United States of America), P. Francescon (Italy), F. Gomez (Spain), D. Gonzalez-Castaño (Spain), S. Kim (United States of America), M. McEwen (Canada), C. Reft (United States of America), F. Sanchez-Doblado (Spain), O.A. Sauer (Germany), T. Zhu (United States of America).

EDITORIAL NOTE

Although great care has been taken to maintain the accuracy of information contained in this publication, neither the IAEA nor its Member States assume any responsibility for consequences which may arise from its use.

This publication does not address questions of responsibility, legal or otherwise, for acts or omissions on the part of any person.

Guidance provided here, describing good practices, represents expert opinion but does not constitute recommendations made on the basis of a consensus of Member States.

The mention of names of specific companies or products (whether or not indicated as registered) does not imply any intention to infringe proprietary rights, nor should it be construed as an endorsement or recommendation on the part of the IAEA.

The IAEA has no responsibility for the persistence or accuracy of URLs for external or third party Internet web sites referred to in this publication and does not guarantee that any content on such web sites is, or will remain, accurate or appropriate.

CONTENTS

1. INTRODUCTION

1.1. BACKGROUND

For conventional radiotherapy, dosimetry is based on widely adopted codes of practice (COPs) such as Technical Reports Series No. 398 (Absorbed Dose Determination in External Beam Radiotherapy: An International Code of Practice for Dosimetry Based on Standards of Absorbed Dose to Water) [1], the American Association of Physicists in Medicine (AAPM) publication titled AAPM's TG-51 Protocol for Clinical Reference Dosimetry of High-Energy Photon and Electron Beams [2] and Refs [3–7]. These and other dosimetry protocols are based on measurements using an ionization chamber with a calibration coefficient in terms of absorbed dose to water, traceable to a primary standards dosimetry laboratory (PSDL) for reference conditions, such as a conventional field size of 10 cm × 10 cm. Departure from reference conditions, such as the determination of absorbed dose to water in beams of different field sizes, were considered in less detail, or not included at all.

However, in radiotherapy there has been an escalation in the use of small static fields that has been facilitated by the generalized availability of standard and add-on multileaf collimators (MLCs) and a variety of treatment machines of new design. This has increased the uncertainty of clinical dosimetry and weakened its traceability to reference dosimetry based on conventional COPs. At the same time, dosimetric errors have become considerably larger than with conventional beams, mostly for two reasons [8]:

(a) The reference conditions recommended by conventional COPs cannot be realized in some machines;
(b) The measurement procedures for determination of absorbed dose to water in small and composite fields are not standardized. In some cases accidents have occurred owing to the use of methods and procedures that are appropriate for large fields but not for small fields [9].

To develop standardized guidance for dosimetry procedures and detectors, an international working group on reference dosimetry of small static fields used in external beam radiotherapy was established by the IAEA in cooperation with the AAPM. In 2008 this working group published a formalism for the dosimetry of small and composite fields [8]. This formalism introduced the concept of two new intermediate calibration fields: (i) a *static machine specific reference* (msr) field for those modalities that cannot establish conventional reference conditions and (ii) a *plan class specific reference* field that is closer to the patient specific

clinical fields and thereby facilitates standardization of composite field dosimetry. Prior to progressing with developing a COP, the members of this IAEA/AAPM working group requested comments from the international medical physics community on the formalism. Since 2008 there have not been comprehensive data available for plan class specific reference fields, so this COP was written for static fields, with the intention of adding the second part of the Code when more data become available. However, there have been many challenges in writing this Code, mainly relating to providing a comprehensive set of relevant data together with associated uncertainties.

Guidance provided here, describing good practices, represents expert opinion but does not constitute recommendations made on the basis of a consensus of Member States.

1.1.1. Definition of small field

In this COP, the requirements of a small field are described in detail. To summarize, at least one of the following three physical conditions will be fulfilled for an external photon beam to be designated small:

(i) There is a loss of lateral charged particle equilibrium (LCPE) on the beam axis;
(ii) There is partial occlusion of the primary photon source by the collimating devices on the beam axis;
(iii) The size of the detector is similar or large compared to the beam dimensions.

The first two characteristics are beam related, while the third one is detector related for a given field size. All three of these conditions result in overlap between the field penumbrae and the detector volume.

1.1.2. Dosimetry equipment

For the msr field it is advised to use an ionization chamber calibrated in terms of absorbed dose to water. The size restriction on an ionization chamber for msr dosimetry is that the outer boundaries of the detector are at least a lateral charged particle distance r_{LCPE} away from the field edges (at 50% absorbed dose level). The preferred approach for reference dosimetry is to obtain a calibration coefficient directly in the msr field, provided the standards laboratory is able to supply such a calibration coefficient. There has been research into the use of calorimeters in small fields, but to date PSDLs are not able to offer calibrations in small fields, although it is expected that they will be available in

the future. In a second approach, the ionization chamber is calibrated for current standard reference conditions and factors are used to convert to the msr field.

Ionization chambers, which have been the 'backbone' of radiotherapy dosimetry, are not always suitable for both reference and relative measurements in small fields. Volume averaging and lack of electronic equilibrium, which requires a sufficiently large region of uniform particle fluence surrounding the detector, complicates the use of certain ionization chambers for the dosimetry of small photon beams. As is well known, any detector perturbs the particle fluence in the medium, and appropriate correction factors are used to account for this effect; however, when relatively large ionization chambers (e.g. of a Farmer type) are used in small fields, the necessary corrections either become excessively large and uncertain or are not known. This implies that the conversion from ionization to absorbed dose to water based on cavity theory and using the currently available perturbation factors used in existing dosimetry COPs or protocols such as Refs [1, 2, 7] is not accurate. Furthermore, spectra, and therefore beam quality, may change as the field size decreases. Hence, for small fields, other detectors for relative dosimetry are discussed and proposed in this Code.

For some treatment units, the use of water phantoms for reference dosimetry is possible but highly inconvenient, and therefore plastic water substitute phantoms may be necessary. Today, plastic materials such as polymethylmethacrylate (PMMA) (Lucite), acrylonitrile butadiene styrene (ABS) and Solid Water® (Sun Nuclear Corp., Melbourne, FL) have well controlled densities, well defined atomic properties, and can be machined for accurate positioning of dosimeters. Therefore, this Code gives a methodology for use of plastic water substitute phantoms that complements the dosimetry in the reference conditions recommended in existing COPs.

1.1.3. Methodology

This COP builds on the established reference dosimetry for conventional 10 cm × 10 cm fields such as that given in Refs [1, 2, 7]. It then extends the dosimetry down to small fields by introducing an msr field and gives the required factors as recommended by Alfonso et al. [8]. It is recommended that the msr field have dimensions as close as possible to those of the conventional reference field and extend at least a distance r_{LCPE} beyond the outer boundaries of the reference ionization chamber. In the case that only fields smaller than the 10 cm × 10 cm reference field can be realized, the msr field will usually be the largest achievable field.

Field size is not uniquely defined for small fields, so for the purpose of applying the procedures in this COP, the field size is the pair of dimensions (in case of rectangular fields) or the diameter (in case of circular fields) that

define(s) the area of the field at the measurement distance. Each dimension is defined by the full width at half maximum (FWHM) of the lateral beam profile measured at a depth sufficient to eliminate the contribution of contaminating electrons; 10 cm is the depth recommended in this COP.

The beam quality indices given in Ref. [1] ($TPR_{20,10}$) and Refs [2, 7] ($\%dd(10)_x$) apply only for a conventional 10 cm × 10 cm field, so this Code gives guidance on how to convert these indices from the msr field to a conventional field size so that conventional dosimetry coefficients can be used. Many modern radiotherapy machines give the option of having a beam that is flattening filter free (FFF); therefore the Code gives details of how to perform dosimetry for small, FFF beams.

Owing to the difficulty of measuring field output factors, this Code gives the option to move away from reference conditions and gives a methodology and factors to determine field output factors. The determination of field output factors is treated as formally as reference dosimetry, and requires explicit correction factors to be applied.

1.1.4. Data

All of the data presented in this COP are based on values published in peer reviewed journals, determined using Monte Carlo calculations and measurements, following the considerable amount of research undertaken on small megavoltage photon beam dosimetry during recent years. Unfortunately, the published data are rather scattered for certain field sizes, especially for the smallest fields, and lack homogeneity with regard to the source-to-surface distance (SSD) or source-to-detector distance (SDD) used, the depth of measurement or calculation, the definition of field size at the surface or at a reference depth, etc. Further complicating the determination of average values for the different detectors and their subsequent statistical analysis is the fact that most of the published data lack a proper estimation of the uncertainty in the various steps involved in the determination of the correction factors given by the different authors. Values of the correction for the small field of interest are limited to a maximum value of 5% in this COP.

1.1.5. Expression of uncertainties

Uncertainty estimates have been derived following as closely as possible Ref. [10], according to a procedure adapted from Ref. [11]. A detailed analysis of the estimated uncertainties for factors used in reference and relative dosimetry is given in the appendices of this COP.

1.1.6. Quantities and symbols

Most of the symbols used in this COP are comparable to those used in Ref. [1], although some are new in the context of small field dosimetry. For completeness, Table 1 contains a summary of all the quantities used in this COP.

TABLE 1. QUANTITIES AND SYMBOLS USED IN THIS PUBLICATION

Symbol	Definition
$\%dd(10,10)$	Percentage depth dose at 10 cm depth in a water phantom for a field size of 10 cm × 10 cm at an SSD of 100 cm.
$\%dd(10,10)_x$	Percentage depth dose at 10 cm depth in a water phantom due to photons only (i.e. excluding the contribution of electron contamination) for a field size of 10 cm × 10 cm at an SSD of 100 cm.
$\%dd(10,S)_x$	Percentage depth dose at 10 cm depth in a water phantom due to photons only (i.e. excluding the contribution of electron contamination) for an equivalent square field size of S cm × S cm at an SSD of 100 cm.
$D_{w,Q}$	Absorbed dose to water at the reference depth, z_{ref}, in a water phantom irradiated by a beam of quality Q (unit: Gy).
f_{msr}	Machine specific reference field.
f_{ref}	Conventional reference field (i.e. 10 cm × 10 cm, at an SDD of 100 cm), used for calibration at the standards laboratory and for reference dosimetry, according to COPs such as Refs [1, 2, 7], at a depth of 10 g/cm^2 in water.
f_{clin}	Clinical non-reference field.
$k_{Q_1,Q_2}^{f_1,f_2}$	Generic form of a correction factor that accounts for the differences between the response of a detector in a field f_2 in a beam of quality Q_2 and a field f_1 in a beam of quality Q_1. If f_1 and f_2 represent the same field (i.e. field size, reference depth, phantom, etc.), the superscript 'f_1,f_2' is replaced with a single 'f_1'.
$k_{Q_{msr}}^{w,plastic}$	Phantom dose conversion factor, for measurements performed in plastic water substitute phantoms.
M_Q	Reading of a dosimeter at the quality Q, corrected for influence quantities other than beam quality (unit: C or meter reading (rdg)).

TABLE 1. QUANTITIES AND SYMBOLS USED IN THIS PUBLICATION (cont.)

Symbol	Definition
M_Q^f	Reading of a detector in a field f in a beam of quality Q, corrected for influence quantities other than beam quality.
$M_{\text{plastic},Q}^f$	Reading of a detector in a plastic water substitute phantom in a field f in a beam of quality Q, corrected for influence quantities other than beam quality.
$M_{\text{w},Q}^f$	As M_Q^f, but used when a distinction has to be made between measurements in a water phantom and in a plastic water substitute phantom.
$N_{D,\text{w},Q_0}^{f_{\text{ref}}}$	Calibration coefficient in terms of absorbed dose to water for an ionization chamber at a reference beam quality Q_0 in the conventional reference field f_{ref}.
$N_{D,\text{w},Q_{\text{msr}}}^{f_{\text{msr}}}$	Calibration coefficient in terms of absorbed dose to water for an ionization chamber in a machine specific reference field f_{msr} at the beam quality Q_{msr}.
$\Omega_{Q_{\text{clin}},Q}^{f_{\text{clin}},f_{\text{ref}}}$	Field output factor of a clinical, non-reference field f_{clin} with respect to the conventional 10 cm × 10 cm reference field f_{ref}.
$\Omega_{Q_{\text{clin}},Q_{\text{msr}}}^{f_{\text{clin}},f_{\text{msr}}}$	Field output factor of a clinical, non-reference field f_{clin} with respect to the machine specific reference field f_{msr}.
OAR(x,y)	Off-axis ratio, the lateral beam profile at the measurement depth normalized to unity on the central axis.
Q	General symbol to indicate the quality of a radiation beam. A subscript "0", i.e. Q_0, indicates the reference quality used for the calibration of an ionization chamber or a dosimeter.
Q_{msr}	Beam quality of a machine specific reference beam.
Q_{clin}	Beam quality of a clinical, non-reference beam.
r_{LCPE}	Lateral charged particle equilibrium range.
$\text{TPR}_{20,10}(10)$	Tissue phantom ratio in water at the depths of 20 and 10 g/cm^2, for a field size of 10 cm × 10 cm defined at an SDD of 100 cm.

TABLE 1. QUANTITIES AND SYMBOLS USED IN THIS PUBLICATION (cont.)

Symbol	Definition
$TPR_{20,10}(S)$	Tissue phantom ratio in water at the depths of 20 and 10 g/cm^2, for an equivalent field size of S cm × S cm defined at an SDD of 100 cm.
$w(x,y)$	Weighting function representing the extension of the sensitive volume of a detector along the beam axis as a function of the lateral coordinates x and y.[a]
z_{max}	Depth of maximum dose (in g/cm^2).
z_{ref}	Reference depth (in g/cm^2) in water for in-phantom measurements.
$z_{eq,plastic}$	Depth in plastic water substitute phantom (in g/cm^2), equivalent to the reference depth in water, scaled according to the ratio of electron densities.

[a] See Appendix I for its definition and examples of its usage.

1.2. OBJECTIVES

This is the first international COP dedicated to reference and relative dosimetry of small static fields used in radiotherapy. It will provide consistent reference dosimetry traceable to metrological primary standards and enable common procedures to be followed within a country for small field dosimetry.

1.3. SCOPE

This COP addresses the reference and relative dosimetry of small static fields used for external beam photon radiotherapy of energies with nominal accelerating potential up to 10 MV. It does not address other radiotherapy modalities such as electron, proton and orthovoltage beams.

This COP consists of six sections. The first two are introductory sections describing the rationale of the COP and the physics of small field dosimetry. The COP is based on the concepts and formalism introduced by Alfonso et al. [8]; these are described in Section 3. The fourth section discusses the detectors and equipment that are suitable for use in msr fields and for relative dosimetry in small fields. The fifth section is the COP for reference dosimetry in msr fields for both beams with flattening filter (WFF) and FFF. The sixth section is the COP for

relative dosimetry for small fields. Sections 5 and 6 give data required to use the COP. Appendix I discusses the origin of the beam quality correction factors for reference dosimetry and their associated uncertainties, and Appendix II discusses the origin of the field output correction factors and their associated uncertainties.

1.4. STRUCTURE

In this COP, an overview of the physics of small field dosimetry is presented first, followed by a general formalism for reference dosimetry in small fields. Guidelines for its practical implementation using suitable detectors and methods for the determination of field output factors are given for specific clinical machines that use small static fields. Guidance for relative dosimetry including detectors, procedures and data is also provided.

2. PHYSICS OF SMALL FIELD DOSIMETRY

Small fields in external radiotherapy are created by downstream collimation of a flattened or unflattened photon beam. Different collimation types are used, including jaws, MLCs and, in some cases, cones or adjustable tertiary collimators. Small photon fields differ from conventional reference fields[1] in their lateral dimensions, causing the penumbrae at both sides of the field to overlap and making most of the commonly used detectors large relative to the radiation field size. This has physical repercussions on dosimetry, which have in general been described well in the literature. Until the publication of Institute of Physics and Engineering in Medicine (IPEM) Report 103 [12], however, those repercussions had not been comprehensively reviewed. This section discusses the physics aspects that are relevant for reference dosimetry and for the determination of field output factors in small static photon fields. It is not meant to present a comprehensive literature overview similar to that in Ref. [12]. Rather it focuses on those small field issues that are of particular relevance to reference dosimetry and on the determination of field output factors. There is some overlap with Ref. [12], but a number of other aspects are introduced, such as the measurement of beam quality when conventional reference conditions cannot be met, equivalent square msr fields and equivalent square small fields, the use of plastic water substitute phantoms for reference dosimetry and a formal approach for the determination of field output factors. Additionally, this section provides a brief overview of the current status of primary standards of absorbed dose to water for small fields, of the current practice of performing reference dosimetry and of the determination of field output factors.

2.1. PARAMETERS DESCRIBING SMALL FIELDS AND PROBLEMS OF SMALL FIELD DOSIMETRY

2.1.1. Small field conditions

At least one of the following three physical conditions will be fulfilled for an external photon beam to be designated small:

[1] In this COP the term ‘conventional reference fields’ refers to the reference fields (and conditions) for the user’s beam calibration prescribed in COPs such as those mentioned in Section 1. In the future, new reference conditions such as those introduced by Alfonso et al. [8] may become conventional for small field dosimetry, but they are not used that way at present.

(i) There is a loss of LCPE on the beam axis (Fig. 1);
(ii) There is partial occlusion of the primary photon source by the collimating devices on the beam axis (Fig. 2);
(iii) The size of the detector is similar or large compared to the beam dimensions (Fig. 3).

The first two characteristics are beam related, while the third one is detector related for a given field size. All three of these conditions result in overlap between the field penumbrae and the detector volume.

2.1.1.1. Beam related conditions

Loss of LCPE occurs in photon beams if the beam half width or radius is smaller than the maximum range of secondary electrons that contribute measurably to the absorbed dose. This condition has been quantified by evaluating the minimum radius of a circular photon field for which collision kerma in water and absorbed dose to water have reached the values determined by broad beam transient charged particle equilibrium (TCPE) conditions (for the definition of TCPE refer to Attix [13], chapter 2, section VII). An illustration is shown in Fig. 1 [14]. Absence of LCPE is problematic for dosimetry using

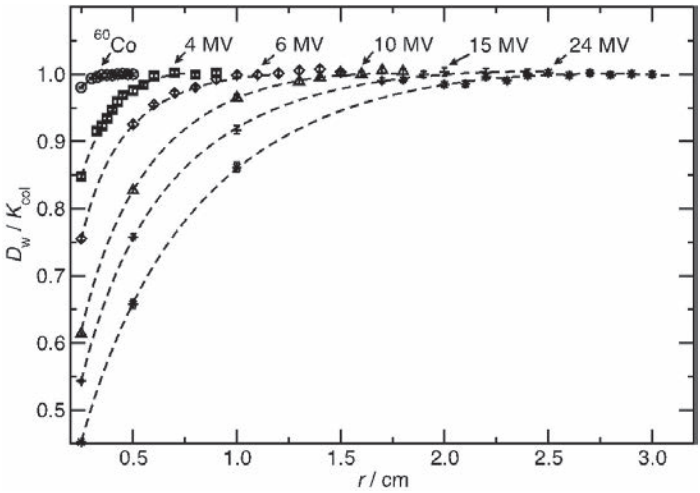

FIG. 1. Ratios of dose-to-water to water-collision-kerma calculated by Monte Carlo simulation in water at 5 cm depth on the central axis of high energy photon beams. The data are plotted as a function of the radius of clinical narrow beams defined at 100 cm SSD for the high energy X ray beams and 80 cm SSD for ^{60}Co (reproduced from Ref. [14] with the permission of P. Papaconstadopoulos, McGill University, Canada).

non-water detector materials, as will be discussed in Sections 2.1.1.2 and 2.1.5. A practical parameter that quantitatively determines when field sizes are small is the lateral charged particle equilibrium range (r_{LCPE}), defined as the minimum radius of a circular photon field for which collision kerma in water and absorbed dose to water are equal at the centre of the field (aside from a correction for the centre of electron production in TCPE). This parameter will be discussed in more detail in Section 3.1.3.

The second condition is illustrated in Fig. 2 and is related to the finite size of the primary photon beam source, the extended focal spot, which is usually determined by the FWHM of the bremsstrahlung photon fluence distribution exiting the target. A small field created by collimation that shields part of the finite primary photon source will produce a lower beam output on the beam axis compared to field sizes where the source is not partially blocked. This primary source occlusion effect becomes important when the field size is comparable to or smaller than the size of the primary photon source. For modern linear accelerators where the primary photon source size is not larger than 5 mm, direct source occlusion usually occurs at field sizes smaller than those where lateral electron disequilibrium starts [12]. Partial occlusion of the primary photon source influences the particle spectrum and is a source of steep local absorbed dose gradients, both of which can have a large effect on the detector response.

The loss of LCPE and the primary photon source occlusion effect are both responsible for a sharp drop in beam output with decreasing field size. This drop

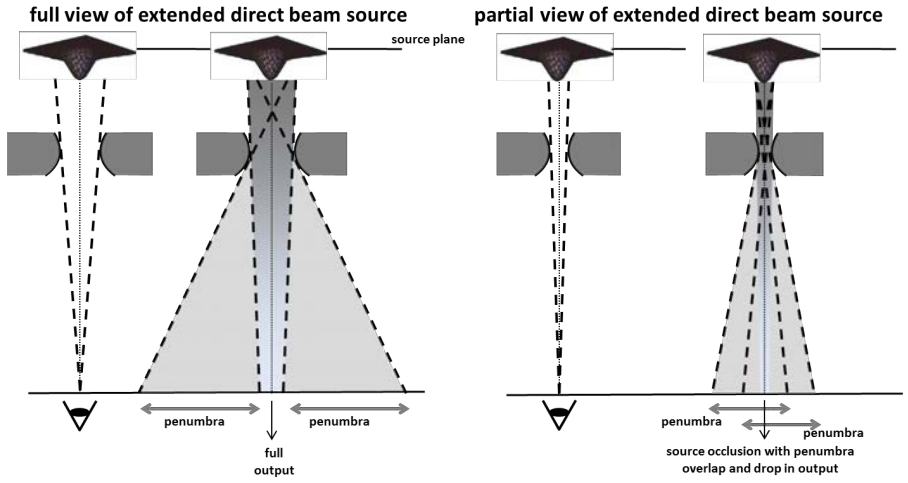

FIG. 2. Schematic illustration of the source occlusion effect (replotted from Ref. [12] with the permission of the Institute of Physics and Engineering in Medicine).

becomes more pronounced when the photon beam energy increases or the density of the medium decreases (in both cases the electron ranges increase).

2.1.1.2. Detector related conditions

The third feature that characterizes a small field is the size of the detector relative to the size of the radiation field. A detector produces a signal that is proportional to the mean absorbed dose over its sensitive volume and this signal is affected by the homogeneity of the absorbed dose over the detection volume (volume averaging). The effect in a small field is illustrated in Fig. 3. A deconvolution process would be required to derive the absorbed dose to water at a point from this signal.

Besides volume averaging, the perturbation of the charged particle fluence (and thus the deviation from Bragg–Gray cavity theory conditions) due to the presence of a detector is an important issue and it must be noted that both effects are always entangled. In the presence of large dose gradients and in the absence of LCPE conditions, fluence perturbations become large and difficult

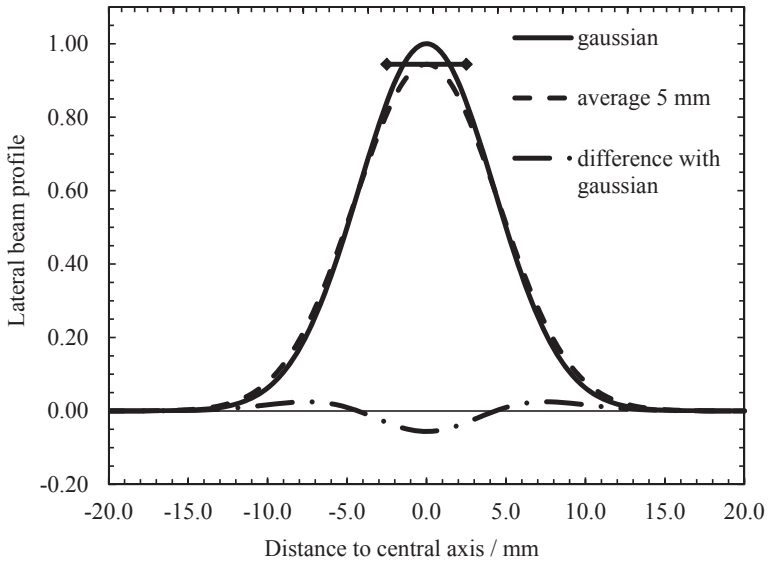

FIG. 3. Schematic illustration of the volume averaging effect in one dimension. The black curve is a Gaussian curve approximating a small field profile; the dashed black curve represents what a detector of 5 mm length would measure. The double arrow represents the dimension of the detector along the scanning axis. The dash-dotted line shows the difference between the two curves as a fraction of the maximum dose (replotted from Ref. [15] with the permission of the International Organization for Medical Physics).

to model. Corrections for volume averaging will also have a larger uncertainty. The dosimetric difficulties thus caused start to show up as soon as the effects of lateral absorbed dose gradients and charged particle disequilibrium reach the detector volume. For these reasons, small field conditions can be assumed to exist when the external edge of the detector volume is at a distance from the field edge smaller than the r_{LCPE} in the medium. To avoid this condition in central axis measurements, the beam half width or radius has to be at least as large as r_{LCPE} plus half the size of the external volume of the detector.

2.1.2. Definition of field size

The International Electrotechnical Commission provides definitions for two differently termed field sizes [16]:

— The *geometrical field size* is defined as the geometrical projection of the collimator opening by the radiation source on a plane perpendicular to the axis of the beam;
— The *irradiation field size* is defined in terms of the dimensions of an area in a plane perpendicular to the radiation beam axis defined by specified isodose lines.

The geometrical field size corresponds with an aligned light field which equals the collimator setting for focused flat edged collimators. For cylindrical collimators, the relation between geometrical field size and collimator settings is a quadratic curve [17]. In broad beams, the FWHM of the lateral profiles, i.e. the irradiation field size specified at the 50% relative dose level, equals the collimator setting and is thus congruent with the geometrical field size. The field size defined by the collimator setting thus corresponds well with the FWHM of the lateral beam profile at the isocentre depth, and measuring the FWHM is a common way of verifying the field size setting. In small fields, however, owing to partial occlusion of the finite primary photon source and loss of LCPE, resulting in a drastic reduction of beam output, this congruence breaks down as is shown in Fig. 4(c) [12, 18]. Because the central axis maximum dose value is reduced, the FWHM is determined by a lower position on the penumbral curve (see Fig. 4). The FWHM of the resulting field is therefore not consistent with the geometrical definition of the field. The irradiation field size specified at 50% relative dose level thus becomes broader than the geometrical field size defined by the projected collimator settings, an effect called apparent field widening. For a given SDD, this effect is dependent on the source-to-collimator distance.

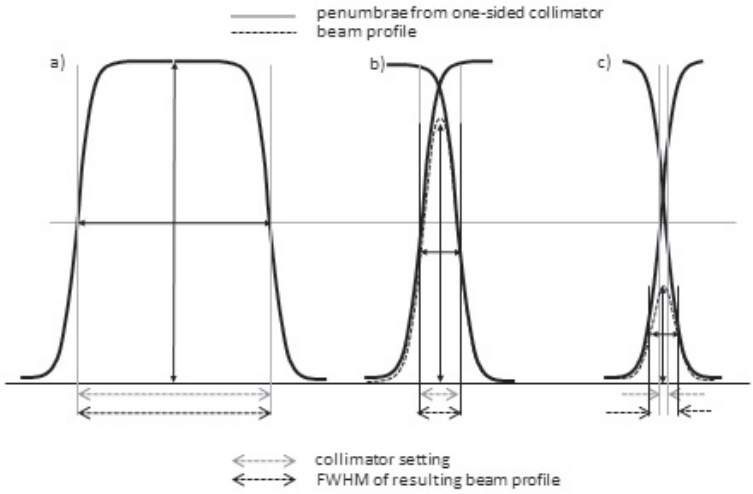

FIG. 4. Effect of overlapping penumbrae on the FWHM of the lateral beam profile for small fields illustrating the apparent field widening compared to the collimator settings (reproduced from Ref. [18] with the permission of the American Association of Physicists in Medicine).

The absence of information on whether the size of a field has been specified in terms of FWHM of the lateral beam profile or of the projected collimator setting complicates the interpretation of field output factor data published in the literature. This COP advises that publication of all small field data such as field output factors be accompanied by unambiguous statements on how the field size is defined. It has been shown that the detector response and perturbation depend on the irradiation field size specified at 50% relative dose level, i.e. the FWHM, at the measurement depth rather than on the collimator setting [19]. The analysis of published data on detector perturbation corrections indicates that the errors made when choosing an incorrect field size specification are substantial [20]. It is advised that the FWHM be used for selecting detector perturbations as a function of field size. It is thus concluded that the FWHM of the lateral beam profile is the most representative and essential field size parameter for accurate small field dosimetry, and field size for small field dosimetry is, in this COP, defined as the irradiation field size or the FWHM of the field. If another field size parameter is referred to, such as geometrical field size, then this will be explicitly mentioned. To facilitate establishing a relationship between FWHM and collimator setting, it is also advised that both the FWHM and the geometrical field size be recorded when reporting small field data. The accurate measurement of profiles for small

fields involves careful procedures; these will be discussed in Section 6 and measurement guidelines are provided in that section.

2.1.3. Hardening of the energy spectrum of small fields

The collimator that defines a small field not only occludes the primary photon source but also shields photons that are scattered from different components inside the linac head, including flattening filter and primary collimator. Thus, the number of low energy photons scattered from the primary collimator, flattening filter and other components in the linac head reaching the centre of the small field is reduced. For off-axis fields, however, there may be an increased relative contribution of photons scattered in the treatment head, and whether this leads to softening or hardening depends on the shape and materials of the flattening filter (if present). Additionally, the amount of phantom scatter also decreases for a small field as compared with a broad field. For most depths, this has a larger effect than the reduced head scatter. These two effects result in a hardening of the photon energy spectrum at any point on the beam axis with decreasing field size and an increase in the average photon energy in comparison with broad beam conditions. This results in a change of the ratio of mass energy absorption coefficients between water and the detector material (e.g. ratio of mass energy absorption coefficients of water to silicon will increase with decreasing field size) and a potential change of the stopping-power ratio between water and the detector material (e.g. the water to air stopping-power ratio will decrease with decreasing field size). An additional effect that plays a role is that when the field is too small for achieving LCPE, there will be a deficit of low energy electrons reaching the central axis, resulting in an increase of the mean electron energy, which can also affect the stopping-power ratio.

Monte Carlo simulations indicate that, although the photon fluence spectrum changes considerably as a function of field size, the charged particle spectrum produced in water is much less affected. Thus, the influence of field size on the water to air stopping-power ratio is found to decrease by not more than 0.5% at a depth of 10 cm in a 6 MV photon beam over a range of field sizes from the 10 cm × 10 cm reference field down to 0.3 cm × 0.3 cm for square fields and a 0.3 cm diameter for circular fields [21, 22]. Even over a range of depths from the depth of dose maximum to 30 cm, the variation is not larger than 1% [21]. The increased average photon energy of the beam does affect the response of silicon based diode detectors because of the large variation of the water to silicon mass energy absorption coefficient ratio for photon energies below 100 keV. Simulations show a variation of 3–4% in the response of unshielded diodes over a range of field sizes from 10 cm × 10 cm to 0.5 cm × 0.5 cm at a measurement

depth of 10 cm as a result of the reduced phantom scatter [23], and this is supported by experimental data [24].

2.1.4. Beam quality of small fields and msr fields

Conventional reference dosimetry of a high energy photon beam with quality Q using an ionization chamber requires an absorbed dose to water calibration coefficient in the beam quality Q or, if that is not available, an absorbed dose to water calibration coefficient in a calibration beam quality Q_0 and a beam quality and chamber dependent beam quality correction factor k_{Q,Q_0}. The subscript Q_0 is omitted when the reference quality is ^{60}Co gamma radiation (i.e. the reduced notation k_Q always corresponds to the reference quality ^{60}Co) [1]. The beam quality for high energy photon beams is specified in Ref. [1] and most other absorbed dose to water based dosimetry protocols by a single beam quality index, the tissue phantom ratio in water at depths of 20 and 10 g/cm^2 for a field size of 10 cm × 10 cm and SDD of 100 cm, here denoted $TPR_{20,10}(10)$[2]. In Refs [2, 7], the beam quality specifier or index is the percentage depth dose at 10 cm depth in a water phantom due to photons only, here denoted $\%dd(10,10)_x$. The beam quality indices in these protocols are used for the selection of the beam quality correction factor k_{Q,Q_0}, required when reference dosimetry is performed with an ionization chamber in a beam with quality different from that used for its calibration; they are also used by standards laboratories to specify the beam quality of high energy beams used for calibration.

In Ref. [1], the preferred approach is to use experimental k_{Q,Q_0} values measured for the user's chamber at specific beam qualities Q in a PSDL or a secondary standards dosimetry laboratory (SSDL). The difference between beam qualities at the standards laboratory and at the user's facility would give preference to k_{Q,Q_0} factors determined for a specific clinical radiotherapy machine, a possibility that only exists if the PSDL or SSDL calibrates chambers in the beam of the particular clinical machine or the same machine type. Some PSDLs and SSDLs provide high energy photon beam calibrations using clinical linacs; this option is realistic given the small differences between calibration coefficients in different machines of the same type. Indeed, with modern radiotherapy technology, differences between machines of the same type have been reduced significantly and, within a certain tolerance, the beam quality for a given photon beam energy at a given machine type is found to vary only modestly from machine to machine. Thus, it is conceivable that a unique beam

---

[2] Note that the symbols used differ from those used to denote the beam quality index in Ref. [1] ($TPR_{20,10}$) and in Refs [2, 7] ($\%dd(10)_x$), because in this COP an additional parameter in brackets is used to specify the field size.

quality correction factor could be used for a particular combination of ionization chamber type and radiotherapy machine type and the dosimetry at these machines could, in principle, be done without a need for beam quality indices. This has to some extent been demonstrated for Gamma Knife® (Elekta AB, Stockholm), Cyberknife® (Accuray Inc., Sunnyvale, CA) and TomoTherapy® (Accuray Inc., Sunnyvale, CA) machines. Likewise, for conventional radiotherapy machines with fields collimated by jaws or MLCs, machine uniformity has improved [25–27]. It must be emphasized though that this does not remove the necessity of verifying that the beam quality index is within the normal range for a given machine type and that even if the determination of the beam quality index is not needed to look up beam quality correction factors, it remains an essential part of commissioning and quality assurance (QA) procedures. Another point is that most intensity modulated radiotherapy (IMRT) and stereotactic treatments are delivered with photon beams of nominal energies not exceeding 10 MV, where the sensitivity of k_{Q,Q_0} to the beam quality specifier is rather small [1, 2]. The multitude of add-ons used for IMRT and stereotactic treatments, however, makes it difficult to tabulate factors for all combinations of basic radiotherapy machines, add-ons and chamber types. Overall, the current situation is that for a wide range of high energy photon treatment machines, k_{Q,Q_0} for specific machine/ionization chamber combinations is not available. Consequently, one has to continue to rely on the use of beam quality indices to link the calibration beam quality to individual end user machines.

For the dosimetry of small fields, two practical questions remain to be considered: Is the beam quality specification for the conventional 10 cm × 10 cm reference field appropriate and sufficient for the dosimetry of smaller fields in the same machine? If the answer to this question is yes, how can the beam quality index be determined for radiation generators that cannot establish the conventional reference conditions prescribed for the measurement of beam quality?

The first question has already been partially answered in the previous section: the very small variation of water to air stopping-power ratios with field size suggests that for ionization chambers the beam quality index of the broad field would be sufficient for all field sizes. The variation of stopping-power ratios and perturbation factors with field size can then be incorporated into a field dependent output correction factor.

Various approaches have been suggested to address the second question. For those types of generators, Alfonso et al. [8] introduced the concept of an msr field, f_{msr}. For TomoTherapy machines, one study [28] introduced a specific beam quality index similar in definition to $\%dd(10,10)_x$ but measured under different conditions achievable in these treatment machines. Monte Carlo calculated k_Q values as a function of this specific index were then compared with values as

a function of the conventional beam quality index to establish a relation between the machine specific index and the conventional index. This approach has been adopted by Ref. [29]. Another approach relies on the measurement of $TPR_{20,10}(S)$, the ratio of absorbed dose to water values at the depths of 20 and 10 g/cm^2 in water for a square field size of S cm × S cm defined at an SDD of 100 cm. $TPR_{20,10}(S)$ values are measured for the non-conventional machine at a series of square field sizes S and compared with the variation for a machine where the conventional reference conditions can be established, enabling extrapolation of the measured data [30]. A related approach used in several publications [30, 31] is to extrapolate measurements as a function of field size using data for the same range of field sizes from the generic set in Ref. [32]. Mainly based on these data, a generic expression was formulated for deriving the beam quality index of the conventional 10 cm × 10 cm reference field, $TPR_{20,10}(10)$, from a measurement of $TPR_{20,10}(S)$ [33].

It was demonstrated by Sauer [33] that the model works well also for non-square (e.g. circular or rectangular) fields using the equivalent square field method (Ref. [32]), and even for FFF beams applying a correction for the scatter deficiency caused by their conical lateral beam profiles. It is important to be aware of the slightly different relation between stopping-power ratios and beam quality index between FFF beams and beams with flattening filter (WFF) [34–37].

Consistent formulas for $TPR_{20,10}(10)$ and $\%dd(10,10)_x$ for a narrower range of square field sizes (S between 4 cm and 12 cm, the relevant range for this COP) have been derived [38] based on the same data from Ref. [32] and are illustrated for $TPR_{20,10}(10)$ in Fig. 5. The expressions are given in Section 5.

2.1.5. Detector response

In radiotherapy dosimetry it is well known that the characteristics of a detector may affect its response to ionizing radiation considerably. For example, the particle fluence that is sampled by the detector differs, sometimes substantially, from the fluence that exists in a homogeneous medium in the absence of the detector. This is caused by the size, shape and materials in the detector, which result in deviations from the ideal small volume concept underlying the Bragg–Gray principle. For a real detector, the application of Bragg–Gray cavity theory based on medium-to-detector stopping-power ratios requires a modification using perturbation correction factors. All dosimetry protocols for conventional reference dosimetry based on a theoretical determination of all perturbation correction factors necessary to correct the detector response from the calibration beam quality to the user's beam quality explicitly or implicitly include such perturbation correction factors [1, 2, 39, 40]. When measurements are performed in CPE or TCPE conditions, any variation in stopping-power ratio

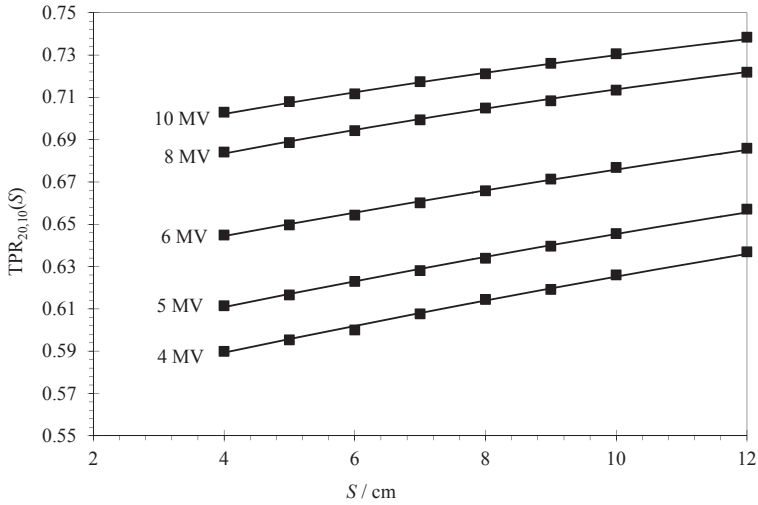

FIG. 5. Dependence of $TPR_{20,10}(S)$ on the field size S based on data from Ref. [32] (square symbols), and according to the model of Palmans [38] (curves) for field sizes between 4 cm and 12 cm and nominal photon beam energies between 4 MV and 10 MV (reproduced from Ref. [38] with the permission of the American Association of Physicists in Medicine).

is evaluated independently of perturbation correction factors for wall effects, the presence, if any, of a central electrode, electron in-scattering effects, volume of the medium displaced by the detector, etc. [41], all assumed to be small and independent. In recent years there has been a renewed interest in accurate determinations of perturbation correction factors for ionization chambers. In particular, Monte Carlo methods have analysed in detail the various types of perturbation effects in a stepwise fashion [42–44], leading to a total perturbation correction factor for an ionization chamber in a given beam quality.

Studies on perturbation effects of small ionization chambers in small static beams are scarce. One of the earliest comprehensive studies pertaining to this area is the work by Crop et al. [45]. The results of this Monte Carlo study, of which the data at the centre of a 0.8 cm × 0.8 cm field are shown in Fig. 6, indicated that the central electrode and wall perturbation correction factors were, even though different from those in a broad beam, close to unity. The major perturbations were caused by the volume averaging effect and the difference between the mass density of the detector and that of the medium, and both corrections were rather large and of similar size. The perturbations were considerably larger for off-axis measurements. This shows that for small fields, perturbation effects even for small detectors are considerably larger than for conventional ionization chambers in broad beams. In the smallest fields of interest, some perturbations become so large

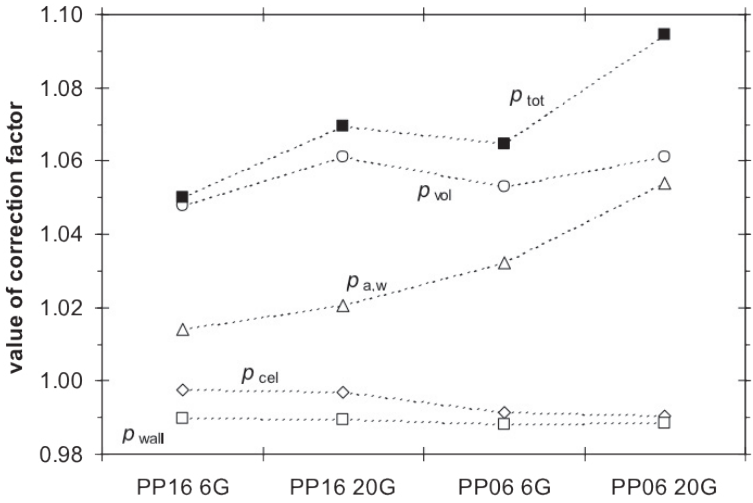

FIG. 6. Contributions to the Monte Carlo calculated overall perturbation correction factor in the centre of a 0.8 cm × 0.8 cm field in a 6 MV photon beam resulting from the non-water equivalence of the wall (p_{wall}), the presence of the central electrode (p_{cel}), the perturbation from replacing water with air ($p_{a,w}$) and volume averaging (p_{vol}) for two types of PinPoint chambers (PP16 = PTW 31016 and PP06 = PTW 31006 with nominal volumes of 0.016 cm^3 and 0.015 cm^3, respectively) and two electron spot sizes (6G and 20G = 0.6 mm and 2.0 mm FWHM, respectively). The data are not in any particular order and the dotted lines serve only the purpose of visually connecting data points that represent the same contributing factor. Note that, for comparison, the value of the total perturbation correction factor p_{tot} in a 10 cm × 10 cm field amounts to 0.99 (reproduced from Ref. [45] with the permission of IOP Publishing).

that the various contributions to the overall perturbation correction factors are no longer independent. This situation, which differs from broad beam conditions, undermines our current approach of applying Bragg–Gray cavity theory. Monte Carlo calculations based on a ratio of absorbed dose to water and absorbed dose to the detector material for the entire detector geometry are then preferable for calculating an overall conversion factor. It might still be of scientific interest to study the contributions in a stepwise fashion but not with the aim of proposing independent values for the various factors that could be reproduced via different routes. Decreasing the relative detector-to-beam size, misalignments, or primary photon source size can in addition, lead to unpredictably large effects. Figure 7 illustrates the uncertainty contribution to the absorbed dose determination using a PTW 60012 diode due to a uniformly distributed displacement error of 1 mm in all directions perpendicular to the beam axis.

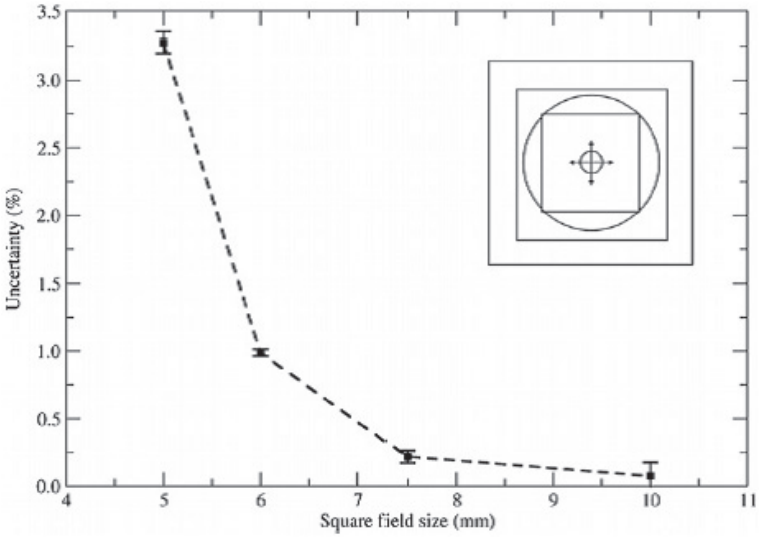

FIG. 7. Uncertainty contribution to the absorbed dose determination using a PTW 60012 diode due to a uniformly distributed displacement error of 1 mm in all directions perpendicular to the beam axis only calculated by Monte Carlo (reproduced from Ref. [46] with the permission of IOP Publishing).

More recently, a number of authors have studied the components of small field perturbation factors by Monte Carlo simulations in a more systematic way [47–50]. Scott et al. [47] defined the ratio of absorbed dose to water at the measurement point in the water phantom and the mean absorbed dose over a volume of water replacing the entire detector's sensitive volume as the volume averaging correction factor. Any other factor is then related to the non-water equivalence of detector materials in the sensitive volume, the electrodes and the encapsulation. It was then observed that, next to volume averaging, the main additional contribution to small field perturbation factors is the difference in density between the detector materials and water, especially in the variation of perturbation factors with field size. Not only is the density of the material in the sensitive volume of importance, but so is that of surrounding materials such as the epoxy encapsulation of diode detectors [51, 52], thin metallic electrodes and presence of small air gaps [53].

Differences in interaction data, while important in the overall conversion factor, are found to make only a small contribution to the variation of the perturbation correction factor with field size. Following up on those observations, Monte Carlo studies have investigated the possibility of compensating for small field perturbations by 'mass density compensation' [54, 55].

It is emphasized that small solid state detectors may also exhibit some level of volume averaging, which, considering their size, is shown only for the smallest therapeutic fields, i.e. those smaller than 1 cm [47, 56–58]. For these detectors, other perturbation effects may play a role as well (e.g. backscattering from metallic electrodes). The energy and angular dependence of some detectors, such as diodes, plays an important role. Owing to the fact that silicon has a higher mass energy absorption coefficient than water, unshielded diodes over-respond in large fields because of the significant phantom scatter component of low energy photons. The consequence is an underestimation of field output factors when they are normalized to a large field size (e.g. the conventional 10 cm × 10 cm reference field). In large fields, the over-response is usually compensated by adding a layer of high Z material around the sides and the bottom of the silicon chip that filters out the low energy scattered photons. These high Z caps are, however, undesirable in very small fields, as they may cause large perturbation effects that are difficult to determine accurately even with Monte Carlo calculations, as detector-to-detector differences are complicated to simulate [59].

2.1.6. Energy range of interest

Photon beams with nominal accelerator potentials greater than 10 MV are often thought necessary for deep seated tumours. Compared to lower energy beams, these create electrons with longer ranges so that full buildup occurs at greater depths, resulting in a lower absorbed dose to water at shallow depths. In addition to the longer forward electron range, higher energy beams also have a longer lateral electron range that increases the penumbral width significantly. This is particularly noticeable for small field sizes and within low density tissues such as the lung.

In IMRT, fluence modulation is primarily determined by beam transmission through open and closed leaf positions but is also heavily influenced by the penumbrae of the lateral beam profiles. A simple illustrative example is shown in Fig. 8 whereby the profiles created by alternating open and closed leaves are compared for 18 and 6 MV beams. The peak doses are higher and the valley doses are lower for 6 MV beams, indicating better modulation for lower energy beams. In addition, at least part of the reason for the lower valley depth is the lower collimator transmission for 6 MV beams. Neutron production from high energy photons is a particular problem for IMRT because a significant number of (γ,n) reactions occur in the high atomic number collimation components. For example, at 18 MV the cross-section for neutron production by collimation is two orders of magnitude greater than for 10 MV photons [60]. Not only do neutrons produce unwanted radiation exposure to the patient, but they also cause activation of linac components that leads to extra exposure to staff and service personnel.

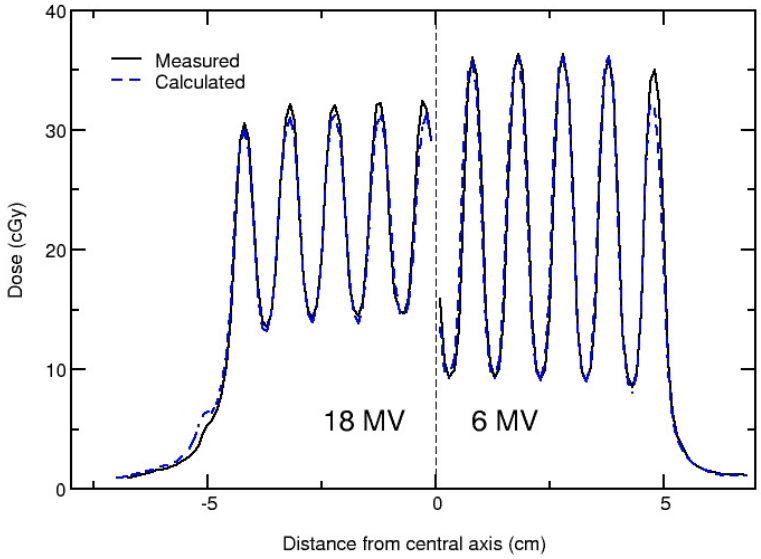

FIG. 8. Absorbed dose to water profiles for alternating open and closed MLC leaves. Both measurement and Monte Carlo calculation show improved modulation for the lower energy beam. For the higher energy beam, a larger fraction of electrons scatter from the open to closed field region and the MLC transmission is higher (courtesy of Jeffrey Siebers, Virginia Commonwealth University).

Based on these observations, the International Commission on Radiation Units and Measurements (ICRU) stated that the use of higher energy beams is not justified for IMRT [61]. For these reasons, guidance in this COP is only provided for high energy photon beams with nominal accelerating potential up to 10 MV. The predominance of the use of these beams also provides a robust argument to restrict the applicability of this COP to potentials below or equal to 10 MV. Data from IAEA's Directory of Radiotherapy Centres (DIRAC) database show that about 80% of beams used at linacs installed after the year 2000 used for all forms of radiotherapy have nominal energies of 10 MV or lower [62]. Furthermore, data from the Imaging and Radiation Oncology Core (IROC) Houston QA Center indicate that, for lung stereotactic radiotherapy, about 96.4% of the beams used are of 6 MV and 3.2% of 10 MV, whereas for liver stereotactic radiotherapy the figures are 80% and 15.7% respectively [63]. The availability of data for small field dosimetry is also dominated by the 6–10 MV range.

2.1.7. Summary of small field characterization for dosimetry

Based on the discussion in the previous sections, a summary is given here of the parameters that need to be determined to enable accurate dosimetry of small fields:

— It is advised that to allow lookup of output correction factors from tables, the field size be specified by the FWHM of the lateral beam profile at the measurement depth (see Section 2.1.2). The depth of measurement is such that electron contamination originating from the materials in the beam path is negligible (in this COP, 10 cm is recommended). The reference distance will usually be the isocentric distance. The collimator setting, which is the aperture size projected to a reference position (isocentre or reference distance from the source), could be recorded as well to enable the link with the beam data management and treatment planning systems.
— The beam quality of a small field, representing the energy spectrum of the beam, is characterized by the determination of a beam quality index ($TPR_{20,10}(10)$ or $\%dd(10,10)_x$) for a conventional 10 cm × 10 cm reference field at the beam. For machines that cannot establish this conventional reference field, modified procedures exist to derive the beam quality index from quantities measurable in smaller fields (see Section 2.1.4).
— A distinction between small and large fields is made by introducing the concept of the beam energy dependent r_{LCPE}. Because detector perturbations are influenced substantially by the absence of equilibrium conditions, small field conditions are also assumed to exist when any point within the outer boundaries of the detector volume is less than r_{LCPE} away from any field edge (at 50% absorbed dose level). Equations are provided of the dependence of r_{LCPE} on the beam quality index.

2.2. ABSORBED DOSE TO WATER STANDARDS FOR SMALL FIELDS

In small field radiotherapy, as in conventional radiotherapy, all dosimetric measurements need to be traceable to primary radiation standards. Traceability is obtained by the process of detector calibration and the entire path between a clinical measurement and a standard is referred to as the calibration chain. QA programmes need to be in place to ensure the quality of the calibration chain. For broad reference fields (10 cm × 10 cm), primary standards of absorbed dose to water exist. These instruments allow for the determination of the absorbed dose to water according to its definition. They are normally maintained in PSDLs. User instruments can be directly calibrated against these primary standards, but

more often they are calibrated against secondary standards, which themselves are calibrated against primary standards. Secondary standards are maintained in SSDLs or Accredited Dosimetry Calibration Laboratories (ADCLs) in North America. The exact roles and positions of PSDLs, SSDLs, the Bureau International des Poids et Mesures (BIPM) and the role of key comparisons are explained by the BIPM web pages (www.bipm.org) and, particularly in terms of how they relate to radiotherapy dosimetry, in Ref. [1].

The most common primary standard for absorbed dose to water in conventional reference fields is calorimetry, although standards based on other methods, such as ionization chambers and chemical dosimeters, are also available. Water calorimetry is the most direct method for the measurement of absorbed dose to water. Graphite calorimeters are also common given their higher sensitivity and robustness as compared to water calorimeters. An extensive review of calorimetric absorbed dose standards for external beams can be found in Seuntjens and Duane [64] and McEwen and DuSautoy [65]. However, only a few studies deal with the application of calorimetry to small field dosimetry; for example, Krauss [66] has applied the primary standard water calorimeter of the Physikalisch-Technische Bundesanstalt (PTB), the National Metrology Institute of Germany, to determine absorbed dose to water and to calibrate ionization chambers in 5 cm × 5 cm and 3 cm × 3 cm fields [67–69]. One of the main technical complications of using a water calorimeter designed for measurements in a 10 cm × 10 cm field in small fields is the increasing correction for heat conduction across the lateral profile. De Prez [70] simulated heat loss corrections for the VSL (Dutch Primary Standards Laboratory) water calorimeter and found that these corrections were within 5% for field sizes down to 3 cm × 3 cm and increased dramatically for smaller field sizes (up to 60% for a 1.8 cm × 1.8 cm field). These corrections depend on the measurement time, which, in turn, depends on the available dose rate. However, if the irradiation time could be shortened, absorbed dose to water determination in a small field using water calorimetry could be feasible; although a substantial increase in absorbed dose rates would be needed for this purpose. This is possible with FFF photon beams. While graphite calorimeters that are used as primary standards instruments have cores that are too large for small field dosimetry, small core graphite calorimeter probes that can be used in water or a water equivalent phantom have been constructed [71, 72] for dosimetry in small photon fields and IMRT fields. Following on the suggestion to derive field output factors from integrated lateral dose or ionization profiles [73, 74], dose–area product calorimeters have been proposed. The BIPM calorimeter [75] has this capability for a limited range of field sizes with its core diameter of 45 mm.

For practical reasons, transfer standards are often used in standards laboratories to calibrate individual user instruments. Also, given that in

most calorimeters, the phantom is part of the construction and thus there is no flexibility on phantom shape, transfer standards are used to establish the calibration quantity in different phantoms. Ionization chambers, ferrous sulphate chemical dosimeters and alanine/electron spin resonance (ESR) have been used for that purpose. Of these, alanine/ESR has also been used as a transfer standard for dose determination in small fields. Because the density of alanine pellets is close to the density of water, the overall correction can be determined with good accuracy as it is dominated by volume averaging. Even for a 0.5 cm diameter field, volume averaging corrections from 3-D dose distributions obtained by gel dosimetry bring the alanine response into good agreement with the response of a range of small detectors [76]. One of its disadvantages is its relatively low sensitivity; however, a type-A standard uncertainty of 0.5% can be achieved for absorbed dose to water values of 10 Gy [77, 78]. For high energy photon fields, a difference of 0.3% to 0.6% in detector response has been reported as compared to ^{60}Co [79, 80].

2.3. OVERVIEW OF CURRENT REFERENCE AND RELATIVE DOSIMETRY OF RADIOTHERAPY BEAMS

2.3.1. Reference dosimetry

2.3.1.1. Conventional reference beams

Guidance for the determination of absorbed dose to water in high energy photon beams based on standards of absorbed dose to water has been provided in various national and international COPs (including Refs [1, 2, 4, 5, 7]). These use common reference conditions for the determination of the beam quality and for the determination of absorbed dose to water: a field size of 10 cm × 10 cm at the phantom surface or at the measurement depth, and an SSD or SDD of 100 cm. These formalisms are very similar and can be described by that given in Ref. [1], which is used as the basis for the formalism in this report and briefly summarized here.

The absorbed dose to water at the reference depth z_{ref} in water for a user beam quality Q and in the absence of the chamber is given by:

$$D_{\text{w},Q} = M_Q N_{D,\text{w},Q} \tag{1}$$

where M_Q is the reading of the ionization chamber at the user's beam quality Q, corrected to the reference values of influence quantities other than beam quality, for which the calibration coefficient is valid, and $N_{D,\text{w},Q}$ is the calibration

coefficient in terms of absorbed dose to water of the ionization chamber measured at a standards laboratory for the user's beam quality Q.

In most countries, direct calibrations in clinical beam qualities are not available, and even when they are available, the calibration beam quality Q_0 is usually different from the user's beam quality Q. In that case, Eq. (1) is replaced by:

$$D_{w,Q} = M_Q N_{D,w,Q_0} k_{Q,Q_0} \tag{2}$$

where N_{D,w,Q_0} is the calibration coefficient in terms of absorbed dose to water of the ionization chamber measured at a standards laboratory for the calibration beam quality Q_0, and k_{Q,Q_0} is the factor that corrects N_{D,w,Q_0} for the difference between the reference beam quality Q_0 and the actual user quality Q.

2.3.1.2. Non-conventional reference beams

Several modern radiation generators that are purposely developed for stereotactic treatments or IMRT cannot establish the reference conditions prescribed in the COPs mentioned. Issues related to the determination of the beam quality index for such machines have been described in Section 2.1.4. For reference dosimetry, the common practice is to use the same formulas as for conventional beams, but performing reference dosimetry in the field size closest to 10 cm × 10 cm (often the largest field available) and in most cases assuming that the beam quality correction factors are the same. Specific procedures are often followed for a particular type of radiotherapy machine. For FFF beams it has been determined that an additional volume averaging correction factor may be required to correct for the non-homogeneity of the lateral profile [81, 82].

For TomoTherapy, a 5 cm × 10 cm reference field at a distance of 85 cm from the source is recommended in Ref. [29], and for the selection of the beam quality correction factor, a generic relation between a TomoTherapy specific beam quality index and the conventional beam quality index from Refs [2, 7] is given. The formalism of Alfonso et al. [8] is followed and a factor to correct for the difference between the ionization chamber's response in a virtual 10 cm × 10 cm reference field and the 5 cm × 10 cm TomoTherapy specific reference field is advised. The value of this factor was based on Monte Carlo simulations and is close to unity.

For CyberKnife, the largest fixed collimator defined field is taken as the reference field. This field is circular and has a nominal 6 cm diameter at a distance of 80 cm from the source. For the determination of the beam quality index, equivalent field and interpolation methods using data from Ref. [32], similar to those described by Sauer [33], have been used for deriving $TPR_{20,10}(10)$ [83] and

$\%dd(10,10)_x$ [31] from measurements in the largest circular field. Beam quality correction factors for ionization chambers in this field are found to be close to those for other 6 MV machines, but for the relatively long Farmer type chambers, a correction greater than 1% needs to be applied for volume averaging over the projected effective area of the ionization chamber [81, 82].

The Gamma Knife is a special case because a treatment field is always composed of a superposition of multiple small fields. Nevertheless, it is considered a case to be categorized under static small field dosimetry rather than composite field dosimetry. The maximum field size diameter is 1.8 cm or 1.6 cm, depending on the machine model, and reference dosimetry for that field size is performed in the centre of a plastic sphere using a microchamber calibrated in ^{60}Co without the use of a beam quality correction factor [84–86]. An air kerma based approach has also been suggested [87].

For Brainlab add-ons, the reference SDD or SSD of 100 cm can be established, but the field size cannot be set to exactly 10 cm × 10 cm, so the nearest field size is used. By choosing one dimension larger than 10 cm and the other smaller, one can achieve a field area which is almost identical to a 10 cm × 10 cm field (e.g. 9.6 cm × 10.4 cm), in which case no special considerations for the determination of beam quality and for reference dosimetry are required.

A formal treatment of the dosimetry of non-standard[3] beams was published by Alfonso et al. [8], and their formalism will be followed in this COP.

2.3.2. Relative dosimetry

2.3.2.1. Field output factors

A field output factor is defined as the ratio of absorbed dose to water in any non-reference field to that in a reference field at a given depth. In conventional broad beams, it is derived from a ratio of detector readings because of the practical independence of dosimetric quantities on field size. In small field dosimetry, however, such independence does not exist, notably for perturbation factors, and a field output factor will in most cases require an output correction factor to be applied to the measured detector reading ratio. It will thus in most cases be incorrect to report a ratio of readings as a field output factor, a mistake which is, unfortunately, all too often encountered in clinical practice as well as in the scientific literature [88]. Many examples have been published showing large discrepancies between the ratio of readings measured with different types of detectors for a particular beam compared with the actual ratio of absorbed

[3] 'Non-conventional' in the nomenclature of this COP.

dose to water values [18, 24, 73]. These discrepancies are mainly field size and detector dependent and can be unacceptably high when measured with detectors that have a large volume compared to the size of the small field. The common practice of reporting ratios of detector readings as field output factors is a mistake that has led to much confusion, potentially to serious errors and, in some of the worst cases, to real accidents. For example, the use of inappropriate detectors for measuring field output factors without further corrections has been reported as the main cause of an accidental overdosage of patients for beams defined by the Brainlab m3 micro MLC [89]. A comparison of beam data measured in different centres in France with microchambers for the 0.6 cm × 0.6 cm beam of different Varian Clinac models, under identical measuring conditions (6 MV photons, micro MLC type, SSD, depth, type and orientation of the detector), showed a discrepancy of about 15% in the extreme values of the detector output ratios as uncorrected estimates for field output factors, as shown in Fig. 9. The report by the French Society of Medical Physics (SFPM), which was the result of a follow-up effort after this accident, advises using at least two different detectors for the measurement of field output factors [89].

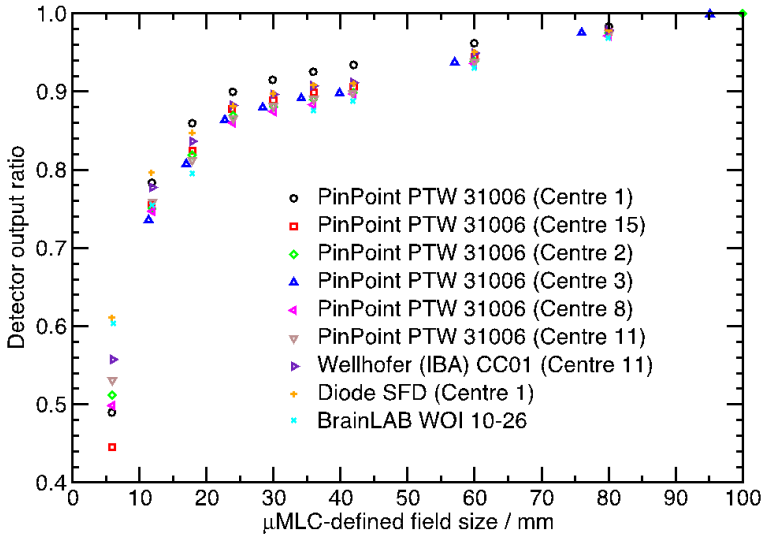

FIG. 9. Detector output ratios as uncorrected estimates for field output factors determined in different centres in France for 6 MV photon beams and the Brainlab m3 micro MLC (SSD = 100 cm, depth = 5.0 cm) using three different detector types. The Brainlab WOI 10-26 data correspond to manufacturer guidance data. (Reproduced from Ref. [89] with the permission of the Institut de radioprotection et de sûreté nucléaire.)

Alfonso et al. [8] have emphasized the distinction between ratios of detector readings and ratios of absorbed dose to water values by explicitly including an output correction factor in the expression for the field output factor.

In large reference fields, output correction factors are required for detectors exhibiting an energy dependent response due to low energy scattered photons originating in the treatment head and in the phantom combined with the different mass energy absorption coefficient for those low energy photons. This is for example the case for silicon based devices such as unshielded diodes and metal oxide semiconductor field-effect transistors (MOSFETs), as described in Section 2.1.5, and it results in a more or less linear increase of the response with increasing field size as illustrated in Fig. 10. From these observations, the approach employed to obtain field output factors is to use an ionization chamber for field sizes down to the one where volume averaging sets in, and use a small detector (e.g. a diode, diamond, liquid ionization chamber or organic scintillator) for smaller fields. The field output factors derived from the measurements with the small detectors are renormalized at the smallest field size where the ionization chamber is used; this is referred to as the intermediate field method in this COP. This method has sometimes been called "daisy-chaining" [90].

For determination of field output factors in small fields, another approach has been proposed that suggests using a large area parallel plane ionization chamber (LAC) in combination with radiographic or radiochromic film [73, 74]. From the signal produced by the two dimensional fluence distribution over the area of the LAC, the value of the dose–area product (DAP) can be determined. With accurate film dosimetry at the same plane of measurement as the LAC, the field size and a two dimensional relative absorbed dose distribution can be determined. From this and the DAP value, the absorbed dose to water is derived at the region of interest. While this is an interesting area of research, there is not enough experience and information at present to provide guidance on this method.

2.3.2.2. Lateral beam profiles

The lateral beam profile is defined as the distribution of absorbed dose to water at the reference depth in the phantom, perpendicular to the beam axis and parallel to the phantom surface. The difficulties of measuring lateral beam profiles in small photon fields are associated with the dimension of the detector's sensitive volume, defined as the geometrical dimension of the measuring volume in the scan direction, in relation with the beam penumbra size. Even for conventional broad fields, when tertiary collimation is used for reduction of their penumbra, the effect of the detector's finite volume can lead to inaccuracies in the determination of the penumbra width. This becomes a crucial problem in

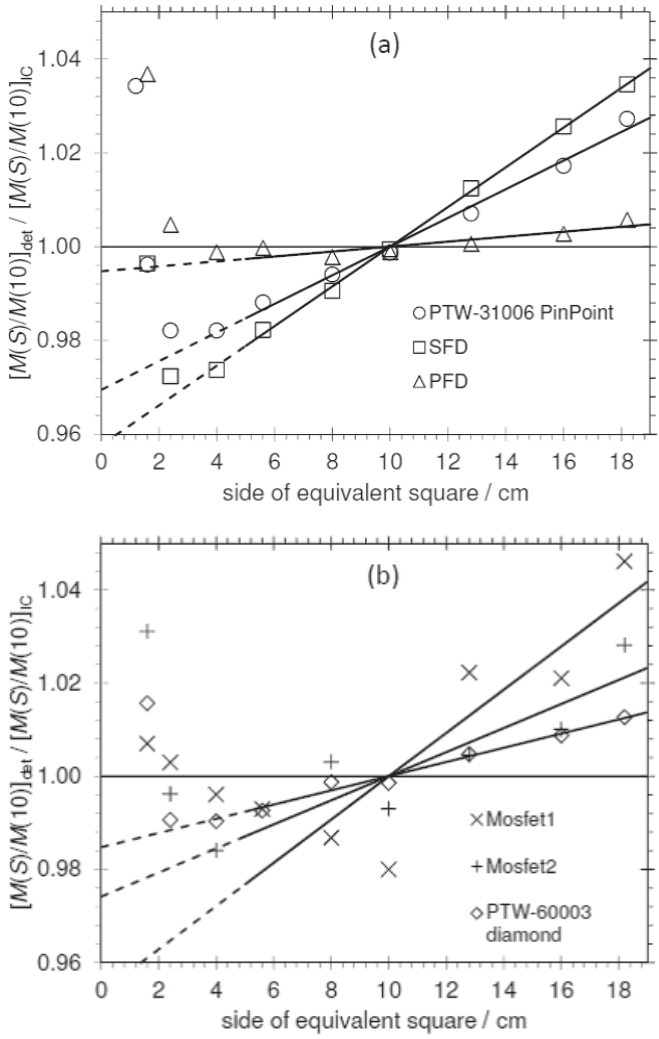

FIG. 10. Ratio of the relative readings of various detectors and the relative reading of a PTW 31010 Semiflex ionization chamber. The relative readings of all detectors were normalized at the value for 10 cm equivalent square field size. This figure illustrates the field size dependence of solid detectors for large fields and the perturbation of ionization chambers in small fields for (a) a PTW 31006 PinPoint ionization chamber, a Scanditronix Stereotactic Field Diode (SFD) and a Scanditronix Photon Field Diode (PFD), and (b) two Thomson Nielsen Si-MOSFETS of the same type (Mosfet1 and Mosfet2) and a PTW 60003 diamond detector (replotted from Ref. [24]). The full lines are linear fits to the data points for field sizes larger than 5 cm × 5 cm and the dashed lines extrapolations of those fits to smaller field sizes to illustrate the field size dependence of the diode response solely due to phantom scatter, i.e. ignoring the effect of fluence perturbations. (Reproduced from Ref. [24] with the permission of the American Association of Physicists in Medicine.)

very small fields, as the penumbra represents an important portion of the field. Because for these small fields detector perturbation factors show a very steep dependence on field size, small errors in penumbra measurements can result in substantial dosimetric errors.

Suitable detectors to resolve the penumbra in small photon fields are tissue equivalent radiochromic film, diodes (stereotactic, shielded or unshielded and oriented parallel to central axis), diamond detectors, small air filled ionization chambers and liquid ionization chambers [12]. Even those detectors require special measures to avoid various artefacts (e.g. the readout procedure for radiochromic film needs to be well conducted). For scanning detectors, the orientation needs to be considered and effects of stem and cable irradiation taken into account. A method has been published to derive corrected penumbrae from measurements with a series of different sized detectors [91]. A paper by Francescon et al. [58] investigated the variation of the perturbation of various small detectors as a function of off-axis position. This is very helpful in advising on the type of detector to be used for profile measurements, but it is important to be aware that owing to detector-to-detector variations combined with the extreme sensitivity of these perturbations to detector dimensions, it is advised that these not be regarded as providing generic output correction factors for profile measurements.

Another approach which has been suggested is to deconvolve the lateral beam profile from the measured profile using Monte Carlo calculated detector specific kernels [92] or simply Gaussian kernels [93] based on the observation that despite the lateral fluence convolution kernels for many detectors being quite complicated, the dose convolution kernels are blurred by the lateral range of secondary electrons and the effects of the detector construction details are lost, making Gaussian kernels adequate.

An interesting observation was made by Underwood et al. [54], who suggested that, while most detectors either under-respond or over-respond on the central axis, i.e. in the measurement of field output factors, in small fields, this is actually compensated by an opposing over-response or under-response, respectively, in the profile tails, and that the integral dose measured for many detectors would be accurate without any output correction factors. Figure 11 illustrates this for three types of detectors. In IMRT, the integral dose contribution of a small field is indeed more important than the absorbed dose to water in the centre of the field itself. This approach would of course only make sense if the same detector is used to measure the field output factor and to measure the profile, while in practice often a combination of a point detector for the field output factor and radiochromic film for the profiles would be used.

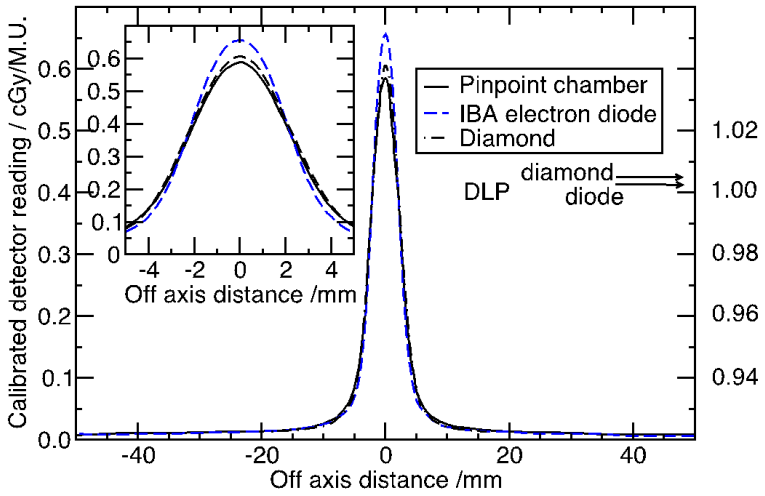

FIG. 11. Lateral beam profiles of a 0.5 cm × 40 cm field (along the short axis of the rectangular field) in a 6 MV beam measured using three different detectors. These profiles are expressed in terms of absorbed dose in cGy per monitor unit (MU) by calibration of the detectors in a large field, denoted as "Calibrated detector reading". This figure shows the under-response of the larger detectors around the dose maximum, as schematically explained in Fig. 3. The arrows on the right hand side vertical axis indicate the ratio of the dose length product (DLP) of the solid detectors (diamond, diode) to the DLP of the PinPoint ionization chamber, illustrating that for the diamond detector and the IBA unshielded diode, the DLP is the same, despite their differences on the axis of the field. (Reproduced from Ref. [54] with the permission of the American Association of Physicists in Medicine.)

3. CONCEPTS AND FORMALISM

This section presents the formalism and concepts underlying the small field dosimetry procedures described in this COP. A distinction will be made between situations where data are available for specific radiation generator/detector combinations and for other situations where procedures have to rely on the less favourable generic approach of using beam quality characterization to look up beam quality correction factors in tabulated data. Note that for completeness, some concepts described in the preceding section are also reproduced here.

3.1. CONCEPTS OF SMALL FIELDS

3.1.1. Definition of field size

For the purpose of applying the procedures in this COP, the field size is the pair of dimensions (in the case of rectangular fields) or the diameter (in the case of a circular field) that define(s) the area of the field at the measurement distance. Each dimension is defined by the FWHM of the lateral beam profile measured at a depth sufficient to eliminate the contribution of contamination electrons. 'Field size' is thus used as synonym for 'irradiation field size' as defined by the International Electrotechnical Commission [16]. A depth of 10 cm in water with the detector's reference point at the isocentre is advised because this is adequate to eliminate contamination electrons and because beam flatness has historically been defined at 10 cm depth. It is advised that the measurement be made with a dosimeter capable of sufficient spatial resolution. There is no need for a calibrated dosimeter for this task because many dosimeter types that have an adequate spatial resolution can be used (for example film, diodes or diamond detectors), none of which are reference class dosimeters.

It is advised to record, in addition, the collimator settings as a nominal identification for practical purposes. For example, the treatment planning system, the electronic patient record and the record and verify system all use the nominal field setting rather than the FWHM relative to which the profile data, patient treatment plan and radiation delivery are referenced. This guidance is analogous to that of stating the nominal accelerating potential (MV) to refer in practice to a beam with a certain quality index.

In this COP, output correction factors for small fields are tabulated as a function of the equivalent square small field size. For non-square fields, a method is provided to determine the equivalent square small field size for which

the output correction factors are the same. This method simply equates the areas of the non-square and square small fields as explained in Section 6.5.2.

Note that, distinct from this, for beam quality specification in non-square msr fields, equivalent square msr fields have to be determined. These are based on equating the amount of phantom scatter, as explained in Section 2.1.2.

3.1.2. The msr field

In high energy photon beam generators where the conventional 10 cm × 10 cm reference field cannot be established, an msr field is introduced which has dimensions that are as close as possible to those of the conventional reference field and extend at least a distance r_{LCPE} beyond the outer boundaries of the reference ionization chamber (see Section 4). In the case that only fields smaller than the 10 cm × 10 cm reference field can be realized, the msr field will usually be the largest achievable field. Examples of msr fields specific for different radiotherapy treatment machines are summarized in Section 3.3 and presented in more detail in Section 5.3.1.

3.1.3. Lateral charged particle equilibrium range

The r_{LCPE} is an important parameter for establishing the relation between the field size and the minimum detector size for which LCPE conditions exist. The r_{LCPE} depends on the beam energy and has been quantified by Li et al. [94], who performed Monte Carlo simulations of absorbed dose to water and water kerma in water for photon beams of different nominal energies. The r_{LCPE} was derived as the minimum radius of a circular field for which the absorbed dose to water in the centre of the field is related by a constant factor to the water kerma in water. Updated Monte Carlo calculations [14] have been performed for this parameter, and expressed as a function of the conventional photon beam quality index $\mathrm{TPR}_{20,10}(10)$, r_{LCPE} (in cm) is given by:

$$r_{\mathrm{LCPE}} = 8.369 \times \mathrm{TPR}_{20,10}(10) - 4.382 \tag{3}$$

Its use is described in Section 5.2.1. When the beam quality index $\%dd(10,10)_{\mathrm{x}}$ is used, r_{LCPE} can be derived using an approximate relation between $\%dd(10,10)_{\mathrm{x}}$ and $\mathrm{TPR}_{20,10}(10)$ [95]:

$$r_{\mathrm{LCPE}} = 77.97 \times 10^{-3} \times \%dd(10,10)_{\mathrm{x}} - 4.112 \tag{4}$$

3.1.4. Volume averaging

The volume averaging correction factor is defined as the ratio of the absorbed dose to water at the reference point in the water phantom in the absence of the detector and the mean absorbed dose to water over the sensitive volume of the detector (still in the absence of the detector). It can be derived from an integration of the 3-D dose distribution in the water phantom over the volume of the detector [56, 96–100]. In the case of plane-parallel detector geometry (e.g. plane-parallel ionization chamber, diode or diamond) with the parallel electrodes oriented perpendicular to the beam axis, this integration can be simplified to a 2-D integration of the lateral beam profile over the sensitive area of the detector facing the beam. In the case of a cylindrical ionization chamber, an integration over the 2-D area of the sensitive volume projected perpendicularly to the beam axis includes a weighting function to account for the fraction of the sensitive volume at different lateral offsets from the beam axis, although an unweighted integration over the projected area could be sufficient in many cases [81]. A suitable, high resolution detector is used for lateral profile measurements with special consideration of the detector orientation. Details are provided in Section 6. The generic equation to calculate the volume averaging correction factor is:

$$k_{\mathrm{vol}} = \frac{\iint_A w(x,y)\,\mathrm{d}x\,\mathrm{d}y}{\iint_A w(x,y)\,\mathrm{OAR}(x,y)\,\mathrm{d}x\,\mathrm{d}y} \tag{5}$$

where x and y are the coordinates on the axes orthogonal to the beam central axis, A is the area of the projection of the sensitive volume of the chamber on a plane orthogonal to the beam axis, OAR(x,y) is the off-axis ratio, which is the lateral beam profile at the measurement depth normalized to unity on the central axis, and $w(x,y)$ is a weighting function representing the extension of the air cavity of the ionization chamber along the beam axis (z) as a function of the beam lateral coordinates (x and y). For plane-parallel detector geometry, $w(x,y)$ is unity over the integration area. Examples of the calculation of the volume averaging correction factor are given in Appendix I.

3.1.5. Beam quality

The option preferred in this COP for beam quality characterization, to be discussed in Section 3.2.1, is to rely on data derived for specific radiation generators as, currently, machine-to-machine differences for a given generator model are rather small and, for the purpose of reference dosimetry, the beam

quality index can be easily verified to be within tolerance for the data to be valid. When data are not available, the common approach of characterizing the beam in terms of a quality index has to be used. As mentioned in Section 2.1.4, there are currently two beam quality indices used for conventional high energy photon beams: $TPR_{20,10}(10)$, used in Ref. [1] and most other COPs, and $\%dd(10,10)_x$, used in Refs [2, 7]. The guidance given here is restricted to these two beam quality indices.

If a 10 cm × 10 cm reference field cannot be established, it is advised to measure $TPR_{20,10}(S)$ or $\%dd(10,S)_x$ for the largest possible square field size S (or in case of a circular or rectangular field, an equivalent square msr field size S) and derive $TPR_{20,10}(10)$ or $\%dd(10,10)_x$, using the expressions of Palmans [38] (these are given in Section 5.3.3). If the SSD is not 100 cm, an additional correction is required to account for the inverse square law, for the difference in electron contamination and for the different scatter conditions (also given in Section 5.3.3).

For photon beams WFF, the determination of an equivalent square msr field for a circular or rectangular field is based on the guidance in Ref. [32]. The equivalent square msr field is defined as the one that produces an equal amount of scatter on the central axis at the measurement depth as the circular or rectangular field. For a FFF beam which exhibits a non-flat lateral beam profile, the lateral integration of the scatter function [32] is included in the lateral fluence distribution because the on-axis scatter is the sum of all scatter contributions from each off-axis elemental volume. This is proportional to the lateral fluence distribution, which is as a first order approximation given by the lateral beam profile.

Note that the issue of equivalent field size is very different for small fields. In the absence of head scatter and any substantial phantom scatter, the equivalence of small fields is in this COP based on fields that exhibit the same detector perturbation factors. It has been shown that for this purpose, the geometric mean of the length and width of a rectangular field (provided the field is not too elongated) is adequate to represent the equivalent square small field size [19]. This means that the equivalent square small field has the same area as the rectangular field, and the assumption is made that this is also valid for deriving the square small field equivalent of a circular small field. Given that for square field sizes below 4 cm, phantom scatter factors are independent of collimation and linac type and only dependent on measurement depth and the field area [19], 4 cm is taken as the borderline value between the broad beam equivalent field size method and the small field equivalent field size method.

3.2. FORMALISM FOR THE DETERMINATION OF THE REFERENCE ABSORBED DOSE TO WATER

The formalism published by Alfonso et al. [8] for the reference dosimetry of small fields is followed in this COP with minor modifications. It is based on the use of an ionization chamber for which a calibration coefficient in terms of absorbed dose to water in a reference beam is available from a standards laboratory. For the dosimetry of small photon fields, two steps are considered: (a) reference dosimetry following the formalism outlined in the following sections and (b) relative dosimetry following the guidance that will be given for the determination of field output factors. The practical procedures based on this formalism will be presented in Sections 5 and 6.

In radiation generators where a conventional 10 cm × 10 cm reference field can be established, reference dosimetry is performed according to the guidance given in Refs [1–7] or an equivalent protocol. In generators where a conventional 10 cm × 10 cm reference field cannot be established, an msr field is introduced which, whenever possible[4], has dimensions as close as possible to the conventional reference field and extends at least a distance r_{LCPE} beyond the outer boundaries of the reference ionization chamber. In other words, if the size of the detector is d (greatest distance between two points on the outer boundary of the detector), the FWHM of the field has to fulfil the following condition:

$$\text{FWHM} \geq 2r_{LCPE} + d \tag{6}$$

As an example, let us assume a photon beam with quality $TPR_{20,10}(10) = 0.677$, for which Eq. (3) yields $r_{LCPE} = 12.8$ mm. An IBA CC08 ion chamber has a cavity length $l = 4$ mm, a cavity radius $r = 3$ mm and a wall thickness $t_{wall} = 0.07$ g/cm^2 (see Table 5 in Section 4.1.1.2); with ρ(C-552) = 1.76 g/cm^3, $t_{wall} = 0.40$ mm. In the longitudinal direction, the chamber outer size will be $d_l = l + t_{wall} = 4.4$ mm and radially $d_r = 2(r + t_{wall}) = 6.8$ mm. As $d_r > d_l$, the largest detector size is $d = d_r$ and Eq. (6) yields a field size having a FWHM = 2 × 12.8 + 6.8 = 32.5 mm at a depth of 100 mm in water. Proceeding in this manner it can be verified that for the chambers listed in Table 5, the FWHM varies between 29.1 mm (Exradin A16 micro) and 38.2 mm (Victoreen Radocon II 555) for this beam, i.e. for the chambers in this table the dominant contribution to the required FWHM is the term $2r_{LCPE}$.

[4] There are some special radiation generators which offer no option for that, such as the Gamma Knife. These will have to be considered on a case by case basis, but for the case of the Gamma Knife, for example, the second required condition of LCPE can still be fulfilled for sufficiently small ionization chambers.

3.2.1. Approaches for the reference dosimetry of msr fields

3.2.1.1. Chamber calibrated specifically for the msr field

The preferred approach for the reference dosimetry is to obtain a calibration coefficient directly in the msr field (f_{msr}), provided the standards laboratory is able to supply such a calibration coefficient. In this case, the absorbed dose to water at the reference depth z_{ref} in water in the absence of the ionization chamber is given by:

$$D_{w,Q_{msr}}^{f_{msr}} = M_{Q_{msr}}^{f_{msr}} \, N_{D,w,Q_{msr}}^{f_{msr}} \tag{7}$$

where Q_{msr} is the beam quality of the msr field (note that this can be different from the beam quality of a conventional reference field owing to the influence of the field size on the particle spectrum); $M_{Q_{msr}}^{f_{msr}}$ is the reading of the dosimeter in the msr field f_{msr} corrected for influence quantities, such as pressure, temperature, incomplete charge collection, polarity effects, etc.; and $N_{D,w,Q_{msr}}^{f_{msr}}$ is the calibration coefficient in terms of absorbed dose to water of the ionization chamber measured by the standards laboratory for the msr field f_{msr} of quality Q_{msr}.

Although it is not widely available yet, some standards laboratories provide calibrations of ionization chambers in the hospital's msr field. A calibration coefficient could also be available via a cross-calibration, a procedure that will be described in Section 5.5.

3.2.1.2. Chamber calibrated for a conventional reference field, with generic beam quality correction factors available

In most cases, the ionization chamber calibration coefficient is measured in a calibration beam of quality Q_0 for a conventional 10 cm × 10 cm reference field f_{ref}. In that case, a beam quality correction factor is required for the use of the calibration coefficient in a beam of a different quality than the one used for the chamber calibration. The absorbed dose to water for the msr field is then given by:

$$D_{w,Q_{msr}}^{f_{msr}} = M_{Q_{msr}}^{f_{msr}} \, N_{D,w,Q_0}^{f_{ref}} \, k_{Q_{msr},Q_0}^{f_{msr},f_{ref}} \tag{8}$$

where $M_{Q_{msr}}^{f_{msr}}$ is the reading of the dosimeter in the msr field f_{msr} corrected for influence quantities, such as pressure, temperature, incomplete charge collection, polarity effects, etc.; $N_{D,w,Q_0}^{f_{ref}}$ is the calibration coefficient in terms of absorbed dose to water of the ionization chamber measured at the standards laboratory for a conventional 10 cm × 10 cm reference calibration field f_{ref} with beam quality

Q_0; and $k_{Q_{msr},Q_0}^{f_{msr},f_{ref}}$ is a factor to correct for the difference between the response of the ionization chamber in a conventional reference calibration field f_{ref} with beam quality Q_0 at the standards laboratory and the response of the ionization chamber in the msr field f_{msr} with beam quality Q_{msr}.

The beam quality correction factor $k_{Q_{msr},Q_0}^{f_{msr},f_{ref}}$ is defined as the ratio of the ionization chamber's calibration coefficients in the machine specific and conventional reference fields:

$$k_{Q_{msr},Q_0}^{f_{msr},f_{ref}} = \frac{N_{D,w,Q_{msr}}^{f_{msr}}}{N_{D,w,Q_0}^{f_{ref}}} = \frac{D_{w,Q_{msr}}^{f_{msr}} \Big/ M_{Q_{msr}}^{f_{msr}}}{D_{w,Q_0}^{f_{ref}} \Big/ M_{Q_0}^{f_{ref}}} \tag{9}$$

In most cases Q_0 will be a ^{60}Co gamma ray beam, but it could also be a high energy X ray beam. Ideally, the beam quality correction factor is determined directly by calibration of the ionization chamber in the calibration reference and msr fields. A few standards laboratories have developed the capability of performing such calibrations for clinical machines, but such services are not widely available. However, given the increased uniformity in physical characteristics of series of treatment machines of the same type, generic experimental values for the beam quality correction factors may be available. For the same reason, generic Monte Carlo calculated beam quality correction factors may be determined for a particular ionization chamber type in such machines as:

$$k_{Q_{msr},Q_0}^{f_{msr},f_{ref}} = \frac{D_{w,Q_{msr}}^{f_{msr}} \Big/ \bar{D}_{air,Q_{msr}}^{f_{msr}}}{D_{w,Q_0}^{f_{ref}} \Big/ \bar{D}_{air,Q_0}^{f_{ref}}} \tag{10}$$

where all quantities on the right hand side of the equation are calculated in the Monte Carlo simulation, D_w is the absorbed dose to water at the measurement point, which, in practice, is calculated as the mean absorbed dose to water over a small volume around the measurement point (the suitable size of which depends on the field size) and D_{air} is the mean absorbed dose to air in the cavity of the ionization chamber.

Where generic experimental or Monte Carlo calculated beam quality correction factors are available for particular treatment machine/ionization chamber combinations, they are tabulated in Section 5. Machines for which such data are available are Gamma Knife, CyberKnife and TomoTherapy for a limited number of chamber types.

Note that a standards laboratory may be able to provide a calibration coefficient $N_{D,w,Q_0}^{f_{msr}}$ for an msr field that does not have exactly the same beam quality as the clinical msr field. In that case:

$$D_{w,Q_{msr}}^{f_{msr}} = M_{Q_{msr}}^{f_{msr}} \; N_{D,w,Q_0}^{f_{msr}} \; k_{Q_{msr},Q_0}^{f_{msr},f_{msr}} \tag{11}$$

3.2.1.3. Chamber calibrated for the conventional reference field, without generic beam quality correction factors available

In the case that no generic beam quality correction factors for the calibration field with reference to the msr field are available, a third approach has to be followed. In this case, the absorbed dose to water for the msr field is given by:

$$D_{w,Q_{msr}}^{f_{msr}} = M_{Q_{msr}}^{f_{msr}} \; N_{D,w,Q_0}^{f_{ref}} \; k_{Q,Q_0}^{f_{ref}} \; k_{Q_{msr},Q}^{f_{msr},f_{ref}} \tag{12}$$

where $M_{Q_{msr}}^{f_{msr}}$ is the reading of the dosimeter in the msr field f_{msr} corrected for influence quantities, such as pressure, temperature, incomplete charge collection, polarity effects, etc., $N_{D,w,Q_0}^{f_{ref}}$ is the calibration coefficient in terms of absorbed dose to water of the ionization chamber measured at the standards laboratory for a conventional 10 cm × 10 cm reference calibration field f_{ref} with beam quality Q_0, $k_{Q,Q_0}^{f_{ref}}$ is a factor to correct for the difference between the response of the ionization chamber in a conventional calibration field f_{ref} with beam quality Q_0 at the standards laboratory and the response of the ionization chamber in a conventional 10 cm × 10 cm reference field f_{ref} with a beam quality Q using the same machine as the msr field f_{msr}, and $k_{Q_{msr},Q}^{f_{msr},f_{ref}}$ is a factor to correct for the difference between the response of the ionization chamber in a conventional 10 cm × 10 cm reference field f_{ref} with beam quality Q using the same machine as the machine specific reference field f_{msr} and the response of the ionization chamber in the msr field f_{msr} with beam quality Q_{msr}.

As previously explained, the need for an msr field arose from the impossibility of realizing a 10 cm × 10 cm field using the treatment machine to perform dosimetry according to a conventional dosimetry protocol. Where a 10 cm × 10 cm field cannot be realised, f_{ref} is referred to as a *hypothetical* 10 cm × 10 cm reference field [8]. The beam quality correction factor $k_{Q,Q_0}^{f_{ref}}$ can thus be obtained from Ref. [1] or Refs [2, 7], for which the beam quality Q of the hypothetical 10 cm × 10 cm reference field needs to be determined according to the guidance in Section 5.3.3.

Since the hypothetical reference field f_{ref} cannot be established experimentally, a direct measurement of $k_{Q_{msr},Q}^{f_{msr},f_{ref}}$ is not possible. If an experimental determination of $k_{Q_{msr},Q_0}^{f_{msr},f_{ref}}$ were available (e.g. measured by a PSDL), a value could be inferred as:

$$k_{Q_{\mathrm{msr}},Q}^{f_{\mathrm{msr}},f_{\mathrm{ref}}} = \frac{k_{Q_{\mathrm{msr}},Q_0}^{f_{\mathrm{msr}},f_{\mathrm{ref}}}}{k_{Q,Q_0}^{f_{\mathrm{ref}}}} \tag{13}$$

where $k_{Q,Q_0}^{f_{\mathrm{ref}}}$ is taken from Ref. [1] or Refs [2, 7].

With a Monte Carlo simulation, it is possible to establish a 10 cm × 10 cm reference field virtually and calculate the beam quality correction factor as:

$$k_{Q_{\mathrm{msr}},Q}^{f_{\mathrm{msr}},f_{\mathrm{ref}}} = \frac{D_{\mathrm{w},Q_{\mathrm{msr}}}^{f_{\mathrm{msr}}} \Big/ \bar{D}_{\mathrm{air},Q_{\mathrm{msr}}}^{f_{\mathrm{msr}}}}{D_{\mathrm{w},Q}^{f_{\mathrm{ref}}} \Big/ \bar{D}_{\mathrm{air},Q}^{f_{\mathrm{ref}}}} \tag{14}$$

In some cases, establishing the hypothetical reference field in the Monte Carlo simulation may not only require modification to the secondary and tertiary collimators, but also to the primary collimator (as for example is the case in CyberKnife), which could have a substantial influence on the beam quality.

For beams with a flattening filter providing a uniform lateral beam profile, the factor $k_{Q_{\mathrm{msr}},Q}^{f_{\mathrm{msr}},f_{\mathrm{ref}}}$ equals unity in most cases for the detectors recommended in this COP. Comparing Eqs (12) and (11) shows that this is equivalent to assuming that $k_{Q_{\mathrm{msr}},Q_0}^{f_{\mathrm{msr}},f_{\mathrm{ref}}}$ equals $k_{Q,Q_0}^{f_{\mathrm{ref}}}$. For practical implementation of these equations it may be sufficient to estimate an uncertainty on the assumption that $k_{Q_{\mathrm{msr}},Q}^{f_{\mathrm{msr}},f_{\mathrm{ref}}} = 1$.

Figure 12 summarizes the three approaches.

For the application to FFF beams, the complication arises that the value $k_{Q,Q_0}^{f_{\mathrm{ref}}}$ for the FFF beam may be different from those tabulated in existing COPs, such as Ref. [1] or Refs [2, 7]. For this reason, $k_{Q,Q_0}^{f_{\mathrm{ref}}}$ in Eq. (12) is replaced with the product of two factors to account for the difference between the response of the ionization chamber in the hypothetical FFF beam of quality $Q^{\mathrm{FFF}} = Q$ and that in a beam WFF with beam quality Q^{WFF}, for which the beam quality index is the same as for the beam quality Q[5]. For clarity, a superscript index 'FFF' has been included for all beam qualities of FFF beams and a superscript index 'WFF' has been included for all beam qualities of beams WFF:

$$D_{\mathrm{w},Q_{\mathrm{msr}}^{\mathrm{FFF}}}^{f_{\mathrm{msr}}} = M_{Q_{\mathrm{msr}}^{\mathrm{FFF}}}^{f_{\mathrm{msr}}} \, N_{D,\mathrm{w},Q_0}^{f_{\mathrm{ref}}} \, k_{Q^{\mathrm{WFF}},Q_0}^{f_{\mathrm{ref}}} \, k_{Q^{\mathrm{FFF}},Q^{\mathrm{WFF}}}^{f_{\mathrm{ref}}} \, k_{Q_{\mathrm{msr}}^{\mathrm{FFF}},Q^{\mathrm{FFF}}}^{f_{\mathrm{msr}},f_{\mathrm{ref}}} \tag{15}$$

where $k_{Q^{\mathrm{WFF}},Q_0}^{f_{\mathrm{ref}}}$ is the beam quality correction factor obtained from Refs [1, 2, 7] or an equivalent COP for a beam WFF with the same beam quality index as the one determined for the FFF beam and $k_{Q^{\mathrm{FFF}},Q^{\mathrm{WFF}}}^{f_{\mathrm{ref}}}$ is the factor that accounts for the

[5] This condition means that $\mathrm{TPR}_{20,10}(10)[Q^{\mathrm{WFF}}] = \mathrm{TPR}_{20,10}(10)[Q]$ or $\%dd(10,10)_x[Q^{\mathrm{WFF}}] = \%dd(10,10)_x[Q]$, but the beam qualities are not identical.

$$D_{w,Q_{\mathrm{msr}}}^{f_{\mathrm{msr}}} = M_{Q_{\mathrm{msr}}}^{f_{\mathrm{msr}}} \cdot N_{D,\mathrm{w},Q_{\mathrm{msr}}}^{f_{\mathrm{msr}}} \quad (1)$$

$$= M_{Q_{\mathrm{msr}}}^{f_{\mathrm{msr}}} \cdot N_{D,\mathrm{w},Q_0}^{f_{\mathrm{ref}}} \cdot k_{Q_{\mathrm{msr}},Q_0}^{f_{\mathrm{msr}},f_{\mathrm{ref}}} \quad (2)$$

$$= M_{Q_{\mathrm{msr}}}^{f_{\mathrm{msr}}} \cdot N_{D,\mathrm{w},Q_0}^{f_{\mathrm{ref}}} \cdot k_{Q,Q_0}^{f_{\mathrm{ref}}} \cdot k_{Q_{\mathrm{msr}},Q}^{f_{\mathrm{msr}},f_{\mathrm{ref}}} \quad (3)$$

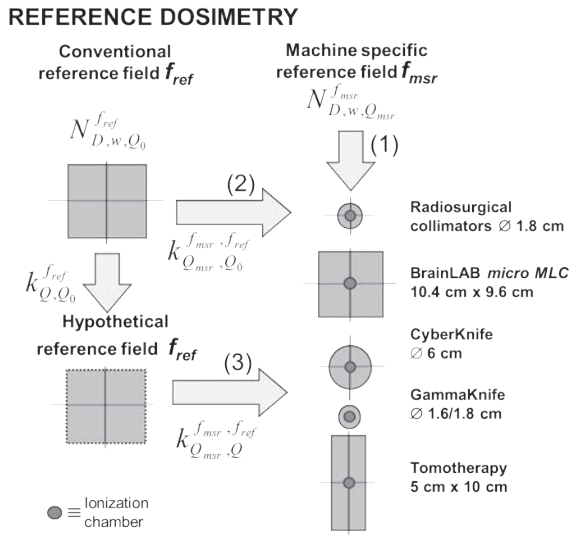

FIG. 12. Schematic overview of the dosimetry of small static fields with reference to a machine specific reference field according to the formalism of this COP. The arrows and formulas labelled (1), (2) and (3) correspond with the approaches of Section 3.2.1.1, 3.2.1.2 and 3.2.1.3, respectively. (Reproduced from Ref. [8] with the permission of the American Association of Physicists in Medicine.)

different response of the ionization chamber in the FFF and the WFF beam. Two effects contribute to the value of $k_{Q^{\mathrm{FFF}},Q^{\mathrm{WFF}}}^{f_{\mathrm{ref}}}$: one is the different response of the ionization chamber due to the different charged particle spectra of both beam qualities changing stopping-power ratios and perturbation correction factors, and the second one is the volume averaging because of the non-uniformity of the lateral beam profile in the FFF beam (the typical quasi-conical 2-D profile)[6]. The volume averaging correction factor can differ significantly from unity if there is substantial field non-uniformity as is the case in FFF beams. Details of the calculation of $k_{Q^{\mathrm{FFF}},Q^{\mathrm{WFF}}}^{f_{\mathrm{ref}}}$ are given in Appendix I.

[6] Note that this approach is different from the one adopted in Ref. [7], where the volume averaging correction factor is not considered as a contribution to the beam quality correction factor but is included as a correction factor to the ionization chamber reading.

3.2.2. Measurement in plastic water substitute phantoms

While current dosimetry protocols (Refs [1, 2, 7]) advise determination of absorbed dose to water in a water phantom at a reference depth z_{ref}, it is acknowledged that there are situations when, for the user, it is more convenient to perform the measurements in a plastic water substitute phantom but still determine the absorbed dose to water, D_w, from these measurements.

For the absorbed dose to water formalism, Seuntjens et al. [101] introduced a modification to the basic equation that, applied to Eq. (8), can be translated into:

$$D_{w,Q_{msr}}^{f_{msr}}\left(z_{ref}\right) = M_{plastic,Q_{msr}}^{f_{msr}}\left(z_{eq,plastic}\right) N_{D,w,Q_0}^{f_{ref}} \, k_{Q_{msr},Q_0}^{f_{msr},f_{ref}} \, k_{Q_{msr}}^{w,plastic} \tag{16}$$

where $M_{plastic,Q_{msr}}^{f_{msr}}\left(z_{eq,plastic}\right)$ is the ionization chamber reading in a plastic water substitute phantom corrected for influence quantities and $k_{Q_{msr}}^{w,plastic}$ is called the *phantom dose conversion factor*. The depth in a plastic water substitute phantom $z_{eq,plastic}$ is equivalent to the reference depth in water z_{ref}, scaled according to the ratio of electron densities (see Attix eq. (13.49a) [13]). In general, an equivalent point is defined as a point where the photon fluence is the same. With the assumption that Compton scattering dominates photon interactions, ensuring equivalence in photon fluence requires scaling, by electron density, of *all* dimensions involved (i.e. depth, field size, phantom size), while keeping the SDD constant. In practice, for phantoms with electron density similar to that of water, the effect of scaling of some of these dimensions (i.e. phantom size and field size) introduces a negligible effect, while corrections can be introduced when the SDD cannot be preserved.

The phantom dose conversion factor $k_{Q_{msr}}^{w,plastic}$ can be determined experimentally as a ratio of ionization chamber readings corrected for influence quantities in the water phantom at depth z_{ref} and in the plastic water substitute phantom at depth $z_{eq,plastic}$. Its theoretical determination is more complicated and relies on Monte Carlo calculations or on the application of the scaling theorem (see Ref. [13] for details). As an example for broad beams, values of $k_{Q_{msr}}^{w,plastic}$ for Solid Water and for PMMA, calculated by Seuntjens et al. [101], are shown in Fig. 13 as a function of the photon beam quality specifiers $TPR_{20,10}(10)$ and $\%dd(10,10)_x$. It can be seen that $k_{Q_{msr}}^{w,plastic}$ varies between approximately 0.960 and 0.980 for PMMA, and between approximately 0.997 and 1.010 for Solid Water.

For a PMMA phantom, $k_{Q_{msr}}^{w,plastic}$ from Monte Carlo calculations and experiments agree within 0.2% despite the rather large depth scaling correction. For Solid Water, larger differences have been found between Monte Carlo calculations and experiments, notably from phantom to phantom, which although yielding an average difference of 0.3% (Monte Carlo always larger) still point to a variation in the water equivalency between different phantoms. This is

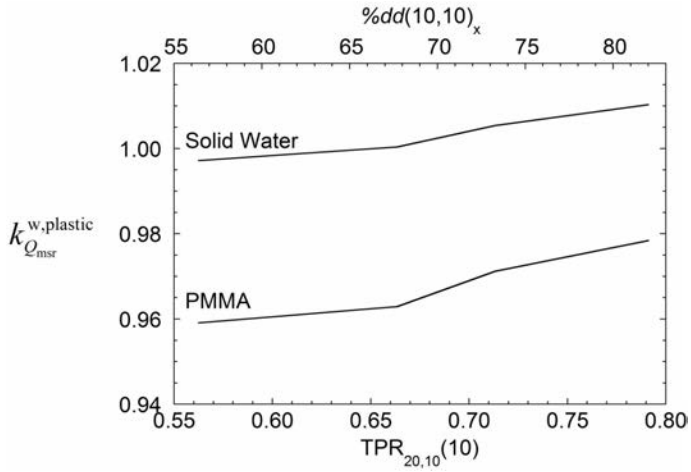

*FIG. 13. Example values of the phantom dose conversion factor for Solid Water (Gammex RMI 457) and PMMA in a 10 cm × 10 cm reference field based on Monte Carlo calculations. Note that the correspondence between %*dd*$(10,10)_x$ and $TPR_{20,10}(10)$ is only approximate. (Reproduced from Ref. [101] with the permission of the American Association of Physicists in Medicine.)*

associated with heterogeneities in the phantom due to manufacturing variability in the plastic. Computed tomography scanning or radiographing of the plastic water substitute material may help in QA for the purpose of reference dosimetry in such phantoms [102].

3.2.3. Determination of field output factors

For the dosimetry of clinical fields, relative to the reference dosimetry of an msr field, field output factors are used (see Section 2.3.2.1). These factors are also called total scatter factors [12, 32, 103], or relative dose factors [104]. The field output factor $\Omega_{Q_{clin},Q_{msr}}^{f_{clin},f_{msr}}$ with respect to the machine specific reference field f_{msr} is defined as the ratio of absorbed dose to water in the clinical field f_{clin} with beam quality Q_{clin} and absorbed dose to water in the machine specific reference field f_{msr} with beam quality Q_{msr}:

$$\Omega_{Q_{clin},Q_{msr}}^{f_{clin},f_{msr}} = \frac{D_{w,Q_{clin}}^{f_{clin}}}{D_{w,Q_{msr}}^{f_{msr}}} \tag{17}$$

These field output factors are used to convert absorbed dose to water for the machine specific reference field f_{msr} to the absorbed dose to water for the clinical field f_{clin}. For machines that can establish the conventional 10 cm × 10 cm reference field f_{ref}, 'msr' in Eq. (17) and accompanying text is replaced with 'ref'. This applies to the remainder of this section.

Field output factors are derived from a ratio of detector readings according to:

$$\Omega_{Q_{clin},Q_{msr}}^{f_{clin},f_{msr}} = \frac{M_{Q_{clin}}^{f_{clin}}}{M_{Q_{msr}}^{f_{msr}}} k_{Q_{clin},Q_{msr}}^{f_{clin},f_{msr}} \tag{18}$$

It is clear from this equation that a ratio of readings is not equal to a field output factor; rather such ratios will need to be multiplied by an output correction factor to obtain the field output factor. Only if the reading of the detector is directly proportional to the absorbed dose to water at a point and the proportionality factor remains constant does the output correction factor become unity. Even calorimeters or transfer instruments require output correction factors for the smallest fields. For some detectors that are very small and have an energy independent response, such as radiochromic film, a liquid ionization chamber or an organic scintillator, the output correction factors may be close to unity. The perfect small field detector, however, does not exist.

The output correction factor $k_{Q_{clin},Q_{msr}}^{f_{clin},f_{msr}}$ can be determined as a directly measured value, an experimental generic value or a Monte Carlo calculated generic value:

$$k_{Q_{clin},Q_{msr}}^{f_{clin},f_{msr}} = \frac{D_{w,Q_{clin}}^{f_{clin}} \Big/ \bar{D}_{det,Q_{clin}}^{f_{clin}}}{D_{w,Q_{msr}}^{f_{msr}} \Big/ \bar{D}_{det,Q_{msr}}^{f_{msr}}} \tag{19}$$

As explained in Section 2.3.2.1, if a suitable detector for the entire range of field sizes from f_{msr} to f_{clin} is not available, it is advised to use an ionization chamber for field sizes down to an intermediate field f_{int} as small as possible but without small field conditions, and to use a suitable small field detector such as a diode only for measurements in smaller fields, thereby limiting the effect of the energy dependence. Using this intermediate field method (IFM), the field output factor is obtained through the equation:

$$\Omega_{Q_{clin},Q_{msr}}^{f_{clin},f_{msr}} = \left[\Omega_{Q_{clin},Q_{int}}^{f_{clin},f_{int}}\right]_{det} \left[\Omega_{Q_{int},Q_{msr}}^{f_{int},f_{msr}}\right]_{IC} \tag{20}$$

where ‘det’ refers to the small field detector and ‘IC’ refers to the ionization chamber.

Using the definition of the field output factor given in Eq. (18), this equation becomes:

$$\Omega_{Q_{\text{clin}},Q_{\text{msr}}}^{f_{\text{clin}},f_{\text{msr}}} = \left[\frac{M_{Q_{\text{clin}}}^{f_{\text{clin}}}}{M_{Q_{\text{int}}}^{f_{\text{int}}}} k_{Q_{\text{clin}},Q_{\text{int}}}^{f_{\text{clin}},f_{\text{int}}}\right]_{\text{det}} \left[\frac{M_{Q_{\text{int}}}^{f_{\text{int}}}}{M_{Q_{\text{msr}}}^{f_{\text{msr}}}} k_{Q_{\text{int}},Q_{\text{msr}}}^{f_{\text{int}},f_{\text{msr}}}\right]_{\text{IC}} \tag{21}$$

making it clear that two output correction factors are required, one for each detector. However, in the absence of small field conditions for the intermediate field, $\left[k_{Q_{\text{int}},Q_{\text{msr}}}^{f_{\text{int}},f_{\text{msr}}}\right]_{\text{IC}} \approx 1$ for well designed ionization chambers. Having to correct only from the intermediate field f_{int} to the clinical field f_{clin} minimizes the contribution from the small field detector to the overall correction, especially the influence of low energy photon scatter.

3.3. REFERENCE CONDITIONS

Reference conditions are described by a set of values of influence quantities for which a calibration coefficient is valid without further correction factors. The reference conditions for calibrations in terms of absorbed dose to water are, for example, the geometrical arrangement (distance and depth); the field size; the material and dimensions of the irradiated phantom; and the ambient temperature, pressure and relative humidity.

For radiotherapy machines that can generate the conventional 10 cm × 10 cm reference field at 100 cm SSD or SDD, the reference conditions given in COPs like Refs [1, 2, 7] are used. For machines where the conventional 10 cm × 10 cm reference field cannot be established, specific reference conditions related to the msr field are used. The reference conditions for the determination of beam quality and absorbed dose to water for msr fields are given in Section 5.3. A compilation of msr fields for some common radiotherapy machines is given in Table 2.

TABLE 2. msr FIELDS FOR COMMON RADIOTHERAPY MACHINES

Machine type	msr field
CyberKnife	6 cm diameter fixed collimator
TomoTherapy	5 cm × 10 cm field
Gamma Knife	1.6 cm or 1.8 cm diameter collimator helmet, all sources simultaneously out
Brainlab micro MLC add-on	For example 9.8 cm × 9.8 cm or 9.6 cm × 10.4 cm
SRS cone add-ons	The closest to a 10 cm × 10 cm equivalent square msr field achievable

4. DETECTORS AND EQUIPMENT

This chapter provides a general background on the characteristics of detectors suitable for reference dosimetry of msr fields and relative dosimetry of small fields, and provides guidance on detectors to be used for applying this COP. Distinction has to be made between detector requirements for dosimetry of the conventional 10 cm × 10 cm reference field and those for dosimetry of smaller fields; particularly for the relative dosimetry of small (non-msr) fields, the requirements can be substantially different. For a review on characteristics of radiation detectors for dosimetry and imaging see Ref. [105].

4.1. EQUIPMENT FOR MACHINE SPECIFIC REFERENCE DOSIMETRY

Accuracy requirements for conventional reference dosimetry and for msr dosimetry are expected to be the same. The reference conditions will, however, be different. Although this places some restrictions on the type of equipment that can be used, the requirements for equipment used for msr dosimetry are expected to be largely the same as those applicable to the dosimetry of conventional reference fields [1, 2]. Equipment considered for msr dosimetry will include, but not be limited to, smaller ionization chambers and phantoms with geometries and materials different from those used for conventional reference dosimetry. Thus, only ionometric measurements are considered for reference dosimetry in this COP. The basic advice remains that for msr dosimetry, an ionization chamber be used in a water phantom to determine the reference absorbed dose to water at the user's radiotherapy machine.

Traditionally, an ionometric dosimeter system for radiotherapy contains the following components [106]:

(a) One or more ionization chambers, including the permanently attached cable and connector. It is advised that the ionization chambers chosen be specifically designed for the intended purpose (modality, radiation quality etc.).
(b) One or more phantoms with waterproof sleeves if needed.
(c) A measuring assembly (electrometer), often separately calibrated in terms of charge or current per scale division.
(d) One or more stability check devices, specifically designed for the chosen ionization chamber.
(e) Calibrated thermometer and barometer.

Component (a) will be reviewed in Section 4.1.1 and component (b) in Section 4.1.2. The other components (c, d and e) are adequately documented in existing protocols and no special requirements relating to them will be discussed in this COP.

4.1.1. Ionization chambers for msr reference dosimetry

Ideally, ionization chambers used for photon beam measurements in a water phantom are water equivalent and do not perturb the radiation fluence, and have a dose rate and directionally independent response, high sensitivity (good signal to noise ratio, reasonable time to acquire the signal), good stability (short and long term), linear response with absorbed dose to water, limited energy dependence, low leakage and negligible cable effect. While many of these characteristics can only be met approximately, thimble ionization chambers have been proven to be robust, simple and suitable for clinical reference dosimetry in msr fields in water or solid phantoms.

The size restriction on an ionization chamber for msr dosimetry is that the outer boundaries of the detector be at least a distance r_{LCPE} away from the field edges (at 50% absorbed dose level). In use, the chamber needs to be aligned in such a way that the radiation fluence is approximately uniform over the chamber cavity. The construction of the chamber is to be as homogeneous as possible, but it is recognized that for technical reasons the central electrode is likely to be made of a material different from that of the chamber walls. Indeed, the choice of materials may play an important role in ensuring that the energy response of the chamber does not vary considerably. It is also necessary for the air cavity not to be sealed so that it will equilibrate rapidly with the ambient temperature and air pressure. Finally, it is preferable that the reference ionization chambers be waterproof, so they can be used directly in water phantoms.

As an ionization chamber is an instrument of high precision, it is advised that the performance of the chamber type be sufficiently tested in radiotherapy beams. Guidance for commercially available ion chambers to be used in generic msr fields with dimensions equal to or larger than 6 cm × 6 cm will be covered in Section 4.1.1.1, while guidance for fields smaller than 6 cm × 6 cm will be given in Section 4.1.1.2. The rationale for this field size limit is based on the largest ionization chamber dimensions (i.e. Farmer types) used for conventional reference dosimetry and the r_{LCPE} of the highest energy beams advised in this COP (note for example that for an 18 MV beam the field size limit would be larger).

4.1.1.1. Equivalent square msr field size $f_{msr} \geq 6$ cm × 6 cm

Modern radiotherapy machines have two main generic designs, namely with and without a beam flattening filter. For beams WFF, the reference ionization chambers are robust air filled chambers that are often waterproof and are simple to use for reference in-phantom measurements. The chamber cavity volumes are between about 0.3 cm^3 and 1 cm^3 (many have a volume around 0.6 cm^3), a size range that balances between the need for sufficient sensitivity and the ability to measure at a point. Chambers with these volumes also have good signal to noise ratio and negligible leakage effects [107]. The requirements are met in cylindrical chambers with an air cavity of internal diameter around 6.4 mm and an internal length around 24 mm, which is typical for Farmer type chambers. In use, the chamber needs to be aligned in such a way that the radiation fluence is approximately uniform over the cross-section of the chamber cavity. It is advised for FFF beams that the reference ionization chamber have a length shorter than that of a typical Farmer type chamber given the non-uniformity of the lateral beam profile [108]. Typical volumes for these chambers are between 0.1 cm^3 and 0.3 cm^3. If Farmer type chambers are used, a correction for the profile non-uniformity has to be applied which can amount to 1.5% for 6 MV FFF beams [76, 81].

A critical analysis of 27 cylindrical ionization chambers used in conventional megavoltage photon beams was published in Ref. [107] in which most of the Farmer type chambers as well as the NE 2611 chambers were found to show good performance compared with the specifications for reference class chambers listed in Table 3. Also, a number of smaller-volume chambers were found to be suitable for reference dosimetry. The characteristics of a number of commercially available ionization chambers for msr dosimetry are given in Table 4. The performance of each individual ionization chamber has to be verified to comply with the criteria given in Table 3.

4.1.1.2. Equivalent square msr field size $f_{msr} < 6$ cm × 6 cm

Since LCPE conditions are a requirement for machine specific reference fields, the field edges are at least a distance r_{LCPE} away from the outer boundaries of the reference ionization chamber. Based on their size, msr fields are not small fields (except in the case of Gamma Knife machines, see below), but some common reference detectors are too large to fulfil the r_{LCPE} criterion mentioned. For example, for 6 MV beams between 3 cm × 3 cm and 5 cm × 5 cm LCPE exists, but a Farmer type chamber is too large for such field sizes; dosimetry under these circumstances would result in an underestimation of the absorbed

TABLE 3. SPECIFICATIONS FOR REFERENCE CLASS IONIZATION CHAMBERS FOR REFERENCE DOSIMETRY OF msr FIELDS, f_{msr} [107]

Parameter	Specification
Chamber settling	Monitoring chamber response with accumulated dose: equilibrium is reached in less than 5 minutes; the initial and equilibrium readings agree within 0.5%.
Leakage	Smaller than 0.1% of the chamber reading.
Polarity effect	Smaller than 0.4% of the chamber reading. The polarity energy dependence is less than 0.3% between ^{60}Co and 10 MV photons.
Recombination correction	1. The correction is linear with dose per pulse. 2. Initial recombination (the dose rate or dose per pulse independent part of the total charge recombination) is below 0.2% at polarizing voltages around 300 V. 3. For pulsed beams, a plot of $1/M_Q$ (charge reading) vs $1/V$ (polarizing voltage) is linear at least for practical values of V. 4. For continuous beams, a plot of $1/M_Q$ vs $1/V^2$ is linear, describing the effect of general recombination. The presence of initial recombination disturbs the linearity but this is normally a small effect, which may be neglected. 5. The difference in the initial recombination correction obtained with opposite polarities is less than 0.1%.
Chamber stability	Change in calibration coefficient over a typical recalibration period of 2 years below 0.3%. Same figure for long term (>5 y) stability.
Chamber material	Wall material not exhibiting temperature and humidity effects.

Note: Chamber types that potentially do not meet these criteria but have been proven to be suitable for reference dosimetry of the Gamma Knife are marked in Table 5.

dose to water on the central axis because of volume averaging and other effects described in Section 2.1.1.2.

Le Roy et al. [109] evaluated 24 small volume ionization chambers (0.007 cm^3 to 0.057 cm^2) of eight different types to determine whether these could be used for reference dosimetry in high energy photon beams with field sizes down to 2 cm × 2 cm (only measurements in a ^{60}Co gamma ray beam were performed). They advise that the polarization voltage across the chamber be chosen such that the electric field strength is between 100 and 200 V/mm. Based upon this study, the authors concluded that only three of the chamber types tested

TABLE 4. CHARACTERISTICS OF CYLINDRICAL IONIZATION CHAMBERS FOR REFERENCE DOSIMETRY OF msr FIELDS $f_{msr} \geq 6$ cm × 6 cm

Ionization chamber type	Cavity volume (cm^3)	Cavity length (mm)	Cavity radius (mm)	Wall material	Wall thickness (g/cm^2)	Central electrode material	Waterproof
Capintec PR-06C/G Farmer	0.65	22.0	3.2	C-552[a]	0.050	C-552[a]	N
Exradin A2 Spokas	0.53	11.4	4.8	C-552[a]	0.176	C-552[a]	Y
Exradin A12 Farmer	0.65	24.2	3.1	C-552[a]	0.088	C-552[a]	Y
Exradin A12S	0.25	11.6	3.1	C-552[a]	0.088	C-552[a]	Y
Exradin A19	0.63	25.0	3.1	C-552[a]	0.088	C-552[a]	Y
FZH TK 01	0.4	12.0	3.5	Delrin[c]	0.071	—[b]	Y
Nuclear Assoc 30-751 Farmer	0.69	23.0	3.1	Delrin[c]	0.056	Aluminium	Y
Nuclear Assoc 30-752 Farmer	0.69	23.0	3.1	Graphite	0.072	Aluminium	Y
NE 2505/3, 3A Farmer	0.6	24.0	3.2	Graphite	0.065	Aluminium	N
NE 2571 Farmer	0.6	24.0	3.2	Graphite	0.065	Aluminium	N

TABLE 4. CHARACTERISTICS OF CYLINDRICAL IONIZATION CHAMBERS FOR REFERENCE DOSIMETRY OF msr FIELDS $f_{msr} \geq 6$ cm × 6 cm (cont.)

Ionization chamber type	Cavity volume (cm^3)	Cavity length (mm)	Cavity radius (mm)	Wall material	Wall thickness (g/cm^2)	Central electrode material	Waterproof
NE 2611	0.33	9.2	3.7	Graphite	0.090	Aluminium (hollow)	N
PTW 23331 rigid	1.0	22.0	4.0	PMMA[d,e]	0.060	Aluminium	N
PTW 23332 rigid	0.3	18.0	2.5	PMMA[d,e]	0.054	Aluminium	N
PTW 23333 (3 mm cap)	0.6	21.9	3.1	PMMA[d,e]	0.059	Aluminium	N
PTW 30001 Farmer	0.6	23.0	3.1	PMMA[d,e]	0.045	Aluminium	N
PTW 30010 Farmer	0.6	23.0	3.1	PMMA[d,e]	0.057	Aluminium	N
PTW 30002/30011 Farmer	0.6	23.0	3.1	Graphite	0.079	Graphite	N
PTW 30004/30012 Farmer	0.6	23.0	3.1	Graphite	0.079	Aluminium	N
PTW 30006/30013 Farmer	0.6	23.0	3.1	PMMA[d,e]	0.057	Aluminium	Y

TABLE 4. CHARACTERISTICS OF CYLINDRICAL IONIZATION CHAMBERS FOR REFERENCE DOSIMETRY OF msr FIELDS $f_{msr} \geq 6$ cm × 6 cm (cont.)

Ionization chamber type	Cavity volume (cm^3)	Cavity length (mm)	Cavity radius (mm)	Wall material	Wall thickness (g/cm^2)	Central electrode material	Waterproof
PTW 31003/31013 Semiflex	0.3	16.3	2.8	PMMA[d,e]	0.078	Aluminium	Y
SNC 100700-0 Farmer	0.6	24.4	3.1	PMMA[d]	0.060	Aluminium	N
SNC 100700-1 Farmer	0.6	24.4	3.1	Graphite	0.085	Aluminium	N
Victoreen Radocon II 555	0.1	23.0	2.4	Polystyrene	0.117	—[b]	N
Victoreen 30-348	0.3	18.0	2.5	PMMA[d]	0.060	—[b]	N
Victoreen 30-351	0.6	23.0	3.1	PMMA[d]	0.060	—[b]	N
Victoreen 30-349	1.0	22.0	4.0	PMMA[d]	0.060	—[b]	N
Victoreen 30-361	0.4	22.3	2.4	PMMA[d]	0.144	—[b]	N
IBA FC-65P Farmer	0.65	23.1	3.1	Delrin[c]	0.057	Aluminium	Y
IBA FC-65G Farmer	0.65	23.1	3.1	Graphite	0.073	Aluminium	Y

TABLE 4. CHARACTERISTICS OF CYLINDRICAL IONIZATION CHAMBERS FOR REFERENCE DOSIMETRY OF msr FIELDS $f_{msr} \geq 6$ cm × 6 cm (cont.)

Ionization chamber type	Cavity volume (cm^3)	Cavity length (mm)	Cavity radius (mm)	Wall material	Wall thickness (g/cm^2)	Central electrode material	Waterproof
IBA FC-23C Farmer	0.23	8.8	3.1	C-552[a]	0.070	C-552[a]	Y
IBA CC13	0.25	10.0	3.0	C-552[a]	0.070	C-552[a]	Y

[a] Air equivalent electrically conducting plastic consisting of a mixture of polyvinylidene fluoride, carbon black and silica.
[b] —: no information available.
[c] Polyoxymethylene (CH_2O). Delrin is a trade name.
[d] Polymethylmethacrylate ($C_5H_8O_2$), also known as acrylic. Trade names are Lucite, Plexiglas or Perspex.
[e] Like most chamber types with non-conductive plastic walls, the chamber wall has an inner conductive layer made of graphite. For this chamber type, the thickness and density of the graphite layer are supplied in the chamber specifications.

were suitable for use as reference class chambers for small beam dosimetry (Exradin A1SL, IBA CC04 and IBA CC01), whereas issues with ion collection efficiency and polarity effects were noted for some chambers. The chamber specifications given in Table 3 are adopted in this COP for msr dosimetry when the equivalent square msr field size is smaller than 6 cm × 6 cm.

A representative case of very small msr fields corresponds to the circular field of Gamma Knife machines, with diameters of 1.6 cm or 1.8 cm. It is noted that these are still fields that exhibit LCPE given the much smaller r_{LCPE} of ^{60}Co, which is about 0.6 cm [94]. The criterion for the outer boundaries of the reference ionization chamber to be at least that distance away from the field edges limits the range of suitable ionization chambers. Fortunately, some of the microchambers listed in Table 5 that do not fulfil the criteria of Table 3 for high energy X ray beams do fulfil those for Gamma Knife. This can partially be explained by the fact that only a small portion of the stem is irradiated, meaning that the polarity effects observed in broad beams [109] with these chamber types are not observed in Gamma Knife measurements [110].

For msr dosimetry in fields with equivalent square msr field size smaller than 6 cm × 6 cm, the largest chamber cavity dimension is restricted to around 7 mm, and this requirement is usually met in ionization chambers with volumes smaller than about 0.3 cm^3. This criterion could in principle be expressed as a function of field size and energy, but the limit of 7 mm ensures that for a 10 MV beam, all fields with an equivalent square size down to about 4 cm fulfil the condition of LCPE, while for 6 MV this is the case down to about 3 cm, and for ^{60}Co gamma ray beams it is the case down to about 2 cm. The fact that for Gamma Knife fields, the beam quality correction factors for ionization chambers marked in Table 5 remain small, even for the smaller field sizes of 1.8 cm and 1.6 cm, can be understood by the size of the cavity, with typical values between 2 and 4 mm for these detectors such that full lateral charge buildup, which may not be achieved at the outer edges of the detector, is still partially achieved within the additional wall material thickness. This reasoning of course ignores the fact that at the interface between the phantom material and the wall there is an additional component of charged particle disequilibrium, and the interplay of this effect with the absence of LCPE could result in a perturbation correction factor different from the one for a broad beam. Table 5 gives a list of commercial small volume ionization chambers recommended for msr dosimetry in this COP in fields with equivalent square msr field size smaller than 6 cm × 6 cm. The chambers recommended in this COP for Gamma Knife are marked in Table 5.

TABLE 5. CHARACTERISTICS OF IONIZATION CHAMBERS SUITABLE FOR REFERENCE DOSIMETRY OF msr FIELDS f_{msr} < 6 cm × 6 cm

Ionization chamber type	Cavity volume (cm^3)	Cavity length (mm)	Cavity radius (mm)	Wall material	Wall thickness (g/cm^2)	Central electrode material	Waterproof
Capintec PR-05P mini[a]	0.07	5.5	2.0	C-552	0.220	C-552	N
Exradin A1 mini Shonka (2 mm cap)	0.057	5.7	2.0	C-552	0.176	C-552	Y
Exradin A1SL mini Shonka slimline[a]	0.057	5.7	2.1	C-552	0.176	C-552	Y
Exradin A14 micro Shonka[a]	0.016	2.0	2.0	C-552	0.176	C-552	Y
Exradin A14SL micro Shonka slimline[a]	0.016	2.1	2.1	C-552	0.194	C-552	Y
Exradin A14P micro planar[a]	0.002	1.0	2.0	C-552	0.176	C-552	Y
Exradin A16 micro[a]	0.007	1.7	1.2	C-552	0.088	C-552	Y
Exradin A18 thimble	0.125	4.9	2.5	C552	0.176	C-552	Y
IBA CC01[a]	0.01	3.6	1.0	C-552	0.088	Steel	Y
IBA CC04[a]	0.04	3.6	2.0	C-552	0.070	C-552	Y

TABLE 5. CHARACTERISTICS OF IONIZATION CHAMBERS SUITABLE FOR REFERENCE DOSIMETRY OF msr FIELDS f_{msr} < 6 cm × 6 cm (cont.)

Ionization chamber type	Cavity volume (cm^3)	Cavity length (mm)	Cavity radius (mm)	Wall material	Wall thickness (g/cm^2)	Central electrode material	Waterproof
IBA CC08	0.08	4.0	3.0	C-552	0.070	C-552	Y
IBA CC13	0.13	5.8	3.0	C-552	0.070	C-552	Y
IBA CC13-S	0.13	5.8	3.0	PEEK/C-552	0.154	C-552	Y
Nuclear Assoc 30-750	0.03	3.6	2.0	C-552	0.068	C-552	Y
Nuclear Assoc 30-749	0.08	4.0	3.0	C-552	0.068	C-552	Y
Nuclear Assoc 30-744	0.13	5.8	3.0	C-552	0.068	C-552	Y
PTW 31010 Semiflex	0.125	6.5	2.8	PMMA[b,c]	0.078	Aluminium	Y
PTW 31014 PinPoint[a]	0.015	5.0	1.0	PMMA[c]	0.085	Aluminium	Y
PTW 31015 PinPoint	0.030	5.0	1.45	PMMA[c]	0.085	Aluminium	Y

TABLE 5. CHARACTERISTICS OF IONIZATION CHAMBERS SUITABLE FOR REFERENCE DOSIMETRY OF msr FIELDS f_{msr} < 6 cm × 6 cm (cont.)

Ionization chamber type	Cavity volume (cm^3)	Cavity length (mm)	Cavity radius (mm)	Wall material	Wall thickness (g/cm^2)	Central electrode material	Waterproof
PTW 31016 PinPoint 3D[a]	0.016	2.9	1.45	PMMA[c]	0.085	Aluminium	Y
Victoreen Radocon II 555	0.1	4.3	2.5	Delrin[d]	0.529	—[e]	N

[a] Chambers that potentially do not meet the criteria of Table 3 but have been proven to be suitable for reference dosimetry of the Gamma Knife [110].
[b] Polymethylmethacrylate ($C_5H_8O_2$), also known as acrylic. Trade names are Lucite, Plexiglas or Perspex.
[c] Like most chamber types with non-conductive plastic walls, the chamber wall has an inner conductive layer made of graphite. For this chamber type, the thickness and density of the graphite layer are supplied in the chamber specifications.
[d] Polyoxymethylene (CH_2O). Delrin is a trade name.
[e] —: data not available.

4.1.2. Phantoms

Water is advised as the reference medium for measurements leading to the determination of absorbed dose to water and beam quality in photon beams. For some treatment machines, the use of water phantoms for reference dosimetry is possible but impractical, and therefore, solid phantoms may be necessary. In those situations only, a water equivalent plastic or similar solid phantom material may be used for reference dosimetry and for the measurement of beam quality indices. If solid phantoms are used, it is essential that the detector be placed accurately, with its measurement point on the radiation beam's central axis at the water equivalent depth $z_{\mathrm{eq,plastic}}$. Today, commercially available solid materials used in radiotherapy dosimetry have well controlled densities and well defined atomic properties, and can be machined for accurate positioning of dosimeters. Solid phantoms are machined in different forms and shapes, depending on particular applications. They may be shaped as slab phantoms, cubes, cylinders, spheres, hemispheres and other geometrical shapes. For additional details on geometry requirements see Section 5.2.2. Ideally, the solid phantom material is water equivalent, that is, its absorption and scattering properties are the same as those of water. The elemental composition (in fractions by weight), nominal density, mean atomic number, mean excitation energy and depth in plastic equivalent to 10 cm depth in water of some common phantom materials used as water substitutes are provided in Section 5.3.4. Note that for the determination of the phantom dose conversion factor in Eq. (16) and its subsequent use for reference dosimetry, any potential inhomogeneities or air pockets are taken into account if the slab order is kept the same in all measurements performed in that solid phantom.

4.2. EQUIPMENT FOR RELATIVE DOSIMETRY IN SMALL AND NON-REFERENCE FIELDS

The equipment used for relative dosimetry in small fields introduces additional challenges such as the need for using detectors with a small volume, the ability for high spatial resolution measurements and the need to overcome positioning problems. Meeting all quoted requirements is a challenge for detector design. The following sections will first outline generic characteristics of detectors suitable for small field dosimetry, including 'ideal' characteristics, and then provide specific guidance for detectors and phantoms to be used for relative dosimetry.

4.2.1. General characteristics of detectors for small field dosimetry

It is prudent to assume that a detector used for dosimetry in large fields will not perform well in small fields until the contrary is proven by its adequate characterization specifically for use in small fields. For example, ionization chambers are often not suitable in the presence of high absorbed dose gradients. Volume averaging and substantial perturbations in the absence of LCPE compromise their use for dosimetry of small photon fields. Generic characteristics of suitable detectors for small field dosimetry are summarized in Table 6 [12].

TABLE 6. CHARACTERISTICS OF DETECTORS FOR RELATIVE DOSIMETRY IN SMALL FIELDS [12]

Detector properties	Guidance	Comments
Stability	Short term detector response is better than 0.1% for a total accumulated absorbed dose of many hundreds of kGy from multiple exposures.	Correction for instabilities over time can be made provided the effect is consistent and recalibration is not frequently required.
Dose linearity	Linearity is better than 0.1% over an absorbed dose range of at least three orders of magnitude (e.g. 0.01–10 Gy).	
Dose rate linearity	Clinical linear accelerators are typically operated at average dose rates of 0.1–0.4 Gy/s; detector is linear to better than 0.1% over the range of operation of the linac.	The range of dose rates is typical for WFF and FFF beams.
Dose per pulse linearity	A detector's response with changing dose per pulse remains stable to better than 0.1% after correction for ion recombination.	Typical dose per pulse operating conditions are 0.2–2.0 mGy per pulse.
Energy dependence of detector response	The useful energy range of the detectors for small field MV radiotherapy is from ^{60}Co to 10 MV.	An ideal detector is constructed to be energy independent with macroscopic interaction coefficients (μ_{en}/ρ for photons and S/ρ for electrons) having a constant ratio to those of water in the energy interval of interest.

TABLE 6. CHARACTERISTICS OF DETECTORS FOR RELATIVE DOSIMETRY IN SMALL FIELDS [12] (cont.)

Detector properties	Guidance	Comments
Spatial resolution	The choice of a suitable detector in terms of spatial resolution is usually based on a trade-off between a high signal to noise ratio and a small dosimeter size.	The requirement for spatial resolution is set by the gradients in the quantity to be measured.
Size of detector	The detector size is such that the volume averaging correction is not larger than 5%.	
Orientation	The response of a detector is ideally independent of the orientation of the detector with respect to the beam and the variation is less than 0.5% for angles of less than 60° between the beam axis and the detector axis.	Detectors do not, in general, have an isotropic response, and either a correction is required to account for the angular response or, more commonly, the beam incidence is fixed (i.e. irradiation from end or side) to minimize the effect.
Background signal	Any form of signal leakage that would contribute to increased background readings is at least three orders of magnitude lower than the detector response per Gy.	The zero dose reading of a detector will affect the low dose limit of the device and the signal to noise ratio.
Environmental factors	Correction over the full range of working conditions enables any influence to be reduced to better than 0.3%.	Measurements are ideally independent of temperature, atmospheric pressure and humidity changes or are corrected accurately for these influence quantities.

Note: These characteristics are based on the assumption that leakage is negligible and appropriate polarity and recombination corrections are applied.

The ideal detector for small field dosimetry samples the fluence at a point, is water equivalent, and has a linear response, which is energy independent and absorbed dose (fluence) rate independent. Although water calorimeters are the most water equivalent instruments and have no known energy dependent or absorbed dose rate dependent response, they are not practical instruments for

routine use. The most commonly used detector in relative dosimetry is the air filled ionization chamber. The minimum chamber size, however, is determined by considerations related to the magnitude of the ionization produced in the cavity volume as compared to the background signal from other chamber components such as stem and cable. For every ionization chamber there will always be a field size below which volume averaging becomes unacceptably large. Below that size, only liquid ion chambers or solid state detectors are suitable for dosimetry, with even those exhibiting substantial perturbations for the smallest field sizes.

Relative dosimetry of small fields often involves the determination of central axis depth dose distributions, tissue phantom ratios or tissue maximum ratios, lateral beam profiles and field output factors as a function of field size and shape. The choice of the most appropriate detectors for the specific type of measurement is made according to the parameter being measured. As no ideal detector exists, it is advised to use two or three different types of detectors suitable for a particular measurement so that redundancy in the results can provide more confidence and assurance that no significant dosimetry errors are being made.

For the determination of field output factors, the volume averaging effect may be a limiting factor in the choice of detector; therefore the detector size is such that the radiation fluence is fairly uniform over the detector area (see Sections 2.1.5 and 3.1.4). Other properties that affect the performance for field output factor determination are the field size dependence of the response of the detector owing to its energy dependence, absorbed dose (fluence) rate dependence, water equivalence and overall perturbation.

For the experimental determination of beam profiles, a detector's spatial resolution, directional response, energy response and absorbed dose rate dependence are important parameters to consider. Volume averaging effects and detector material properties affect the measurement of the beam penumbra. Non-uniform directional response may lead to distortion of the shape of the measured profile. Absorbed dose rate dependence may manifest itself by an overestimation of absorbed dose values by some percentage in part of the profile. Detectors exhibiting absorbed dose rate dependence are not the appropriate choice, unless a correction is made for the absorbed dose rate effect. This is especially relevant for FFF beams, where dose rates or dose per pulse values are higher than for beams with a flattening filter. Also, the contribution of low energy photons to absorbed dose may be a problem with some detectors. For the determination of depth dose distributions, the influence of low energy scattered photons increases with depth, and therefore the lack of water equivalence, resulting in the energy dependence of some detectors such as diodes, resulting in an over-response. For the smallest fields, where no in-scatter of photons on the

central axis occurs, the effect of beam hardening may dominate over the effect of scatter contributions, resulting in the opposite behaviour.

Fluence perturbation and detector size effects, together with positioning difficulties, are the most important problems encountered in almost all dosimetric systems used for measurements in small photon beams. Detector composition is also important; if high *Z* material is used in the detector's construction, the energy fluence of secondary electrons is altered (see Section 2.1.5). Such detectors (e.g. ionization chambers with a metal central electrode) may exhibit changes in response as field size changes. When such detectors are calibrated under larger beam conditions, their energy response needs to be considered, as there are differences between large and small beams in terms of the energy spectra of the photons and electrons detected. Corrections depend not only on the sensitive medium of the detector but also to a greater extent on the detailed construction of the detector and surrounding materials.

For accurate measurements in small fields, it is thus important that each detector is radiographed before use, at more than one rotational position (e.g. orthogonal views), to identify any potential problems and assess the construction and symmetry of the device. This will also make it possible to determine the location of the sensitive volume of the detector, which may differ from external marks or information provided by the manufacturer to an extent significantly affecting small field dosimetry [111]. Where necessary, the angular response is also measured to confirm any asymmetries and determine how to take these into account [59].

Many types of dosimeters have been used for small beam relative dosimetry, and it must be emphasized that no single detector stands out as having characteristics close to the ideal ones. For this reason, in contrast to the situation for reference dosimetry, it is not possible to advise using a particular type of detector for particular relative measurements. The wide range of detectors whose use is described in the literature includes vented air and liquid ionization chambers, silicon diodes, diamond detectors, plastic and organic scintillators, radiographic and radiochromic films, metal oxide semiconductor field-effect transistors (MOSFETs), thermoluminescent dosimeters (TLDs), optically stimulated luminescence detectors (OSLDs), radio photoluminescence glass rods and alanine. The items below provide an overview of these detectors.

— *Classical vented ionization chambers* of a volume of 0.3–0.6 cm^3 are not suitable for relative dosimetry in small beams as their size is too large and they underestimate the absorbed dose to water on the central axis of a small field [8]. These ion chambers are to be avoided for profile measurements as corrections for volume averaging effects are unacceptably large.

— *Small vented air ionization chambers* of a volume of 0.01–0.3 cm^3 (minichambers, pinpoint chambers) were reported to be suitable for the measurements of field parameters down to 2 cm × 2 cm [91, 109]. They have favourable energy response to low energy photons and uniform directional response. They are also independent of absorbed dose rate. Stem and cable effects need to be checked and corrected for. It is also advised that the polarity effect be carefully checked and corrected for. Examples of small chambers are given in Table 5, but it is advised that their characteristics be checked before use.
— *Microionization chambers* of a volume of 0.002–0.01 cm^3 (microchambers) have a very small measuring volume and the volume averaging effect is less pronounced, but they have limitations with regard to their reduced sensitivity. The reduced response of microchambers to a given absorbed dose to water means that signal leakage can be significant if not corrected for, particularly in low absorbed dose regions of the beam [109, 112, 113]. It is advised that care be exercised when using microchambers in larger beams, as some authors reported that with an increase in the amount of chamber cable irradiated, the magnitude of radiation induced signal increased [112]. Examples of microchambers are given in Table 5, but it is advised that their characteristics be checked before use.
— *Liquid ionization chambers* (LICs) are filled with dielectric liquid instead of air. Because of the higher density of liquid, the chamber signal per detector volume is significantly larger than that for an air filled ionization chamber of the same volume; therefore, these small chambers are particularly attractive for small field dosimetry. In addition, they are nearly water equivalent, which reduces the chamber perturbation effects compared to air filled chambers. LICs require a bias voltage of 800 V or more. Their response is dose rate dependent because of substantial recombination effects, and it is advised that this be corrected for in profile measurements [114–117]. Cable and stem effects need to be checked and corrected for because the signal may increase substantially owing to the irradiation of a part of the cable. Also the temperature dependence of these chambers can have sufficient influence to necessitate corrections [118]. The only commercial liquid ionization chamber was the PTW 31018. This chamber, however, is no longer available.
— *Silicon diodes* generally have a sensitive volume small enough (typically <0.2 mm^3) so that the volume averaging effects are small. However, their angular dependence is not uniform owing to the internal construction and materials used, and can vary by 3% in magnitude [119]. For this reason, it is advised that they only be used with the axis of symmetry parallel to the beam axis. Diodes are known to over-respond to low energy photons

owing to the differences in mass energy absorption coefficients of silicon and water at keV energies. However, in small fields, where the scattered radiation is reduced, the contribution of low energy photons is rather low. Care needs to be taken to select an appropriate type of diode. Unshielded diodes ('electron diodes') were reported to have properties better suited to small field dosimetry than shielded diodes ('photon diodes') [120–123], but output correction factors are needed for field sizes below 1 cm owing to the effect of their mass density compared to water [37]. Shielded diodes are energy compensated, to absorb some of the low energy scattered photons, and contain high density material (e.g. tungsten) [121]. However, the presence of tungsten increases the fluence of secondary electrons in silicon owing to the higher mass energy absorption coefficient of tungsten, for lower energy photon beams. This causes over-response of the diode. It was shown that the response of shielded diodes is not completely independent of changes in field size and the depth of measurement [121]. The increase in the contribution of low energy scattered photons with depth results in an over-response of shielded diodes. However, some diodes have been reported to exhibit under-response at large depths [58, 124] that was attributed to the absorbed dose rate dependent response. In small fields, the use of unshielded diodes is advised. For measurements in very small fields, stereotactic diodes are used. Diodes have a limited lifetime and their sensitivity depends on accumulated absorbed dose. For this reason it is advised that the constancy of their relative response be verified periodically.

— *Diamond detectors* exhibit high sensitivity and their response is almost independent of energy owing to the relatively constant ratio of stopping-power and mass energy absorption coefficients of diamond to water. They have uniform directional response [125]. Natural diamond based detectors are small in one dimension (<0.5 mm), but their lateral sizes vary because of the diamond selection process. Their absorbed dose rate dependence is significant and needs to be corrected for [126–129], and they require substantial pre-irradiation. It is advised that care be taken in ensuring that the diamond detector is biased correctly, otherwise it can be damaged. It is noted that natural diamond detectors are no longer commercially available and have been replaced by artificial chemical vapour deposition (CVD) diamonds [130–132]. The latter detectors are used without bias voltage and have been shown to be suitable for small field dosimetry [57, 133], but output correction factors are needed for field sizes below 1 cm owing to the effect of their mass density compared to water [47].

— *Plastic and organic scintillators* are based on the production of light in the scintillator during its irradiation. The light is carried by an optical fibre to a photomultiplier tube located outside the irradiation room. Scintillator response is generally linear in the absorbed dose to water range of therapeutic interest [134]. Various studies have indicated that perturbation correction factors for plastic and organic scintillators in small fields are close to unity [56, 100, 135, 136]. These detectors are almost water equivalent in terms of electron density and atomic composition. Typically, they match the water mass stopping-power and mass energy absorption coefficient to within ±2% for the range of beam energies in clinical use including the keV region. Scintillators are nearly energy independent and can be used directly for relative absorbed dose determination. Plastic scintillation dosimeters can be made very small (about 1 mm^3 or less) and yet provide adequate sensitivity for clinical dosimetry. The main complication in the use of plastic scintillators is the correction for the Cerenkov light generated in the optical fibre. Various correction methods have been developed, among which spectral filtration and the use of hollow core fibres have proven to be most successful [137]. The signal to noise ratio of plastic scintillators is generally low and their response degrades with accumulated dose, but owing to their high spatial resolution, flat energy dependence and small size, plastic scintillators can be used for small beam dosimetry applications. The only commercially available device is the Exradin W1, which is listed with its characteristics in Table 7.
— *Radiographic and radiochromic film* dosimetry for small field measurements is attractive owing to superior spatial resolution in 2-D, but is to be used with caution. Radiographic films are known for their limited absorbed dose range, energy dependence and orientation dependence [138]. They exhibit over-response at low absorbed dose to water levels outside the field owing to their increased sensitivity to low energy photons. Careful control of the radiographic film processing and readout procedures is essential for accurate dosimetry. This problem is largely resolved by using radiochromic films that self-develop and require no chemical processing to get an image of the absorbed dose distribution [139]. Radiochromic films are not sensitive to ambient light and do not require a darkroom for their processing, but they were reported to be sensitive to ultraviolet radiation [140]. For megavoltage beams, radiochromic films are nearly tissue equivalent and show little energy dependence. However, depending on the composition, they show varying degrees of energy dependence in the kilovoltage X ray region [139, 141]. They are water resistant. Radiochromic films can be read with a suitable (flat-bed) scanner. The readout procedures require accurate absorbed dose to water calibration, including careful

investigation of spatial non-uniformity of the film response, scanner response and dependence of signal on film orientation [142]. The film signal continues to develop for several hours after irradiation; therefore film scanning is performed in the same post-irradiation interval as for the calibration film. Some other disadvantages reported by various authors include film darkening and temperature sensitivity effects [140]. Nevertheless, its high spatial resolution, water resistance, insensitivity to light and lack of need for processing give radiochromic film a considerable advantage over radiographic film. Radiochromic film can be advised for measurements of small beam profiles, penumbrae and field output factors where changes in the spectral components of a beam can occur and can affect the output factor measurements.

— *Other detectors: MOSFETs, TLDs, OSLDs, radiophotoluminescent (RPL) glass dosimeters, alanine*

- *MOSFETs* are generally used for in vivo dosimetry. Owing to their small size, they have high spatial resolution. However, MOSFET detectors exhibit energy and directional dependence, poor signal to noise ratio and inadequate reproducibility [143]. They also have a rather short lifespan [144]. Overall, the literature [24, 144] does not support their use for small field dosimetry.
- *TLDs* are well established for absorbed dose audit programmes and hospital in vivo dosimetry [145, 146]. TLDs most commonly used in medical applications are LiF:Mg,Ti, LiF:Mg,Cu,P and $Li_2B_4O_7$:Mn, because of their tissue equivalence. TLDs are available in various forms (e.g. powder, chips, microchips, rods, ribbon). LiF:Mg,Ti is one of the most commonly used TLD materials. Its response is linear over a range of absorbed dose values, although it increases in the absorbed dose region above 1–2 Gy (supralinear behaviour). To derive the absorbed dose to water from the thermoluminescence reading response, non-linearity corrections have to be applied, together with other correction factors, such as fading and energy correction, if a TLD is calibrated with a different beam quality than that used for the measurement. For accurate small beam dosimetry, TLDs require careful handling and control of readout procedures to achieve measurement uncertainty of 2% or better. They have been shown to require small corrections in small fields [100].
- *OSLDs* are based on a principle similar to that of TLDs. Instead of heat, light (from a laser) is used to release the trapped energy in the form of luminescence. Typical OSLDs use carbon-doped aluminium oxide (Al_2O_3:C) in the form of small chips (≈1 mm^3), rods, mini-dots and nano-dots. They can be coupled with optical fibre and laser based readout systems for on-line readout or used as passive dosimeters, similarly to

TLDs. OSLDs exhibit high sensitivity over the wide range of absorbed dose rates and absorbed dose to water levels used in radiotherapy. OSLDs exhibit similar linearity, energy and dose rate dependence as TLDs. Precise OSL dosimetry is presently performed by some institutions [147].

- *Radiophotoluminescent (RPL) glass dosimeters* are accumulation type solid state dosimeters that use the phenomenon of radiophotoluminescence to measure absorbed dose. The material used is silver activated phosphate glass. The dosimeters come in the shape of small glass rods (e.g. diameter 1.5 mm, length 8–12 mm). When silver activated phosphate glass is exposed to radiation, stable luminescence centres are created in silver ions. The readout technique uses pulsed ultraviolet laser excitation. The readout area is smaller than the dosimeter size, i.e. diameter 1.5 mm, length 6 mm in the standard readout mode and diameter 1.5 mm, length 0.6 mm in the high absorbed dose mode, which is convenient for small beam dosimetry. A photomultiplier tube registers the orange fluorescence emitted by the glass. RPL signal is not erased during the readout, thus the dosimeter can be re-analysed several times, and the measured data reproduced. Glass dosimeters were reported to have adequate reproducibility; they have a linear response in the therapy absorbed dose range, good spatial resolution, flat energy response from keV to MeV energies [148] and very low fading [149]. RPL glass dosimetry systems are commercially available. Their use for small beam dosimetry has been reported by a few authors [148, 149].
- *Alanine* is often quoted as a suitable dosimeter because it is close to water equivalent, but the pellets with which radiotherapy level dosimetry is achieved are usually quite large (e.g. typically 5 mm diameter and 2.5 mm thickness) and are thus also prone to substantial volume averaging. Smaller pellets are available (e.g. 2.5 mm diameter and 2.5 mm nominal length pellets from the UK National Physical Laboratory (NPL) [57] or the minipellets of 1 mm diameter and 3 mm length in Ref. [150]). Another problem with alanine dosimetry is its comparatively low sensitivity, requiring absorbed doses greater than 10 Gy to obtain a reproducibility of less than 0.5%. Nevertheless, the advantage of alanine is that its density and macroscopic interaction coefficients are close to those of water, so the only substantial perturbation is the volume averaging effect, which can be calculated from measured beam profiles (see Eq. (5) and examples in Appendix I). Even though the necessary instrumentation is in general not available in hospitals, readout services are provided by some standards laboratories and universities.

A list of commercially available silicon diode, diamond, liquid ionization chamber and organic scintillator detectors is given in Table 7. For the sake of clarity it is worth mentioning that diodes discussed in this section, usually called 'scanning diodes', have different construction than diodes used for in vivo dosimetry.

To summarize, liquid ion chambers, silicon diodes, diamond detectors, organic scintillators, radiochromic film, TLDs and OSL dosimeters are considered suitable for relative dosimetry of small photon fields and are advised for use in radiotherapy clinics by this COP, after their proper characterization for the purpose.

4.2.2. Phantoms

Dosimetric and geometric phantoms for relative dosimetry and dose verification of small field treatments may include the following:

— Simple water filled calibration phantoms without a scanning system.
— Full scatter 3-D water phantoms (also known as 3-D radiation field analysers) typically used for the measurement of scanned dosimetric data. It is critical that they are commissioned for alignment, orthogonality, distance accuracy and hysteresis effects before use [151].
— Water equivalent plastic cylinders, spheres, hemispheres, cubes and other shapes containing cavities for inserting ionization chambers, diodes or TLDs, possibly including sliced sections for films. Some contain a space for diode or ionization chamber arrays.
— Phantoms with adjustable measurement planes and chamber cavities, which rigidly attach to stereotactic frames or index precisely to imaging and treatment couch tops.

Prior to the use of plastic water substitute phantoms for dosimetry purposes, their commissioning is a mandatory step in order to check the uniformity of the phantom material and derive any relevant correction factors. A computed tomography examination of the solid slabs is a useful QA test that can help in verifying homogeneity. Ionization chamber measurements in plastic water substitute phantoms are prone to effects such as charge buildup and temperature inhomogeneities, and it needs to be verified that they have no effect on the measurements. Plastics usually have low thermal conductivity; the dosimeter temperature needs to be established by direct measurement at the position of the detector and/or by leaving sufficient time for thermal equilibration with the room [152].

TABLE 7. SILICON DIODE, DIAMOND, LIQUID IONIZATION CHAMBER AND ORGANIC SCINTILLATOR DETECTORS FOR SMALL FIELD DOSIMETRY

Detector	Sensitive volume (mm^3)	Geometric form of sensitive area[a]	Diameter or side length of sensitive area (mm)	Thickness of sensitive volume (mm)	Reference point[b] (from flat face/tip) (mm)[c]	Shielded
IBA PFD3G diode	0.19	Disc	2	0.06	<0.9	Y
IBA EFD3G diode	0.19	Disc	2	0.06	<0.9	N
IBA SFD diode	0.017	Disc	0.6	0.06	<0.9	N
PTW 31018 liquid ion chamber[d]	1.7	Disc	2.5	0.35	1.0	Y
PTW 60008 diode[d]	0.03	Disc	1.13	0.03	2.0[c]	Y
PTW 60012 diode[d]	0.03	Disc	1.13	0.03	0.8[c]	N
PTW 60016 diode	0.03	Disc	1.13	0.03	2.4[c]	Y
PTW 60017 diode	0.03	Disc	1.13	0.03	1.3[c]	N
PTW 60018 diode	0.3	Disc	1.13	0.25	1.3[c]	N
PTW 60003 natural diamond	1–6	Variable	<4	0.1–0.4	1.0[c]	N

TABLE 7. SILICON DIODE, DIAMOND, LIQUID IONIZATION CHAMBER AND ORGANIC SCINTILLATOR DETECTORS FOR SMALL FIELD DOSIMETRY (cont.)

Detector	Sensitive volume (mm^3)	Geometric form of sensitive area[a]	Diameter or side length of sensitive area (mm)	Thickness of sensitive volume (mm)	Reference point[b] (from flat face/tip) (mm)[c]	Shielded
PTW 60019 CVD diamond[d]	0.004	Disc	2.2	0.001	1.0[c]	N
Sun Nuclear EDGE Detector	0.019	Square	0.8	0.03	0.3	Y
Exradin W1 (Standard Imaging)	2.4	Cylinder	1.0	3.0	1.5[e]	N

Note: Characteristics stated by the manufacturers.

[a] "Disc" refers to a geometry where the diameter is larger than the thickness of the detectors, while "cylinder" refers to a detector with a diameter smaller than its length.

[b] The reference point quoted is with respect to the flat face of the detector, for the stem orientation parallel to the beams' central axis.

[c] Note that for the PTW detectors, the data represent water equivalent thickness, not geometrical distance.

[d] No longer commercially available.

[e] Location of the centre of the scintillating detection volume when irradiated from top.

5. CODE OF PRACTICE FOR REFERENCE DOSIMETRY OF MACHINE SPECIFIC REFERENCE FIELDS

5.1. GENERAL

This section provides a COP for machine specific reference dosimetry (msr beam calibration) in clinical high energy photon beams. It is based on the use of an ionization chamber that has been calibrated in terms of absorbed dose to water N_{D,w,Q_0} or $N_{D,w,Q_{msr}}$ in a standards laboratory's reference beam of quality Q_0 or Q_{msr}.

5.2. DOSIMETRY EQUIPMENT

5.2.1. Ionization chambers

Guidance regarding ionization chambers is given in Section 4.1.1. Only cylindrical ionization chambers that fulfil the specifications of a reference class ionization chamber as summarized in Table 3 are advised for msr dosimetry in high energy photon beams. For msr fields with equivalent square msr field size equal to or larger than 6 cm × 6 cm, Farmer type chambers or other reference class chambers such as those listed in Table 4 are used. For msr fields with equivalent square msr field size smaller than 6 cm × 6 cm, smaller ionization chambers such as those listed in Table 5 are used to ensure that the outer edges of the detector volume are at least a distance r_{LCPE} away from the field edges (defined at 50% of the dose maximum, in consistency with the definition of field size given in Section 2.1.2). As discussed in Section 3.1.3, the r_{LCPE} (in cm) is given by:

$$r_{LCPE} = 8.369 \times TPR_{20,10}(10) - 4.382 \quad (22)$$

or

$$r_{LCPE} = 77.97 \times 10^{-3} \times \%dd(10,10)_x - 4.112 \quad (23)$$

The reference point of a cylindrical chamber for the purpose of calibration at the standards laboratory and for measurements under reference conditions in the user's beam is taken to be on the chamber axis at the centre of the cavity volume. This point is positioned at the reference depth z_{ref} in a water phantom. For practical considerations on the use of ionization chambers, such as the time required to equilibrate, evaluation of and correction for leakage currents,

and corrections for influence quantities, such as temperature, atmospheric pressure, humidity, polarity effects and recombination, the same guidance as in Ref. [1] applies; this is summarized in Section 5.4. It is advised that if a field instrument is used, it be cross-calibrated against a calibrated reference chamber in the conventional reference field f_{ref} = 10 cm × 10 cm or in the msr field f_{msr} as described in Section 5.5.

5.2.2. Phantoms and chamber sleeves

Guidance regarding phantoms and chamber sleeves is given in conventional COPs [1, 2, 7]. Water is advised as the reference medium for the determination of absorbed dose to water and beam quality in photon beams. It is advised that the phantom extend at least 5 cm beyond all four sides of the field size employed at the depth of measurement and also that it extend to at least 5 cm beyond the maximum depth of measurement.

In horizontal beams, the window of the phantom is made of plastic and is of thickness t_{win} between 0.2 cm and 0.5 cm. The water equivalent thickness (in g/cm^2) of the phantom window is taken into account when evaluating the depth at which the chamber is to be positioned; the thickness is calculated as the product $t_{win}\rho_{plastic}$ where $\rho_{plastic}$ is the mass density of the plastic (in g/cm^3). For non-waterproof chambers, a waterproofing sleeve is used, made of PMMA and preferably not thicker than 1.0 mm. The air gap between the chamber wall and the waterproofing sleeve is sufficient (0.1–0.3 mm) to allow the air pressure in the chamber to equilibrate; for this reason the use of a thin rubber sheath is not advised[7]. The same waterproofing sleeve that was used for calibration of the user's ionization chamber is also used for reference dosimetry. If it is not possible to use the same waterproofing sleeve that was used during calibration at the standards laboratory, then another sleeve of the same material and of similar thickness is used.

There might be situations where it is more convenient to use a plastic water substitute phantom than water. In that case, even though this is not the preferred option, a high quality water equivalent plastic or similar solid phantom material, such as those listed in Table 20, may be used. It is advised that the procedures described in Section 5.3.4 be followed to determine the depth in the plastic water substitute phantom that corresponds to the reference depth in the water phantom and the phantom dose conversion factor.

---

[7] Another known reason is that the talcum powder often used in the sheaths may occlude the ventilation hole, 'sealing' the chamber expected to be open to ambient air.

5.3. DETERMINATION OF ABSORBED DOSE TO WATER IN THE msr FIELD, f_{msr}

5.3.1. Reference conditions

The reference conditions for determination of absorbed dose to water are specified in Table 8 for high energy photon beams, in Table 9 for CyberKnife machines, in Table 10 for TomoTherapy machines and in Table 11 for Gamma Knife machines.

TABLE 8. REFERENCE CONDITIONS FOR THE DETERMINATION OF ABSORBED DOSE TO WATER IN HIGH ENERGY PHOTON BEAMS

Influence quantity	Reference value or reference characteristics
Phantom material	Water
Phantom shape and size	At least 30 cm × 30 cm × 30 cm
Chamber type	Cylindrical
Measurement depth z_{ref}	10 g/cm^2
Reference point of chamber	On the central axis at the centre of the cavity volume
Position of reference point of chamber	At the measurement depth z_{ref}
SSD/SDD	100 cm or the closest achievable[a]
Field size	10 cm × 10 cm[b] or size of the msr field[c]

[a] If the reference absorbed dose to water has to be determined for an isocentric set-up, the source-to-axis distance of the accelerator is used, even if this is not 100 cm.

[b] The field size is defined at the surface of the phantom for an SSD type set-up, whereas for a source-to-axis distance type set-up it is defined at the plane of the detector, placed at the reference depth in the water phantom at the isocentre of the machine.

[c] The equivalent square msr field size, S, as close as possible to 10 cm but not smaller than 4 cm and not larger than 12 cm. The aspect ratio of rectangular fields (largest dimension/smallest dimension) is as close as possible to unity.

TABLE 9. REFERENCE CONDITIONS FOR THE DETERMINATION OF ABSORBED DOSE TO WATER IN HIGH ENERGY PHOTON BEAMS ON CYBERKNIFE MACHINES

Influence quantity	Reference value or reference characteristics
Phantom material	Water
Phantom shape and size	At least 30 cm × 30 cm × 30 cm
Chamber type	Cylindrical
Measurement depth z_{ref}	10 g/cm^2
Reference point of chamber	On the central axis at the centre of the cavity volume
Position of reference point of chamber	At the measurement depth z_{ref}
SDD	80 cm
Field shape and size	Circular, maximum available, fixed collimator (6 cm diameter)

TABLE 10. REFERENCE CONDITIONS FOR THE DETERMINATION OF ABSORBED DOSE TO WATER IN HIGH ENERGY PHOTON BEAMS ON TOMOTHERAPY MACHINES

Influence quantity	Reference value or reference characteristics
Phantom material	Water
Phantom shape and size	At least 30 cm × 30 cm × 30 cm
Chamber type	Cylindrical
Measurement depth z_{ref}	10 g/cm^2
Reference point of chamber	On the central axis at the centre of the cavity volume
Position of reference point of chamber	At the measurement depth z_{ref}
SSD/SDD	85 cm[a]
Field shape and size	Rectangular (5 cm × 10 cm for TomoTherapy HiArt)

[a] The reference SSD or SDD (for source-to-axis distance set-up) is that used for clinical treatments.

TABLE 11. REFERENCE CONDITIONS FOR THE DETERMINATION OF ABSORBED DOSE TO WATER ON GAMMA KNIFE MACHINES

Influence quantity	Reference value or reference characteristics
Phantom material	Water or plastic (polystyrene, ABS, Solid Water, etc.)[a]
Phantom shape and size	Hemispherical atop a cylinder, 16 cm diameter
Chamber type	Microchamber, cylindrical
Measurement depth z_{ref}	Centre of the hemisphere[b]
Reference point of chamber	On the central axis at the centre of the cavity volume
Position of reference point of chamber	At the centre of the hemisphere
SSD	32 cm
Field size	Circular, maximum available (1.6 or 1.8 cm diameter)[c]

[a] Different designs have been reported, but the more common type advised in Gamma Knife systems is the hemisphere atop a water filled or compact polystyrene cylinder.

[b] In polystyrene phantoms this is usually a depth of 8 cm, for PMMA it is 7 cm.

[c] For Gamma Knife machines, the maximum field size available depends on the model: 1.8 cm diameter for the standard model (Gamma Knife 4 or 4C) and 1.6 cm diameter for the Perfexion (PFX) model. For Rotating Gamma System (RGS) machines, the maximum field size available is 1.8 cm diameter. The msr field is the field generated with all sources out.

5.3.2. Machine specific determination of absorbed dose to water

5.3.2.1. High energy X ray WFF beams

The formalism for the determination of absorbed dose to water in the msr field f_{msr} is detailed in Section 3.2.1. The measurement is performed using an ionization chamber with its reference point positioned at the reference depth z_{ref} in a water phantom[8]. Depending on the availability of a calibration coefficient

[8] If a water equivalent plastic phantom is used, the expressions are modified according to the description given in Section 3.2.2.

for the ionization chamber, one of the three different methods outlined in Section 3.2.1 is used to determine the absorbed dose to water in a water phantom:

(a) A calibration coefficient, $N_{D,\mathrm{w},Q_{\mathrm{msr}}}^{f_{\mathrm{msr}}}$, in terms of absorbed dose to water for the ionization chamber in a reference beam of quality Q_{msr} in the msr field f_{msr} is available; this is the preferred option, although at present few standards laboratories offer this type of calibration. The absorbed dose to water for the f_{msr} field, in a beam of quality Q_{msr}, at the reference depth z_{ref} in water and in the absence of the ionization chamber is given by:

$$D_{\mathrm{w},Q_{\mathrm{msr}}}^{f_{\mathrm{msr}}} = M_{Q_{\mathrm{msr}}}^{f_{\mathrm{msr}}} \, N_{D,\mathrm{w},Q_{\mathrm{msr}}}^{f_{\mathrm{msr}}} \tag{24}$$

If the conventional reference field f_{ref} = 10 cm × 10 cm can be established at the machine, in Eq. (24) f_{msr} will be replaced by f_{ref} and the beam quality Q_{msr} by Q.

(b) A calibration coefficient, $N_{D,\mathrm{w},Q_0}^{f_{\mathrm{ref}}}$, in terms of absorbed dose to water for the ionization chamber in a standards laboratory's reference beam of quality Q_0 in the conventional reference field f_{ref} = 10 cm × 10 cm is available, as well as a beam quality correction factor $k_{Q_{\mathrm{msr}},Q_0}^{f_{\mathrm{msr}},f_{\mathrm{ref}}}$ to correct for the use of the calibration coefficient in the f_{msr} field. The absorbed dose to water for the f_{msr} field, in a beam of quality Q_{msr}, at the reference depth z_{ref} in water and in the absence of the ionization chamber is given by:

$$D_{\mathrm{w},Q_{\mathrm{msr}}}^{f_{\mathrm{msr}}} = M_{Q_{\mathrm{msr}}}^{f_{\mathrm{msr}}} \, N_{D,\mathrm{w},Q_0}^{f_{\mathrm{ref}}} \, k_{Q_{\mathrm{msr}},Q_0}^{f_{\mathrm{msr}},f_{\mathrm{ref}}} \tag{25}$$

When the calibration beam quality Q_0 is ^{60}Co, the generalized symbol for the beam quality correction factor $k_{Q_{\mathrm{msr}},Q_0}^{f_{\mathrm{msr}},f_{\mathrm{ref}}}$ can be simplified to $k_{Q_{\mathrm{msr}}}^{f_{\mathrm{msr}},f_{\mathrm{ref}}}$.

If the conventional reference field f_{ref} = 10 cm × 10 cm can be established at the machine, in Eq. (25) f_{msr} will be replaced by f_{ref} and the beam quality Q_{msr} by Q. In addition, as the resulting double superscript f_{ref} in k can be removed (there is no need to consider different types of reference fields), Eq. (25) reduces to the formalism given in conventional COPs, showing consistency between those and the present COP.

While Eq. (25) is meant to be applied using $k_{Q_{\mathrm{msr}},Q_0}^{f_{\mathrm{msr}},f_{\mathrm{ref}}}$ that are directly measured or calculated for the f_{msr} field, based on current knowledge and uncertainty estimates it can be assumed that $k_{Q_{\mathrm{msr}},Q_0}^{f_{\mathrm{msr}},f_{\mathrm{ref}}} = k_{Q,Q_0}^{f_{\mathrm{ref}}}$, where Q refers to the hypothetical conventional reference field of the machine. Data for the beam quality correction factor $k_Q^{f_{\mathrm{ref}}}$, short notation for $k_{Q,Q_0}^{f_{\mathrm{ref}}}$ with reference to Q_0 = ^{60}Co and f_{ref} = 10 cm × 10 cm, in WFF beams are given in Table 12 for a range of ionization chambers, consistent with the k_{Q} data in Refs [1, 2, 7].

TABLE 12. $k_Q^{f_{ref}}$ DATA FOR THE CONVENTIONAL f_{ref} FIELD (10 cm × 10 cm) FOR REFERENCE IONIZATION CHAMBERS IN WFF LINACS, AS A FUNCTION OF THE BEAM QUALITY INDICES $TPR_{20,10}(10)$ AND $\%dd(10,10)_x$

Ion chamber ↓	$TPR_{20,10}(10)$ =	0.630	0.660	0.690	0.720	0.750
	$\%dd(10,10)_x$ =	63.4	65.2	67.6	70.5	73.9
Capintec PR-06C/G Farmer		0.997	0.994	0.991	0.988	0.982
Exradin A2 Spokas		0.998	0.997	0.995	0.992	0.988
Exradin A12 Farmer		0.998	0.996	0.993	0.990	0.984
Exradin A12S		0.996	0.994	0.991	0.987	0.981
Exradin A19		0.996	0.993	0.990	0.985	0.980
Nuclear Assoc 30-751 Farmer		0.996	0.993	0.990	0.985	0.979
Nuclear Assoc 30-752 Farmer		0.997	0.995	0.992	0.989	0.983
NE 2505/3, 3A Farmer		0.996	0.994	0.992	0.989	0.984
NE 2571 Farmer		0.997	0.994	0.992	0.989	0.984
NE 2611		0.996	0.993	0.991	0.988	0.984
PTW 23331 rigid		0.996	0.992	0.989	0.985	0.980

TABLE 12. $k_Q^{f_{ref}}$ DATA FOR THE CONVENTIONAL f_{ref} FIELD (10 cm × 10 cm) FOR REFERENCE IONIZATION CHAMBERS IN WFF LINACS, AS A FUNCTION OF THE BEAM QUALITY INDICES $TPR_{20,10}(10)$ AND $\%dd(10,10)_x$ (cont.)

Ion chamber ↓	$TPR_{20,10}(10)$ =	0.630	0.660	0.690	0.720	0.750
	$\%dd(10,10)_x$ =	63.4	65.2	67.6	70.5	73.9
PTW 23332 rigid		0.996	0.993	0.989	0.984	0.978
PTW 23333 (3 mm cap)		0.996	0.993	0.989	0.985	0.979
PTW 30001 Farmer		0.996	0.993	0.989	0.985	0.979
PTW 30010 Farmer		0.996	0.993	0.989	0.985	0.979
PTW 30002/30011 Farmer		0.996	0.993	0.991	0.987	0.982
PTW 30004/30012 Farmer		0.998	0.995	0.993	0.989	0.984
PTW 30006/30013 Farmer		0.996	0.993	0.989	0.984	0.978
PTW 31003/31013 Semiflex		0.996	0.993	0.989	0.984	0.978
SNC 100700-0 Farmer		0.997	0.994	0.991	0.986	0.979
SNC 100700-1 Farmer		0.998	0.996	0.994	0.990	0.984

TABLE 12. $k_Q^{f_{ref}}$ DATA FOR THE CONVENTIONAL f_{ref} FIELD (10 cm × 10 cm) FOR REFERENCE IONIZATION CHAMBERS IN WFF LINACS, AS A FUNCTION OF THE BEAM QUALITY INDICES $TPR_{20,10}(10)$ AND $\%dd(10,10)_x$ (cont.)

Ion chamber ↓	$TPR_{20,10}(10)$ =	0.630	0.660	0.690	0.720	0.750
	$\%dd(10,10)_x$ =	63.4	65.2	67.6	70.5	73.9
Victoreen Radocon III 555		0.993	0.989	0.985	0.979	0.973
Victoreen 30-348		0.995	0.991	0.988	0.982	0.976
Victoreen 30-351		0.995	0.991	0.988	0.983	0.977
Victoreen 30-349		0.995	0.991	0.988	0.983	0.978
Victoreen 30-361		0.995	0.991	0.988	0.983	0.977
IBA FC-65P (Wellhöfer IC 69) Farmer		0.997	0.994	0.992	0.986	0.979
IBA FC-65G (Wellhöfer IC 70) Farmer		0.998	0.997	0.994	0.989	0.983

Note: See Appendix I for details.

If the calibration beam quality Q_0 is not ^{60}Co, the beam quality correction factor can be derived from the ratio of values for Q and Q_0, as both are relative to ^{60}Co. Hence, $k_{Q,Q_0}^{f_{\text{ref}}}$ is obtained from the values in Table 12 as follows:

$$k_{Q,Q_0}^{f_{\text{ref}}} = \frac{k_Q^{f_{\text{ref}}}}{k_{Q_0}^{f_{\text{ref}}}} \tag{26}$$

(c) A calibration coefficient, $N_{D,\text{w},Q_0}^{f_{\text{ref}}}$, in terms of absorbed dose to water for the ionization chamber in a standards laboratory's reference beam of quality Q_0 in the conventional reference field f_{ref} = 10 cm × 10 cm is available, but there is no beam quality correction factor available to correct for the use of the calibration coefficient in the f_{msr} field. The absorbed dose to water for the f_{msr} field, in a beam of quality Q_{msr}, at the reference depth z_{ref} in water and in the absence of the ionization chamber is given by:

$$D_{\text{w},Q_{\text{msr}}}^{f_{\text{msr}}} = M_{Q_{\text{msr}}}^{f_{\text{msr}}} \; N_{D,\text{w},Q_0}^{f_{\text{ref}}} \; k_{Q,Q_0}^{f_{\text{ref}}} \; k_{Q_{\text{msr}},Q}^{f_{\text{msr}},f_{\text{ref}}} \tag{27}$$

This requires that the beam quality Q of the hypothetical conventional reference field of the machine (see Section 3.2.1.3) be estimated in order to adopt beam quality correction factors $k_Q^{f_{\text{ref}}}$ from Ref. [1] or from Refs [2, 7]. The determination of the beam quality index is detailed in Section 5.3.3, and the values of $k_Q^{f_{\text{ref}}}$ for a range of ionization chambers for generic WFF beams are given in Table 12. Based on current knowledge and uncertainty estimates, it can be assumed that $k_{Q_{\text{msr}},Q}^{f_{\text{msr}},f_{\text{ref}}} = 1$, which is consistent with the assumption $k_{Q_{\text{msr}},Q_0}^{f_{\text{msr}},f_{\text{ref}}} = k_{Q,Q_0}^{f_{\text{ref}}}$ in Eq. (25); note that these equalities hold only within the uncertainty estimates discussed in Appendix I.

In Eqs (24–27), $M_{Q_{\text{msr}}}^{f_{\text{msr}}}$ is the reading of the ionization chamber in the field f_{msr} corrected for influence quantities, such as pressure, temperature, incomplete charge collection, polarity effects, etc. (see Section 5.4).

5.3.2.2. FFF high energy X ray beams

For FFF high energy X ray beams, the formalism is essentially the same; in particular, options (a) and (b) in the previous section remain unaltered. For the application of option (c), values of $k_Q^{f_{\text{ref}}}$ (the short notation for $k_{Q,Q_0}^{f_{\text{ref}}}$ when $Q_0 = {}^{60}$Co) for a range of ionization chambers for FFF photon beams as well as

for the two specific machine types CyberKnife and TomoTherapy are given in Table 13. These data include a generic volume averaging correction factor[9].

5.3.2.3. ^{60}Co gamma ray beams

For ^{60}Co gamma ray beams such as in the Gamma Knife, only option (b) is considered (see Eq. (25)). The factor $k_{Q_{msr},Q_0}^{f_{msr},f_{ref}}$ with reference to a chamber calibration $N_{D,w,Q_0}^{f_{ref}}$ with $Q_0 = {}^{60}$Co is close to unity for most chambers suitable for reference dosimetry in these treatment machines. Note, however, that as reference dosimetry in Gamma Knife beams is usually performed in plastic phantoms (ABS or Solid Water), the correction factors include the conversion to absorbed dose to water. Values of $k_{Q_{msr},Q_0}^{f_{msr},f_{ref}}$ for the Gamma Knife models Perfexion and 4C are given in Table 14.

5.3.3. Determination of the beam quality when the conventional f_{ref} cannot be realized

As already emphasized, some treatment machines cannot realize the conventional reference field of 10 cm × 10 cm. However, case (c) in Sections 5.3.2.1 and 5.3.2.2 is based on the use of the beam quality correction factor $k_{Q,Q_0}^{f_{ref}}$. To this end, data for a hypothetical 10 cm × 10 cm reference field f_{ref} at the same machine as for the f_{msr} field are required for the application of Eq. (27). These data can be taken from Refs [1, 2, 7] using a beam quality index measured for the msr field, which is subsequently related to that of the reference field.

The two beam quality indices defined for a 10 cm × 10 cm reference field, $TPR_{20,10}(10)$ (defined in Ref. [1]) and $\%dd(10,10)_x$ (defined in Refs [2, 7]) are considered in this COP. Both are derived from relevant measurements in a field with equivalent square msr field size S, i.e. $TPR_{20,10}(S)$ and $\%dd(10,S)_x$, respectively. For machines that cannot realize a square field, an equivalent square msr field size needs to be calculated. Both steps are described below.

5.3.3.1. Equivalent square msr field size

For flattened fields that exhibit a homogeneous lateral beam profile over most of the field area, the equivalent square msr field sizes for rectangular and circular fields can be derived from the tables of Ref. [32]. A subset of such data

[9] Users wishing to investigate the data difference using a volume averaging correction factor calculated specifically for their beam can find an example in Appendix I.

TABLE 13. $k_{Q_{msr}}^{f_{msr},f_{ref}}$ DATA FOR THE CONVENTIONAL f_{ref} FIELD (10 cm × 10 cm) FOR REFERENCE IONIZATION CHAMBERS IN FFF LINACS, AS A FUNCTION OF THE BEAM QUALITY INDICES $TPR_{20,10}(10)$ AND $\%dd(10,10)_x$, AND FOR THE CYBERKNIFE AND TOMOTHERAPY MACHINES

Ion chamber ↓	$TPR_{20,10}(10)$ =	0.63	0.66	0.69	0.72	0.75	CyberKnife	TomoTherapy
	$\%dd(10,10)_x$ =	63.8	65.6	68.2	71.7	76.1		
Capintec PR-06C/G Farmer		0.996	0.995	0.992	0.988	0.981	1.000	0.996
Exradin A2 Spokas		0.996	0.996	0.993	0.989	0.983	0.997	0.996
Exradin A12 Farmer		0.998	0.997	0.994	0.991	0.984	1.004	0.998
Exradin A12S		0.994	0.993	0.989	0.984	0.977	0.993	0.994
Exradin A19		0.995	0.995	0.991	0.987	0.981	1.002	0.995
Nuclear Assoc 30-751 Farmer		0.995	0.994	0.991	0.986	0.979	1.000	0.995
Nuclear Assoc 30-752 Farmer		0.997	0.996	0.993	0.990	0.983	1.002	0.997
NE 2505/3, 3A Farmer		0.996	0.996	0.993	0.990	0.985	1.003	0.996
NE 2571 Farmer		0.996	0.995	0.993	0.990	0.985	1.003	0.996
NE 2611		0.994	0.992	0.989	0.985	0.979	0.993	0.993

TABLE 13. $k_{Q_{msr}}^{f_{msr},f_{ref}}$ DATA FOR THE CONVENTIONAL f_{ref} FIELD (10 cm × 10 cm) FOR REFERENCE IONIZATION CHAMBERS IN FFF LINACS, AS A FUNCTION OF THE BEAM QUALITY INDICES $TPR_{20,10}(10)$ AND $\%dd(10,10)_x$, AND FOR THE CYBERKNIFE AND TOMOTHERAPY MACHINES (cont.)

Ion chamber ↓	$TPR_{20,10}(10)$ =	0.63	0.66	0.69	0.72	0.75	CyberKnife	TomoTherapy
	$\%dd(10,10)_x$ =	63.8	65.6	68.2	71.7	76.1		
PTW 23331 rigid		0.995	0.993	0.990	0.985	0.980	0.998	0.994
PTW 23332 rigid		0.995	0.993	0.988	0.983	0.976	0.995	0.994
PTW 23333 (3 mm cap)		0.995	0.993	0.990	0.985	0.978	0.998	0.995
PTW 30001 Farmer		0.995	0.994	0.990	0.986	0.979	0.999	0.995
PTW 30010 Farmer		0.995	0.994	0.990	0.986	0.979	0.999	0.995
PTW 30002/30011 Farmer		0.995	0.994	0.992	0.988	0.982	1.001	0.995
PTW 30004/30012 Farmer		0.997	0.996	0.994	0.990	0.984	1.003	0.997
PTW 30006/30013 Farmer		0.995	0.994	0.990	0.985	0.978	0.999	0.995
PTW 31003/31013 Semiflex		0.995	0.993	0.990	0.985	0.978	0.996	0.994
SNC 100700-0 Farmer		0.996	0.995	0.992	0.987	0.979	1.002	0.996

TABLE 13. $k_{Q_{msr}}^{f_{msr},f_{ref}}$ DATA FOR THE CONVENTIONAL f_{ref} FIELD (10 cm × 10 cm) FOR REFERENCE IONIZATION CHAMBERS IN FFF LINACS, AS A FUNCTION OF THE BEAM QUALITY INDICES $TPR_{20,10}(10)$ AND $\%dd(10,10)_x$, AND FOR THE CYBERKNIFE AND TOMOTHERAPY MACHINES (cont.)

Ion chamber ↓	$TPR_{20,10}(10)$ =	0.63	0.66	0.69	0.72	0.75	CyberKnife	TomoTherapy
	$\%dd(10,10)_x$ =	63.8	65.6	68.2	71.7	76.1		
SNC 100700-1 Farmer		0.998	0.998	0.995	0.991	0.985	1.005	0.998
Victoreen Radocon III 555		0.992	0.990	0.985	0.979	0.973	0.995	0.991
Victoreen 30-348		0.993	0.991	0.987	0.981	0.973	0.994	0.992
Victoreen 30-351		0.994	0.992	0.988	0.984	0.977	0.998	0.993
Victoreen 30-349		0.994	0.992	0.988	0.983	0.978	0.997	0.993
Victoreen 30-361		0.994	0.992	0.988	0.983	0.976	0.998	0.993
IBA FC-65P (Wellhöfer IC 69) Farmer		0.996	0.995	0.992	0.987	0.978	1.002	0.996
IBA FC-65G (Wellhöfer IC 70) Farmer		0.997	0.997	0.994	0.990	0.983	1.004	0.998

Note: The correspondence between $TPR_{20,10}(10)$ and $\%dd(10,10)_x$ is different from that for WFF beams.

TABLE 14. CORRECTION FACTORS $k_{Q_{msr},Q_0}^{f_{msr},f_{ref}}$ FOR THE GAMMA KNIFE MODELS PERFEXION AND 4C [110, 153]

Chamber type	Perfexion f_{msr} = 16 mm ∅			4C f_{msr} = 18 mm ∅		
	Solid Water	ABS	Water	Solid Water	ABS	Water
PTW T31010	1.0037	1.0146	1.0001	0.9958	0.9990	0.9924
PTW T31016	1.0040	1.0110	0.9991	1.0014	1.0025	0.9964
Exradin A1SL	1.0046	1.0138	1.0006	1.0009	1.0014	0.9967
Exradin A14SL	1.0154	1.0194	1.0112	1.0116	1.0060	1.0058
Exradin A16	1.0167	1.0295	1.0127	1.0163	1.0217	1.0104
IBA CC01	1.0213	1.0292	1.0169	1.0203	1.0208	1.0157
IBA CC04	1.0107	1.0117	1.0062	1.0086	1.0049	1.0040
Capintec PR05-P 4.7	1.0059	1.0070	1.0010	1.0007	0.9960	0.9951
Capintec PR05-P 7.6	1.0025	1.0126	0.9976	0.9885	0.9972	0.9844

for the field sizes considered in this COP is given in Table 15. The equivalent square msr field sizes for WFF beams are independent of energy.

For FFF beams, the contribution of scattered photons to the centre of the field varies differently as a function of field size and depends also on the energy of the beam. Data for the equivalent flattened square msr field size, based on average values for 6–7 MV and 10 MV FFF beams described in the literature are given in Tables 16 and 17 (see Appendix I for information on how these are calculated). For Cyberknife, which has a steeper gradient in its lateral beam profile, the 6 cm diameter msr field has an equivalent uniform square msr field size of 5.0 cm.

TABLE 15. EQUIVALENT SQUARE msr FIELD SIZE OF RECTANGULAR FIELDS WITH DIMENSIONS X AND Y AND OF CIRCULAR FIELDS WITH DIAMETER Ø FOR FLATTENED BEAMS

X (cm) \ Y (cm)	12	11	10	9	8	7	6	5	4	3
12	12.0	11.5	10.9	10.3	9.6	8.9	8.1	7.2	6.2	5.1
11		11.0	10.5	9.9	9.3	8.6	7.8	7.0	6.0	5.0
10			10.0	9.5	8.9	8.3	7.5	6.8	5.9	4.8
9				9.0	8.5	7.9	7.2	6.5	5.7	4.7
8					8.0	7.5	6.9	6.2	5.4	4.5
7						7.0	6.5	5.9	5.1	4.3
6							6.0	5.5	4.8	4.1
5								5.0	4.5	3.8
4									4.0	3.4
3										3.0
Ø (cm)	12	11	10	9	8	7	6	5	4	3
	10.7	9.8	8.9	8.0	7.1	6.2	5.4	4.5	3.6	2.7

5.3.3.2. Experimental determination of $TPR_{20,10}(10)$

The beam quality index $TPR_{20,10}(10)$ is determined from the measurement of $TPR_{20,10}$ for the f_{msr} equivalent square field, S, which is subsequently used in the analytical expression of Palmans [38] given below. The experimental set-up for measuring $TPR_{20,10}(S)$ is shown in Fig. 14 and the reference conditions of measurement are given in Table 18. It is advised that the influence of recombination effects at the two measurement depths be investigated and taken into account if there is variation with depth. Although TPR is normally defined

TABLE 16. EQUIVALENT UNIFORM SQUARE msr FIELD SIZE OF RECTANGULAR FIELDS WITH DIMENSIONS X AND Y AND OF CIRCULAR FIELDS WITH DIAMETER Ø FOR 6–7 MV FFF BEAMS

X (cm) \ Y (cm)	12	11	10	9	8	7	6	5	4	3
12	11.2	10.8	10.3	9.8	9.2	8.5	7.8	7.0	6.0	5.0
11		10.4	9.9	9.4	8.9	8.3	7.6	6.8	5.9	4.9
10			9.5	9.1	8.6	8.0	7.3	6.6	5.7	4.8
9				8.7	8.2	7.6	7.0	6.3	5.5	4.6
8					7.8	7.3	6.7	6.1	5.3	4.5
7						6.8	6.3	5.8	5.1	4.3
6							5.9	5.4	4.8	4.0
5								4.9	4.4	3.8
4									4.0	3.4
3										3.0
Ø (cm)	12	11	10	9	8	7	6	5	4	3
	10.2	9.4	8.6	7.8	7.0	6.1	5.3	4.4	3.5	2.7

Note: The values do not apply to CyberKnife beams. For Cyberknife, which has a steeper gradient in its lateral beam profile, the 6 cm diameter msr field has an equivalent uniform square msr field size of 5.0 cm.

strictly in terms of ratios of absorbed dose to water, for ‘non-small’ fields the use of ionization ratios provides acceptable accuracy owing to the slow variation with depth of water/air stopping-power ratios, their practically negligible field size dependence and the assumed constancy of perturbation factors beyond the depth of maximum dose.

TABLE 17. EQUIVALENT UNIFORM SQUARE msr FIELD SIZE OF RECTANGULAR FIELDS WITH DIMENSIONS X AND Y AND OF CIRCULAR FIELDS WITH DIAMETER Ø FOR 10 MV FFF BEAMS

X (cm) \ Y (cm)	12	11	10	9	8	7	6	5	4	3
12	10.5	10.2	9.8	9.3	8.8	8.2	7.5	6.7	5.9	4.9
11		9.8	9.5	9.0	8.5	8.0	7.3	6.6	5.7	4.8
10			9.1	8.7	8.2	7.7	7.1	6.4	5.6	4.7
9				8.3	7.9	7.4	6.8	6.2	5.4	4.5
8					7.5	7.1	6.6	5.9	5.2	4.4
7						6.7	6.2	5.7	5.0	4.2
6							5.8	5.3	4.7	4.0
5								4.9	4.4	3.7
4									3.9	3.4
3										3.0
Ø (cm)	12	11	10	9	8	7	6	5	4	3
	9.7	9.0	8.3	7.6	6.8	6.0	5.2	4.4	3.5	2.7

The beam quality index for the conventional reference field f_{ref} 10 cm × 10 cm, $TPR_{20,10}(10)$, is derived from Ref. [38]:

$$TPR_{20,10}(10) = \frac{TPR_{20,10}(S) + c(10 - S)}{1 + c(10 - S)} \quad (28)$$

where $c = (16.15 \pm 0.12) \times 10^{-3}$, valid for $4 \leq S \leq 12$, S being the equivalent square msr field size in cm.

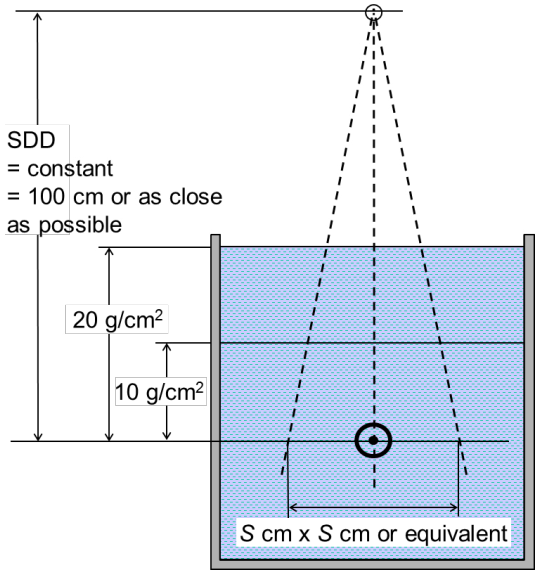

FIG. 14. Experimental set-up for the measurement of $TPR_{20,10}$(S). The SDD is kept constant at 100 cm or as close to that distance as possible, and measurements are made with 10 g/cm^2 and 20 g/cm^2 of water over the reference point of the chamber. The field at the position of the reference point of the chamber has an equivalent square msr field size S. *Either a cylindrical or a plane-parallel ionization chamber can be used (reproduced from Ref. [1]).*

TABLE 18. REFERENCE CONDITIONS FOR THE DETERMINATION OF THE PHOTON BEAM QUALITY INDEX $TPR_{20,10}(S)$ IN HIGH ENERGY PHOTON GENERATORS

Influence quantity	Reference value or reference characteristics
Phantom material	Water
Chamber type	Cylindrical or plane-parallel with sufficient lateral buildup[a]
Measurement depths	20 g/cm^2 and 10 g/cm^2
Reference point of chamber	For cylindrical chambers, on the central axis at the centre of the cavity volume; for plane-parallel chambers, on the inner surface of the entrance window at its centre

TABLE 18. REFERENCE CONDITIONS FOR THE DETERMINATION OF THE PHOTON BEAM QUALITY INDEX $TPR_{20,10}(S)$ IN HIGH ENERGY PHOTON GENERATORS (cont.)

Influence quantity	Reference value or reference characteristics
Position of reference point of chamber	For cylindrical or plane-parallel chambers, at the measurement depths
Orientation of chamber stem	Perpendicular to the beam axis
SDD	100 cm or, for msr fields, the closest to 100 cm achievable
Field shape and size at SDD	10 cm × 10 cm or the msr field (the closest to 10 cm × 10 cm achievable[b])

[a] It is advised that the largest dimension of the chamber be smaller than the smallest side of the field minus twice the r_{LCPE}, or that the outer lateral edge of the detector volume be at least a distance r_{LCPE} away from the nearest field edge.

[b] It is advised that the equivalent square msr field size, S, be as close as possible to 10 cm but not smaller than 4 cm and not larger than 12 cm. The aspect ratio of rectangular fields (largest dimension/smallest dimension) will be as close as possible to unity.

*5.3.3.3. Experimental determination of %*dd*(10,10)$_x$*

The beam quality index $\%dd(10,10)_x$ is determined from the measurement of $\%dd(10)$ for the f_{msr} equivalent square field, S, which is subsequently used in the analytical expression of Palmans [38] given below. The experimental set-up for measuring $\%dd(10,S)_x$ is shown in Fig. 15 and the reference conditions of measurement are given in Table 19.

If the chamber used is cylindrical, its effective point of measurement will be placed at the relevant measurement depths, while for a plane-parallel chamber, the inner front face of the cavity will be positioned at the relevant depths. It is advised that the influence of recombination effects at the two measurement depths be investigated and taken into account if there is variation with depth. Although $\%dd(10,10)$ is strictly defined in terms of ratios of absorbed dose to water, for 'non-small' fields the use of ionization ratios provides acceptable accuracy owing to the slow variation with depth of water/air stopping-power ratios, their practically negligible field size dependence and the assumed constancy of perturbation factors beyond the depth of maximum dose.

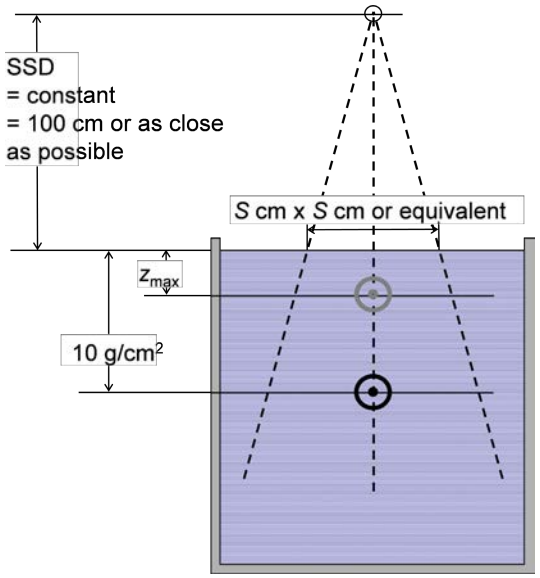

*FIG. 15. Experimental set-up for the determination of %*dd*(10,*S*)$_x$. The SSD is kept constant at 100 cm or as close to that distance as possible, and measurements are made at depths of z_{max} and 10 g/cm^2 (usually derived from a depth-dose distribution). The field at the phantom surface has an equivalent square msr field size* S*. Either a plane-parallel or a cylindrical ionization chamber can be used. In the latter case, the chamber's effective point of measurement is taken into account (see Table 19) by shifting the measured depth ionization curve, with the centre of the cavity as the point of measurement, upstream by 0.6*r*, where r is the inner radius of the cylindrical chamber [7].*

No lead foil needs to be used in the measurements of %*dd*(10,*S*) for WFF beams with energies below 10 MV. However, for FFF beams of any energy, it is recommended to introduce a 1 mm lead foil in the beam to eliminate the potential effect of accelerator-produced electron contamination and obtain %*dd*(10,10)$_{Pb}$. The beam quality specifier %*dd*(10,10)$_x$ can then be obtained from %*dd*(10,10)$_{Pb}$ using the relations in Ref. [2]. It is noted that according to guidance in Refs [2, 7], for the conventional 10 cm × 10 cm reference field in 10 MV beams the measurements are done using a lead foil.

The beam quality index for the conventional reference field f_{ref} 10 cm × 10 cm, %*dd*(10,10), is derived from Ref. [38]:

$$\%dd(10,10) = \frac{\%dd(10,S) + 80c(10-S)}{1 + c(10-S)} \tag{29}$$

TABLE 19. REFERENCE CONDITIONS FOR THE DETERMINATION OF THE PHOTON BEAM QUALITY INDEX $\%dd(10,S)_x$ IN HIGH ENERGY PHOTON GENERATORS

Influence quantity	Reference value or reference characteristics
Phantom material	Water
Chamber type	Cylindrical or plane-parallel with sufficient lateral buildup[a]
Measurement depths	10 g/cm^2 and z_{max}
Reference point of chamber	For cylindrical chambers at P_{eff}[b]; for plane-parallel chambers, on the inner surface of the entrance window at its centre
Position of reference point of chamber	For cylindrical or plane-parallel chambers, at the measurement depths
Orientation of chamber stem	Perpendicular to the beam axis
SSD	100 cm or, for msr fields, the closest to 100 cm achievable
Field shape and size at SSD	10 cm × 10 cm or the msr field (the closest to 10 cm × 10 cm achievable[c])

[a] It is advised that the largest dimension of the chamber be smaller than the field size minus twice the r_{LCPE}, or that the outer lateral edge of the detector volume be at least a distance r_{LCPE} away from the nearest field edge.

[b] The effective point of measurement of a cylindrical chamber, P_{eff}, is located 0.6 times the cavity radius from the chamber axis towards the photon source.

[c] It is advised that the equivalent square msr field size, S, be as close as possible to 10 cm but not smaller than 4 cm and not larger than 12 cm. The aspect ratio of rectangular fields (largest dimension/smallest dimension) will be as close as possible to unity.

where $c = (53.4 \pm 1.1) \times 10^{-3}$, valid for $4 \leq S \leq 12$, S being the equivalent square msr field size in cm. For the range of beam qualities in this COP, the beam quality index is assumed to correspond to $\%dd(10,10)$ [38], i.e.:

$$\%dd(10,10)_x = \%dd(10,10) \tag{30}$$

If the SSD is not equal to 100 cm an additional correction is required. The percentage depth dose at the SSD and a depth of 10 cm, obtained from Eq. (31), is then denoted $\%dd^{\mathrm{SSD}}(10,10)$, and $\%dd(10,10)$ is derived as:

$$\%dd(10,10) = \%dd^{\mathrm{SSD}}(10,10) \times \frac{\mathrm{TMR}(10,11)}{\mathrm{TMR}\left(10,\frac{\mathrm{SSD}+10}{\mathrm{SSD}}10\right)} \times \frac{\mathrm{NPSF}(11)}{\mathrm{NPSF}\left(\frac{\mathrm{SSD}+10}{\mathrm{SSD}}10\right)} \times \left(\frac{100+z_{\max}}{110}\frac{\mathrm{SSD}+10}{\mathrm{SSD}+z_{\max}}\right)^2 \quad (31)$$

where TMR(z,S) is the tissue maximum ratio at depth z in water for an equivalent square field of size S (defined at the depth z) and NPSF(S) is the normalized peak-scatter factor for the field size S (see Ref. [32]). For SSD between 90 and 110 cm, a sufficiently accurate approximation is provided by omitting the TMR and NPSF ratios in Eq. (31).

5.3.4. Measurement in plastic water substitute phantoms

In situations where it is more convenient to use a plastic water substitute phantom than water, the absorbed dose to water can be derived from measurements in a plastic phantom by incorporating a phantom dose conversion factor $k_{Q_{\mathrm{msr}}}^{\mathrm{w,plastic}}$ into Eqs (24, 25, 27). For example, for case (b) in Section 5.3.2.1, Eq. (25) becomes:

$$D_{\mathrm{w},Q_{\mathrm{msr}}}^{f_{\mathrm{msr}}}\left(z_{\mathrm{ref}}\right) = M_{\mathrm{plastic},Q_{\mathrm{msr}}}^{f_{\mathrm{msr}}}\left(z_{\mathrm{eq,plastic}}\right) N_{D,\mathrm{w},Q_0}^{f_{\mathrm{ref}}} k_{Q_{\mathrm{msr}},Q_0}^{f_{\mathrm{msr}},f_{\mathrm{ref}}} k_{Q_{\mathrm{msr}}}^{\mathrm{w,plastic}} \quad (32)$$

where $M_{\mathrm{plastic},Q_{\mathrm{msr}}}^{f_{\mathrm{msr}}}\left(z_{\mathrm{eq,plastic}}\right)$ is the ionization chamber reading in the plastic water substitute phantom corrected for influence quantities and the other quantities have the same meaning as before[10]. The phantom dose conversion factor in Eq. (32) is determined experimentally as a ratio of ionization chamber readings corrected for influence quantities in the water phantom at a depth z_{ref} and in the plastic water substitute phantom at the equivalent depth $z_{\mathrm{eq,plastic}}$:

[10] Note, however, that in the Gamma Knife, the calculations of overall correction factors already incorporate the plastic conversion factor and the depth scaling, so neither the additional correction factor nor an equivalent depth have to be accounted for.

$$k_{Q_{\mathrm{msr}}}^{\mathrm{w,plastic}} = \frac{M_{\mathrm{w},Q_{\mathrm{msr}}}^{f_{\mathrm{msr}}}\left(z_{\mathrm{ref}}\right)}{M_{\mathrm{plastic},Q_{\mathrm{msr}}}^{f_{\mathrm{msr}}}\left(z_{\mathrm{eq,plastic}}\right)} \tag{33}$$

It is emphasized that an accurate experimental determination has the advantage that loss of homogeneity or air pockets originating during the manufacturing process of the phantom material are taken into account provided the plate order is kept unchanged. Note also that, for a given phantom, this experimental procedure needs to be performed only once (it is advised that this be verified periodically, within the standard QA procedures).

In Eqs (32, 33), the depth in plastic water substitute phantom $z_{\mathrm{eq,plastic}}$ is taken to be equivalent to the reference depth in water z_{ref}, scaled according to the ratio of electron densities (see Attix eq. (13.49a) [13]), i.e.:

$$z_{\mathrm{eq,plastic}} = \frac{\rho_{\mathrm{w}}}{\rho_{\mathrm{plastic}}} \frac{\left(\frac{Z}{A}\right)_{\mathrm{w}}}{\left(\frac{Z}{A}\right)_{\mathrm{plastic}}} z_{\mathrm{ref}} \tag{34}$$

Note that it is advised that the field size be scaled according to the ratio of electron densities and that the SDD has to be kept constant in an isocentric set-up (or in case of an SSD set-up the change of SDD has to be corrected for). The effects are small for materials with electron densities close to that of water [101], but differences for PMMA are substantial.

Values of $(Z/A)_{\mathrm{med}}$ can be found in Ref. [154] for some plastic materials, or calculated from the composition of the substance using the Bragg additivity rule, i.e.:

$$\left(\frac{Z}{A}\right)_{\mathrm{med}} = \sum_i w_i \left(\frac{Z_i}{A_i}\right) \tag{35}$$

where w_i is the fraction by weight and Z_i and A_i are the atomic number and atomic mass of the constituent element i. Typical elemental compositions, densities, mean atomic numbers, mean excitation energies, values of $(Z/A)_{\mathrm{med}}$ and depths equivalent to 10 cm of water for some plastic materials used in dosimetry (and for water) are given in Table 20. For the correction for influence quantities in the measurement of the ionization chamber reading in plastic water substitute phantoms, the temperature needs to be monitored at the location of the cavity, or

TABLE 20. ELEMENTAL COMPOSITION (FRACTION BY WEIGHT), NOMINAL AVERAGE DENSITY, MEAN ATOMIC NUMBER, MEAN EXCITATION ENERGY, $(Z/A)_{med}$ AND $Z_{eq,plastic}(10)$ OF COMMON PHANTOM MATERIALS USED AS WATER SUBSTITUTES

Material	Water, liquid[a]	ABS[b]	Plastic Water®[c]	PMMA[a,d]	Polystyrene[a]	RW-1 water eq[a]	RW-2 muscle eq[a]	RW-3	Solid Water RMI-45®[a,e]	Solid Water WT1[a]	Virtual Water™[f]
H	0.111 9	0.054 0	0.092 5	0.080 5	0.077 4	0.132 0	0.070 0	0.075 9	0.080 9	0.081 0	0.077 0
C		0.877 7	0.628 2	0.599 8	0.922 6	0.794 0	0.830 0	0.904 1	0.672 2	0.672 0	0.687
N		0.068 2	0.010 0						0.024 0	0.024 0	0.022 7
O	0.888 1		0.179 4	0.319 6		0.038 0	0.040 0	0.008 0	0.198 4	0.199 0	0.188 6
Mg						0.009 0					
Cl			0.009 6						0.001 3	0.001 0	0.001 3
Ca			0.079 5			0.027 0			0.023 2	0.023 0	0.023 1
Ti							0.060 0	0.012 0			
Br			0.000 3								
Nominal density $\rho_{plastic}$ (g/cm^3)	0.998	1.066	1.030	1.190	1.060	0.970	1.110	1.045	1.030	1.020	1.030

TABLE 20. ELEMENTAL COMPOSITION (FRACTION BY WEIGHT), NOMINAL AVERAGE DENSITY, MEAN ATOMIC NUMBER, MEAN EXCITATION ENERGY, $(Z/A)_{med}$ AND $Z_{eq,plastic}(10)$ OF COMMON PHANTOM MATERIALS USED AS WATER SUBSTITUTES (cont.)

Material	Water, liquid[a]	ABS[b]	Plastic Water®[c]	PMMA[a,d]	Polystyrene[a]	RW-1 water eq[a]	RW-2 muscle eq[a]	RW-3	Solid Water RMI-45®[a,e]	Solid Water WT1[a]	Virtual Water™[f]
$\bar{Z}$[g]	6.60	5.56	6.62	5.85	5.29	5.29	6.25	5.48	5.96	5.95	5.97
I (eV)	78.0	70.0	69.9	74.0	68.7	59.8	71.3	67.1	68.7	68.6	69.2
$(Z/A)_{med}$	0.555 1	0.526 2	0.544 6	0.539 4	0.537 7	0.564 5	0.531 6	0.536 4	0.539 5	0.539 5	0.537 5
$z_{eq,plastic}$ (10)[h]	—	9.88	9.88	8.63	9.72	10.12	9.39	9.88	9.97	10.07	10.01

Note: Owing to significant discrepancies in density quoted by the manufacturers, it is advised that the phantom density always be determined experimentally. For comparison, liquid water is also included.

[a] See Refs [154–156].

[b] Acrylonitrile butadiene styrene (ABS).

[c] Nuclear Associates (New York, NY).

[d] Polymethylmethacrylate, also known as acrylic. Trade names are Lucite, Plexiglas or Perspex.

[e] Gammex/Sun Nuclear (Middleton, WI).

[f] Med-Cal, Inc.

[g] For the definition of mean atomic number, see, for instance, Refs [157, 158].

[h] Equivalent depth in plastic, in cm, of $z_{ref} = 10$ cm. If $z_{ref} \neq 10$ cm, the numbers in this row are multiplied by $z_{ref}/10$ cm.

the plastic phantom needs to be in thermal equilibrium with the room temperature in which the measurement is performed.

5.4. CORRECTION FOR INFLUENCE QUANTITIES

This section summarizes the procedures to correct the raw ionization chamber reading ${}_{\text{raw}}M_{Q_{\text{msr}}}^{f_{\text{msr}}}$ for influence quantities to obtain $M_{Q_{\text{msr}}}^{f_{\text{msr}}}$ using air filled reference ionization chambers[11].

5.4.1. Air density correction

All ionization chambers recommended for reference dosimetry in this COP are open to ambient air. The mass of air in the cavity will thus depend on atmospheric conditions (temperature and pressure). The factor k_{TP} to correct for these conditions is given by:

$$k_{\text{TP}} = \frac{(T + 273.15)}{(T_0 + 273.15)} \frac{P_0}{P} \tag{36}$$

where T is the temperature in °C and P the pressure in kPa of the air in the cavity of the ionization chamber, and T_0 and P_0 are the reference conditions for temperature and pressure for which the calibration coefficient of the ionization chamber is valid, i.e. 20°C (or 22°C for calibrations from standards laboratories in North America) and 101.325 kPa, respectively.

5.4.2. Humidity

No correction is necessary for relative humidity if the ionization chamber is used in a range of 20% to 80% relative humidity and has a calibration coefficient valid at a relative humidity of 50%. In the unlikely case that the relative humidity is outside the range of 20–80%, a correction factor is needed [1, 159].

5.4.3. Electrometer calibration factor k_{elec}

When the ionization chamber and electrometer are calibrated separately, the calibration coefficient for the ionization chamber is given in units Gy/C or

[11] More background and details on these corrections can be found in Refs [1, 2, 7].

a multiple (e.g. mGy/nC or cGy/nC). The calibration factor k_{elec} obtained for the electrometer converts the electrometer reading to charge and is expressed in units C/rdg. If the reading of the electrometer is in terms of charge, the electrometer calibration factor is dimensionless. If the ionization chamber and the electrometer are calibrated together, as one measurement assembly, no separate electrometer calibration factor has to be applied.

5.4.4. Polarity correction

The correction factor for polarity in a given radiation beam is given by:

$$k_{pol} = \frac{|M_+| + |M_-|}{2M} \tag{37}$$

where M_+ and M_- are the electrometer readings obtained at positive and negative polarity, respectively and M is the electrometer reading taken at the polarity used routinely. The polarity used routinely is the same as that used during the calibration of the ionization chamber. For details on the situation where the standards laboratory has not applied this correction during calibration, refer to Ref. [1]. Given the observations discussed in Section 4, it is advised that attention be paid to long stabilization times that may be required for small volume ionization chambers. Polarity effects may also be field size dependent owing to the varying portion of the stem being irradiated, hence it is important that this effect be investigated for every ionization chamber used for small field dosimetry.

5.4.5. Recombination correction

The incomplete collection of charge in an ionization chamber cavity owing to the recombination of ions requires the use of a correction factor k_s. Two separate effects take place: (i) the recombination of ions formed by separate ionizing particle tracks, termed general (or volume) recombination, which depends on the density of ionizing particles and therefore on the dose rate; and (ii) the recombination of ions formed by a single ionizing particle track, referred to as initial recombination, which is independent of the dose rate. Both effects depend on the chamber geometry and on the applied polarizing voltage. In conventional radiotherapy beams, initial recombination is generally less than 0.2%.

In continuous radiation, i.e. ^{60}Co gamma rays, the two voltage method may be used and a correction factor derived using the relation:

$$k_s = \frac{\left(\frac{V_1}{V_2}\right)^2 - 1}{\left(\frac{V_1}{V_2}\right)^2 - \frac{M_1}{M_2}} \tag{38}$$

where M_1 and M_2 are the collected charges at the polarizing voltages V_1 and V_2, M_1 being the ionization chamber reading at the normal operating voltage V_1 and V_2 being a lower voltage. This relation is based on a linear dependence of $1/M$ on $1/V^2$, which describes the effect of general recombination in continuous beams. For clinical purposes, general recombination can be considered negligible in ^{60}Co beams.

For pulsed beams, the recombination correction factor k_s is derived using the two voltage method [160]. This method assumes a linear dependence of $1/M$ on $1/V$ (it is advised that this assumption be verified when commissioning a new chamber) and uses the measured values of the collected charges M_1 and M_2 at the polarizing voltages V_1 and V_2, respectively, measured using the same irradiation conditions. V_1 is the normal operating voltage and V_2 a lower voltage; the ratio V_1/V_2 is ideally equal to or larger than 3. The polarity effect will change with the voltage, and M_1 and M_2 are each corrected for this effect using Eq. (37). The recombination correction factor k_s at the normal operating voltage V_1 is obtained from:

$$k_s = a_0 + a_1\left(\frac{M_1}{M_2}\right) + a_2\left(\frac{M_1}{M_2}\right)^2 \tag{39}$$

where the constants a_i are given in Table 21 for pulsed radiation [161].

For $k_s < 1.03$, the correction can be approximated to within 0.1% using the relation:

$$k_s = 1 + \frac{\left(\frac{M_1}{M_2}\right) - 1}{\left(\frac{V_1}{V_2}\right) - 1} \tag{40}$$

Note that the correction factor k_s evaluated using the two voltage method in pulsed beams corrects for both general and initial recombination. In pulsed beams, where general recombination is dominant, the recombination correction for a given chamber will scale approximately linearly with dose rate.

TABLE 21. QUADRATIC FIT COEFFICIENTS, FOR THE CALCULATION OF k_s BY THE 'TWO VOLTAGE' TECHNIQUE IN PULSED RADIATION, AS A FUNCTION OF THE VOLTAGE RATIO V_1/V_2 [161]

V_1/V_2	a_0	a_1	a_2
2.0	2.337	−3.636	2.299
2.5	1.474	−1.587	1.114
3.0	1.198	−0.875	0.677
3.5	1.080	−0.542	0.463
4.0	1.022	−0.363	0.341
5.0	0.975	−0.188	0.214

If it is not known if the relation between $1/M$ and $1/V$ is linear, or if there is any doubt about this, it is advised that a Jaffé plot of $1/M$ versus $1/V$ be measured. This is especially the case for some small volume ionization chambers in which charge recombination effects may distort the saturation curve. Small volume chambers may also exhibit asymmetric saturation curves for opposing polarities (essentially a voltage dependent polarity effect). Given the observations discussed in Section 4, it is advised that attention be paid to the long stabilization times that may be required for small volume ionization chambers. For FFF beams, where dose per pulse values are substantially larger than in WFF beams, studies have shown that recombination can be treated in the same way and that the two voltage technique is accurate under the same conditions as for WFF beams [162–165].

5.5. CROSS-CALIBRATION IN THE msr FIELD

For cross-calibrating a field ionization chamber in an msr field, the same considerations as in Ref. [1] apply. If a calibration coefficient for a reference chamber ('REF') is available for a given msr field size f_{msr}, a field chamber may be cross-calibrated against the calibrated reference. The chambers are compared by alternately placing them in a water phantom with their reference points at z_{ref}; the readings are corrected for influence quantities.

The calibration coefficient of the field chamber ('FIELD') is given by:

$$\left[N_{D,\mathrm{w},Q_{\mathrm{msr}}}^{f_{\mathrm{msr}}}\right]_{\mathrm{FIELD}} = \frac{\left[M_{Q_{\mathrm{msr}}}^{f_{\mathrm{msr}}}\right]_{\mathrm{REF}}}{\left[M_{Q_{\mathrm{msr}}}^{f_{\mathrm{msr}}}\right]_{\mathrm{FIELD}}} \left[N_{D,\mathrm{w},Q_{\mathrm{msr}}}^{f_{\mathrm{msr}}}\right]_{\mathrm{REF}} \tag{41}$$

The resulting calibration coefficient $\left[N_{D,\mathrm{w},Q_{\mathrm{msr}}}^{f_{\mathrm{msr}}}\right]_{\mathrm{FIELD}}$ can then be used for reference dosimetry in an msr field using Eq. (24) for the same normal atmospheric conditions of temperature and pressure as for the reference chamber 'REF'.

If a calibration of the reference chamber in the msr field is not available, a cross-calibration coefficient can be obtained with:

$$\left[N_{D,\mathrm{w},Q_{\mathrm{msr}}}^{f_{\mathrm{msr}}}\right]_{\mathrm{FIELD}} = \frac{\left[D_{\mathrm{w},Q_{\mathrm{msr}}}^{f_{\mathrm{msr}}}\right]_{\mathrm{REF}}}{\left[M_{Q_{\mathrm{msr}}}^{f_{\mathrm{msr}}}\right]_{\mathrm{FIELD}}} \tag{42}$$

where $\left[D_{\mathrm{w},Q_{\mathrm{msr}}}^{f_{\mathrm{msr}}}\right]_{\mathrm{REF}}$ is obtained with Eqs (25) or (27) using the reference ionization chamber.

6. CODE OF PRACTICE FOR RELATIVE DOSIMETRY OF SMALL FIELDS

A full dosimetric characterization of small fields for clinical use requires not only the calibration of the beam under reference conditions (addressed in the previous section) but also the determination of field output factors, necessary for the calculation of monitor units or treatment time, and measured central axis percentage depth dose (PDD) distributions, tissue phantom ratios (TPR) or tissue maximum ratios (TMR), and lateral beam profiles. This COP provides guidance for measurements of field output factors and lateral beam profiles at the measurement depth because of their importance in the determination of the field size and the volume averaging correction. Guidance for the measurements of relative dose distributions can be found in other publications, such as Ref. [166] and, specifically for small fields, Refs [12, 167, 168].

6.1. EQUIPMENT

6.1.1. Detectors for relative dosimetry

The guidance regarding detectors for relative dosimetry is given in Section 4.2.1. It must be emphasized that no ideal detector exists for measurements in small fields. For the determination of both field output factors and lateral beam profiles, the use of two or preferably three different types of suitable detectors is therefore advised so that redundancy in the results can provide more confidence and assurance that no significant dosimetry errors are being made. An example could be a combination of detectors with correction factors above and below unity (so that the product of these factors is close to one), such as a small air filled ionization chamber, radiochromic film and an unshielded diode, or a diamond, liquid ion chamber and an organic scintillator.

6.1.1.1. Detectors for measuring field output factors

A full discussion on detectors used for measurements of dosimetric parameters for relative dosimetry is given in Chapter 4. As discussed in Section 3.2.3, field output factors (see also the definition in Section 2.3.2.1) are derived from a ratio of detector readings according to:

$$\Omega_{Q_{\text{clin}},Q_{\text{msr}}}^{f_{\text{clin}},f_{\text{msr}}} = \frac{M_{Q_{\text{clin}}}^{f_{\text{clin}}}}{M_{Q_{\text{msr}}}^{f_{\text{msr}}}} k_{Q_{\text{clin}},Q_{\text{msr}}}^{f_{\text{clin}},f_{\text{msr}}} \tag{43}$$

where $k_{Q_{\text{clin}},Q_{\text{msr}}}^{f_{\text{clin}},f_{\text{msr}}}$ is the output correction factor, which can be determined as a directly measured value, an experimental generic value or a Monte Carlo calculated generic value. Data for $k_{Q_{\text{clin}},Q_{\text{msr}}}^{f_{\text{clin}},f_{\text{msr}}}$ as a function of field size are given in Section 6.6 for different detectors and machines.

The minimum field size recommended for measurements with real time detectors (those providing an instantaneous and potentially continuous signal readout) and for off-line detectors (those that provide a readout after post-processing) is such that the detector specific output correction factor is not greater than ±5% for a particular machine. For this reason Tables 23–27 do not include $k_{Q_{\text{clin}},Q_{\text{msr}}}^{f_{\text{clin}},f_{\text{msr}}}$ values outside this interval. It is understood that detectors or machine configurations not included in the tables require an experimental or Monte Carlo determination, but extrapolation of the tabulated values is to be avoided.

As an example, according to the tabulated values, the PTW 60008 and 60016 shielded diodes are not to be used for field sizes smaller than 1 cm (equivalent square) in WFF and FFF machines with 6 MV (Table 26) or 10 MV (Table 27).

For the determination of field output factors, the volume averaging effect will be one of the limiting issues for the choice of a detector. The detector size is such that the volume averaging correction factor $(k_{\text{vol}})_{Q_{\text{clin}}}^{f_{\text{clin}}}$ for the small field of interest, f_{clin}, in the beam of quality Q_{clin}[12], is limited by $0.95 \leq (k_{\text{vol}})_{Q_{\text{clin}}}^{f_{\text{clin}}} \leq 1.05$. The volume averaging correction factor $(k_{\text{vol}})_{Q_{\text{clin}}}^{f_{\text{clin}}}$ is calculated using:

$$(k_{\text{vol}})_{Q_{\text{clin}}}^{f_{\text{clin}}} = \frac{\iint_A w(x,y)\,\mathrm{d}x\,\mathrm{d}y}{\iint_A w(x,y)\,\mathrm{OAR}(x,y)\,\mathrm{d}x\,\mathrm{d}y} \tag{44}$$

where $w(x,y)$ is a weighting function specific to the ionization chamber geometry, described in Appendix I, where examples of the calculation of the volume

[12] Note that no procedure is provided to determine the beam quality Q_{clin} of the clinical field. It should be understood as the beam quality of a small field at a radiotherapy machine for which the beam quality of the reference field is Q_{ref} or Q_{msr}. For the user, the only relevant difference from the reference field is the field size, but the beam quality Q_{clin} is explicitly used to indicate that the charged particle spectrum at the measurement depth will be different from the charged particle spectrum in the reference field.

averaging correction factor are given. It is advised that the field size dependence of the detector's response be smaller than 2% over the range of field sizes measured. This number is a typical variation of the change in the response of unshielded diodes for an increase of the equivalent square field size *S* by 5 cm.

As discussed be Section 4.2.1, a number of specialized detectors (e.g. radiophotoluminescent detectors, plastic and organic scintillators) and techniques to use them are available. Experience on their use is limited to workers with specialized training and access to specialized equipment. It is advised that users of these detectors develop significant expertise before using them for measurements of clinical dosimetric parameters.

Dosimetry of small fields in non-water and heterogeneous media is beyond the scope of this COP, but it is important to be aware that these conditions may introduce significant energy and material dependent perturbations, and using generic data for such conditions can result in significant clinical errors [169–172].

6.1.1.2. Detectors for measuring beam profiles

It is advised that for the experimental determination of lateral beam profiles, detectors have high spatial resolution (requiring the use of detectors with a small area perpendicular to the beam axis or quasi-continuous detectors such as radiochromic film), limited energy dependence in their response and limited dose rate or dose-per-pulse dependence (see Table 6 for limits).

Liquid ion chambers, unshielded diodes, microdiamonds and organic scintillators have a small sensitive volume and are suitable for profile measurements using a scanning system. Given the asymmetries in their construction and the influence of stem irradiation effects, the orientation is always such that the stem is parallel to the beam axis. It is advised that the effect on the profiles of irradiating the stem and parts of the cables always be investigated, minimized and, if possible, corrected for. Also, the effect of charge recombination needs to be assessed and, if necessary, corrected for.

Radiochromic film is very suitable for lateral profile measurements, but needs adequate readout and calibration procedures. Any other detector with a dispersed radiosensitive agent (such as a gel dosimeter) needs to be thoroughly investigated, characterized and benchmarked against other detectors.

6.1.2. Phantoms

Guidance regarding phantoms is given in Section 4.2.2.

6.2. IN-PHANTOM DETECTOR SET-UP

Accurate and reproducible measurements of beam profiles in small fields require not only the choice of an appropriate detector in terms of its size and composition but also the presence of a number of machine and detector QA procedures in place with more stringent tolerances than for broad beam dosimetry. These include procedures that verify jaw and collimator position, beam alignment, alignment of the water phantom and the movement of the scanning system with the beam, detector and electrometer functionality, etc. It is beyond the scope of this COP to provide guidance on these QA procedures, which can be found in other publications [12, 29, 31, 83, 168, 173–175].

For the determination of beam profiles and field output factors, accurate set-up of the detector in a 3-D full scatter water tank is required [166]. For field output factor measurements with off-line detectors that are not waterproof, it could be more practical to perform the measurement in a solid, water equivalent plastic phantom. Guidance on setting up such a detector for that purpose is also given.

6.2.1. Detector orientation

The orientation of the detector axis with respect to the beam axis has an influence on the shape of the measured profile or field output factor. A general rule is that, whenever possible, the detector is oriented such that the smallest dimension of its sensitive volume is perpendicular to the scanning direction. This is, however, not always possible because of detector specific considerations such as asymmetry of construction and the location of the stem.

Some microionization chambers designed specifically for relative dosimetry in small beams show a particular sensitivity to irradiation of stem and cable owing to their very small volume. To minimize this effect, the chamber is oriented with its stem parallel to the beam axis, in order to ensure uniform stem irradiation, while taking care that the cable is positioned to minimize its irradiated length when full travel of the detector is allowed. The scanning orientation to avoid is with the stem perpendicular to beam axis and parallel to the scanning direction (c.f. orientation 3 in Fig. 18).

Scanning diodes have been widely used for the measurement of lateral beam profiles, owing to their superior spatial resolution compared to ionization chambers and higher signal. Shielded and unshielded diodes both have disk shaped active volumes, with larger diameter than depth of their depleted regions, which would reasonably suggest orienting the diode's sensitive disk parallel to the beam axis, in order to make best use of their spatial resolution. However, it has been shown that this orientation produces asymmetric lateral profiles, owing to

distortions caused by the unequal distribution of material around the chip [176]. For scintillating fibre dosimeters, the technique used for the establishment of the Cerenkov correction procedure affects the optimal detector direction for scanning [137].

Advised orientations for various point detectors with respect to the beam's central axis, for relative dosimetry in small photon fields, are given in Table 22.

TABLE 22. DETECTOR ORIENTATION, WITH RESPECT TO THE BEAM CENTRAL AXIS, FOR RELATIVE DOSIMETRY IN SMALL PHOTON FIELDS

Detector type	Detector's geometrical reference	Lateral beam profiles	Field output factors
Cylindrical micro ion chamber	Axis	Parallel or perpendicular	Perpendicular
Liquid ion chamber	Axis	Perpendicular	Parallel
Silicon shielded diode	Axis	Parallel	Parallel
Silicon unshielded diode	Axis	Parallel	Parallel
Diamond detector	Axis	Parallel	Parallel
Radiochromic film	Film surface	Perpendicular	Perpendicular

Note: See Figs 18 and 19.

6.2.2. Placement of the detector's reference point at the reference depth

The detector is placed with its reference point at the reference depth. For each detector, this point may depend on the orientation of the detector with respect to the radiation beam. For cylindrical ionization chambers in the perpendicular orientation (with the major axis of the detector perpendicular to the beam axis), it is the centre of the cavity volume of the chamber on the chamber axis (the location on the central axis is usually specified by the manufacturer as a given distance from the tip of the chamber), or it is sometimes indicated by a fiducial mark. For cylindrical ionization chambers in the parallel orientation (with the major axis of the detector parallel to the beam axis), it is the tip of the ionization chamber. For solid state detectors, the reference point for orientation

of the stem parallel to the beam's axis is usually specified by the manufacturer with respect to the flat face or tip of the detector and often marked with a circle (indicated in Table 7 for the detectors listed). For the perpendicular orientation (with the major axis of the detector perpendicular to the beam axis) the centre of the detector is used.

6.2.3. Detector alignment with beam central axis

For small field dosimetry, it is essential to ensure accurate alignment of the detector with respect to the beam's central axis given the sharp maximum and steep gradients in lateral beam profiles. Figure 16 [90] illustrates that alignment based on laser beams or the machine's light field with typical tolerances of 1 mm is not accurate enough for the measurement of field output factors for small fields. After initial alignment based on lasers or light field, further refinement of the alignment is thus required. This requires measurement of profiles in two dimensions at the measurement depth.

6.2.3.1. Alignment of real time detectors

With real time detectors, the alignment of the detector with the central axis of the beam can be achieved using the scanning system. These scans are

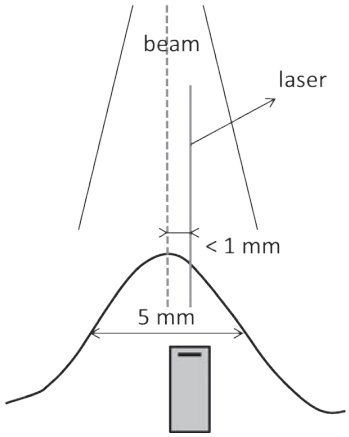

FIG. 16. Demonstration of the influence of clinical set-up accuracy: the beam laser (solid vertical line) is calibrated with a misalignment tolerance of less than 1 mm from the beam's central axis in a field of 5 mm width, but this does not ensure a negligible underestimation of the profile maximum (reproduced from Ref. [90] with the permission of the American Association of Physicists in Medicine).

performed at slow speed, with an appropriate step size for the field (of the order of 0.1 mm for the smallest fields) and with attention to potential effects of hysteresis of the scanning system. The alignment can be performed based either on the centre of the two 50% profile levels or on the profile maximum assuming that the beam profile is symmetric. At the same time this provides a measurement of the FWHM field size specification. Given that tiny changes in the collimator position can result in substantial changes of the absorbed dose to water at the centre of the field, this alignment procedure and FWHM determination is performed every time the field has been set or re-set by moving the collimator for MLC based radiotherapy machines. The alignment has to be performed in two orthogonal directions, and this may require an iterative procedure to determine the centre of the field, accounting for the possibility of tiny phantom misalignments.

Note that for the measurement of depth dose profiles along the beam axis, the centre of the field has to be determined at different depths and, based on that information, the phantom and scanning system needs to be accurately aligned with the beam central axis (CAX correction). For the procedures in this COP, which are restricted to field output factor and lateral beam profile measurements, this is not critical; however for the measurement of lateral beam profiles, it is advised that they be measured at the same depth at which the output factors are determined.

6.2.3.2. Lateral alignment of off-line detectors

The main problem with setting up an off-line detector is that the radiation-induced signal cannot be observed immediately, and any radiation exposure during alignment of the detector contributes to the signal. Thus, the detector itself cannot be used to detect the centre of the field. Various methods have been described to deal with this alignment problem, of which three are discussed below. For MLC based radiotherapy machines, this alignment procedure and FWHM determination is performed every time the field has been set or re-set by moving the collimator.

(a) Off-line detector set-up using attachment system

A specially constructed attachment system on the scanning arm in a scanning phantom can be used to allow a real time detector to be replaced with a passive detector. This requires very accurate machining of the real time and off-line detector holders to ensure accurate positioning of the reference point of both detectors at the same location. Often, ancillary parts (e.g. so-called stop thimbles for ionization chambers) can facilitate the insertion of detectors in their holders with the required positioning

accuracy. The user is referred to the product catalogue of the ionization chamber manufacturer.

(b) Off-line detector set-up using film

This method is particularly suited for measurements in a solid water equivalent phantom [177]. After preliminary lateral positioning of the detector insert in a phantom slab at the correct SDD and aligned with the beam axis based on lasers and/or light field, a radiochromic film is inserted between the slab with the detector insert and the slab further away from beam source to quantify any necessary additional lateral displacement of the phantom. To enhance contrast, a dummy detector made of a high Z material, or with a high Z material bead at the location of the reference point, could be inserted. If necessary the procedure is repeated iteratively. Once alignment within the required tolerance has been achieved, the detector is inserted and the amount of phantom material necessary to position the detector's reference point at the measurement depth is added on top or in front of the slab containing the detector insert. It is essential with each handling for taking away or adding slabs that the lateral alignment of the slab be adequately maintained.
In addition to this alignment procedure, a radiochromic film could be inserted behind the slab containing the detector for each detector irradiation, provided the detector contour can be clearly resolved on the exposed film. This enables a volume averaging correction to be made for each individual detector retrospectively, based on the measured lateral beam profiles and the measured position of the detector with respect to the field. Ideally, a slab with a special insert would be designed for this purpose, such that the slab containing the detector does not have to be removed for every irradiation.

(c) Off-line detector set-up using an electronic portal imaging device

This method is suited for measurements in both a water phantom and a solid water equivalent phantom [100]. After initial positioning of the detector insert in the water phantom or a phantom slab at the correct SDD and aligned with the beam axis based on lasers and/or light field, an image of the irradiation set-up is taken using an electronic portal imaging device (EPID) below or behind the phantom to quantify any necessary additional lateral displacement of the detector holder in the scanning system or of the solid phantom. An example of such an EPID image is shown in Fig. 17. To enhance contrast, a dummy detector made of a high Z material, or with a high Z material bead at the location of the reference point, is inserted.

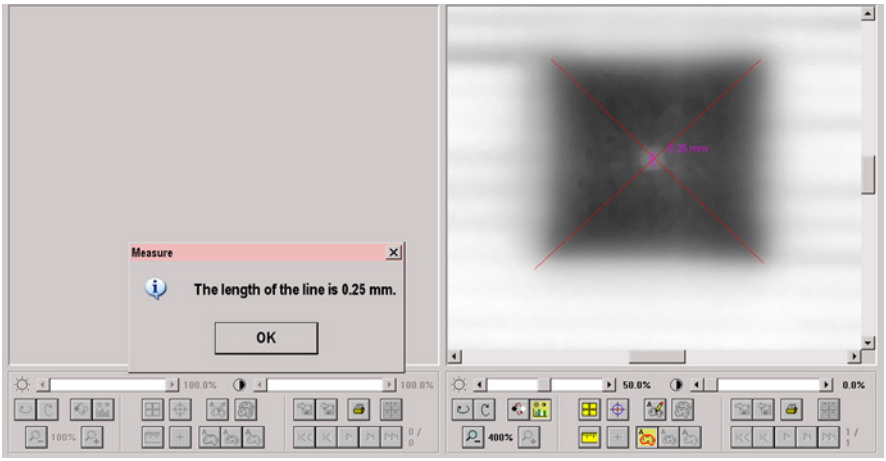

FIG. 17. EPID image showing the detector's position using a marker and measurement of the distance of the centre of the marker from the beam central axis, which was in this illustrative example for a 1.8 cm × 1.8 cm field found to be within 0.25 mm [100] (courtesy of G. Azangwe, National University of Science and Technology, Zimbabwe).

If necessary the procedure is repeated iteratively. Once alignment within the required tolerance has been achieved, the detector is inserted in the detector holder on the scanning system and moved to the previously determined measurement point in the water phantom or, in the case of a solid phantom, the correct amount of phantom material to position the detector's reference point at the measurement depth is added on top or in front of the slab containing the detector insert. It is essential with each handling for taking away or adding slabs that the lateral alignment of the slab be adequately maintained. The EPID image usually does not have sufficient resolution to work out retrospectively the volume averaging correction for each individual detector based on the measured lateral beam profiles and the measured position of the detector with respect to the field.

6.2.4. Set-up of SSD or SAD

The measurement of field output factors and lateral beam profile is performed at the same SSD or source-to-axis distance (SAD) as was used for reference dosimetry. For these relative measurements, the exact distance to the beam source is not critical and tolerances used for reference dosimetry are always sufficient.

6.3. MEASUREMENT OF LATERAL BEAM PROFILES

The detector is set-up as described in Section 6.2. The field is set using the same method of collimation that would be used clinically (e.g. using cones, jaws, MLCs, etc.).

The scanning speed and step size are chosen taking into account the following considerations: (i) the disturbance of the water surface is minimized (this can be checked by focusing the in-room cameras on the water surface), (ii) for small field sizes the speed is at its lowest value over the central beam area, and (iii) the step size is chosen such that there are a large number of steps over the entire range of the beam profile (typically a step size of 0.1 mm is required).

It is advised that the measurements be performed by referencing the signal of the field detector to that of a monitor detector to allow correction for temporal variations in machine output during the measurements. It is important that any device used to obtain the monitor signal not affect the measurement signal; thus for small fields it is not acceptable to place a detector in the corner of the beam as is typically done for large fields. Ideally, the monitor signal is taken from the linac's internal chamber signal, but this may not be possible in a clinical situation. Alternatively, a transmission detector can be placed below the linac head or a thick walled large area plane-parallel ionization chamber can be placed at a larger depth than the field detector within the phantom. Accelerator heads of some of the manufacturers contain dedicated locations for the introduction of a monitor chamber in a manner that does not perturb the radiation field.

As with the use of any detectors that produce small signals, it is advised that care be taken in the detector orientation (see Section 6.2.1) to minimize the effect of extra cameral current due to stem or cable signals. The acceptable orientations for ionization chambers and real time solid state detectors such as diodes and diamonds are illustrated in Figs 18 and 19. Note that for organic scintillators only, orientation (2) in Fig. 19 is acceptable because of the Cerenkov light induced in the cable [137].

Preferably, at least two different types of detectors are used and the results compared to ensure a robust evaluation of beam profiles.

6.4. DETERMINATION OF ABSORBED DOSE AT z_{max}

Section 5.3.2 provides a methodology for determining the absorbed dose at z_{ref}. However, the calibration of clinical treatment machines is often specified at the depth of maximum dose, z_{max}. To determine the absorbed dose at this depth, it is advised that the user, for a given beam, use the central axis depth dose profiles

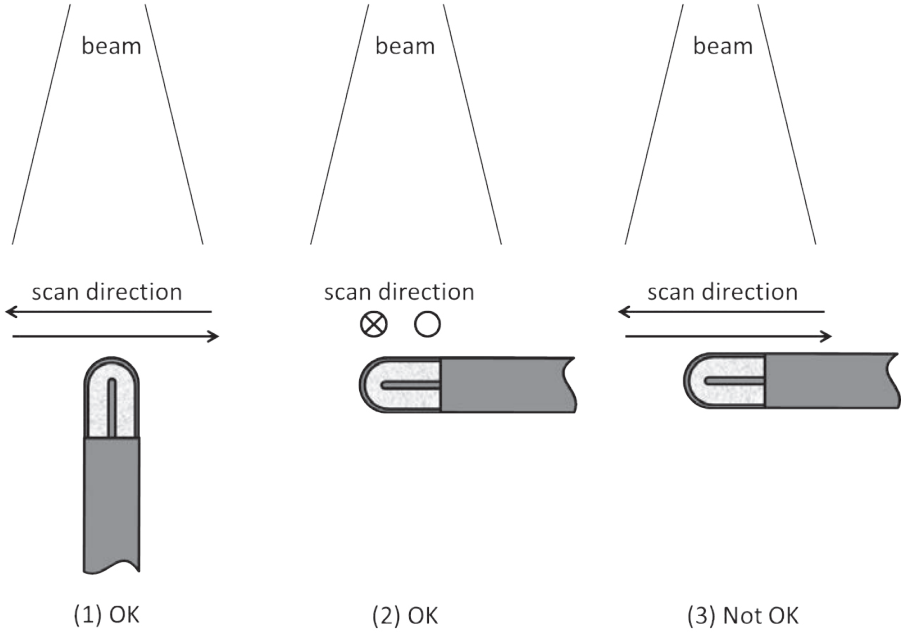

FIG. 18. Possible orientations of an ionization chamber for measurements of lateral beam profiles (arrows indicate scanning directions in the paper plane while circle and crossed circle symbols refer to scanning directions perpendicular to the paper plane).

(percentage depth dose data for SSD set-ups and TPR or TMR for SAD set-ups). It is beyond the scope of this COP to provide guidelines for these measurements (for guidance on the measurements of central axis depth dose profiles, see Ref. [166] and, specifically for small fields, Refs [12, 167, 168]).

6.5. DETERMINATION OF IN-PHANTOM FIELD OUTPUT FACTORS

6.5.1. Reference conditions

In-phantom field output factors for clinical beams f_{clin} are measured at the same reference depth used for measurements in the msr field f_{msr}. Section 5.3.2 provides the methodology for determining the absorbed dose at z_{ref} under machine specific reference conditions. According to Ref. [1], z_{ref} is 10 g/cm^2 for high energy photons. However, at the time of writing this COP, data for CyberKnife machines are only available referenced or defined at the depth of maximum dose

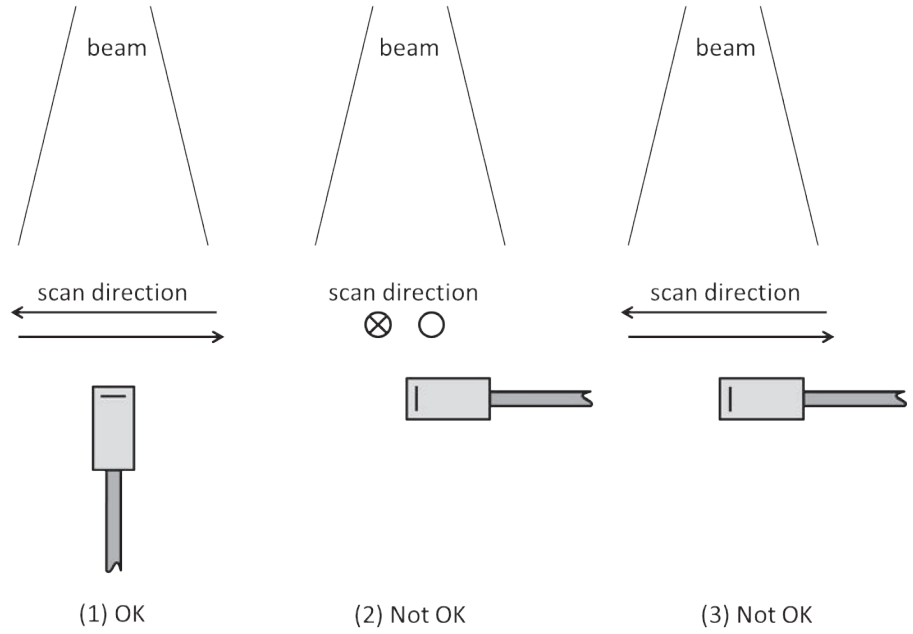

FIG. 19. Possible orientations of a solid state detector (diode, diamond) for measurements of lateral beam profiles (arrows indicate scanning directions in the paper plane while circle and crossed circle symbols refer to scanning directions perpendicular to the paper plane).

z_{max}. Therefore, CyberKnife machines will be considered a special case until more data are available. Note that this COP does not include guidance for the measurement of in-air output factors. Guidance for this purpose can be found in Refs [12, 166, 168, 178].

6.5.2. Determination of the equivalent square small field size

For the purpose of selecting output correction factors for each small field size, the in-plane and cross-plane dosimetric field widths, defined as the FWHM at the detector measurement depth, are derived from the lateral beam profiles obtained as described in Section 6.3.

For rectangular small fields with uneven in-plane and cross-plane FWHMs, the equivalent square small field size is given by the geometric mean [19], i.e.:

$$S_{clin} = \sqrt{A\,B} \tag{45}$$

where A and B correspond to the in-plane and cross-plane dosimetric field widths, defined as the FWHM at the measurement depth. Outside the condition $0.7 < A/B < 1.4$, which is usually not violated except for the smallest equivalent square small field sizes (below 0.6 cm), a larger uncertainty on the output correction factor than that specified in Table 37 should be considered.

For circular small fields with a FWHM radius r:

$$S_{\text{clin}} = r\sqrt{\pi} = 1.77r \tag{46}$$

r corresponds to the radius of the circular field defined by the points where, on average[13], the dose level amounts to 50% of the maximum dose at the measurement depth.

Note that this guidance is based on equal area of field sizes, which is different from the rule used for equivalent square msr field sizes in broad beams, based on equal photon scatter contributions.

6.5.3. Determination of field output factors

Field output factors, relating the absorbed dose to water of a clinical field f_{clin} to that of a reference field, f_{msr} or f_{ref}, are derived from a measured ratio of detector readings multiplied by an adequate correction that converts the ratio of measured readings into a ratio of values of absorbed dose to water. In this section expressions are given for the case of a clinical field relative to a machine specific reference field. They can also be used for a clinical field relative to a conventional 10 cm × 10 cm reference field, in which case 'msr' in the text and equations is replaced with 'ref'.

As already shown in Section 6.1.1.1, the field output factor, $\Omega_{Q_{\text{clin}},Q_{\text{msr}}}^{f_{\text{clin}},f_{\text{msr}}}$, relative to the f_{msr} is defined by:

$$\Omega_{Q_{\text{clin}},Q_{\text{msr}}}^{f_{\text{clin}},f_{\text{msr}}} = \frac{M_{Q_{\text{clin}}}^{f_{\text{clin}}}}{M_{Q_{\text{msr}}}^{f_{\text{msr}}}} k_{Q_{\text{clin}},Q_{\text{msr}}}^{f_{\text{clin}},f_{\text{msr}}} \tag{47}$$

where $M_{Q_{\text{clin}}}^{f_{\text{clin}}}$ and $M_{Q_{\text{msr}}}^{f_{\text{msr}}}$ are the readings of the detector (corrected for influence quantities) in the clinical field and the msr field, respectively. Values of the output correction factor $k_{Q_{\text{clin}},Q_{\text{msr}}}^{f_{\text{clin}},f_{\text{msr}}}$ for a range of detectors are given in Tables 23 to 27,

[13] To account for potential slight polar asymmetries and/or the effects of measurement fluctuations.

valid at 10 cm depth in water (except for the CyberKnife, for which they are valid at z_{max}). These factors include generic values for the volume averaging effect.

If the field output factor is determined with the intermediate field method using two detectors, i.e. an ionization chamber down to an intermediate field f_{int}, as small as possible but without small field conditions (which means that the outer edge of the detector is at least a distance r_{LCPE} away from any field edges), and a suitable small field detector such as a diode for smaller fields, thereby limiting the effect of energy dependence, then the field output factor is obtained as follows:

$$\Omega_{Q_{clin},Q_{msr}}^{f_{clin},f_{msr}} = \left[\frac{M_{Q_{clin}}^{f_{clin}}}{M_{Q_{int}}^{f_{int}}} k_{Q_{clin},Q_{int}}^{f_{clin},f_{int}}\right]_{det} \left[\frac{M_{Q_{int}}^{f_{int}}}{M_{Q_{msr}}^{f_{msr}}} k_{Q_{int},Q_{msr}}^{f_{int},f_{msr}}\right]_{IC} \tag{48}$$

where 'det' refers to the small field detector and 'IC' to the ionization chamber. The output correction factor $\left[k_{Q_{clin},Q_{int}}^{f_{clin},f_{int}}\right]_{det}$ is obtained from the tabulated output correction factors with respect to the msr field as follows:

$$\left[k_{Q_{clin},Q_{int}}^{f_{clin},f_{int}}\right]_{det} = \frac{\left[k_{Q_{clin},Q_{msr}}^{f_{clin},f_{msr}}\right]_{det}}{\left[k_{Q_{int},Q_{msr}}^{f_{int},f_{msr}}\right]_{det}} \tag{49}$$

In the absence of small field conditions for the intermediate field f_{int}, the output correction factor for the ionization chamber $\left[k_{Q_{int},Q_{msr}}^{f_{int},f_{msr}}\right]_{IC}$ is assumed to be unity for the ionization chambers recommended in this COP.

6.5.4. Some practical considerations

While the determination of the field output factors is based on a relative measurement, it is still important to correct all readings of ionization chambers for influence quantities. Since measurement sequences are often long, atmospheric conditions can vary substantially. Recombination and polarity correction factors can also depend on the field size. Note also that the response of many solid state detectors also exhibits temperature dependence, and that recombination (or dose rate dependence) may also be considerable and thus vary as the field output changes.

The overall measurement sequence consists of individual field size measurements interleaving the reference field measurements. This means that the reference field measurement is done before and after the measurement for each non-reference field. This procedure is time consuming and may not be practical in all clinical situations, but the number of different field sizes interleaved between two reference field measurements is limited based on the known stability characteristics of the beam. This enables correction for drifts of the beam output and can help ensure that the reading for the reference field does not vary beyond acceptable tolerance levels.

In the clinical treatment delivery sequence the collimator setting can be approached in different ways (i.e. from a smaller or from a larger field size). If the collimator control system allows for it, it is worth characterizing field output factors for the treatment planning system as averages of the measurements taken in the following two situations: (i) after the collimator is moved to a larger field size and then back to the correct field size, and (ii) after the collimator is moved to a smaller field size and then back to the correct field size. In this manner, the influence of the hysteresis of the collimator is minimized by averaging the effect.

6.6. TABLES OF FIELD OUTPUT CORRECTION FACTORS

Detector specific field output correction factors as a function of the field size are given in Tables 23 to 27 for CyberKnife, Tomotherapy and Gamma Knife machines, and for 6 MV and 10 MV WFF and FFF linacs for which the msr field has an equivalent square msr field size of 10 cm (if the msr field has a smaller size the output correction factor can be derived as explained in Appendix II; cf. Eq. (63)). The determination of the field output correction factors together with an estimate of their uncertainty are given in Appendix II.

It is noted that at present there are no $k_{Q_{\text{clin}},Q_{\text{msr}}}^{f_{\text{clin}},f_{\text{msr}}}$ data available for other detector types and for the Gamma Knife model 4C to include in Table 25.

Due to the rather large values of the output correction factors for some air filled ionization chambers in certain field sizes, such chambers are unsuitable for Gamma Knife output measurements with the 4 mm collimator. The chambers PTW T31002 and T31010, which in addition are unsuitable with the 8 mm collimator, have been excluded from Table 25.

TABLE 23. FIELD OUTPUT CORRECTION FACTORS $k_{Q_{clin},Q_{msr}}^{f_{clin},f_{msr}}$ FOR CYBERKNIFE MACHINES, AS A FUNCTION OF THE DIAMETER OF CIRCULAR FIELDS (COLLIMATOR SETTING) FOR THE DETECTOR ORIENTATIONS SPECIFIED IN TABLE 22

Detector	Circular field diameter (cm)											
	5.0	4.0	3.5	3.0	2.5	2.0	1.5	1.2	1.0	0.8	0.6	0.5
Ionization chambers												
Exradin A14SL micro Shonka slimline	1.000	1.000	1.000	1.000	1.001	1.002	1.010	1.026	1.047	—	—	—
Exradin A16 micro	1.000	1.000	1.000	1.000	1.001	1.003	1.007	1.014	1.021	1.032	1.050	—
IBA/Wellhöfer CC01	1.000	1.001	1.001	1.001	1.001	1.002	1.003	1.005	1.009	1.016	1.031	1.043
IBA/Wellhöfer CC04	1.000	1.000	1.000	1.000	1.001	1.002	1.009	1.020	1.035	—	—	—
IBA/Wellhöfer CC13/IC10/IC15	1.000	1.000	1.000	1.001	1.003	1.009	1.027	—	—	—	—	—
PTW 31002 Flexible	1.000	1.001	1.002	1.004	1.009	1.022	—	—	—	—	—	—
PTW 31010 Semiflex	1.000	1.000	1.000	1.001	1.003	1.008	1.022	1.043	—	—	—	—
PTW 31014 PinPoint	1.000	1.000	1.001	1.002	1.004	1.008	1.019	1.032	1.044	—	—	—
PTW 31016 PinPoint 3D	1.000	1.000	1.000	1.001	1.002	1.004	1.011	1.021	1.031	1.046	—	—

TABLE 23. FIELD OUTPUT CORRECTION FACTORS $k_{Q_{clin},Q_{msr}}^{f_{clin},f_{msr}}$ FOR CYBERKNIFE MACHINES, AS A FUNCTION OF THE DIAMETER OF CIRCULAR FIELDS (COLLIMATOR SETTING) FOR THE DETECTOR ORIENTATIONS SPECIFIED IN TABLE 22 (cont.)

Detector	Circular field diameter (cm)											
	5.0	4.0	3.5	3.0	2.5	2.0	1.5	1.2	1.0	0.8	0.6	0.5
Real time solid state dosimeters												
IBA PFD3G shielded diode	1.000	0.999	0.998	0.996	0.993	0.989	0.983	0.978	0.974	0.969	0.963	0.959
IBA EFD3G unshielded diode	1.001	1.001	1.001	1.001	1.001	1.000	0.997	0.994	0.991	0.987	0.981	0.978
IBA SFD unshielded diode (stereotactic)	1.001	1.002	1.003	1.003	1.004	1.003	1.000	0.996	0.991	0.983	0.972	0.965
PTW 60008 shielded diode	1.000	1.000	0.999	0.998	0.996	0.991	0.981	0.972	0.962	0.951	—	—
PTW 60012 unshielded diode	1.001	1.001	1.002	1.001	1.001	0.999	0.994	0.989	0.984	0.977	0.968	0.962
PTW 60016 shielded diode	1.000	0.999	0.998	0.996	0.993	0.987	0.978	0.969	0.962	0.953	—	—
PTW 60017 unshielded diode	1.000	1.001	1.001	1.000	0.999	0.997	0.992	0.987	0.981	0.975	0.966	0.960
PTW 60018 unshielded diode (stereotactic)	1.000	1.001	1.000	1.000	0.998	0.995	0.990	0.984	0.979	0.973	0.965	0.961
PTW 60003 natural diamond	1.000	1.000	1.000	1.000	1.000	1.000	1.000	1.001	1.003	1.009	1.023	1.037

TABLE 23. FIELD OUTPUT CORRECTION FACTORS $k_{Q_{clin},Q_{msr}}^{f_{clin},f_{msr}}$ FOR CYBERKNIFE MACHINES, AS A FUNCTION OF THE DIAMETER OF CIRCULAR FIELDS (COLLIMATOR SETTING) FOR THE DETECTOR ORIENTATIONS SPECIFIED IN TABLE 22 (cont.)

Detector	Circular field diameter (cm)											
	5.0	4.0	3.5	3.0	2.5	2.0	1.5	1.2	1.0	0.8	0.6	0.5
PTW 60019 CVD diamond	1.000	1.000	1.000	0.999	0.999	0.998	0.995	0.991	0.988	0.984	0.978	0.975
PTW 31018 liquid ion chamber	1.000	0.999	0.999	0.999	0.998	0.998	0.998	0.998	0.999	1.002	1.010	1.019
Sun Nuclear EDGE Detector	1.000	1.000	1.000	0.999	0.998	0.995	0.989	0.982	0.975	0.966	0.954	—
Standard Imaging W1 plastic scintillator	1.000	1.000	1.000	1.000	1.000	1.000	1.000	1.000	1.000	1.000	1.000	1.000

Note: The msr field is 6 cm diameter and the reference depth is 1.5 cm.

TABLE 24. FIELD OUTPUT CORRECTION FACTORS $k_{Q_{clin},Q_{msr}}^{f_{clin},f_{msr}}$ FOR TOMOTHERAPY MACHINES, AS A FUNCTION OF THE EQUIVALENT SQUARE FIELD SIZE

Detector	Equivalent square field size, S_{clin} (cm)												
	5.0	4.0	3.5	3.0	2.5	2.0	1.5	1.2	1.0	0.8	0.6	0.5	0.4
Ionization chambers													
Exradin A14SL micro Shonka slimline	1.000	1.000	1.000	1.000	1.000	1.002	1.010	1.027	—	—	—	—	—
Exradin A16 micro	1.000	1.000	1.000	1.000	1.001	1.003	1.008	1.017	1.027	1.043	—	—	—
IBA/Wellhöfer CC01	1.002	1.003	1.004	1.005	1.005	1.006	1.007	1.010	1.014	1.024	1.044	—	—
IBA/Wellhöfer CC04	1.000	1.000	1.000	1.000	1.000	1.002	1.009	1.022	1.041	—	—	—	—
IBA/Wellhöfer CC13/IC10/IC15	1.000	1.000	1.000	1.001	1.002	1.009	1.030	—	—	—	—	—	—
PTW 31002 Flexible	1.000	1.001	1.001	1.004	1.009	1.023	—	—	—	—	—	—	—
PTW 31010 Semiflex	1.000	1.000	1.000	1.001	1.002	1.008	1.025	—	—	—	—	—	—
PTW 31014 PinPoint	1.000	1.000	1.001	1.002	1.004	1.009	1.023	1.041	—	—	—	—	—
PTW 31016 PinPoint 3D	1.000	1.000	1.000	1.001	1.001	1.004	1.013	1.025	1.039	—	—	—	—

TABLE 24. FIELD OUTPUT CORRECTION FACTORS $k_{Q_{clin},Q_{msr}}^{f_{clin},f_{msr}}$ FOR TOMOTHERAPY MACHINES, AS A FUNCTION OF THE EQUIVALENT SQUARE FIELD SIZE (cont.)

Detector	Equivalent square field size, S_{clin} (cm)												
	5.0	4.0	3.5	3.0	2.5	2.0	1.5	1.2	1.0	0.8	0.6	0.5	0.4
Real time solid state dosimeters													
IBA PFD3G shielded diode	0.999	0.998	0.997	0.995	0.992	0.986	0.976	0.968	0.961	0.952	—	—	—
IBA EFD3G unshielded diode	1.005	1.007	1.008	1.009	1.009	1.009	1.006	1.002	0.997	0.991	0.982	0.976	0.969
IBA SFD unshielded diode (stereotactic)	1.009	1.013	1.015	1.017	1.018	1.019	1.017	1.012	1.006	0.995	0.978	0.966	0.951
PTW 60008 shielded diode	1.000	1.000	0.999	0.998	0.995	0.990	0.977	0.962	—	—	—	—	—
PTW 60012 unshielded diode	1.005	1.008	1.009	1.010	1.010	1.008	1.003	0.996	0.988	0.978	0.963	0.953	—
PTW 60016 shielded diode	1.000	0.999	0.998	0.995	0.991	0.984	0.970	0.956	—	—	—	—	—
PTW 60017 unshielded diode	1.004	1.005	1.006	1.006	1.006	1.003	0.997	0.989	0.981	0.971	0.956	—	—
PTW 60018 unshielded diode (stereotactic)	1.004	1.005	1.005	1.005	1.004	1.001	0.993	0.985	0.977	0.968	0.955	—	—
PTW 60003 natural diamond	1.000	1.000	1.000	1.000	1.000	1.000	1.000	1.001	1.003	1.009	1.026	1.045	—
PTW 60019 CVD diamond	1.000	1.000	1.000	1.000	0.999	0.997	0.993	0.989	0.984	0.977	0.968	0.962	0.955

TABLE 24. FIELD OUTPUT CORRECTION FACTORS $k_{Q_{clin},Q_{msr}}^{f_{clin},f_{msr}}$ FOR TOMOTHERAPY MACHINES, AS A FUNCTION OF THE EQUIVALENT SQUARE FIELD SIZE (cont.)

Detector	Equivalent square field size, S_{clin} (cm)												
	5.0	4.0	3.5	3.0	2.5	2.0	1.5	1.2	1.0	0.8	0.6	0.5	0.4
PTW 31018 liquid ion chamber	0.997	0.995	0.994	0.994	0.993	0.992	0.991	0.991	0.992	0.994	1.003	1.015	1.038
Sun Nuclear EDGE Detector	1.000	1.000	1.000	0.999	0.998	0.994	0.986	0.976	0.966	0.951	—	—	—
Standard Imaging W1 plastic scintillator	1.000	1.000	1.000	1.000	1.000	1.000	1.000	1.000	1.000	1.000	1.000	1.000	1.000

Note: The msr field is 5 cm × 10 cm and the reference depth is 10 cm.

TABLE 25. FIELD OUTPUT CORRECTION FACTORS $k_{Q_{clin},Q_{msr}}^{f_{clin},f_{msr}}$ FOR THE GAMMA KNIFE MODEL PERFEXION, AS A FUNCTION OF THE DIAMETER OF THE CIRCULAR COLLIMATOR [179]

Model	Type	4 mm Ø	8 mm Ø	16 mm Ø
PTW T31006	Ionization chamber	—[a]	1.025	1.000
PTW T31014	Ionization chamber	—[a]	1.030	1.000
PTW T31015	Ionization chamber	—[a]	—[a]	1.000
PTW T31016	Ionization chamber (PinPoint 3D)	—[a]	1.032	1.000
PTW T60008	Diode (photon/shielded)	0.951	0.971	1.000
PTW T60012	Diode (electron/unshielded)	0.965	0.996	1.000
PTW T60016	Diode (photon/shielded)	0.958	0.981	1.000
PTW T60017	Diode (electron/unshielded)	0.961	0.997	1.000
PTW T60003	Diamond detector (natural)	—[a]	1.006	1.000
PTW T60019	Diamond detector (synthetic)	0.993	1.005	1.000

[a] A large correction factor makes this chamber unsuitable for output measurements with this collimator.

TABLE 26. FIELD OUTPUT CORRECTION FACTORS $k_{Q_{clin},Q_{msr}}^{f_{clin},f_{msr}}$ FOR FIELDS COLLIMATED BY AN MLC OR SRS CONE AT 6 MV WFF AND FFF MACHINES, AS A FUNCTION OF THE EQUIVALENT SQUARE FIELD SIZE

Detector	Equivalent square field size, S_{clin} (cm)												
	8.0	6.0	4.0	3.0	2.5	2.0	1.5	1.2	1.0	0.8	0.6	0.5	0.4
Ionization chambers													
Exradin A14SL micro Shonka slimline	1.000	1.000	1.000	1.000	1.000	1.002	1.010	1.027	—	—	—	—	—
Exradin A16 micro	1.000	1.000	1.000	1.000	1.001	1.003	1.008	1.017	1.027	1.043	—	—	—
IBA/Wellhöfer CC01	1.002	1.004	1.007	1.008	1.008	1.009	1.011	1.013	1.018	1.027	1.047	—	—
IBA/Wellhöfer CC04	1.000	1.000	1.000	1.000	1.000	1.002	1.009	1.022	1.041	—	—	—	—
IBA/Wellhöfer CC13/IC10/IC15	1.000	1.000	1.000	1.001	1.002	1.009	1.030	—	—	—	—	—	—
PTW 31002 Flexible	1.000	1.000	1.001	1.004	1.009	1.023	—	—	—	—	—	—	—
PTW 31010 Semiflex	1.000	1.000	1.000	1.001	1.002	1.008	1.025	—	—	—	—	—	—
PTW 31014 PinPoint	1.000	1.000	1.000	1.002	1.004	1.009	1.023	1.041	—	—	—	—	—
PTW 31016 PinPoint 3D	1.000	1.000	1.000	1.001	1.001	1.004	1.013	1.025	1.039	—	—	—	—

TABLE 26. FIELD OUTPUT CORRECTION FACTORS $k_{Q_{clin},Q_{msr}}^{f_{clin},f_{msr}}$ FOR FIELDS COLLIMATED BY AN MLC OR SRS CONE AT 6 MV WFF AND FFF MACHINES, AS A FUNCTION OF THE EQUIVALENT SQUARE FIELD SIZE (cont.)

Detector	Equivalent square field size, S_{clin} (cm)												
	8.0	6.0	4.0	3.0	2.5	2.0	1.5	1.2	1.0	0.8	0.6	0.5	0.4
Real time solid state dosimeters													
IBA PFD3G shielded diode	1.000	1.000	0.998	0.995	0.992	0.986	0.976	0.968	0.961	0.952	—	—	—
IBA EFD3G unshielded diode	1.005	1.009	1.014	1.016	1.016	1.015	1.012	1.008	1.004	0.998	0.988	0.983	0.976
IBA SFD unshielded diode (stereotactic)	1.008	1.017	1.025	1.029	1.031	1.032	1.030	1.025	1.018	1.007	0.990	0.978	0.963
PTW 60008 shielded diode	1.000	1.000	1.000	0.998	0.995	0.990	0.977	0.962	—	—	—	—	—
PTW 60012 unshielded diode	1.005	1.010	1.015	1.017	1.017	1.016	1.010	1.003	0.996	0.985	0.970	0.960	—
PTW 60016 shielded diode	1.000	1.000	0.999	0.995	0.991	0.984	0.970	0.956	—	—	—	—	—
PTW 60017 unshielded diode	1.004	1.007	1.010	1.011	1.011	1.008	1.002	0.994	0.986	0.976	0.961	0.952	—
PTW 60018 unshielded diode (stereotactic)	1.004	1.007	1.010	1.011	1.009	1.006	0.998	0.990	0.983	0.973	0.960	0.952	—
PTW 60003 natural diamond	1.000	1.000	1.000	1.000	1.000	1.000	1.000	1.001	1.003	1.009	1.026	1.045	—
PTW 60019 CVD diamond	1.000	1.000	1.000	1.000	0.999	0.997	0.993	0.989	0.984	0.977	0.968	0.962	0.955

TABLE 26. FIELD OUTPUT CORRECTION FACTORS $k_{Q_{clin},Q_{msr}}^{f_{clin},f_{msr}}$ FOR FIELDS COLLIMATED BY AN MLC OR SRS CONE AT 6 MV WFF AND FFF MACHINES, AS A FUNCTION OF THE EQUIVALENT SQUARE FIELD SIZE (cont.)

Detector	Equivalent square field size, S_{clin} (cm)												
	8.0	6.0	4.0	3.0	2.5	2.0	1.5	1.2	1.0	0.8	0.6	0.5	0.4
PTW 31018 liquid ion chamber	0.997	0.994	0.991	0.989	0.988	0.988	0.987	0.987	0.987	0.990	0.999	1.011	1.033
Sun Nuclear EDGE Detector	1.000	1.000	1.000	0.999	0.998	0.994	0.986	0.976	0.966	0.951	—	—	—
Standard Imaging W1 plastic scintillator	1.000	1.000	1.000	1.000	1.000	1.000	1.000	1.000	1.000	1.000	1.000	1.000	1.000

Note: The reference depth is 10 cm.

TABLE 27. FIELD OUTPUT CORRECTION FACTORS $k_{Q_{clin},Q_{msr}}^{f_{clin},f_{msr}}$ FOR SMALL FIELDS COLLIMATED BY AN MLC OR SRS CONE AT 10 MV WFF AND FFF MACHINES, AS A FUNCTION OF THE EQUIVALENT SQUARE FIELD SIZE

Detector	Equivalent square field size, S_{clin} (cm)												
	8.0	6.0	4.0	3.0	2.5	2.0	1.5	1.2	1.0	0.8	0.6	0.5	0.4
Ionization chambers													
Exradin A14SL micro Shonka slimline	1.000	1.000	1.000	1.000	1.000	1.002	1.010	1.027	—	—	—	—	—
Exradin A16 micro	1.000	1.000	1.000	1.000	1.001	1.003	1.008	1.017	1.027	1.043	—	—	—
IBA/Wellhöfer CC01	1.001	1.003	1.004	1.005	1.005	1.006	1.007	1.009	1.014	1.023	1.043	—	—
IBA/Wellhöfer CC04	1.000	1.000	1.000	1.000	1.000	1.002	1.009	1.022	1.041	—	—	—	—
IBA/Wellhöfer CC13/IC10/IC15	1.000	1.000	1.000	1.001	1.002	1.009	1.030	—	—	—	—	—	—
PTW 31002 Flexible	1.000	1.000	1.001	1.004	1.009	1.023	—	—	—	—	—	—	—
PTW 31010 Semiflex	1.000	1.000	1.000	1.001	1.002	1.008	1.025	—	—	—	—	—	—
PTW 31014 PinPoint	1.000	1.000	1.000	1.002	1.004	1.009	1.023	1.041	—	—	—	—	—
PTW 31016 PinPoint 3D	1.000	1.000	1.000	1.001	1.001	1.004	1.013	1.025	1.039	—	—	—	—

TABLE 27. FIELD OUTPUT CORRECTION FACTORS $k_{Q_{clin},Q_{ref}}^{f_{clin},f_{ref}}$ FOR SMALL FIELDS COLLIMATED BY AN MLC OR SRS CONE AT 10 MV WFF AND FFF MACHINES, AS A FUNCTION OF THE EQUIVALENT SQUARE FIELD SIZE (cont.)

Detector	Equivalent square field size, S_{clin} (cm)												
	8.0	6.0	4.0	3.0	2.5	2.0	1.5	1.2	1.0	0.8	0.6	0.5	0.4
Real time solid state dosimeters													
IBA PFD3G shielded diode	1.000	1.000	0.998	0.995	0.992	0.986	0.976	0.968	0.961	0.952	—	—	—
IBA EFD3G unshielded diode	1.003	1.005	1.008	1.009	1.009	1.008	1.005	1.000	0.996	0.989	0.980	0.974	0.967
IBA SFD unshielded diode (stereotactic)	1.005	1.010	1.015	1.018	1.018	1.018	1.015	1.010	1.003	0.992	0.974	0.962	—
PTW 60008 shielded diode	1.000	1.000	1.000	0.998	0.995	0.990	0.977	0.962	—	—	—	—	—
PTW 60012 unshielded diode	1.003	1.006	1.009	1.010	1.010	1.008	1.002	0.994	0.986	0.976	0.960	0.951	—
PTW 60016 shielded diode	1.000	1.000	0.999	0.995	0.991	0.984	0.970	0.956	—	—	—	—	—
PTW 60017 unshielded diode	1.002	1.004	1.006	1.006	1.005	1.003	0.996	0.988	0.980	0.969	0.954	—	—
PTW 60018 unshielded diode (stereotactic)	1.002	1.004	1.006	1.006	1.004	1.000	0.992	0.984	0.976	0.966	0.953	—	—
PTW 60003 natural diamond	1.000	1.000	1.000	1.000	1.000	1.000	1.000	1.001	1.003	1.009	1.026	1.045	—

TABLE 27. FIELD OUTPUT CORRECTION FACTORS $k_{Q_{clin},Q_{ref}}^{f_{clin},f_{ref}}$ FOR SMALL FIELDS COLLIMATED BY AN MLC OR SRS CONE AT 10 MV WFF AND FFF MACHINES, AS A FUNCTION OF THE EQUIVALENT SQUARE FIELD SIZE (cont.)

Detector	Equivalent square field size, S_{clin} (cm)												
	8.0	6.0	4.0	3.0	2.5	2.0	1.5	1.2	1.0	0.8	0.6	0.5	0.4
PTW 60019 CVD diamond	1.000	1.000	1.000	1.000	0.999	0.997	0.993	0.989	0.984	0.977	0.968	0.962	0.955
PTW 31018 liquid ion chamber	0.998	0.996	0.994	0.994	0.993	0.993	0.992	0.992	0.993	0.995	1.005	1.017	1.039
Sun Nuclear EDGE Detector	1.000	1.000	1.000	0.999	0.998	0.994	0.986	0.976	0.966	0.951	—	—	—
Standard Imaging W1 plastic scintillator	1.000	1.000	1.000	1.000	1.000	1.000	1.000	1.000	1.000	1.000	1.000	1.000	1.000

Note: The reference depth is 10 cm.

Appendix I

DETERMINATION OF BEAM QUALITY CORRECTION FACTORS FOR REFERENCE DOSIMETRY AND THEIR UNCERTAINTY ESTIMATES

This appendix describes the procedures used to derive detector specific values of the beam quality correction factors $k_Q^{f_{ref}}$ and $k_{Q_{msr}}^{f_{msr},f_{ref}}$ for the reference dosimetry of WFF linac beams, FFF beams, including CyberKnife and TomoTherapy beams, and Gamma Knife ^{60}Co beams; the values are given in Chapter 5. For WFF beams, values of $k_Q^{f_{ref}}$, short notation for $k_{Q,Q_0}^{f_{ref}}$ with reference to Q_0 = ^{60}Co and f_{ref} = 10 cm × 10 cm (see Eqs (25, 27) and related text), are given in Table 12. These values have been derived from data in Refs [1, 7]. For FFF beams, additional information from the literature has been used to determine volume averaging corrections, water to air stopping-power ratios and equivalent square field sizes, leading to the $k_Q^{f_{ref}}$ correction factors given in Table 13. For Gamma Knife beams, the values of $k_{Q_{msr}}^{f_{msr},f_{ref}}$, short notation for $k_{Q_{msr},Q_0}^{f_{msr},f_{ref}}$ with reference to Q_0 = ^{60}Co, given in Table 14 have been taken directly from the literature.

I.1. LINAC BEAMS WITH FLATTENING FILTER (WFF BEAMS)

I.1.1. $k_Q^{f_{ref}}$ values for WFF beams

$k_Q^{f_{ref}}$ values from Ref. [1], where they were denoted by k_Q, for most chambers recommended in this COP for the reference dosimetry of f_{ref} = 10 cm × 10 cm fields are given in Table 28. Values for these ionization chambers that have also been provided in Ref. [7] are given in Table 29 along with values for three chambers not included in Ref. [1]. The stated values of $\%dd(10,10)_x$ have been optimized such that for chambers included in both protocols the sum of the squares of the differences between the $k_Q^{f_{ref}}$ values in both tables is minimized. Using this procedure, the recommended data for $k_Q^{f_{ref}}$ for WFF beams given in Table 29 were determined as a function of both beam quality indices, $TPR_{20,10}(10)$ and $\%dd(10,10)_x$.

TABLE 28. $k_Q^{f_{ref}}$ DATA FOR THE f_{ref} = 10 cm × 10 cm FIELD FOR REFERENCE IONIZATION CHAMBERS IN WFF LINACS AS A FUNCTION OF $TPR_{20,10}(10)$ [1]

Ion chamber $TPR_{20,10}(10)$ =	0.630	0.660	0.690	0.720	0.750
Capintec PR-06C/G Farmer	0.997	0.994	0.991	0.988	0.982
Exradin A2 Spokas	0.998	0.997	0.995	0.992	0.988
Exradin A12 Farmer	0.998	0.996	0.993	0.990	0.984
Exradin A12S[a]	—	—	—	—	—
Exradin A19[a]	—	—	—	—	—
Nuclear Assoc 30-751 Farmer	0.996	0.993	0.990	0.985	0.979
Nuclear Assoc 30-752 Farmer	0.997	0.995	0.992	0.989	0.983
NE 2505/3, 3A Farmer	0.996	0.994	0.992	0.989	0.984
NE 2571 Farmer	0.997	0.994	0.992	0.989	0.984
NE 2611	0.996	0.993	0.991	0.988	0.984
PTW 23331 rigid	0.996	0.992	0.989	0.985	0.980
PTW 23332 rigid	0.996	0.993	0.989	0.984	0.978
PTW 23333 (3 mm cap)	0.996	0.993	0.989	0.985	0.979
PTW 30001 Farmer	0.996	0.993	0.989	0.985	0.979
PTW 30010 Farmer	0.996	0.993	0.989	0.985	0.979
PTW 30002/30011 Farmer	0.996	0.993	0.991	0.987	0.982
PTW 30004/30012 Farmer	0.998	0.995	0.993	0.989	0.984
PTW 30006/30013 Farmer	0.996	0.993	0.989	0.984	0.978
PTW 31003/31013 Semiflex	0.996	0.993	0.989	0.984	0.978

TABLE 28. $k_Q^{f_{ref}}$ DATA FOR THE f_{ref} = 10 cm × 10 cm FIELD FOR REFERENCE IONIZATION CHAMBERS IN WFF LINACS AS A FUNCTION OF $TPR_{20,10}(10)$ [1] (cont.)

Ion chamber	$TPR_{20,10}(10)$ =	0.630	0.660	0.690	0.720	0.750
SNC 100700-0 Farmer		0.997	0.994	0.991	0.986	0.979
SNC 100700-1 Farmer		0.998	0.997	0.994	0.990	0.984
Victoreen Radocon III 555		0.993	0.988	0.985	0.979	0.973
Victoreen 30-348		0.995	0.991	0.988	0.982	0.976
Victoreen 30-351		0.995	0.991	0.988	0.983	0.977
Victoreen 30-349		0.995	0.991	0.988	0.983	0.978
Victoreen 30-361		0.995	0.991	0.988	0.983	0.977
IBA FC-65P (Wellhöfer IC 69) Farmer		0.997	0.994	0.992	0.986	0.979
IBA FC-65G (Wellhöfer IC 70) Farmer		0.998	0.997	0.994	0.989	0.983

[a] Data not given in Ref. [1].

TABLE 29. $k_Q^{f_{ref}}$ DATA FOR THE f_{ref} = 10 cm × 10 cm FIELD FOR REFERENCE IONIZATION CHAMBERS IN WFF LINACS AS A FUNCTION OF $\%dd(10,10)_x$ [7]

Ion chamber	$\%dd(10,10)_x$ =	63.4	65.2	67.6	70.5	73.9
Capintec PR-06C/G Farmer		0.997	0.995	0.993	0.989	0.984
Exradin A2 Spokas[a]		—	—	—	—	—
Exradin A12 Farmer		0.997	0.994	0.991	0.987	0.981
Exradin A12S		0.996	0.994	0.991	0.987	0.981
Exradin A19		0.996	0.993	0.990	0.985	0.980

TABLE 29. $k_Q^{f_{ref}}$ DATA FOR THE f_{ref} = 10 cm × 10 cm FIELD FOR REFERENCE IONIZATION CHAMBERS IN WFF LINACS AS A FUNCTION OF $\%dd(10,10)_x$ [7] (cont.)

Ion chamber	$\%dd(10,10)_x$ =	63.4	65.2	67.6	70.5	73.9
Nuclear Assoc 30-751 Farmer[a]		—	—	—	—	—
Nuclear Assoc 30-752 Farmer[a]		—	—	—	—	—
NE 2505/3, 3A Farmer[a]		—	—	—	—	—
NE 2571 Farmer		0.996	0.994	0.991	0.987	0.981
NE 2611		0.999	0.996	0.993	0.989	0.984
PTW 23331 rigid[a]		—	—	—	—	—
PTW 23332 rigid[a]		—	—	—	—	—
PTW 23333 (3 mm cap)[a]		—	—	—	—	—
PTW 30001 Farmer[a]		—	—	—	—	—
PTW 30010 Farmer		0.997	0.994	0.991	0.987	0.981
PTW 30002/30011 Farmer		0.997	0.994	0.991	0.987	0.982
PTW 30004/30012 Farmer		0.998	0.996	0.993	0.989	0.984
PTW 30006/30013 Farmer		0.995	0.993	0.990	0.986	0.980
PTW 31003/31013 Semiflex		0.996	0.994	0.991	0.986	0.981
SNC 100700-0 Farmer[a]		—	—	—	—	—
SNC 100700-1 Farmer[a]		—	—	—	—	—
Victoreen Radocon III 555[a]		—	—	—	—	—
Victoreen 30-348[a]		—	—	—	—	—
Victoreen 30-351[a]		—	—	—	—	—

TABLE 29. $k_Q^{f_{ref}}$ DATA FOR THE f_{ref} = 10 cm × 10 cm FIELD FOR REFERENCE IONIZATION CHAMBERS IN WFF LINACS AS A FUNCTION OF $\%dd(10,10)_x$ [7] (cont.)

Ion chamber	$\%dd(10,10)_x$ =	63.4	65.2	67.6	70.5	73.9
Victoreen 30-349[a]		—	—	—	—	—
Victoreen 30-361[a]		—	—	—	—	—
IBA FC-65P (Wellhöfer IC 69) Farmer		0.996	0.994	0.990	0.986	0.980
IBA FC-65G (Wellhöfer IC 70) Farmer		0.996	0.994	0.991	0.987	0.981

[a] Data not given in Ref. [7].

I.1.2. Uncertainties of the $k_Q^{f_{ref}}$ values for WFF beams

The relative standard uncertainty of the $k_Q^{f_{ref}}$ values in Ref. [1] was estimated to be 1%, while the uncertainty quoted in Ref. [7] was 0.5%. As the latter estimate was based on more recent comparisons of measured and Monte Carlo calculated data, it seems a priori reasonable to assume that Ref. [1] slightly overestimated the overall uncertainty of the beam quality correction factors. Further discussions [180] have, on the other hand, indicated that the lower estimate in Ref. [7] may be more applicable to particular reference chambers, such as the NE 2571 (for which a considerable amount of experimental data exist), while an underestimation could occur for chambers having less or no experimental data available in other publications.

It is advised that the $k_Q^{f_{ref}}$ values given in Table 12 as a function of $\%dd(10,10)_x$ be assigned an uncertainty component for the matching of $\%dd(10,10)_x$ to $TPR_{20,10}(10)$ data. After the optimization procedure described above, the maximum difference in $k_Q^{f_{ref}}$ at the highest beam qualities amounted to 0.3%; therefore it can be assumed that the relative standard uncertainty for this matching does not exceed 0.2%.

Based on current knowledge and uncertainty estimates, it is assumed throughout this COP that in situations where a hypothetical field f_{ref} = 10 cm × 10 cm needs to be considered (see Section 3.2.1.3), the same beam quality correction factors can be used for the f_{msr} and f_{ref} fields in WFF beams; hence, $k_{Q_{msr}}^{f_{msr},f_{ref}}$ equals $k_Q^{f_{ref}}$ for the hypothetical conventional reference field of a machine. Additionally, as water to air stopping-power ratios are known to vary by not more than 0.2% for field sizes from 10 cm × 10 cm down to about

3 cm × 3 cm, the range covering the f_{msr} field sizes for linac beams, a relative standard uncertainty of 0.15% can be estimated for the $s_{w,air}$ contribution. These two contributions will only marginally increase the overall uncertainty of $k_{Q_{msr}}^{f_{msr},f_{ref}}$ values compared with that of $k_Q^{f_{ref}}$.

Given that the 1% relative standard uncertainty in Ref. [1] appears to be a conservative estimate, it can be assumed that the combined relative standard uncertainty of $k_Q^{f_{ref}}$ and $k_{Q_{msr}}^{f_{msr},f_{ref}}$, including the two additional contributions mentioned, will not exceed 1%. Because it is not the purpose of this COP to review the data in Refs [1, 7], the recommended $k_Q^{f_{ref}}$ values given in Table 12 are estimated to have a relative standard uncertainty of 1%. If the chamber calibration is made with a high energy photon beam of quality Q_0, there is a correlation in the ratio of two values with respect to ^{60}Co (see Eq. (26)), and the relative standard uncertainty of $k_{Q,Q_0}^{f_{ref}}$ with reference to a calibration beam quality $Q_0 \neq {}^{60}$Co is assumed to be 1% as well.

I.1.3. Equivalent square msr field sizes of WFF beams

For WFF beams in which a 10 cm × 10 cm conventional reference field cannot be established, the measured values of $TPR_{20,10}(S)$ and $\%dd(10,S)_x$ in a machine specific reference field, f_{msr}, are converted to the beam quality indices $TPR_{20,10}(10)$ and $\%dd(10,10)_x$ following the procedure described in Section 5.3.3.

If the f_{msr} field is not square, then an equivalent square field size, S, has to be determined based on the condition that the scatter component in equivalent field sizes is the same. Using scatter functions from Ref. [32], it can be shown that equivalent square field sizes of rectangular and circular fields depend very little on the exact shape of the scatter function. It has been found that the scatter function proposed in Ref. [32]:

$$s = \frac{SC(r)}{SC(\infty)} = 1 - e^{-\lambda r} - \mu\lambda r e^{-\lambda r} \tag{50}$$

with $\mu = 0.5$, $\lambda = 0.18$ and $SC(r)$ being the scatter component of a circular field with radius r, fits well measured scatter components when the expression is integrated over WFF beams of various field sizes, and therefore this function has been used for this COP. The integration is performed over the field area using the expression:

$$SC_{field} = \frac{1}{2\pi}\iint_{field\ area}\left(\lambda(1-\mu)\frac{e^{-\lambda r}}{r} + \mu\lambda^2 e^{-\lambda r}\right) r\,dr\,d\theta \tag{51}$$

Figure 20 illustrates how the equivalent square field size of a rectangular field is derived from the scatter components of rectangular and square fields. The equivalent square msr field sizes in Table 15 have been calculated according to this procedure.

I.2. FFF LINAC BEAMS

No $k_Q^{f_{ref}}$ data were given for FFF beams in Ref. [1], and discussions in the literature indicate that data for FFF beams or beams with light filtration are slightly different from those for WFF beams when $k_Q^{f_{ref}}$ is given as a function of $TPR_{20,10}(10)$ [34, 35, 37, 181–184]. Even though it is generally assumed that data in Refs [2, 7] are valid for both WFF and FFF beams, there is also evidence that $k_Q^{f_{ref}}$ values given as a function of $\%dd(10,10)_x$ are slightly different for WFF and FFF beams [34, 35, 37, 181–184], though the differences are smaller than for

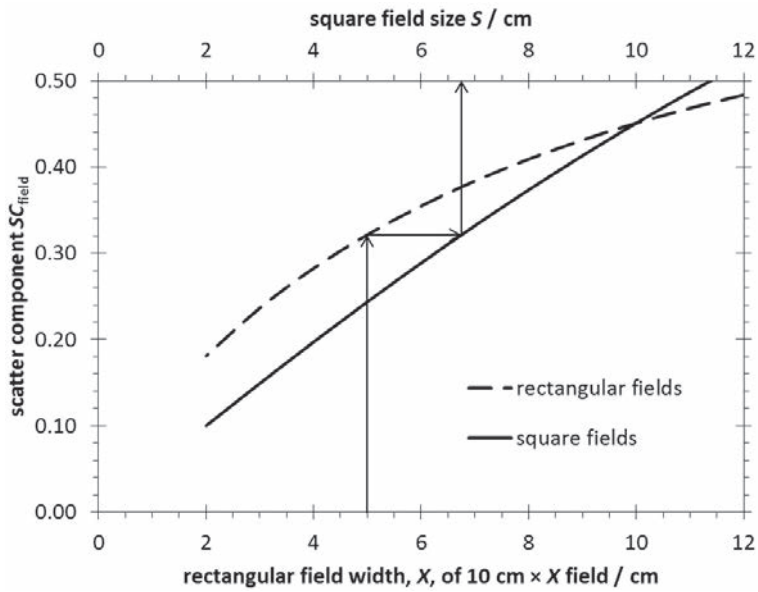

FIG. 20. Scatter components for 10 cm × X cm rectangular fields (dashed curve, lower horizontal axis) and square fields of size S *(continuous curve, upper horizontal axis) in a WFF beam calculated using Eq. (51). The example illustrates that a 10 cm × 5 cm rectangular field has an equivalent square field size of 6.8 cm.*

$TPR_{20,10}(10)$. There are three main issues to consider that lead to the differences in $k_Q^{f_{ref}}$ data between WFF and FFF beams:

(a) Differences in water to air stopping-power ratios $(s_{w,air})_Q$ as a function of the beam quality index $TPR_{20,10}(10)$ or $\%dd(10,10)_x$;
(b) Differences in all types of ionization chamber perturbation correction factors except for volume averaging as a function of the beam quality index $TPR_{20,10}(10)$ or $\%dd(10,10)_x$;
(c) Volume averaging due to the non-uniform lateral beam profile of reference fields in FFF beams.

The third issue is addressed in Ref. [7] as an additional correction factor in the expression to determine absorbed dose to water, but no correction factors or procedures for their determination were provided. A fourth issue to consider is the reduced scatter component at the reference depth in FFF beams as compared to WFF beams, which makes the equivalent square field size smaller than that defined by the beam penumbrae [33]. To this end, either the field size for the determination of the beam quality has to be larger than the 10 cm × 10 cm reference field, such that the equivalent square field size is 10 cm × 10 cm, or the equivalent square field size S of the 10 cm × 10 cm reference field has to be determined so that the measured values of $TPR_{20,10}(S)$ and $\%dd(10,S)_x$ can be converted to the beam quality indices $TPR_{20,10}(10)$ and $\%dd(10,10)_x$ as described in Section 5.3.3.

I.2.1. Water to air stopping-power ratios for FFF beams

The difference in water to air stopping-power ratios $(s_{w,air})_Q$ between heavily filtered and unfiltered or lightly filtered beams has been the subject of debate since the 1980s [34, 35, 37, 181–184]. Many of these discussions were based on beams that either had non-clinical characteristics, such as those used in the past in some national metrology institutes, or on clinical beams not in current use. A relatively recent paper that compared Monte Carlo calculated water to air stopping-power ratios for FFF and WFF beams assumed that FFF beams have no filtration at all [34], while FFF beams in clinical use always have some minimal filtration to prevent electrons emerging from the target from reaching the patient and to reduce backscatter from the collimator into the monitor chamber, which would complicate the modelling of beam output as a function of field size and shape [108].

The only set of $(s_{w,air})_Q$ data available for FFF beams currently in clinical use is from the Monte Carlo calculations by Dalaryd et al. [37], and these data have been used to calculate the WFF–FFF differences as a function of beam

quality for this COP. The data are shown in Fig. 21, where the values of the beam quality indices are those reported in the publication. Strictly speaking, these $(s_{w,air})_Q$ values need to be corrected for the effect of the reduced equivalent square field size, but this was found to result in very small differences, about 0.06% for the data as a function of $\%dd(10,10)_x$, and varying from less than 0.03% to 0.1% for the data as a function of $TPR_{20,10}(10)$. One data point of the dataset (marked as a triangle in Fig. 21) was disregarded because it represented a FFF beam with a very low beam quality index and it skewed the difference because no corresponding low beam quality value for the WFF beams was present in the dataset. It is assumed that even though the extrapolation of the curves in Fig. 21 to lower beam quality indices is less accurate (potentially closer estimates are provided by the dashed lines), the difference between the two curves is better represented by omitting this data point.

Thus, for FFF beams, the $k_Q^{f_{ref}}$ values from Refs [1, 7] have been corrected for these differences; the applied correction factors as a function of $TPR_{20,10}(10)$ and $\%dd(10,10)_x$ are given in Table 30. The values chosen for $\%dd(10,10)_x$ in this table are the result of the optimization to match $k_Q^{f_{ref}}$ for FFF beams as a function of $TPR_{20,10}(10)$ and $\%dd(10,10)_x$ described in Section I.2.4.

I.2.2. Ionization chamber perturbation correction factors for FFF beams

There are at present no data in the literature on the difference in ionization chamber perturbation correction factors between WFF and FFF beams as a function of the beam quality indices. For the chamber wall perturbation correction factor, it is known that it depends on the water to air stopping-power ratio as well as on the wall to air stopping-power ratio, and that the dependence on beam quality index is smaller than the dependence on water to air stopping-power ratio.

Given the lack of data, it is assumed in this COP that the dependence of ionization chamber perturbation correction factors as a function of the beam quality indices is the same as for WFF beams, and the $k_Q^{f_{ref}}$ data are not corrected for this potential difference.

I.2.3. Volume averaging correction factors for FFF beams

The non-uniformity of the lateral beam profiles of reference fields in FFF beams results in an under-response of the reference ionization chambers that is relatively large compared to the scale of the dose variation at the centre of these reference fields. It has, for example, been shown that the dose averaged over the dimensions of a Farmer ionization chamber in the 6 cm diameter reference field of a CyberKnife machine is about 1% lower than the dose at the centre of the field [76, 81]. Reference [7] explicitly introduced a new correction factor

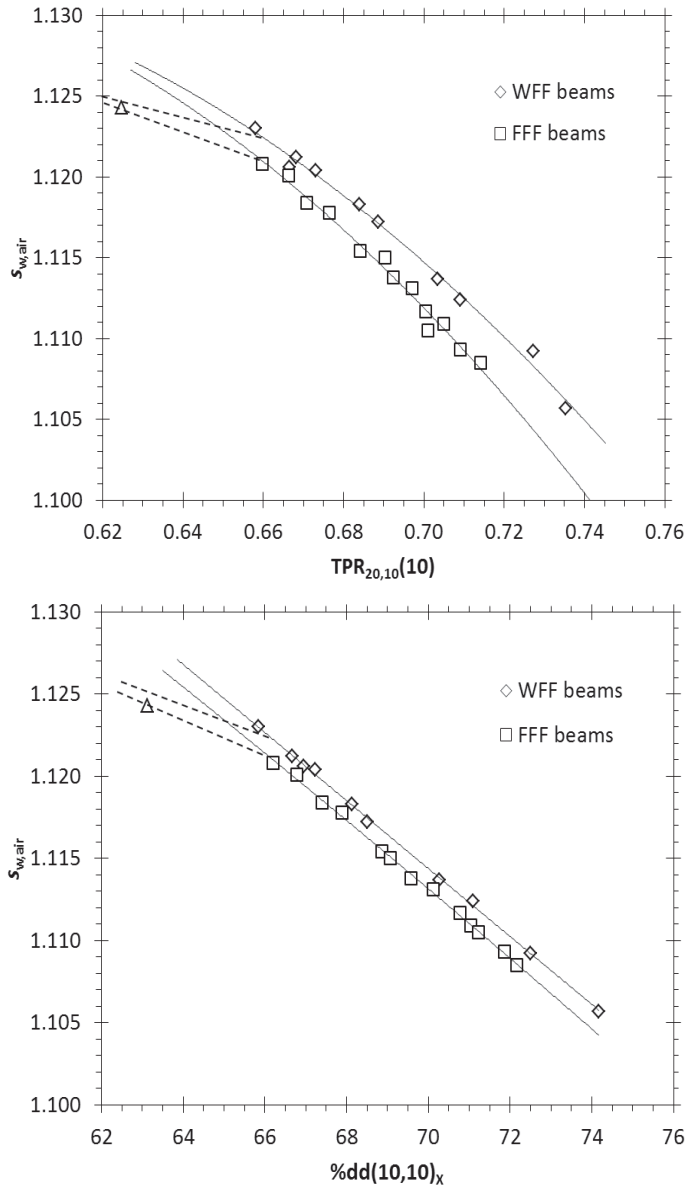

FIG. 21. Water to air stopping-power ratios $(s_{w,air})_Q$ for clinical WFF and FFF beams calculated by the Monte Carlo method [37]. The triangular data point on the left was disregarded in the analysis, as explained in the text. The solid lines represent quadratic fits used to calculate the difference in $(s_{w,air})_Q$ between WFF and FFF beams. The dashed lines represent potentially better estimates for the extrapolations to low beam quality indices, but it can be assumed that the differences are well described by the extrapolated solid curves (reproduced with the permission of the American Association of Physicists in Medicine).

TABLE 30. RATIOS OF WATER TO AIR STOPPING-POWER RATIOS FOR FFF AND WFF BEAMS USED AS CORRECTION FACTORS IN THIS CODE AS A FUNCTION OF THE BEAM QUALITY INDICES $TPR_{20,10}(10)$ AND $\%dd(10,10)_x$

$TPR_{20,10}(10)$	0.630	0.660	0.690	0.720	0.750
$\left(s_{w,air}\right)^{FFF}_{TPR_{20,10}(10)} \Big/ \left(s_{w,air}\right)^{WFF}_{TPR_{20,10}(10)}$	0.999	0.998	0.997	0.996	0.994
$\%dd(10,10)_x$	63.8	65.6	68.2	71.7	76.1
$\left(s_{w,air}\right)^{FFF}_{\%dd(10,10)_x} \Big/ \left(s_{w,air}\right)^{WFF}_{\%dd(10,10)_x}$	0.998	0.998	0.998	0.998	0.998

in the equation to determine absorbed dose to water accounting for this volume averaging effect, but no values were provided for the correction factors.

The volume averaging correction factor is defined as the dose averaged over a volume of water in homogeneous water where the water volume coincides with the volume displaced by the ionization chamber. Kawachi et al. [81] proposed an expression for calculating the volume averaging correction factor from measured lateral beam profiles:

$$\left(k_{vol}\right)^{f_{ref}}_{Q} = \frac{\iint_A \mathrm{d}x\mathrm{d}y}{\iint_A \mathrm{OAR}(x,y)\mathrm{d}x\mathrm{d}y} \tag{52}$$

where x and y are the coordinates on the axes orthogonal to the beam central axis, A is the area of the projection of the sensitive volume of the chamber on a plane orthogonal to the beam axis and OAR(x,y) is the off-axis ratio, which is the 2-D lateral beam profile at the measurement depth normalized to the central axis. Equation (52), however, does not account for the change of the longitudinal extent of an ionization chamber depending on the lateral position. A more accurate expression is given by:

$$\left(k_{vol}\right)^{f_{ref}}_{Q} = \frac{\iint_A w(x,y)\mathrm{d}x\mathrm{d}y}{\iint_A w(x,y)\mathrm{OAR}(x,y)\mathrm{d}x\mathrm{d}y} \tag{53}$$

where $w(x,y)$ is a weighting function representing the extension of the air cavity of the ionization chamber along the beam axis as a function of the beam lateral coordinates.

As an example, the volume averaging correction factor is calculated for a Farmer chamber in the 6 cm diameter reference field of a CyberKnife machine using Eqs (52, 53) for the four geometrical models of varying simplification of the ionization chamber described in Fig. 22.

For the four models in Fig. 22, the weights $w(x,y)$ in Eq. (53) are calculated as the length of the chord defined by the intersection of the line at lateral offsets x and y parallel to the beam axis and the chamber:

$$\text{A: } w(x,y) = 1, \ -L/2 \leq y \leq L/2 \text{ and } x = 0$$

$$\text{B: } w(x,y) = \sqrt{R^2 - x^2}, \ -L/2 \leq y \leq L/2 \text{ and } x \leq R$$

$$\text{C: } \begin{cases} w(x,y) = \sqrt{R^2 - x^2}, & -L/2 \leq y < L_{ce} - L/2 \text{ and } x \leq R \\ w(x,y) = \sqrt{R^2 \dfrac{(y - L/2)^2}{(L_{ce} - L)^2} - x^2}, & L_{ce} - L/2 \leq y \leq L/2 \text{ and } x \leq R \dfrac{y - L/2}{L_{ce} - L} \end{cases}$$

$$\text{D: } \begin{cases} w(x,y) = \sqrt{R^2 - x^2} - \sqrt{R_{ce}{}^2 - x^2}, & -L/2 \leq y < L_{ce} - L/2 \text{ and } x < R_{ce} \\ w(x,y) = \sqrt{R^2 - x^2}, & -L/2 \leq y < L_{ce} - L/2 \text{ and } R_{ce} \leq x \\ w(x,y) = \sqrt{R^2 \dfrac{(y - L/2)^2}{(L_{ce} - L)^2} - x^2}, & L_{ce} - L/2 \leq y \leq L/2 \text{ and } x \leq R \dfrac{y - L/2}{L_{ce} - L} \end{cases}$$

and $w(x,y) = 0$ for any point at a position not defined in the expressions above. The resulting volume averaging correction factors are given in Table 31.

If model D is considered to be the most accurate chamber representation, then Eq. (52) overestimates slightly the volume averaging effect because it assigns too much weight to the peripheral radial regions of the chamber. However, it is clear that all models yield results within reasonable agreement. For this reason, the volume averaging correction is calculated in this COP for FFF beam types in clinical use according to model A, i.e. a simple integration over a line having the length of the thimble ionization chamber.

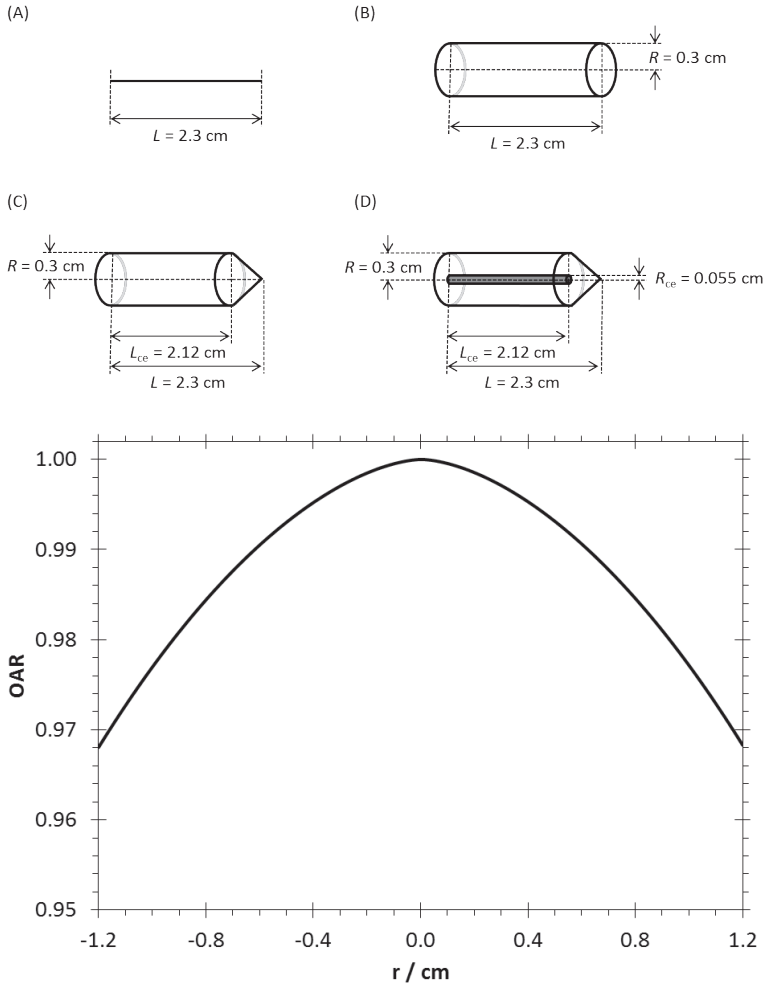

FIG. 22. Upper panel: illustration (not to scale) of the four models considered for the calculation of the volume averaging correction for a thimble ionization chamber in an FFF beam: (A) a line shaped detector of 2.3 cm length, (B) a cylinder of 2.3 cm length and 0.6 cm diameter, (C) a cylinder of 2.12 cm length and 0.6 cm diameter with a conical tip of 0.18 cm length (corresponding to a Farmer type cavity volume without a central electrode), and (D) a cylinder of 2.12 cm length and 0.6 cm diameter with a conical tip of 0.18 cm length and a cylindrical central electrode of 2.12 cm length and 0.11 cm diameter (corresponding to a Farmer type chamber with central electrode). Lower panel: lateral beam profile of a CyberKnife [83] used for illustrating the calculation of the volume averaging correction.

TABLE 31. VOLUME AVERAGING CORRECTION FACTORS $\left(k_{\mathrm{vol}}\right)_{Q}^{f_{\mathrm{ref}}}$

(calculated with Eqs (52) or (53) using the weighting factors w(x,y) *of the four models illustrated in Fig. 22)*

Method	$\left(k_{\mathrm{vol}}\right)_{Q}^{f_{\mathrm{ref}}}$
Eq. (52) (Kawachi)	1.011 6
Eq. (53) Model A	1.010 8
Eq. (53) Model B	1.011 4
Eq. (53) Model C	1.010 5
Eq. (53) Model D	1.010 5

Measured lateral beam profiles were extracted from the literature for Varian TrueBeam [27], Siemens Artiste [185], TomoTherapy HiArt [186] and CyberKnife [83] machines. For the FFF beams in an Elekta Versa HD, beam profiles were kindly provided by W. Lechner from the Medical University of Vienna. For the Varian TrueBeam and Elekta Versa HD, profiles for nominal accelerator potentials of 6 MV and 10 MV were included in the calculations. Figure 23 shows the volume averaging effect (the reciprocal of the volume averaging correction factor) for these beam profiles. It can be observed that, except for the CyberKnife, the volume averaging effect is very similar for all beams with nominal accelerator potentials of 6–7 MV. The same can be concluded for 10 MV beams. The much larger volume averaging effect for CyberKnife can be explained by a combination of the influence of the closer measuring distance and the narrower primary collimator.

As a result of a fitting procedure for these data it was found that, except for the CyberKnife, the volume averaging effects in Fig. 23 are reproduced within 0.05% for chamber lengths up to 2.4 cm by the following expression for the correction factor:

$$\left(k_{\mathrm{vol}}\right)_{Q}^{f_{\mathrm{ref}}} = 1 + \left(6.2\times10^{-3}\cdot \mathrm{TPR}_{20,10}(10) - 3.57\times10^{-3}\right)\cdot\left(\frac{100}{\mathrm{SDD}}\right)^{2}\cdot L^{2} \qquad (54)$$

where L is the length, in cm, of the thimble ionization chamber and SDD is the source-to-detector distance (which equals the source-to-surface distance, SSD,

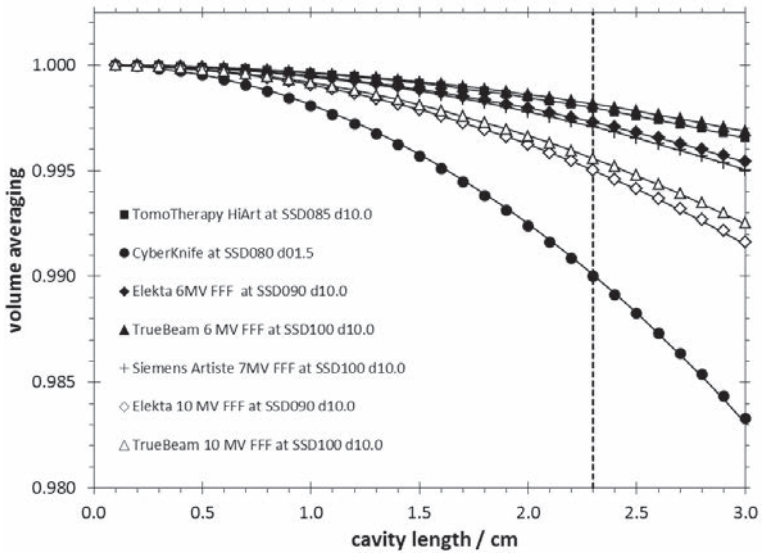

FIG. 23. Volume averaging effect (the reciprocal of the volume averaging correction factor) for various FFF beams based on measured profiles and calculated using Eq. (53) according to model A in Fig. 22. Source-to-surface distances (SSD) and depths (d), both in cm, for which the profiles have been measured are indicated in the legends. The full lines are quadratic fits with only the coefficient of the second order term as free parameter (the zero-th and first order terms being fixed at 1 and 0).

plus the measurement depth), in cm. The assumption is made that the field size is defined at a distance of 100 cm from the photon source.

Using $\%dd(10,10)_x$ the following expression was found to provide similar accuracy:

$$\left(k_{\mathrm{vol}}\right)_Q^{f_{\mathrm{ref}}} = 1 + \left(5.9\times10^{-5}\cdot\%dd(10,10)_{\mathrm{X}} - 3.38\times10^{-3}\right)\cdot\left(\frac{100}{\mathrm{SDD}}\right)^2\cdot L^2 \qquad (55)$$

For CyberKnife machines, these expressions are not adequate due to the considerably larger volume averaging effects. An accurate expression for the volume averaging correction factor for CyberKnife machines at an SSD of 80 cm and a measurement depth of 1.5 cm was found to be:

$$\left(k_{\mathrm{vol}}\right)_Q^{f_{\mathrm{ref}}} = 1 + 1.9\times10^{-3}\cdot L^2 \qquad (56)$$

Table 32 gives the generic volume averaging correction factors for different ionization chambers as a function of $\mathrm{TPR}_{20,10}(10)$ or beam type used in this COP. They are all based on Eq. (54) and an SDD of 100 cm, except for

CyberKnife where they are based on Eq. (56). For TomoTherapy machines, $TPR_{20,10}(10) = 0.645$ was selected as a typical value derived from literature data; it corresponds to a 10 cm × 10 cm hypothetical reference field. These values have been used in the calculation of the generic values of $k_Q^{f_{ref}}$ for FFF beams given in Table 13.

If the measurement is performed at a different SDD or if a specific $\left(k_{vol}\right)_Q^{f_{ref}}$ is available, determined directly from a measured lateral beam profile, the generic $k_Q^{f_{ref}}$ can be multiplied by the ratio of the specific volume averaging correction factor as follows (values are given in Table 32):

$$\left(k_Q^{f_{ref}}\right)^{specific} = \left(k_Q^{f_{ref}}\right)^{Table\,12} \frac{\left[\left(k_{vol}\right)_Q^{f_{ref}}\right]^{specific}}{\left[\left(k_{vol}\right)_Q^{f_{ref}}\right]^{Table\,32}} \tag{57}$$

where $\left[\left(k_{vol}\right)_Q^{f_{ref}}\right]^{specific}$ represents the 'better' estimate of $\left(k_{vol}\right)_Q^{f_{ref}}$.

I.2.4. $k_Q^{f_{ref}}$ values for FFF beams

$k_Q^{f_{ref}}$ values (with reference to $Q_0 = {}^{60}Co$) for FFF beams as a function of $TPR_{20,10}(10)$ have been obtained as the product of the $k_Q^{f_{ref}}$ values for WFF beams in Table 12, correction factors for the difference in water to air stopping-power ratio from Table 30 and the volume averaging correction factors from Table 32. The recommended set of $k_Q^{f_{ref}}$ values for FFF beams is given in Table 13.

To obtain the $\%dd(10,10)_x$ corresponding to the $TPR_{20,10}(10)$ values in the table in a way similar to that used for WFF beams, a separate table of $k_Q^{f_{ref}}$ as a function of $\%dd(10,10)_x$ was built for a range of initial $\%dd(10,10)_x$ estimates. These $k_Q^{f_{ref}}$ values were obtained as the product of interpolated $k_Q^{f_{ref}}$ values from Table 12, correction factors for the difference in water to air stopping-power ratio derived from the fits in Fig. 21 and volume averaging corrections calculated with Eq. (55). New estimates of the corresponding $\%dd(10,10)_x$ were then obtained by iteratively minimizing the sum of the squares of differences between the $k_Q^{f_{ref}}$ values in both tables and recalculating the correction factors for the difference in water to air stopping-power ratios and the volume averaging corrections for the new estimates of $\%dd(10,10)_x$ in each step of the iteration. This procedure leads to the values of $\%dd(10,10)_x$ given in Table 30, and the product of the three factors results in the $k_Q^{f_{ref}}$ values of Table 13. Note that $k_{Q_{msr}}^{f_{msr},f_{ref}}$ values are assumed to be identical to the tabulated $k_Q^{f_{ref}}$ values.

There is evidence from measured or Monte Carlo calculated data to support these values, but it is mostly restricted to CyberKnife or TomoTherapy machines. For the CyberKnife beams, an experimental investigation compared the response

TABLE 32. GENERIC VOLUME AVERAGING CORRECTION FACTORS $\left(k_{\mathrm{vol}}\right)_{Q}^{f_{\mathrm{ref}}}$

Ion chamber	$TPR_{20,10}(10)$ =	0.63	0.66	0.69	0.72	0.75	CyberKnife	(TomoTherapy HiArt)[a]
Capintec PR-06C/G Farmer		1.002	1.003	1.003	1.004	1.005	1.009	1.002
Exradin A2 Spokas		1.000	1.001	1.001	1.001	1.001	1.002	1.001
Exradin A12 Farmer		1.002	1.003	1.004	1.005	1.006	1.011	1.003
Exradin A12S		1.000	1.001	1.001	1.001	1.001	1.003	1.001
Exradin A19		1.002	1.003	1.004	1.006	1.007	1.012	1.003
Nuclear Assoc 30-751 Farmer		1.002	1.003	1.004	1.005	1.006	1.010	1.002
Nuclear Assoc 30-752 Farmer		1.002	1.003	1.004	1.005	1.006	1.010	1.002
NE 2505/3, 3A Farmer		1.002	1.003	1.004	1.005	1.006	1.011	1.002
NE 2571 Farmer		1.002	1.003	1.004	1.005	1.006	1.011	1.002
NE 2611		1.000	1.000	1.001	1.001	1.001	1.002	1.000
PTW 23331 rigid		1.002	1.003	1.003	1.004	1.005	1.009	1.002
PTW 23332 rigid		1.001	1.002	1.002	1.003	1.003	1.006	1.001

TABLE 32. GENERIC VOLUME AVERAGING CORRECTION FACTORS $\left(k_{\mathrm{vol}}\right)_{Q}^{f_{\mathrm{ref}}}$ (cont.)

Ion chamber	$TPR_{20,10}(10)$ =	0.63	0.66	0.69	0.72	0.75	CyberKnife	(TomoTherapy HiArt)[a]
PTW 23333 (3 mm cap)		1.002	1.003	1.003	1.004	1.005	1.009	1.002
PTW 30001 Farmer		1.002	1.003	1.004	1.005	1.006	1.010	1.002
PTW 30010 Farmer		1.002	1.003	1.004	1.005	1.006	1.010	1.002
PTW 30002/30011 Farmer		1.002	1.003	1.004	1.005	1.006	1.010	1.002
PTW 30004/30012 Farmer		1.002	1.003	1.004	1.005	1.006	1.010	1.002
PTW 30006/30013 Farmer		1.002	1.003	1.004	1.005	1.006	1.010	1.002
PTW 31003/31013 Semiflex		1.001	1.001	1.002	1.002	1.003	1.005	1.001
SNC 100700-0 Farmer		1.002	1.003	1.004	1.005	1.006	1.011	1.003
SNC 100700-1 Farmer		1.002	1.003	1.004	1.005	1.006	1.011	1.003
Victoreen Radocon III 555		1.002	1.003	1.004	1.005	1.006	1.010	1.002
Victoreen 30-348		1.001	1.002	1.002	1.003	1.003	1.006	1.001
Victoreen 30-351		1.002	1.003	1.004	1.005	1.006	1.010	1.002

TABLE 32. GENERIC VOLUME AVERAGING CORRECTION FACTORS $\left(k_{\mathrm{vol}}\right)_{Q}^{f_{\mathrm{ref}}}$ (cont.)

Ion chamber	$TPR_{20,10}(10)$ =	0.63	0.66	0.69	0.72	0.75	CyberKnife	(TomoTherapy HiArt)[a]
Victoreen 30-349		1.002	1.003	1.003	1.004	1.005	1.009	1.002
Victoreen 30-361		1.002	1.003	1.004	1.004	1.005	1.009	1.002
IBA FC-65P (Wellhöfer IC 69) Farmer		1.002	1.003	1.004	1.005	1.006	1.010	1.002
IBA FC-65G(Wellhöfer IC 70) Farmer		1.002	1.003	1.004	1.005	1.006	1.010	1.002

Note: Calculated using Eq. (56) for the CyberKnife and Eq. (54) at an SDD = 100 cm for all other FFF beams.

[a] For TomoTherapy machines, $TPR_{20,10}(10) = 0.645$ is used as a typical value derived from literature data; it corresponds to a 10 cm × 10 cm hypothetical reference field.

of a PTW 30013 Farmer chamber in water at 5 cm depth with that of alanine dosimeters [76, 82]. The results were presented in the form of $k_{Q_{msr},Q}^{f_{msr},f_{ref}}$, but from the data reported, the value of $k_{Q_{msr}}^{f_{msr},f_{ref}}$ can be calculated to be 0.991 ± 0.016 [76] and 0.989 ± 0.016 [82]. While these results are approximately 1% lower than the value given in Table 13, the difference is within the uncertainties of the measurement. Various authors have calculated $k_{Q_{msr}}^{f_{msr},f_{ref}}$ data by the Monte Carlo method, either from detailed simulations of the ionization chamber geometry [51] or by calculation of the contributing factors in the equation for beam quality correction factors [81, 187, 188]. Because the latter three papers only include values not corrected for volume averaging, data with and without the volume averaging correction factors from Table 32 applied are shown in Table 33. Good agreement between the Monte Carlo calculated data and the data of Table 13 can be observed for all chambers investigated.

For TomoTherapy machines, only two experimental investigations are related to ionization chamber types recommended in this COP for reference dosimetry [189, 190]. The response of a NE 2611 chamber was compared with that of alanine, resulting in $k_{Q_{msr}}^{f_{msr},f_{ref}} = 0.996$ [189], which can be compared to the 0.993 value in Table 13. Another publication compared the response of NE 2611 and NE 2571 chambers with alanine, obtaining $k_{Q_{msr}}^{f_{msr},f_{ref}}$ values of 0.992 and 1.010, respectively [190]; these can be compared to the corresponding values of 0.993 and 1.003 in Table 13. Other experimental studies [190, 191], as well as Monte Carlo calculations [28, 30], have confirmed that the data for an A1SL chamber also agree with values calculated using the method described in this Appendix to arrive at the data in Table 13. Monte Carlo calculations for some of the chambers recommended in this COP, obtained either from detailed simulations of the chamber geometry [186] or by calculation of the contributing factors in the equation for beam quality correction factors, have also been reported [192]; they are compared in Table 34 with the values recommended in this COP, and they again show good agreement.

I.2.5. Uncertainties of $k_Q^{f_{ref}}$ values for FFF beams

The uncertainty of $k_Q^{f_{ref}}$ values for WFF beams needs to be combined with those for the correction of the water to air stopping-power ratio, the assumption that perturbation correction factors are the same as for WFF beams and the volume averaging correction factor.

The uncertainty on the correction of the water to air stopping-power ratio has been estimated by assuming an asymmetric triangular distribution with the WFF data as upper limit, the Xiong and Rogers data [35] as lower limit and the values from Dalaryd et al. [37] as mode. For the data as a function of $TPR_{20,10}(10)$ this results in a relative standard uncertainty of 0.2%, while for the data as a

TABLE 33. COMPARISON OF MONTE CARLO CALCULATED VALUES OF $k_{Q_{msr}}^{f_{msr},f_{ref}}$ [a] FOR CYBERKNIFE MACHINES FROM FOUR REFERENCES AND THOSE OBTAINED IN THIS CODE

Ionization chamber	$k_{Q_{msr}}^{f_{msr},f_{ref}}$				
Reference	[51]	[187]	[81]	[188]	This COP
Exradin A12	1.006	0.996 (1.007)		0.995 (1.006)	0.993 1.004
Exradin A12S			0.995 (0.998)		0.991 0.993
NE 2571	1.003				0.992 1.003
NE 2561/2611			0.994 (0.996)		0.991 0.993
PTW 30001		0.989 (0.999)			0.989 0.999
PTW 30002		0.992 (1.002)			0.991 0.999
PTW 30004		0.993 (1.003)			0.993 1.003
PTW 30006/30013	1.000	0.989 (0.999)		0.991 (1.001)	0.989 0.999

Note: For each chamber, the upper row corresponds to values without a volume averaging correction factor and the lower row to corrected values (those within parenthesis have been derived from the published values using the generic volume averaging correction factors in Table 32).

[a] $k_{Q_{msr},Q_0}^{f_{msr},f_{ref}}$ with reference to $Q_0 = {}^{60}$Co.

function of $\%dd(10,10)_x$ the resulting relative standard uncertainty is negligible (<0.05%).

For the generic volume averaging correction factors used in the calculations, a relative standard uncertainty of 0.2% has been assumed based on (i) the agreement of the generic data with those calculated for the individual beams, (ii) the simplification made by using model A in Fig. 22, (iii) uncertainties of the ionization chamber geometries, and (iv) the assumption of generic beam profiles

TABLE 34. COMPARISON OF MONTE CARLO CALCULATED VALUES OF $k_{Q_{msr}}^{f_{msr},f_{ref}}$ [a] FOR TOMOTHERAPY HIART MACHINES FROM TWO REFERENCES AND THOSE USED IN THIS CODE

Ionization chamber	$k_{Q_{msr}}^{f_{msr},f_{ref}}$ [a]		
Reference	[186]	[192]	This COP
Exradin A12	1.000		0.996 0.998
NE 2571	0.997	0.995 (0.997)	0.994 0.996
PTW 30006/30013	0.997	0.995 (0.997)	0.993 0.995

Note: For each chamber, the upper row corresponds to values without a volume averaging correction factor and the lower row to corrected values (those within parenthesis have been derived from the published values using the generic volume averaging correction factors in Table 32).

[a] $k_{Q_{msr},Q_0}^{f_{msr},f_{ref}}$ with reference to $Q_0 = {}^{60}$Co.

established from variations of profiles measured by different authors for the same machine type.

Given the slow variation of other correction factors with beam quality, the assumption that they are the same for FFF and WFF beams was estimated to result in an additional uncertainty contribution of not more than 0.1%. The resulting estimation of the combined relative standard uncertainty of the recommended $k_Q^{f_{ref}}$ values for FFF beams given in Table 13 is therefore 1%. Based on current knowledge and uncertainty estimates, it is assumed that $k_{Q_{msr}}^{f_{msr},f_{ref}}$ equals $k_Q^{f_{ref}}$ for the hypothetical conventional reference field of the machine. No data are available on the variation of the water to air stopping-power ratios with field size, but given that the photon scatter contribution at the measurement point is smaller for FFF beams than for WFF beams, it can be assumed that this variation of water to air stopping-power will be even smaller for FFF beams. Thus, the same relative standard uncertainty of 0.15% for the $s_{w,air}$ contribution is deemed appropriate. This contribution will only marginally increase the overall uncertainty of $k_{Q_{msr}}^{f_{msr},f_{ref}}$ values as compared to the uncertainty of $k_Q^{f_{ref}}$ values.

Similar considerations as for WFF beams apply concerning the uncertainty component for the matching of $\%dd(10,10)_x$ to $TPR_{20,10}(10)$ data and when the calibration beam quality Q_0 is not ^{60}Co, but another FFF linac beam.

I.2.6. Equivalent uniform square field sizes of FFF beams

In FFF beams, the scatter for a given field size is smaller than in WFF beams due to the non-uniform lateral beam profile. As a result, for a 10 cm × 10 cm reference field, the equivalent uniform square field side is smaller than 10 cm.

Measured ratios of ionization chamber readings as a function of field size show that the scatter function of FFF beams is very similar to that of WFF beams and, especially for equivalent square field sides smaller than 12 cm, cannot be distinguished; hence, the scatter function given in Eq. (50) can be used for FFF beams. In the integration over the field area, however, a function $F(r)$ describing the radial dependence of the lateral beam profile has to be introduced[14]:

$$SC_{\text{field}} = \frac{1}{2\pi} \iint_{\text{field area}} \left(\lambda(1-\mu)\frac{e^{-\lambda r}}{r} + \mu\lambda^2 e^{-\lambda r} \right) F(r)\, r\, \mathrm{d}r\, \mathrm{d}\theta \tag{58}$$

Note that Eq. (51) for WFF beams is only a special case of Eq. (58), with $F(r) = 1$. Using the same approach as for WFF beams, i.e. defining field sizes to be equivalent if their scatter components, calculated with Eq. (58), are the same, equivalent uniform square field sizes were calculated for square, circular and rectangular fields in FFF beams using published lateral beam profiles measured at the depth of maximum dose. The results for 6–7 MV and 10 MV beams were obtained as averages of all available data for each nominal accelerating potential, and provided as generic values for 6–7 MV and 10 MV beams in Tables 16 and 17, respectively.

Samples of the values are shown in Fig. 24, which illustrates the dependence of the relation between different field shapes for 6–7 MV and 10 MV beams; these differ due to the difference in the non-uniform lateral beam profiles. The equivalent flattened square field size on the ordinate axis is not to be confused with an equivalent square field in a WFF beam but rather here is a (virtual) uniform field with the same photon spectrum as the non-uniform msr or ref field in the FFF beam. Since having different FFF fields with the same equivalent uniform square field size means that they have the same scatter component, equivalent square field sizes of circular or rectangular FFF fields can be obtained from Fig. 24 using the same procedure as in Fig. 20.

[14] For simplicity it is assumed that FFF beams have radial symmetry, but any 2-D profile could be used in the integration.

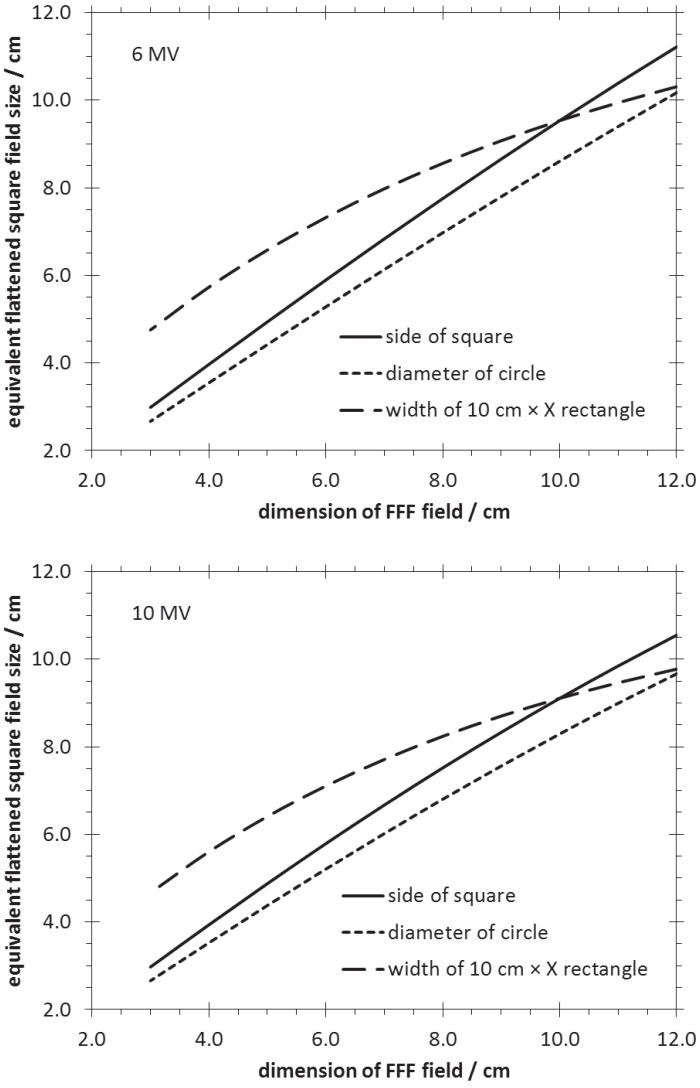

FIG. 24. Equivalent uniform square field sizes of msr fields of various shapes and dimensions in FFF beams with nominal accelerating potentials of 6 MV (upper panel) and 10 MV (lower panel). The dimension of the FFF field, represented on the horizontal axis, refers to the size of square fields, the diameter of circular fields or the width X of rectangular fields with a length of 10 cm.

Appendix II

DETERMINATION OF FIELD OUTPUT CORRECTION FACTORS AND THEIR UNCERTAINTY ESTIMATES

Following the considerable amount of research in small megavoltage photon beam dosimetry during recent years, there is a large amount of experimental and Monte Carlo calculated data available for detector specific[15] output correction factors, $k_{Q_{\text{clin}},Q_{\text{msr}}}^{f_{\text{clin}},f_{\text{msr}}}$, particularly for certain solid state detectors and ionization chambers on the central axis of 6 MV beams. Unfortunately, the published data are rather scattered for certain field sizes, especially for the smallest fields, and lack homogeneity with regard to the SSD or SDD used, the depth of measurement or calculation, the definition of field size at the surface or at a reference depth, etc. To further complicate the determination of average values for the different detectors and their subsequent statistical analysis, most of the published data lack a proper estimation of the uncertainty in the various steps involved in the determination of the correction factors given by the different authors.

II.1. SELECTION OF DATASETS FOR DERIVING FIELD OUTPUT CORRECTION FACTORS

To derive small field output correction factors from the literature for the range of small field detectors considered in this COP, three types of datasets have been considered:

(i) Reference detectors, perturbation free except for volume averaging

When available, experimental data were obtained by comparing the field size dependence of the small field detector with that of another small field (reference) detector which can be assumed to be perturbation free except for volume averaging. This is the case for reference detectors with radiological properties and densities that are not too different from the corresponding values for water, and, since they enter Eq. (47) as a ratio, it can be assumed that no other correction than volume averaging is required. Examples of such reference detectors are alanine, TLDs, organic scintillators and radiochromic film. For these detectors, the $k_{Q_{\text{clin}},Q_{\text{msr}}}^{f_{\text{clin}},f_{\text{msr}}}$ values for the small field detector were derived from the published data as follows:

[15] Monte Carlo calculations of simplified detector geometries are not considered in this section.

$$k_{Q_{\text{clin}},Q_{\text{msr}}}^{f_{\text{clin}},f_{\text{msr}}}[\text{sfd}] = \frac{M_{Q_{\text{clin}}}[\text{ref}] \times k_{\text{vol}}[\text{ref}] / M_{Q_{\text{msr}}}[\text{ref}]}{M_{Q_{\text{clin}}}[\text{sfd}] / M_{Q_{\text{msr}}}[\text{sfd}]} \tag{59}$$

where the generic notation M_Q[#] denotes the reading of detector # in the field of quality Q, 'ref' refers to the reference detector, which is assumed to be perturbation free except for volume averaging, and 'sfd' stands for the small field detector. The factor k_{vol}[ref] is the volume averaging correction factor for the reference detector in the clinical small field; this correction is assumed to be unity for the reference field (i.e. no volume averaging correction is required for the 10 cm × 10 cm field).

In some cases the published data had already been calculated in this manner by the authors. In other cases the authors had corrected both the small field readings of the reference detector and those of the small field detector for volume averaging and reported 'residual' correction factors, i.e. a correction accounting for all fluence perturbation effects except for volume averaging. In the latter case, the reported 'residual' correction factors have been multiplied by an estimated k_{vol}[sfd], i.e. the volume averaging correction factor for the small field detector in the clinical small field. In most cases, the values according to Eq. (59) have been derived from the raw data provided in the publication's tables, by private communication with the authors or, if neither of these two was available, by digitizing graphs from the publications. If more than one reference dosimeter fulfilling the criterion of being 'perturbation free except for volume averaging' was used in a study, average values of the numerator of Eq. (59) for those detectors were used. This was the case, for example, with the Azangwe et al. dataset [100], which reported values for a number of detector types, including two types of TLDs, two alanine systems and two organic scintillators.

(ii) Reference detector with known output correction factors

Many publications are available in which a range of small field detectors have been compared but none of them can be considered 'perturbation free except for volume averaging'. If output correction factors are available for one of these detectors, which based on a substantial set of independent data differ from one another by not more than 5%, experimental output correction factors for the other detectors have been derived as follows:

$$k_{Q_{\text{clin}},Q_{\text{msr}}}^{f_{\text{clin}},f_{\text{msr}}}[\text{sfd}] = \frac{M_{Q_{\text{clin}}}[\text{ref}] \times k_{Q_{\text{clin}},Q_{\text{msr}}}^{f_{\text{clin}},f_{\text{msr}}}[\text{ref}] / M_{Q_{\text{msr}}}[\text{ref}]}{M_{Q_{\text{clin}}}[\text{sfd}] / M_{Q_{\text{msr}}}[\text{sfd}]} \tag{60}$$

Examples of such suitable reference detectors are unshielded diodes, stereotactic diodes, natural and artificially grown diamonds and liquid ionization chambers.

(iii) Monte Carlo calculated output correction factors

Output correction factors from Monte Carlo simulations were derived according to the expressions given in the international formalism by Alfonso et al. [8] (see eq. (10)), i.e.:

$$k_{Q_{\text{clin}},Q_{\text{msr}}}^{f_{\text{clin}},f_{\text{msr}}}[\text{sfd}] = \frac{D_{\text{w},Q_{\text{clin}}} / D_{\text{w},Q_{\text{msr}}}}{D_{\text{det},Q_{\text{clin}}}[\text{sfd}] / D_{\text{det},Q_{\text{msr}}}[\text{sfd}]} \tag{61}$$

where the generic notation $D_{\text{w},Q}$ stands for the average absorbed dose to water scored in a small voxel at the reference point in homogeneous water in a field of quality Q and $D_{\text{det},Q}$[sfd] is the average dose scored in the small field detector in a field of quality Q. In most publications, the output correction factors according to Eq. (61) were calculated by the authors, and in some cases they have been derived from published raw data.
Data obtained with a 'hybrid procedure', combining Monte Carlo calculated field output factors in water, determined from the dose scored in a small water voxel, with measured ratios of detector readings (as for example in Ref. [193]) were not used because even for the best commissioned Monte Carlo model it cannot be assumed that the simulation and the measurement correspond to the same particle fluence distribution. Such 'hybrid' data can, however, play an important role in the commissioning of a Monte Carlo model [194, 195].

The field size used for each data point was the equivalent field size at the measurement depth. For a SAD set-up, the nominal or stated field size corresponds to the size at the detector position. For SSD set-ups, the field size specified at the phantom surface has been scaled accounting for the divergence of the beam, i.e. at measurement depths of 5 cm and 10 cm this requires multiplying the stated field size by a factor 1.05 and 1.10, respectively. Preference has been given to measured field sizes, but if these were not available, nominal field sizes have been used. All data were assumed to apply to a measurement depth of 10 cm in water. Values obtained at the depth of maximum dose were not considered. For detectors not showing a substantial field size dependence in square field sizes above 3 cm, published data obtained at 5 cm depth were assumed to be valid at 10 cm depth. For detectors exhibiting a substantial field size dependence for sizes

above 3 cm, such as unshielded diodes, a linear field size dependent correction was applied based on data from publications where measurements at both depths were reported.

All the selected published results were renormalized to a 10 cm × 10 cm reference field size (hence f_{ref} = 10 cm × 10 cm). In many publications, data had been normalized to a smaller intermediate field size (commonly square field sizes of 3 cm, 4 cm or 5 cm), but data for a 10 cm × 10 cm reference field had been given as well. In situations where data for a 10 cm × 10 cm reference field were not available, average ratios of the output correction factors for the same detector in the intermediate field size obtained from other publications have been used to renormalize the data. For field sizes that were slightly non-square (e.g. even if they are nominally square, measured FWHM field sizes could be rectangular), as well as for circular collimated fields, the equivalent square of small field sizes was taken as the square having the same area as the rectangular or circular collimated field following the observations by Cranmer-Sargison et al. [19].

II.2. MEAN VALUES AND UNCERTAINTY ESTIMATES

Mean values of the field output correction factors and uncertainty estimates have been derived following as closely as possible Ref. [10], according to a procedure adapted from Ref. [11]:

(i) Based on the detailed uncertainty estimates made by some authors [50, 136, 196], uncertainties for the datasets used in the present analysis have been taken as 1% for all the field sizes in Monte Carlo calculations, 1% for the experimental values with fields larger than 1 cm × 1 cm, and 2% for the experimental values with fields equal to or smaller than 1 cm × 1 cm. These uncertainties are considered overall uncertainties of type B, henceforth referred to as u_{B_1}. This common choice precludes any bias due to the uncertainties quoted by the authors of the different datasets, here assumed to be identical for all the sets within each modality, experimental or Monte Carlo.

It is emphasized that measurements for the smallest field sizes are always troublesome, mainly due to the alignment of each detector, which justifies the criteria above. Monte Carlo calculations for these fields are in principle not affected by this constraint, although there are other important contributions to their uncertainty (see step (iii)).

(ii) For each detector, the entire set of data for all field sizes (experimental and Monte Carlo) has been fitted with respect to the field size S by a function having the form:

$$k_{Q_{\text{clin}},Q_{\text{ref}}}^{f_{\text{clin}},f_{\text{ref}}}(S)=\frac{1+d\cdot e^{-\frac{10-a}{b}}}{1+d\cdot e^{-\frac{S-a}{b}}}+c\cdot(S-10) \tag{62}$$

where the data are weighted by the uncertainties of step (i). The coefficient d can only take the binary values of $d = +1$ or $d = -1$. Data outside the 99% confidence level prediction interval are filtered out and the fit re-done to determine the final coefficients a, b and c. This step thus yields estimates of the weighted mean $k_{Q_{\text{clin}},Q_{\text{ref}}}^{f_{\text{clin}},f_{\text{ref}}}$ values as a function of the field size. Note that the equation contains a normalization forcing the fit to be equal to 1 for the 10 cm × 10 cm field size. For machines that cannot establish the 10 cm × 10 cm reference field, $k_{Q_{\text{clin}},Q_{\text{msr}}}^{f_{\text{clin}},f_{\text{msr}}}$ values were derived from the values given by Eq. (62) as follows:

$$k_{Q_{\text{clin}},Q_{\text{msr}}}^{f_{\text{clin}},f_{\text{msr}}}(S)=\frac{k_{Q_{\text{clin}},Q_{\text{ref}}}^{f_{\text{clin}},f_{\text{ref}}}(S)}{k_{Q_{\text{msr}},Q_{\text{ref}}}^{f_{\text{msr}},f_{\text{ref}}}(S_{\text{msr}})} \tag{63}$$

where S_{msr} is the equivalent square small field size of the machine specific reference field f_{msr}.

(iii) An overall type B standard uncertainty, u_B, for each field size and detector type has been estimated from the range of data values, including the experimental and Monte Carlo values. This is evaluated by assuming that the limiting values $\pm L$ of the data range for each field size correspond to the 95% confidence limits of a normal (Gaussian) distribution; thus $u_B = L/2$. Note that this is a compromise between assuming a rectangular $\left(u_B = L/\sqrt{3}\right)$ or a triangular $\left(u_B = L/\sqrt{6}\right)$ distribution for the data (see Refs [111, 197]). This overall u_B is assumed to correspond to the contribution of possibly correlated items and details not accounted for in the different publications. For example, the reading of many detectors often requires elaborate procedures and corrections, and all measurements are relative to a given reference detector (of diverse type) whose response often also requires non-trivial corrections. Also, Monte Carlo data do not account for the possible influence of the radiation source type (which is particularly important for the smallest field sizes), there are unknown differences between a detector's design (blueprints on which the simulation geometry is based) and its actual production by the manufacturer, and there are details about the detector's operation that cannot be simulated [114]. In both modalities of data, differences between detectors of the same model and manufacturer and accelerator-to-accelerator differences are also often ignored.

For some detectors and/or field sizes, there are only one or two datasets available and the method does not yield a realistic estimate of u_B; in those few cases the uncertainty has been taken to be as for a similar detector type.

(iv) The combined standard uncertainty for the mean $k_{Q_{clin},Q_{msr}}^{f_{clin},f_{msr}}$ values, u_c, becomes strongly dominated by the u_B above, which is about one order of magnitude larger than u_{B_1}, especially for the smallest beam sizes. Adding u_{B_1} to u_B in u_c would involve some degree of double counting; hence, the uncertainty weights in the fits of step (ii) are used only to weight differently experimental vs Monte Carlo data for certain field sizes.

II.3. DATASETS AND GRAPHS OF THE STATISTICAL ANALYSIS

Details on the sources of experimental data used in this COP to derive small field output correction factors $k_{Q_{clin},Q_{msr}}^{f_{clin},f_{msr}}$ are given in Table 35, along with information on the reference detectors and experimental conditions used for deriving output correction factors in each dataset. Table 36 gives the corresponding information for the Monte Carlo calculated correction factors. Detector and machine specific field output correction factors are given in Tables 23 to 27.

The most substantial collection of data is available for linac beams with nominal accelerating potentials of 6 MV at a measurement depth of 10 cm. No indication for significant differences in field output correction factors was found between MLC collimated beams and stereotactic cone shaped beams, represented as a function of the equivalent square small field size, confirming earlier observations [56, 136, 198]. Similarly, no significant differences in data between FFF and WFF beams were observed, confirming earlier findings reported in the literature [57, 196, 216].

All the data for 6 MV beams at the reference depth of 10 cm and with reference to 10 cm × 10 cm conventional reference fields are shown in Figs 25–30 and discussed in the following two paragraphs. In the legends of these six figures, a distinction is made between experimentally derived values and Monte Carlo calculated data; additional information is given for some data to distinguish between different datasets from the same publication. The thick continuous line and uncertainty bars (enveloped by thin continuous lines) describe the weighted mean values and their combined expanded uncertainty with a coverage factor of $k = 2$ (i.e. at 95% confidence level). The horizontal line sets the limits (0.95–1.05) within which correction factors are recommended in this COP. Data indicated by an arrow are discarded during the fitting procedure because they differ by more than 3 standard deviations from the fitted values.

Text cont. on p. 186.

TABLE 35. SOURCES OF MEASURED DATA, REFERENCE DETECTORS AND EXPERIMENTAL CONDITIONS FOR THE DETERMINATION OF SMALL SQUARE (SF) AND CIRCULAR (CF) FIELD OUTPUT CORRECTION FACTORS FOR 6 MV AND 10 MV LINAC BEAMS

Publication	Small field detectors	Reference detector	Eq.	Beam type/field range	SSD (cm)	Measurement depth (cm)
Archambault et al. [198]	Exradin A16, IBA CC13	Organic scintillator	(59)	Varian Clinac iX/standard MLC, SF 1–5 cm	90	10
Azangwe et al. [100]	IBA SFD, IBA PFD, IBA EFD, PTW 60003, PTW 60019, PTW 31018, IBA CC01, IBA CC04, IBA CC13, PTW 31014, PTW 31016, PTW 31010, PTW 31013	TLD-100, TLD microcubes, alanine (NPL), alanine (Technical University of Denmark (DTU)), two organic scintillators (DTU)	(59)	Elekta Synergy/Brainlab micro MLC, SF 0.6–6 cm	90	10
Bassinet et al. [177]	Sun Nuclear EDGE, PTW 60016, PTW 60017, PTW 31018, PTW 60003, PTW 31014, IBA SFD	EBT2 radiochromic film, TLD microcubes	(59)	Novalis/m3 micro MLC & Varian Clinac 2100/m3 micro MLC, SF 0.6–8 cm	100	10
Bucciolini et al. [199]	PTW 31006	Scanditronix-SFD unshielded diode	(60)	Elekta SL75-5/standard MLC, SF 1–9 cm	95	5

TABLE 35. SOURCES OF MEASURED DATA, REFERENCE DETECTORS AND EXPERIMENTAL CONDITIONS FOR THE DETERMINATION OF SMALL SQUARE (SF) AND CIRCULAR (CF) FIELD OUTPUT CORRECTION FACTORS FOR 6 MV AND 10 MV LINAC BEAMS (cont.)

Publication	Small field detectors	Reference detector	Eq.	Beam type/field range	SSD (cm)	Measurement depth (cm)
Cranmer-Sargison et al. [200]	PTW 60008, PTW 60012, PTW 60016, PTW 60017	IBA SFD unshielded diode	(60)	Varian iX + standard MLC, Elekta Synergy/MLCi2, SF 0.55–5.5 cm,	100	10
Crop et al. [201]	PTW 31006, PTW 60003	PTW 60003 natural diamond or radiochromic film	(60)	Elekta SLi plus/ModuLeaf, SF 1–7 cm	95	5
Eaton et al. [202]	PTW 31010	PTW 60003 natural diamond	(60)	Siemens Oncor/ModuLeaf, SF 1.05–9.45 cm	95	5
Fippel et al. [203]	PTW 60008, PTW 31006, PTW 31002	PTW 60003 natural diamond	(60)	Elekta SLi plus/standard MLC, SF 2.2–5.5 cm	100	10
Francescon et al. [50]	PTW 31014	PTW 60012 unshielded diode	(60)	Siemens Primus/ standard MLC & Elekta Synergy/standard MLC, SF 0.45–3 cm	90	10

TABLE 35. SOURCES OF MEASURED DATA, REFERENCE DETECTORS AND EXPERIMENTAL CONDITIONS FOR THE DETERMINATION OF SMALL SQUARE (SF) AND CIRCULAR (CF) FIELD OUTPUT CORRECTION FACTORS FOR 6 MV AND 10 MV LINAC BEAMS (cont.)

Publication	Small field detectors	Reference detector	Eq.	Beam type/field range	SSD (cm)	Measurement depth (cm)
Godwin et al. [204]	Sun Nuclear EDGE, Exradin A16, IBA CC01, IBA CC13	EBT2 radiochromic film	(59)	Elekta Synergy/mini MLC Apex SF 0.5–13 cm	100	10
Griessbach et al. [205]	PTW 60003, PTW 60008, PTW 60012	PTW 60003 natural diamond or PTW 60012 unshielded diode	(60)	Siemens Mevatron KD-2/Brainlab m3 micro MLC, SF 0.63–8.4 cm	100	5
Haryanto et al. [206]	PTW 60008, PTW 31006, PTW 31002	PTW 60003 natural diamond	(60)	Elekta SLi plus/standard MLC, SF 1.1–5.5 cm	100	10
Krauss [207]	PTW 60008, PTW 60012, PTW 31002, PTW 31016	PTW 31018 liquid ion chamber	(60)	Varian Clinac 2300C-D/standard MLC, SF 1–7 cm	90	10
Lambert et al. [208]	PTW 60003, PTW 31002	Organic scintillator	(50)	Varian Clinac 21iX/standard MLC, SF 1.05–9.45 cm	100	5

TABLE 35. SOURCES OF MEASURED DATA, REFERENCE DETECTORS AND EXPERIMENTAL CONDITIONS FOR THE DETERMINATION OF SMALL SQUARE (SF) AND CIRCULAR (CF) FIELD OUTPUT CORRECTION FACTORS FOR 6 MV AND 10 MV LINAC BEAMS (cont.)

Publication	Small field detectors	Reference detector	Eq.	Beam type/field range	SSD (cm)	Measurement depth (cm)
Lechner et al. [57]	IBA PFD, IBA EFD, IBA SFD, PTW 60008, PTW 60019, PTW 31018, IBA CC01, IBA CC04, IBA CC13, PTW 31014, PTW 31016, PTW 31010	Mini-alanine (NPL)	(59)	Elekta Synergy/Brainlab micro MLC, SF 0.65–4.25 cm	90	10
Marsolat et al. [132]	PTW 60003	PTW 60017 unshielded diode	(60)	Varian Clinac 2100/microMLC, SF 0.6–8 cm	100	10
Martens et al. [193]	PTW 31006	PTW 60003 natural diamond	(60)	Elekta SLi plus/standard MLC, SF 1–8 cm	95	5
Ralston et al. [56]	IBA PFD, IBA EFD, IBA SFD, PTW 60012	Organic scintillator	(59)	Varian Novalis Tx/high definition MLC, SF and CF 0.35–6 cm	90	10
Ralston et al. [133]	PTW 60019	Organic scintillator	(59)	Varian Novalis Tx/high definition MLC, SF and CF 0.35–6 cm	90	10

TABLE 35. SOURCES OF MEASURED DATA, REFERENCE DETECTORS AND EXPERIMENTAL CONDITIONS FOR THE DETERMINATION OF SMALL SQUARE (SF) AND CIRCULAR (CF) FIELD OUTPUT CORRECTION FACTORS FOR 6 MV AND 10 MV LINAC BEAMS (cont.)

Publication	Small field detectors	Reference detector	Eq.	Beam type/field range	SSD (cm)	Measurement depth (cm)
Sauer and Wilbert [24]	IBA SFD, IBA PFD, PTW 60003, PTW 31006	PTW 60003 natural diamond or Scanditronix-SFD unshielded diode	(60)	Elekta Synergy/ microMLC, SF 0.4–8 cm	100	5
Schwedas et al. [194]	PTW 60008, PTW 60012, PTW 31002, PTW 31006	PTW 60003 natural diamond	(60)	Siemens Primus/standard MLC, SF 1–5 cm	90	10
Stasi et al. [195]	Wellhöfer IC15, Exradin A14SL, Exradin A16, PTW 31006	PTW 60003 natural diamond	(60)	Varian Clinac 600 C-D/standard MLC, SF 1.1–5.5 cm	100	10
Tanny et al. [196]	Sun Nuclear EDGE, Exradin A14SL, Exradin A16, Exradin A26, PTW 31014	Exradin W1 organic scintillator	(59)	Varian TrueBeam/micro MLC, SF and CF 0.66–3.3 cm	100	10
Underwood et al. [197]	PTW 60017, PTW 60019	Exradin W1 organic scintillator	(59)	Varian TrueBeam STx/micro MLC, SF and CF 0.66–3.3 cm	95	5

TABLE 36. SOURCES OF MONTE CARLO DATA, COMPUTER CODE USED AND CONDITIONS FOR THE CALCULATION OF SMALL SQUARE (SF) FIELD OUTPUT CORRECTION FACTORS

Publication	Small field detectors	Monte Carlo system/ code	Beam type/field range	SSD (cm)	Calculation depth (cm)
Andreo et al. [11]	PTW 60019	Penelope/penEasy EGSnrc/egs_chamber	Varian Clinac iX/standard MLC, SF 0.55–4.4 cm	100	10
Benmakhlouf [209] Benmakhlouf et al. [210]	PTW 60016, PTW 60017, PTW 60018, PTW 60019, PTW 31016, PTW 31018, PTW 60003, IBA PFD, IBA EFD, IBA SFD, IBA CC01	Penelope/penEasy	Varian Clinac iX/standard MLC, SF 0.55–4.4 cm	100	10
Cranmer-Sargison et al. [211]	PTW 60016, PTW 60017, IBA SFD	BEAMnrc/DOSRZnrc	Varian iX/standard MLC, SF 0.50–5.5 cm	100	10
Czarnecki et al. [48, 49]	PTW 60016, PTW 60017, PTW 31010, PTW 31014, PTW 31016	BEAMnrc/EGSnrc	Siemens KD/standard MLC, SF 0.5–4 cm	90	10
Francescon et al. [50]	PTW 60012, Sun Nuclear EDGE, PTW 31014, PTW 31018, Exradin A16	BEAMnrc/egs_chamber	Novalis Tx/standard MLC, SF 0.53–2.1 cm	90	10

TABLE 36. SOURCES OF MONTE CARLO DATA, COMPUTER CODE USED AND CONDITIONS FOR THE CALCULATION OF SMALL SQUARE (SF) FIELD OUTPUT CORRECTION FACTORS (cont.)

Publication	Small field detectors	Monte Carlo system/ code	Beam type/field range	SSD (cm)	Calculation depth (cm)
Kamio et al. [212]	Exradin W1, PTW 60012, PTW 31018, PTW 60003, Exradin A14, Exradin A1SL, alanine	BEAMnrc/EGSnrc	Varian Clinac 21EX/Millennium MLC, SF 0.5–3 cm	90	10
Papaconstadopoulos et al. [213]	Exradin W1, Exradin D1V, PTW 60019, PTW 31018	BEAMnrc/EGSnrc	Novalis Tx/standard MLC, SF 0.53–2.1 cm	90	5
Underwood et al. [214]	Exradin W1, PTW 60012, PTW 31018, PTW 60003, Exradin A14, Exradin A1SL, alanine	BEAMnrc/egs_chamber	Varian Clinac iX, SF 0.26–1.6 cm	100	5
Wang et al. [215]	IBA CC01	EGSnrc/Cavity	Varian Clinac iX, SF 0.5–6 cm	100	5

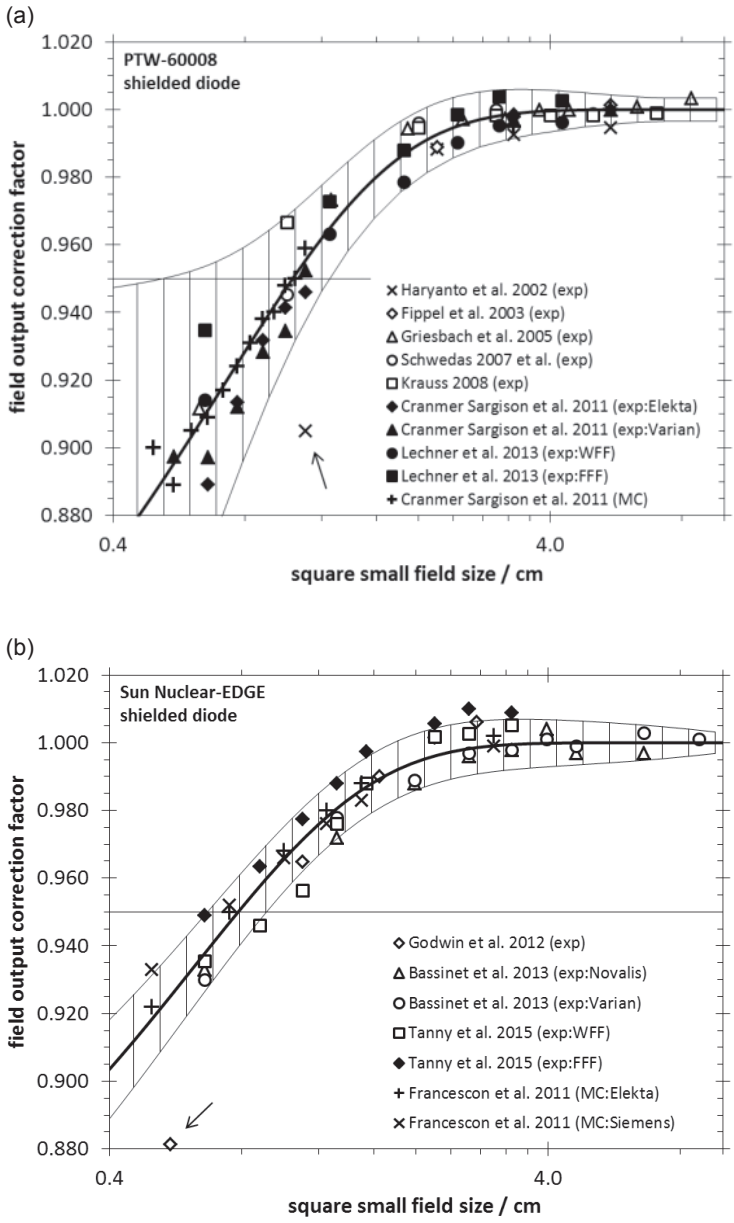

FIG. 25. Detector specific output correction factors, $k_{Q_{clin},Q_{ref}}^{f_{clin},f_{ref}}(S)$*, as a function of the field size (in logarithmic scale) and at a depth of 10 cm, for a reference field size 10 cm × 10 cm, in water on the central axis of 6 MV photon beams, for two shielded diodes, two unshielded diodes and two microionization chambers. The uncertainty estimates shown correspond to those for the individual detectors, which exclude the data indicated by arrows (see Section II.2).*

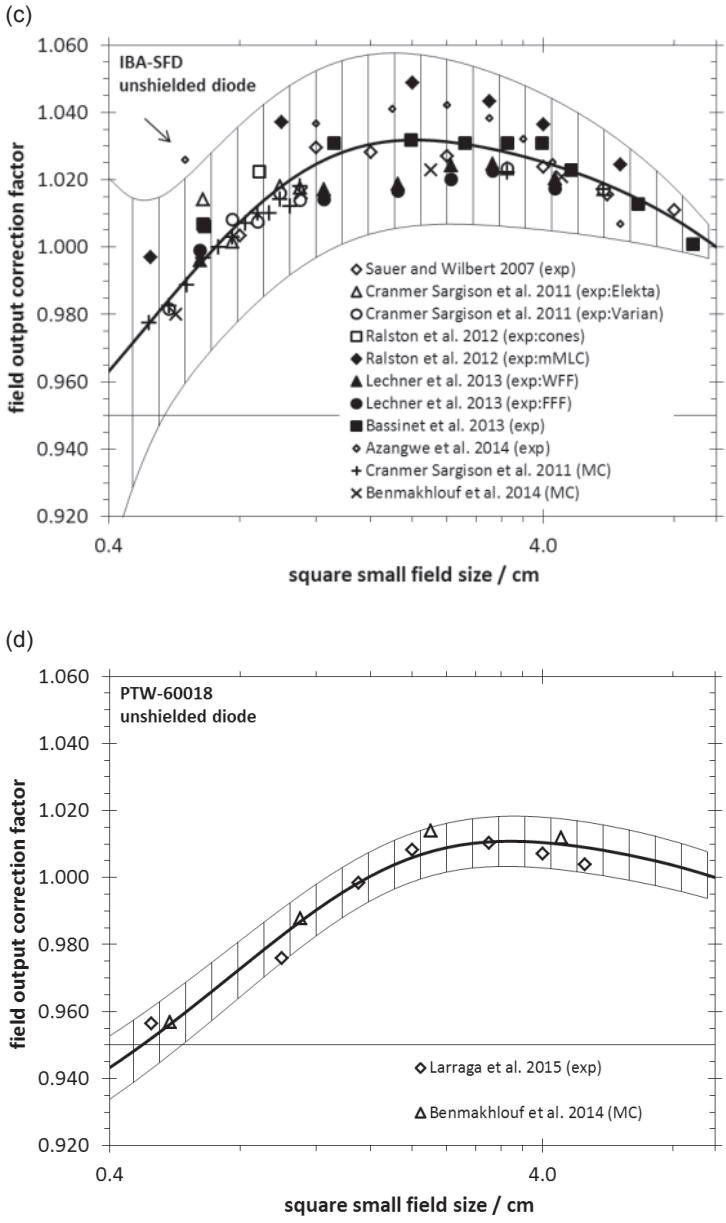

FIG. 25. (cont.) Detector specific output correction factors, $k_{Q_{clin},Q_{ref}}^{f_{clin},f_{ref}}(S)$*, as a function of the field size (in logarithmic scale) and at a depth of 10 cm, for a reference field size 10 cm × 10 cm, in water on the central axis of 6 MV photon beams, for two shielded diodes, two unshielded diodes and two microionization chambers. The uncertainty estimates shown correspond to those for the individual detectors, which exclude the data indicated by arrows (see Section II.2).*

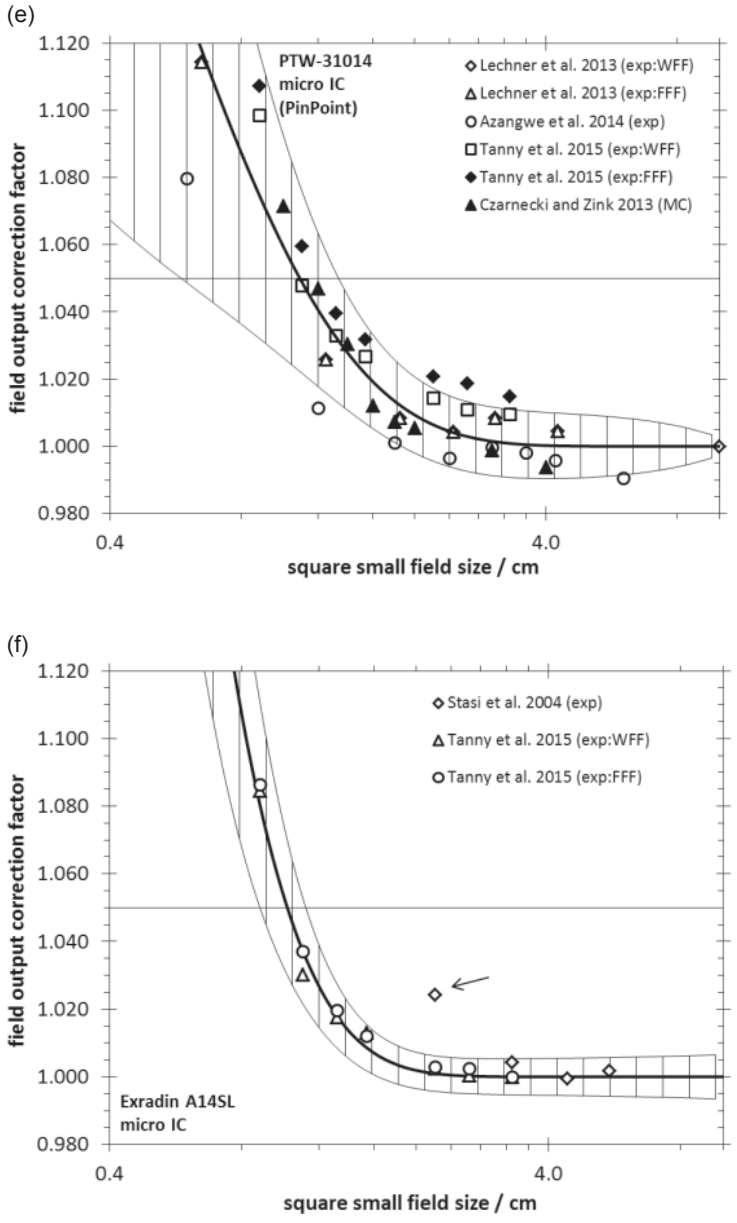

FIG. 25. (cont.) Detector specific output correction factors, $k_{Q_{clin},Q_{ref}}^{f_{clin},f_{ref}}(S)$*, as a function of the field size (in logarithmic scale) and at a depth of 10 cm, for a reference field size 10 cm × 10 cm, in water on the central axis of 6 MV photon beams, for two shielded diodes, two unshielded diodes and two microionization chambers. The uncertainty estimates shown correspond to those for the individual detectors, which exclude the data indicated by arrows (see Section II.2).*

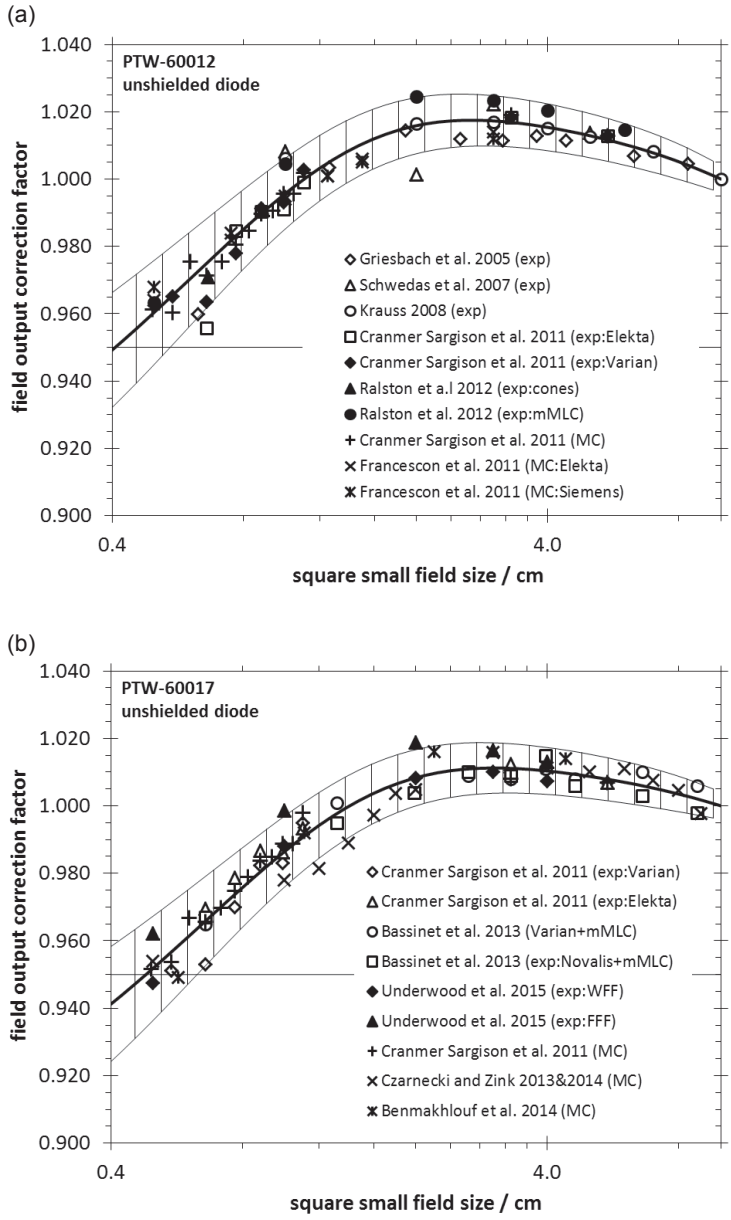

FIG. 26. Detector specific output correction factors, $k_{Q_{clin},Q_{ref}}^{f_{clin},f_{ref}}(S)$*, as a function of the field size (in logarithmic scale) and at a depth of 10 cm, for a reference field size 10 cm × 10 cm in water on the central axis of 6 MV photon beams, for unshielded diodes and the PTW 60019 microdiamond. The uncertainty estimates shown correspond to the global values for detectors of a given type provided in Table 37.*

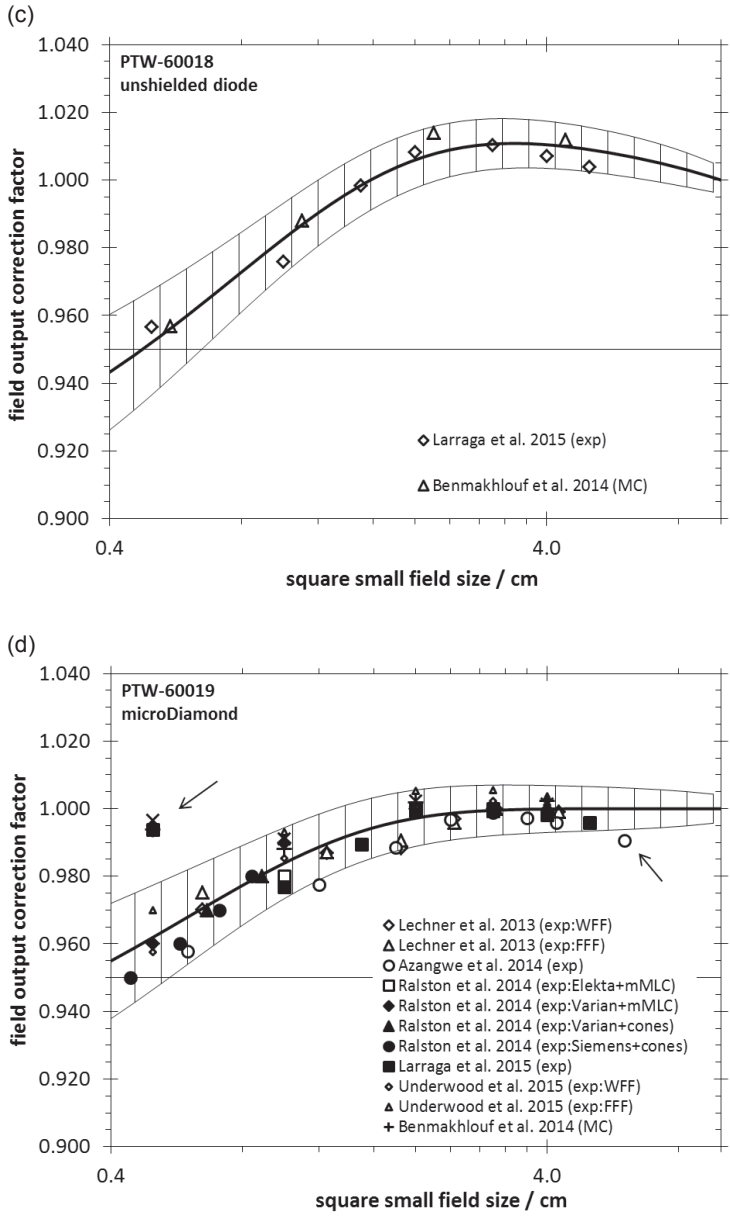

FIG. 26. (cont.) Detector specific output correction factors, $k_{Q_{clin},Q_{ref}}^{f_{clin},f_{ref}}(S)$*, as a function of the field size (in logarithmic scale) and at a depth of 10 cm, for a reference field size 10 cm × 10 cm in water on the central axis of 6 MV photon beams, for unshielded diodes and the PTW 60019 microdiamond. The uncertainty estimates shown correspond to the global values for detectors of a given type provided in Table 37.*

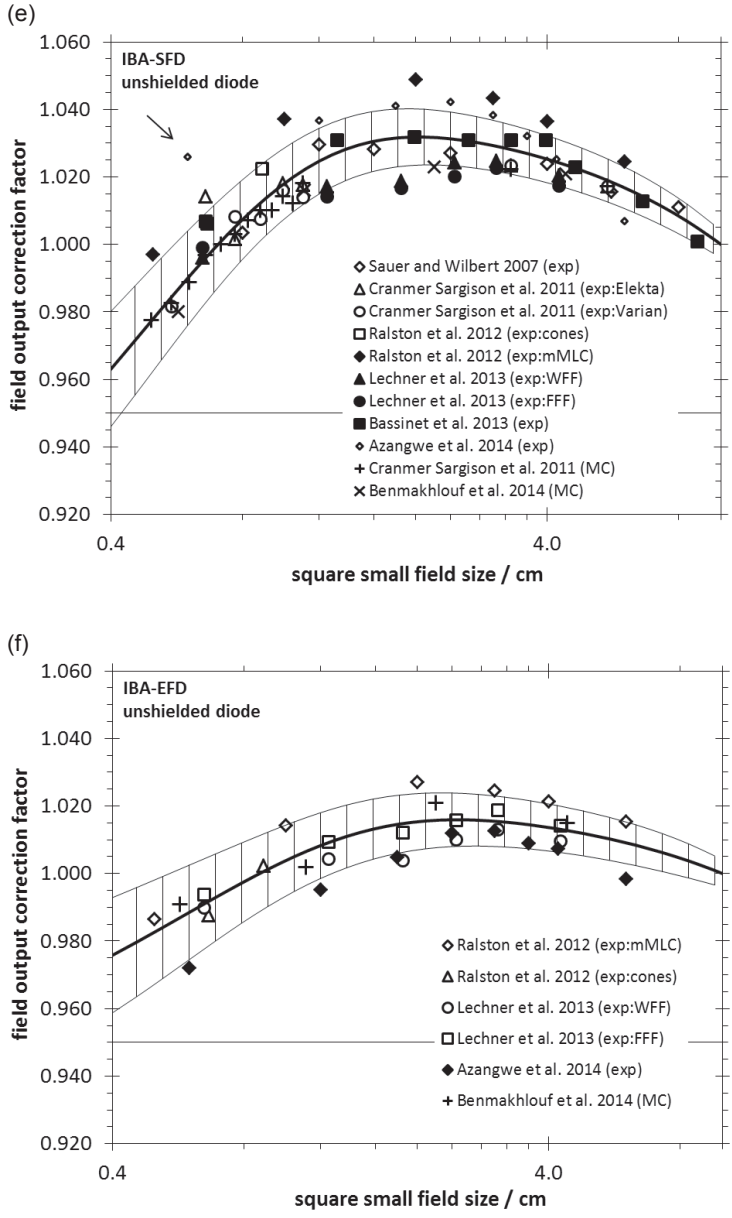

FIG. 26. (cont.) Detector specific output correction factors, $k_{Q_{clin},Q_{ref}}^{f_{clin},f_{ref}}(S)$*, as a function of the field size (in logarithmic scale) and at a depth of 10 cm, for a reference field size 10 cm × 10 cm in water on the central axis of 6 MV photon beams, for unshielded diodes and the PTW 60019 microdiamond. The uncertainty estimates shown correspond to the global values for detectors of a given type provided in Table 37.*

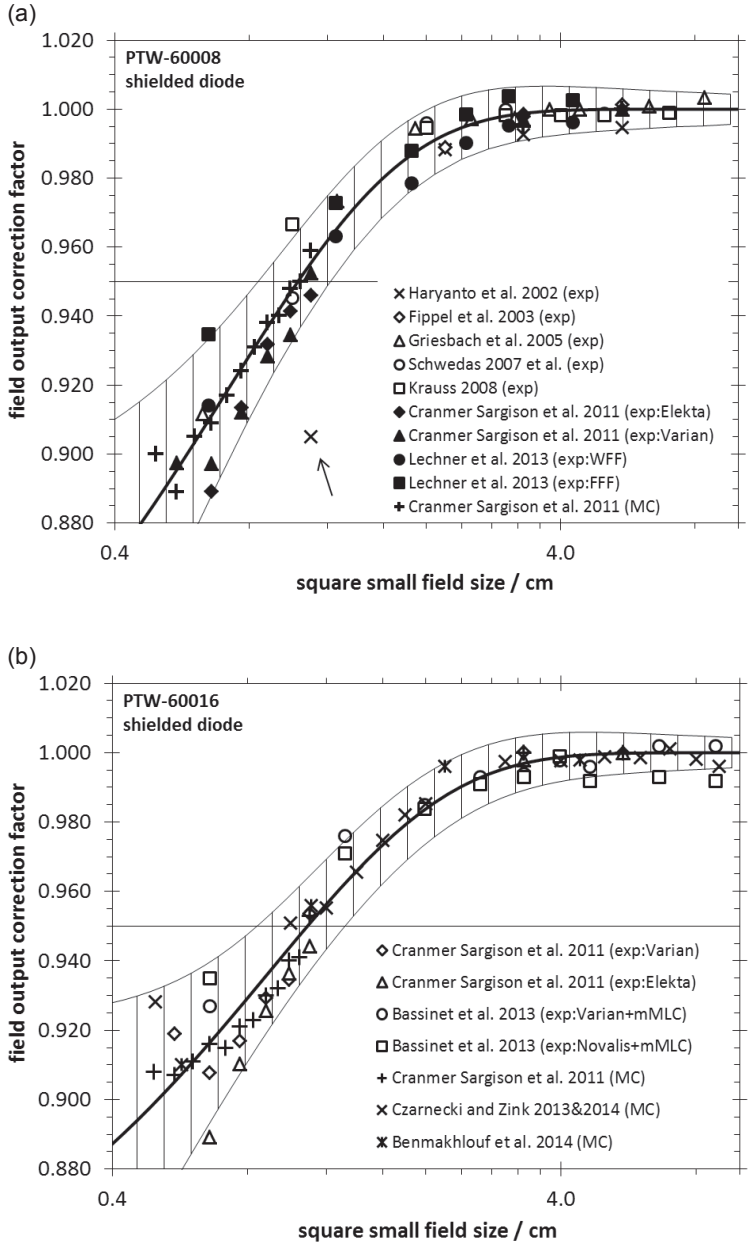

FIG. 27. Detector specific output correction factors, $k_{Q_{\text{clin}},Q_{\text{ref}}}^{f_{\text{clin}},f_{\text{ref}}}(S)$*, as a function of the field size (in logarithmic scale) and at a depth of 10 cm, for a reference field size 10 cm × 10 cm in water on the central axis of 6 MV photon beams, for shielded diodes. The uncertainty estimates shown correspond to the global values for detectors of a given type provided in Table 37.*

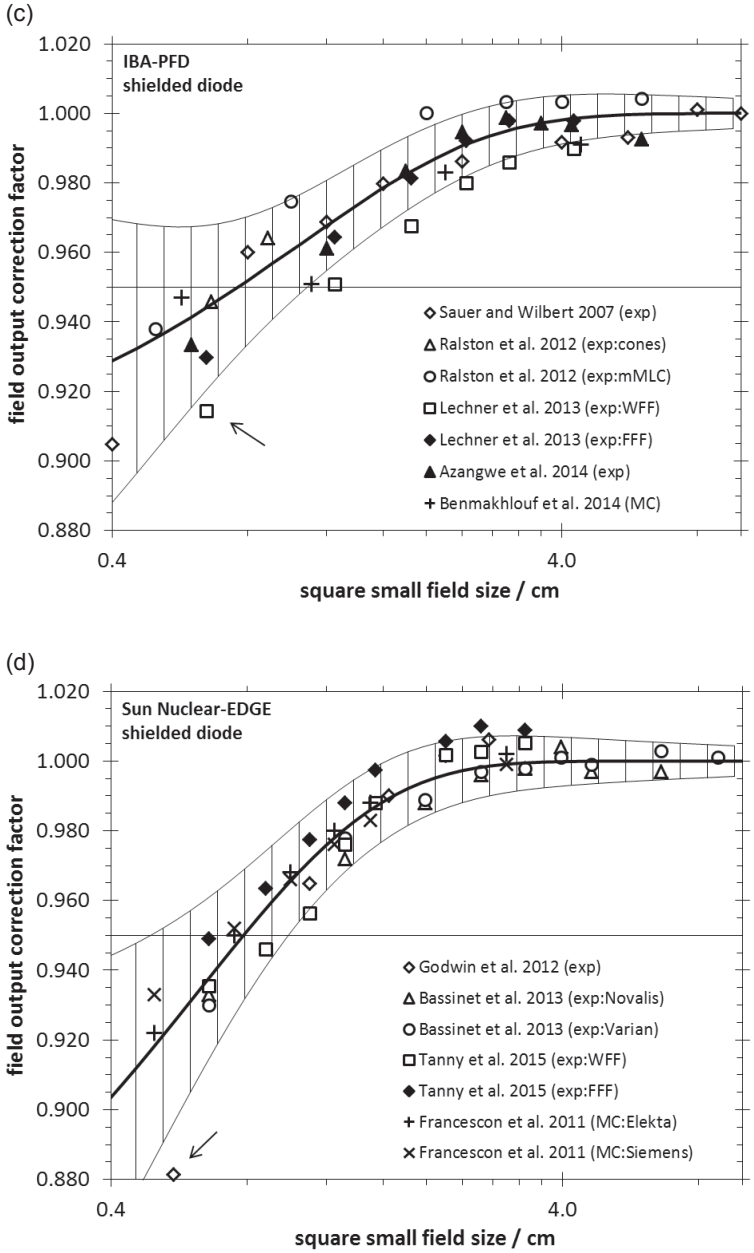

FIG. 27. (cont.) Detector specific output correction factors, $k_{Q_{clin},Q_{ref}}^{f_{clin},f_{ref}}(S)$*, as a function of the field size (in logarithmic scale) and at a depth of 10 cm, for a reference field size 10 cm × 10 cm in water on the central axis of 6 MV photon beams, for shielded diodes. The uncertainty estimates shown correspond to the global values for detectors of a given type provided in Table 37.*

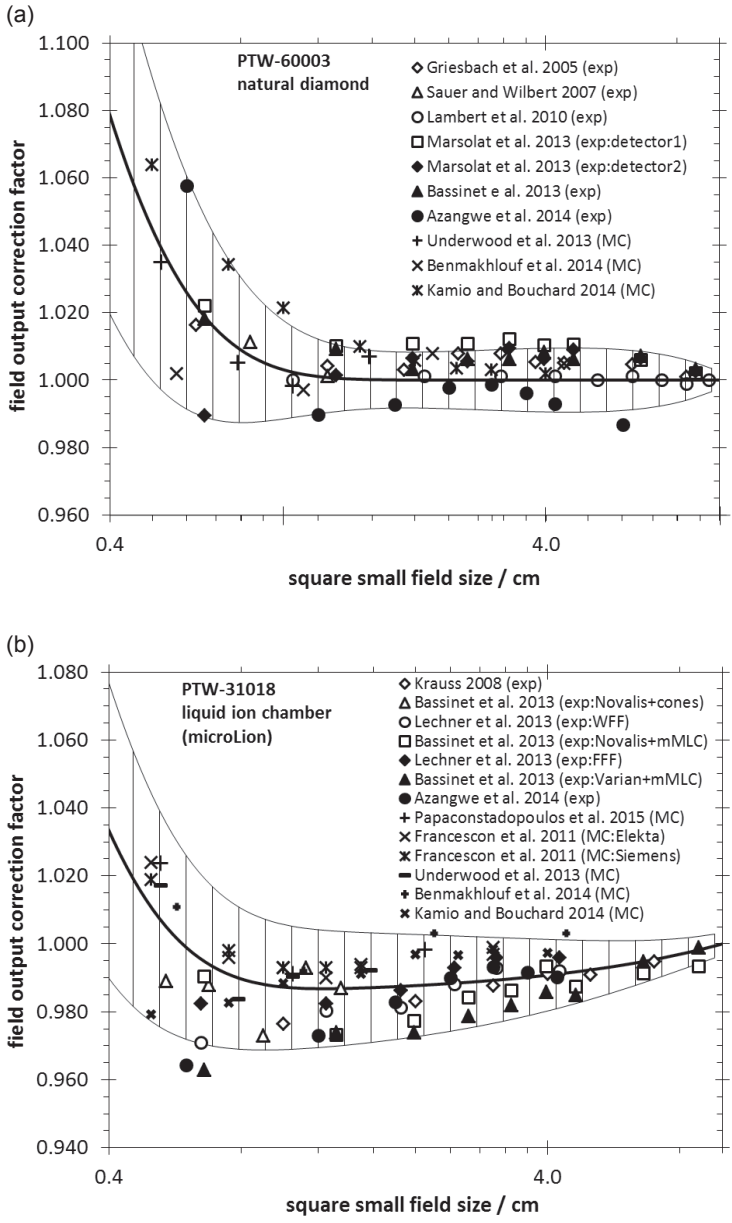

FIG. 28. Detector specific output correction factors, $k_{Q_{clin},Q_{ref}}^{f_{clin},f_{ref}}(S)$*, as a function of the field size (in logarithmic scale) and at a depth of 10 cm, for a reference field size 10 cm × 10 cm in water on the central axis of 6 MV photon beams, for the PTW 60003 natural diamond detector and the PTW 31018 liquid ion chamber. The uncertainty estimates shown correspond to the global values for detectors of a given type provided in Table 37.*

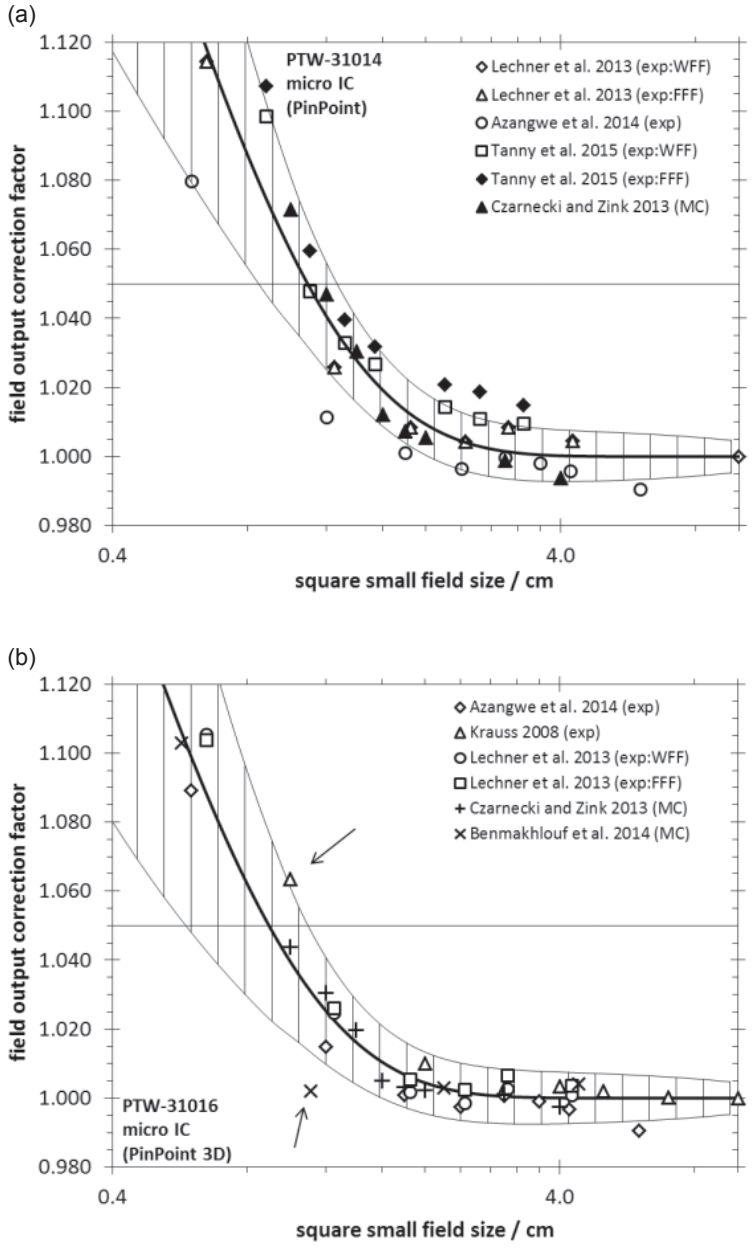

FIG. 29. Detector specific output correction factors, $k_{Q_{clin},Q_{ref}}^{f_{clin},f_{ref}}(S)$*, as a function of the field size (in logarithmic scale) and at a depth of 10 cm, for a reference field size 10 cm × 10 cm in water on the central axis of 6 MV photon beams, for microionization chambers. The uncertainty estimates shown correspond to the global values for detectors of a given type provided in Table 37.*

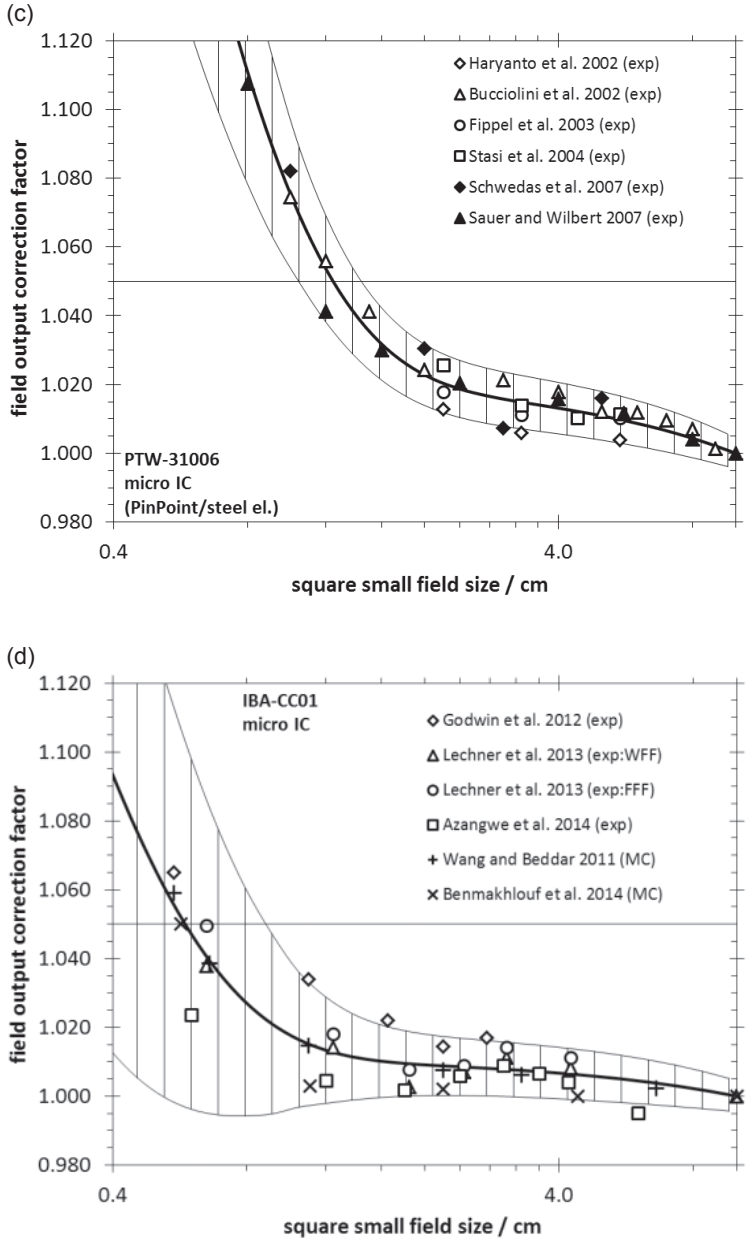

FIG. 29. (cont.) Detector specific output correction factors, $k_{Q_{clin},Q_{ref}}^{f_{clin},f_{ref}}(S)$*, as a function of the field size (in logarithmic scale) and at a depth of 10 cm, for a reference field size 10 cm × 10 cm in water on the central axis of 6 MV photon beams, for microionization chambers. The uncertainty estimates shown correspond to the global values for detectors of a given type provided in Table 37.*

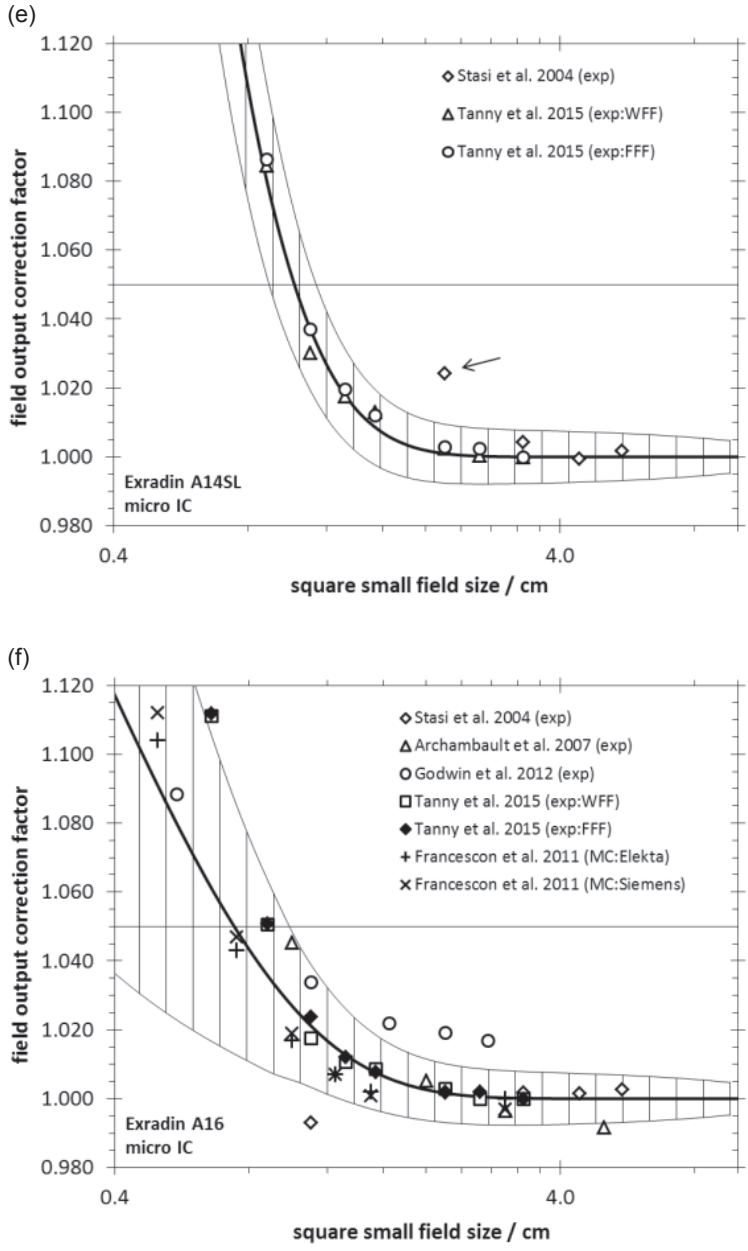

FIG. 29. (cont.) Detector specific output correction factors, $k_{Q_{clin},Q_{ref}}^{f_{clin},f_{ref}}(S)$*, as a function of the field size (in logarithmic scale) and at a depth of 10 cm, for a reference field size 10 cm × 10 cm in water on the central axis of 6 MV photon beams, for microionization chambers. The uncertainty estimates shown correspond to the global values for detectors of a given type provided in Table 37.*

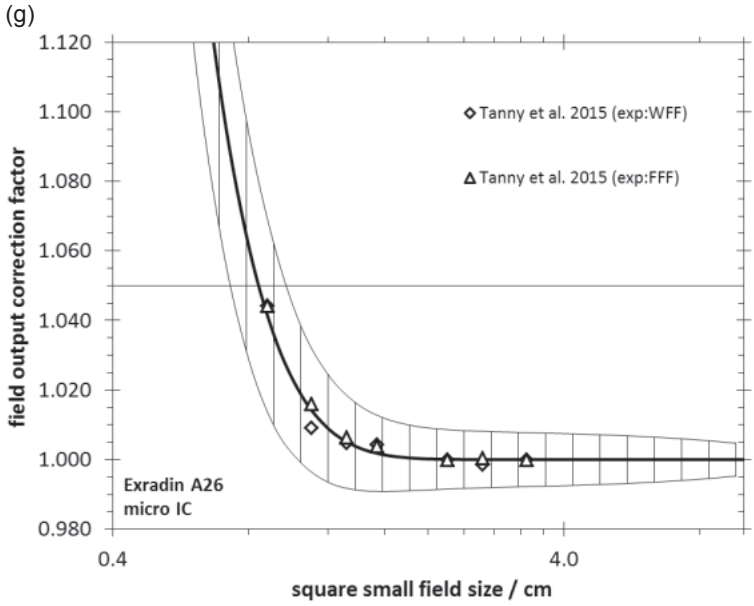

FIG. 29. (cont.) Detector specific output correction factors, $k_{Q_{clin},Q_{ref}}^{f_{clin},f_{ref}}(S)$*, as a function of the field size (in logarithmic scale) and at a depth of 10 cm, for a reference field size 10 cm × 10 cm in water on the central axis of 6 MV photon beams, for microionization chambers. The uncertainty estimates shown correspond to the global values for detectors of a given type provided in Table 37.*

For six small field detectors, Fig. 25 shows the data compilation for linac beams with nominal accelerating potentials of 6 MV at 10 cm depth, the results of the fits according to Eq. (62) and the uncertainties estimated according to the procedure outlined in this Appendix. This figure shows data for pairs of similar detector types (two shielded diodes, two unshielded diodes and two microionization chambers) to illustrate that the procedure used for uncertainty estimation yields values that depend substantially on the nature and amount of data available for a given detector. They are, for example, less reliable when only a small number of data sets are available. Given that there is no reason to assume that for similar detectors the uncertainties vary significantly, detectors have been grouped as follows: shielded diodes, unshielded diodes, microionization chambers and mini-ionization chambers. The average uncertainty estimates for each of these groups have been accepted as applicable to all the detectors of that group. The PTW 60019 microdiamond detector has been added to the group of unshielded diodes because its correction factors and uncertainty estimates are very similar. The PTW 60003 natural diamond and PTW 31018 liquid ionization chamber have been considered separately because no similar detector types

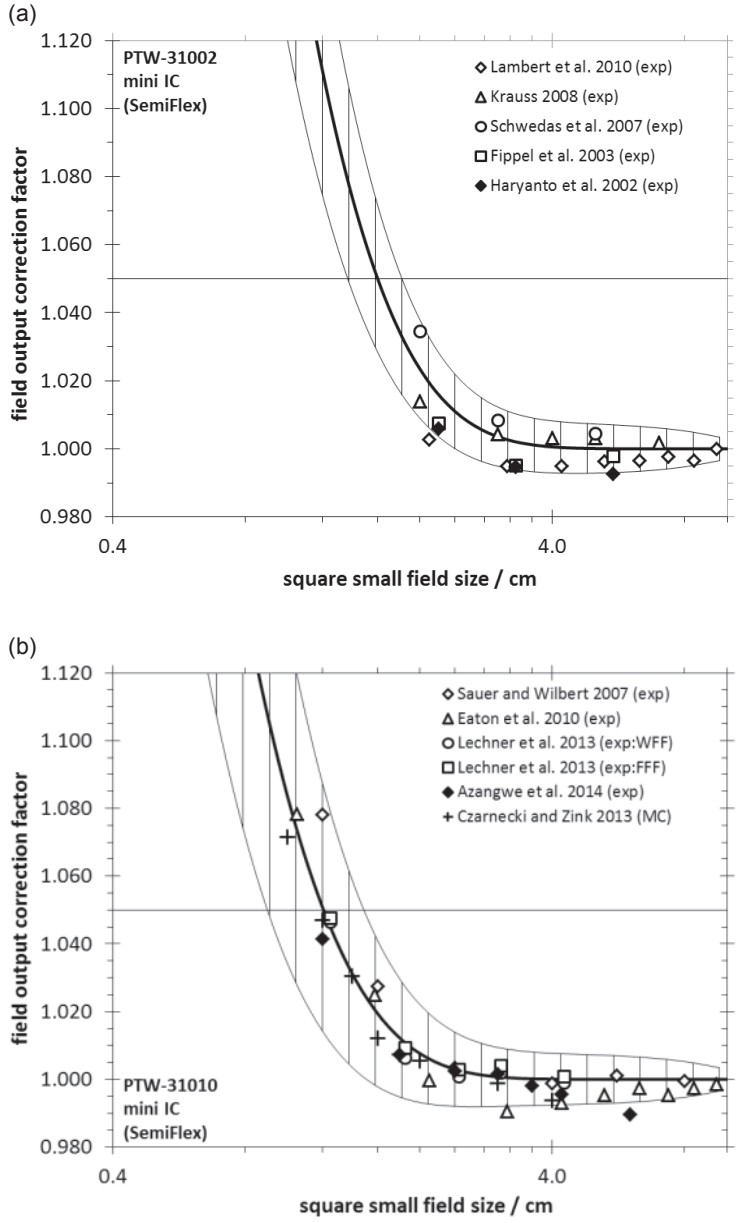

FIG. 30. Detector specific output correction factors, $k_{Q_{clin},Q_{ref}}^{f_{clin},f_{ref}}(S)$*, as a function of the field size (in logarithmic scale) and at a depth of 10 cm, for a reference field size 10 cm × 10 cm in water on the central axis of 6 MV photon beams, for mini-ionization chambers (note that some data points at small field sizes fall outside the plotted area). The uncertainty estimates shown correspond to the global values for detectors of a given type provided in Table 37.*

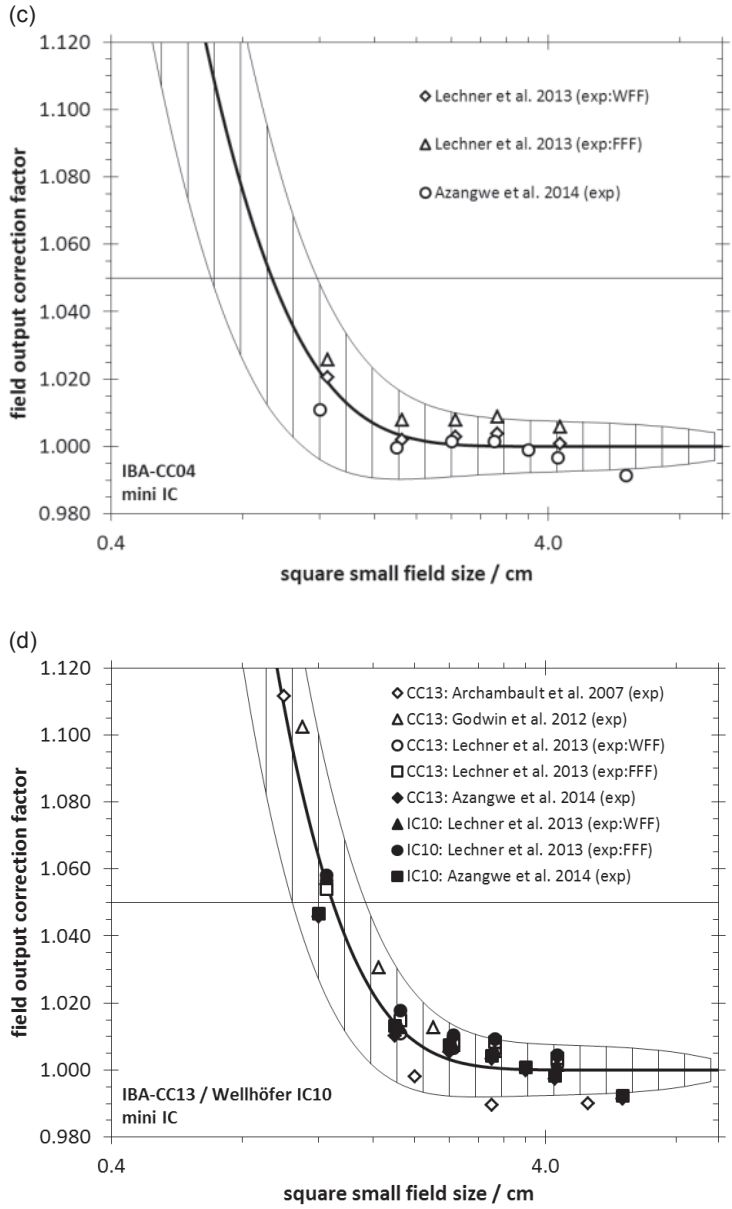

FIG. 30. (cont.) Detector specific output correction factors, $k_{Q_{clin},Q_{ref}}^{f_{clin},f_{ref}}(S)$*, as a function of the field size (in logarithmic scale) and at a depth of 10 cm, for a reference field size 10 cm × 10 cm in water on the central axis of 6 MV photon beams, for mini-ionization chambers (note that some data points at small field sizes fall outside the plotted area). The uncertainty estimates shown correspond to the global values for detectors of a given type provided in Table 37.*

are present in the data compilation. For the PTW 60003 natural diamond, an additional reason for this separate treatment is that the spread of data points can be assumed to account for the range of the natural diamond sizes used in the detector construction, as specified by the manufacturer, and its influence on the volume averaging correction. Based on this approach, all available data for 6 MV beams with their fits and uncertainty estimates, according to the grouping described, are shown in Figs 26–30.

For nominal beam accelerating potentials other than 6 MV and for measurement depths other than 10 cm, the amount of data is limited. Using the available data, a comparison has been made between 6 MV and 10 MV beams and for three different measurement depths (10 cm, 5 cm and z_{max}). The fitting procedures were exactly the same as for the 6 MV beams at 10 cm depth. Figure 31 shows the fits for the two energies and at the three depths for the PTW 60017 unshielded diode, illustrating, as a representative example, the observations made for all detectors. Because it was observed that the linear term in Eq. (62) is always smaller in absolute value for 10 MV beams than for 6 MV beams and also systematically decreases in absolute value with decreasing depth, graphs (b) and (d) show the same data with the linear term subtracted. In summary, the following observations were made:

— On average, the ratio of the linear terms (i.e. coefficient c in Eq. (62)) for 10 MV and 6 MV beams is 0.6; this can be explained by the higher mean energy of the primary beam and thus also the higher mean energy of the scatter component.
— On average, the ratio of the linear terms (i.e. coefficient c in Eq. (62)) at 5 cm depth and at 10 cm depth amounts to 0.85, while the ratio of the linear terms at z_{max} and at 10 cm depth amounts to 0.35; this can be explained by the increase of the scatter component with depth.
— After subtracting the linear term in Eq. (62) the remaining part of the correction factors was always within the expanded uncertainty interval of the fit to all 6 MV data at 10 cm depth; nevertheless, the fit to the data at z_{max} was found to be systematically closer to unity than at the other depths, which was reflected in a reduction of the sigmoid term in Eq. (62) by 20–60% depending on the detector type.
— When taking into account the equivalent square small field size at the measurement depth, the field output correction factors do not depend on the SDD (observations made for the CyberKnife at distances ranging from 65 cm to 100 cm [217]).

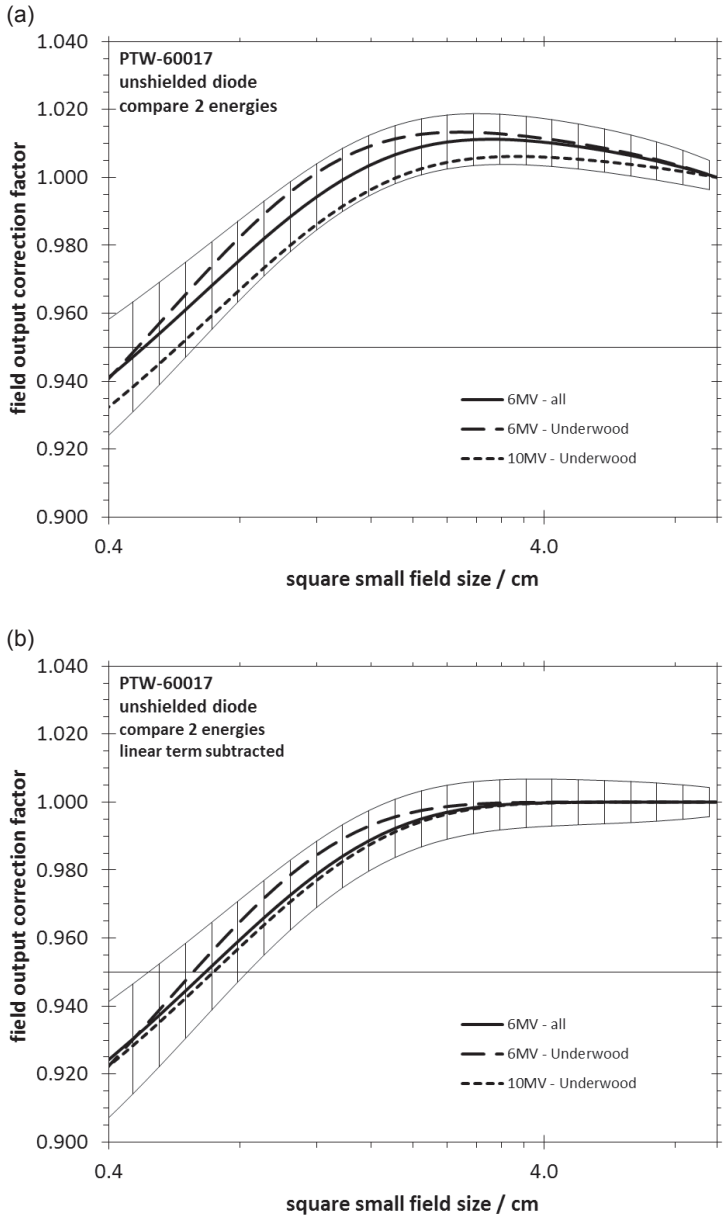

FIG. 31. Fits to detector specific output correction factors, $k_{Q_{clin},Q_{ref}}^{f_{clin},f_{ref}}(S)$*, as a function of the field size (in logarithmic scale) for the PTW 60017 unshielded diode for 6 MV and 10 MV photon beams at a depth of 10 cm in water (graphs (a) and (b)) and for 6 MV photon beams at depths of 10 cm, 5 cm and* z_{max} *(graphs (c) and (d)), for a reference field size 10 cm × 10 cm. Graphs (b) and (d) represent the same data as graphs (a) and (c) but with the linear term of Eq. (62) subtracted.*

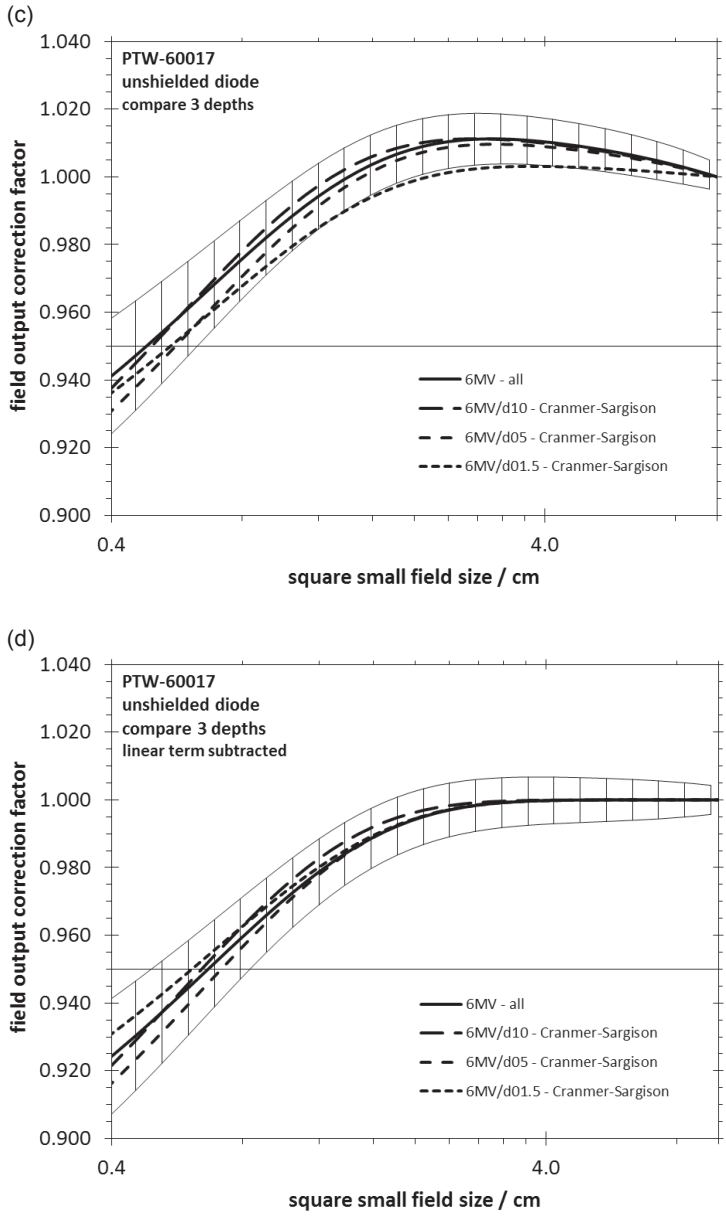

FIG. 31. (cont.) Fits to detector specific output correction factors, $k_{Q_{clin},Q_{ref}}^{f_{clin},f_{ref}}(S)$*, as a function of the field size (in logarithmic scale) for the PTW 60017 unshielded diode for 6 MV and 10 MV photon beams at a depth of 10 cm in water (graphs (a) and (b)) and for 6 MV photon beams at depths of 10 cm, 5 cm and* z_{max} *(graphs (c) and (d)), for a reference field size 10 cm × 10 cm. Graphs (b) and (d) represent the same data as graphs (a) and (c) but with the linear term of Eq. (62) subtracted.*

The only exception to these observations was the Sun Nuclear EDGE shielded diode, for which the difference between data for 6 MV and 10 MV beams was larger than the expanded uncertainty. This could be due to the particular construction of this detector with the stem and contacts lateral to the position of the diode, but since this was related to a limited set of data it could also be an isolated outlier; hence this detector has not been treated differently from the others in the generation of the data tables.

The fitting parameters a, b, c and d obtained for the 6 MV beams at a measurement depth of 10 cm (i.e. the fits shown in Figs 26–30) were used to calculate the data in Table 26. The relative standard uncertainties (coverage factor $k = 1$) for the different groups of detectors are given in Table 37. The calculation of the field output correction factors in Table 27 for 10 MV beams at a depth of 10 cm in water used the same parameters a, b and d in Eq. (62) as for the 6 MV beam data in Table 26, while the value used for parameter c was 0.6 times the value for 6 MV beams.

For the CyberKnife, data in Table 23 have been calculated with a reduction of 40% applied to the sigmoid term, and the value used for parameter c was 0.35 times the value for 6 MV beams at a depth of 10 cm, consistent with the observations above. By this approach, good agreement was found between published data for the CyberKnife [51, 76, 136, 217–219] and the data from Table 23. For TomoTherapy machines, data in Table 24 used the fitting parameters for the 6 MV beams at a measurement depth of 10 cm, but normalized to the equivalent square field size of the 5 cm × 10 cm msr field.

TABLE 37. RELATIVE STANDARD UNCERTAINTIES OF THE FIELD OUTPUT CORRECTION FACTORS IN TABLE 26

Square small field size S/cm	Unshielded diodes and PTW 60019 microDiamond (%)	Shielded diodes (%)	Mini IC (%)	Micro IC (%)	PTW 60003 natural diamond (%)	PTW 31018 liquid ion chamber (%)
0.4	0.9	—	—	—	2.9	2.2
0.5	0.8	—	—	3.2	2.2	1.7
0.6	0.7	1.3	—	2.5	1.7	1.4
0.8	0.6	0.9	3.4	1.6	1.1	1.0
1.0	0.5	0.7	2.5	1.1	0.7	0.9
1.2	0.5	0.6	1.8	0.8	0.6	0.9
1.5	0.5	0.6	1.2	0.6	0.4	0.8
2.0	0.4	0.5	0.7	0.4	0.4	0.8
2.5	0.4	0.4	0.5	0.4	0.4	0.7
3.0	0.4	0.4	0.4	0.4	0.4	0.6
3.5	0.4	0.4	0.4	0.4	0.5	0.6

TABLE 37. RELATIVE STANDARD UNCERTAINTIES OF THE FIELD OUTPUT CORRECTION FACTORS IN TABLE 26 (cont.)

Square small field size S/cm	Unshielded diodes and PTW 60019 microDiamond (%)	Shielded diodes (%)	Mini IC (%)	Micro IC (%)	PTW 60003 natural diamond (%)	PTW 31018 liquid ion chamber (%)
4.0	0.3	0.4	0.4	0.4	0.5	0.5
5.0	0.3	0.3	0.4	0.4	0.5	0.4
6.0	0.3	0.3	0.3	0.3	0.4	0.4
8.0	0.3	0.2	0.3	0.3	0.3	0.2

Note: Listed per group of small field detector types as described in the text.

REFERENCES

[1] INTERNATIONAL ATOMIC ENERGY AGENCY, Absorbed Dose Determination in External Beam Radiotherapy: An International Code of Practice for Dosimetry Based on Standards of Absorbed Dose to Water, Technical Reports Series No. 398, IAEA, Vienna (2000).

[2] ALMOND, P.R., et al., AAPM's TG-51 protocol for clinical reference dosimetry of high-energy photon and electron beams, Med. Phys. **26** (1999) 1847–1870.

[3] BERLAND, V.A., et al., "Determination of the absorbed dose of photon (1–50 MeV) and electron beams (5–50 MeV) in external radiation therapy", National Code of Practice RD-50-691-89 (STANDARTOV, I., Ed.), Izdatelstvo Standartov, Moscow (1990) (in Russian).

[4] LILLICRAP, S.C., OWEN, B., WILLIAMS, J.R., WILLIAMS, P.C., Code of Practice for high-energy photon therapy dosimetry based on the NPL absorbed dose calibration service, Phys. Med. Biol. **35** (1990) 1355–1360.

[5] DEUTSCHES INSTITUT FÜR NORMUNG, Dosismessverfahren nach der Sondenmethode für Photonen- und Elektronenstrahlung, Teil 2: Ionisationsdosimetrie, Deutsche Norm DIN 6800-2, DIN, Berlin (1997).

[6] NETHERLANDS COMMISSION ON RADIATION DOSIMETRY, Code of Practice for the Absorbed Dose Determination in High Energy Photon and Electron Beams, Rep. NCS-18, NSC, Delft (2008).

[7] McEWEN, M., et al., Addendum to the AAPM's TG-51 protocol for clinical reference dosimetry of high-energy photon beams, Med. Phys. **41** (2014) 041501-1–20.

[8] ALFONSO, R., et al., A new formalism for reference dosimetry of small and nonstandard fields, Med. Phys. **35** (2008) 5179–5186.

[9] INTERNATIONAL COMMISSION ON RADIOLOGICAL PROTECTION, Preventing Accidental Exposures from New External Beam Radiation Therapy Technologies, Publication 112, Pergamom Press, Elsevier, Amsterdam (2009).

[10] BIPM JOINT COMMITTEE FOR GUIDES IN METROLOGY, Evaluation of Measurement Data: Guide to the Expression of Uncertainty in Measurement (GUM), JCGM 100:2008, BIPM, Sévres (2008).

[11] ANDREO, P., BURNS, D.T., SALVAT, F., On the uncertainties of photon mass energy-absorption coefficients and their ratios for radiation dosimetry, Phys. Med. Biol. **57** (2012) 2117–2136.

[12] INSTITUTE OF PHYSICS AND ENGINEERING IN MEDICINE, Small Field MV Photon Dosimetry, IPEM Rep. 103, IPEM, York (2010).

[13] ATTIX, F.H., Introduction to Radiological Physics and Radiation Dosimetry, John Wiley & Sons, New York (1986).

[14] PAPACONSTADOPOULOS, P., On the Detector Response and the Reconstruction of the Source Intensity Distribution in Small Photon Fields, PhD Thesis, McGill Univ. (2016).

[15] WUERFEL, J., Dose measurements in small fields, Med. Phys. Int. **1** (2013) 81–90.

[16] INTERNATIONAL ELECTROTECHNICAL COMMISSION, Medical Electrical Equipment: Glossary of Defined Terms, IEC TR 60788, IEC, Geneva (2004).

[17] DE VLAMYNCK, K., et al., Dose measurements compared with Monte Carlo simulations of narrow 6 MV multileaf collimator shaped photon beams, Med. Phys. **26** (1999) 1874–1882.
[18] DAS, I.J., DING, G.X., AHNESJÖ, A., Small fields: Nonequilibrium radiation dosimetry, Med. Phys. **35** (2008) 206–215.
[19] CRANMER-SARGISON, G., CHARLES, P.H., TRAPP, J.V., THWAITES, D.I., A methodological approach to reporting corrected small field relative outputs, Radiother. Oncol. **109** (2013) 350–355.
[20] DERREUMAUX, S., et al., Mesure de la dose absorbée dans les faisceaux de photons de très petites dimensions utilisés en radiothérapie stéréotaxique, Rep. DRPH/SER 2008-18, Institut de radioprotection et de sûreté nucléaire, Fontenay-aux-Roses (2008).
[21] EKLUND, K., AHNESJÖ, A., Fast modelling of spectra and stopping-power ratios using differentiated fluence pencil kernels, Phys. Med. Biol. **53** (2008) 4231–4247.
[22] SANCHEZ-DOBLADO, F., et al., Ionization chamber dosimetry of small photon fields: A Monte Carlo study on stopping-power ratios for radiosurgery and IMRT beams, Phys. Med. Biol. **48** (2003) 2081–2099.
[23] EKLUND, K., AHNESJÖ, A., Modeling silicon diode dose response factors for small photon fields, Phys. Med. Biol. **55** (2010) 7411–7423.
[24] SAUER, O.A., WILBERT, J., Measurement of output factors for small photon beams, Med. Phys. **34** (2007) 1983–1988.
[25] HUQ, M.S., University of Pittsburgh Cancer Institute and UPMC CancerCenter, personal communication, 2014.
[26] SJÖSTRÖM, D., BJELKENGREN, U., OTTOSSON, W., BEHRENS, C.F., A beam-matching concept for medical linear accelerators, Acta Oncol. **48** (2009) 192–200.
[27] CHANG, Z., et al., Commissioning and dosimetric characteristics of TrueBeam system: Composite data of three TrueBeam machines, Med. Phys. **39** (2012) 6981–7018.
[28] THOMAS, S.D., MacKENZIE, M., ROGERS, D.W.O, FALLONE, B.G., A Monte Carlo derived TG-51 equivalent calibration for helical tomotherapy, Med. Phys. **32** (2005) 1346–1353.
[29] LANGEN, K.M., et al., QA for helical tomotherapy: Report of the AAPM Task Group 148, Med. Phys. **37** (2010) 4817–4853.
[30] ZEVERINO, M., AGOSTINELLI, S., PUPILLO, F., TACCINI, G., Determination of the correction factors for different ionization chambers used for the calibration of the helical tomotherapy static beam, Radiother. Oncol. **100** (2011) 424–428.
[31] SHARMA, S.C., OTT, J.T., WILLIAMS, J.B., DICKOW, D., Commissioning and acceptance testing of a CyberKnife linear accelerator, J. Appl. Clin. Med. Phys. **8** (2007) 119–125.
[32] BRITISH INSTITUTE OF RADIOLOGY, Central Axis Depth Dose Data for Use in Radiotherapy Departments: 1996, BJR Supplement 25, BIR, London (1996).
[33] SAUER, O.A., Determination of the quality index (Q) for photon beams at arbitrary field sizes, Med. Phys. **36** (2009) 4168–4172.
[34] ANDREO, P., On the beam quality specification of high-energy photons for radiotherapy dosimetry, Med. Phys. **27** (2000) 434–440.

[35] XIONG, G., ROGERS, D.W.O., Relationship between $\%dd(10)_x$ and stopping-power ratios for flattening filter free accelerators: A Monte Carlo study, Med. Phys. **35** (2008) 2104–2109.
[36] PALMANS, H., National Physical Laboratory, personal communication, 2015.
[37] DALARYD, M., KNÖÖS, T., CEBERG, C., Combining tissue-phantom ratios to provide a beam-quality specifier for flattening filter free photon beams, Med. Phys. **41** (2014) 111716-1–6.
[38] PALMANS, H., Determination of the beam quality index of high-energy photon beams under nonstandard reference conditions, Med. Phys. **39** (2012) 5513–5519.
[39] TASK GROUP 21, RADIATION THERAPY COMMITTEE, AMERICAN ASSOCIATION OF PHYSICISTS IN MEDICINE, A protocol for the determination of absorbed dose from high-energy photon and electron beams, Med. Phys. **10** (1983) 741–771.
[40] INTERNATIONAL ATOMIC ENERGY AGENCY, Absorbed Dose Determination in Photon and Electron Beams: An International Code of Practice, Technical Reports Series No. 277, IAEA, Vienna (1987).
[41] ANDREO, P., NAHUM, A., "Absolute dose determination under reference conditions", Handbook of Radiotherapy Physics: Theory and Practice (MAYLES, P., NAHUM, A., ROSENWALD, J.-C., Eds), Taylor & Francis, Boca Raton, FL (2007) 333–366.
[42] CAPOTE, R., et al., An EGSnrc Monte Carlo study of the microionization chamber for reference dosimetry of narrow irregular IMRT beamlets, Med. Phys. **31** (2004) 2416–2422.
[43] BOUCHARD, H., SEUNTJENS, J., Ionization chamber-based reference dosimetry of intensity modulated radiation beams, Med. Phys. **31** (2004) 2454–2465.
[44] WULFF, J., ZINK, K., KAWRAKOW, I., Efficiency improvements for ion chamber calculations in high energy photon beams, Med. Phys. **35** (2008) 1328–1336.
[45] CROP, F., et al., The influence of small field sizes, penumbra, spot size and measurement depth on perturbation factors for microionization chambers, Phys. Med. Biol. **54** (2009) 2951–2969.
[46] BOUCHARD, H., SEUNTJENS, J., KAWRAKOW, I., A Monte Carlo method to evaluate the impact of positioning errors on detector response and quality correction factors in nonstandard beams, Phys. Med. Biol. **56** (2011) 2617–2637.
[47] SCOTT, A.J., KUMAR, S., NAHUM, A.E., FENWICK, J.D., Characterizing the influence of detector density on dosimeter response in non-equilibrium small photon fields, Phys. Med. Biol. **57** (2012) 4461–4476.
[48] FENWICK, J.D., KUMAR, S., SCOTT, A.J., NAHUM, A.E., Using cavity theory to describe the dependence on detector density of dosimeter response in non-equilibrium small fields, Phys. Med. Biol. **58** (2013) 2901–2923.
[49] CZARNECKI, D., ZINK, K., Monte Carlo calculated correction factors for diodes and ion chambers in small photon fields, Phys. Med. Biol. **58** (2013) 2431–2444.
[50] CZARNECKI, D., ZINK, K., Corrigendum: Monte Carlo calculated correction factors for diodes and ion chambers in small photon fields, Phys. Med. Biol. **59** (2014) 791–794.

[51] FRANCESCON, P., CORA, S., SATARIANO, N., Calculation of $k_{Q_{\text{clin}},Q_{\text{msr}}}^{f_{\text{clin}},f_{\text{msr}}}$ for several small detectors and for two linear accelerators using Monte Carlo simulations, Med. Phys. **38** (2011) 6513–6527.
[52] FRANCESCON, P., KILBY, W., SATARIANO, N., CORA, S., Monte Carlo simulated correction factors for machine specific reference field dose calibration and output factor measurement using fixed and iris collimators on the CyberKnife system, Phys. Med. Biol. **57** (2012) 3741–3758.
[53] CHARLES, P.H., et al., The effect of very small air gaps on small field dosimetry, Phys. Med. Biol. **57** (2012) 6947–6960.
[54] UNDERWOOD, T.S.A., WINTER, H.C., HILL, M.A., FENWICK, J.D., Detector density and small field dosimetry: Integral versus point dose measurement schemes, Med. Phys. **40** (2013) 082102-1–082102-16.
[55] CHARLES, P.H., et al., Monte Carlo-based diode design for correction-less small field dosimetry, Phys. Med. Biol. **58** (2013) 4501–4512.
[56] RALSTON, A., LIU, P., WARRENER, K., McKENZIE, D., SUCHOWERSKA, N., Small field diode correction factors derived using an air core fibre optic scintillation dosimeter and EBT2 film, Phys. Med. Biol. **57** (2012) 2587–2602.
[57] LECHNER, W., PALMANS, H., SÖLKNER, L., GROCHOWSKA, P., GEORG, D., Detector comparison for small field output factor measurements in flattening filter free photon beams, Radiother. Oncol. **109** (2013) 356–360.
[58] FRANCESCON, P., BEDDAR, S., SATARIANO, N., DAS, I.J., Variation of $k_{Q_{\text{clin}},Q_{\text{ms}}}^{f_{\text{clin}},f_{\text{msr}}}$ for the small-field dosimetric parameters percentage depth dose, tissue-maximum ratio, and off-axis ratio, Med. Phys. **41** (2014) 101708-1–14.
[59] McKERRACHER, C., THWAITES, D.I., Notes on the construction of solid-state detectors, Radiother. Oncol. **79** (2006) 348–351.
[60] DAS, I.J., KASE, K.R., Higher energy: Is it necessary, is it worth the cost for radiation oncology? Med. Phys. **19** (1992) 917–925.
[61] INTERNATIONAL COMMISSION ON RADIATION UNITS AND MEASUREMENTS, Prescribing, Recording, and Reporting Photon-Beam Intensity-Modulated Radiotherapy Therapy (IMRT), ICRU Rep. 83, ICRU Bethesda, MD (2010).
[62] IZEWSKA, J., International Atomic Energy Agency, personal communication, 2014.
[63] FOLLOWILL, D., IROC Houston Quality Assurance Center, personal communication, 2014.
[64] SEUNTJENS, J., DUANE, S., Photon absorbed dose standards, Metrologia **46** (2009) S39–S58.
[65] McEWEN, M.R., DuSAUTOY, A.R., Primary standards of absorbed dose for electron beams, Metrologia **46** (2009) S59–S79.
[66] KRAUSS, A., The PTB water calorimeter for the absolute determination of absorbed dose to water in ^{60}Co radiation, Metrologia **43** (2006) 259–272.
[67] KRAUSS, A., KAPSCH, R.-P., Calorimetric determination of k_Q factors for NE 2561 and NE 2571 ionization chambers in 5 cm × 5 cm and 10 cm × 10 cm radiotherapy beams of 8 MV and 16 MV photons, Phys. Med. Biol. **52** (2007) 6243–6259.

[68] KRAUSS, A., KAPSCH, R.-P., Corrigendum: Calorimetric determination of k_Q factors for NE 2561 and NE 2571 ionization chambers in 5 cm × 5 cm and 10 cm × 10 cm radiotherapy beams of 8 MV and 16 MV photons, Phys. Med. Biol. **53** (2008) 1151–1152.
[69] KRAUSS, A., KAPSCH, R.-P., ROUIJAA, M., "Calorimetric determination of k_Q factors for NE2561 ionization chambers in 3 cm × 3 cm beams of 6 MV and 10 MV photons", Standards, Applications and Quality Assurance in Medical Radiation Dosimetry (IDOS) (Proc. Int. Symp. Vienna, 2010), Vol. 1, IAEA, Vienna (2011) 209–218.
[70] DE PREZ, L.A., "Small field dosimetry in high energy photon beams based on water calorimetry", Standards, Applications and Quality Assurance in Medical Radiation Dosimetry (IDOS) (Proc. Int. Symp. Vienna, 2010), Book of Extended Synopses, IAEA, Vienna (2011) CD-ROM, 291–292.
[71] DUANE, S., et al., An absorbed dose calorimeter for IMRT dosimetry, Metrologia **49** (2012) S168–S173.
[72] RENAUD, J., MARCHINGTON, D., SEUNTJENS, J., SARFEHNIA, A., Development of a graphite probe calorimeter for absolute clinical dosimetry, Med. Phys. **40** (2013) 020701-1–6.
[73] SANCHEZ-DOBLADO, F., et al., A new method for output factor determination in MLC shaped narrow beams, Phys. Med. **23** (2007) 58–66.
[74] DJOUGUELA, A., et al., The dose-area product, a new parameter for the dosimetry of narrow photon beams, Z. Med. Phys. **16** (2006) 217–227.
[75] PICARD, S., BURNS, D.T., ROGER, P., "The BIPM graphite calorimeter standard for absorbed dose to water", Standards, Applications and Quality Assurance in Medical Radiation Dosimetry (IDOS) (Proc. Int. Symp. Vienna, 2010), Vol. 1, IAEA, Vienna (2011) 55–65.
[76] PANTELIS, E., et al., On the implementation of a recently proposed dosimetric formalism to a robotic radiosurgery system, Med. Phys. **37** (2010) 2369–2379.
[77] SHARPE, P.H.G., SEPHTON, J.P., "Alanine dosimetry at NPL: The development of a mailed reference dosimetry service at radiotherapy dose levels", Techniques for High Dose Dosimetry in Industry, Agriculture and Medicine (Proc. Symp. Vienna, 1998), IAEA-TECDOC-1070, IAEA, Vienna (1999) 183–189.
[78] ANTON, M., Uncertainties in alanine/ESR dosimetry at the Physikalisch-Technische Bundesanstalt, Phys. Med. Biol. **51** (2006) 5419–5440.
[79] SHARPE, P.H.G., SEPHTON, J.P., "Therapy level alanine dosimetry at the NPL", Alanine Dosimetry for Clinical Applications (Proc. 216th PTB Seminar, Braunschweig, 2006), PTB-Dos-51, Physikalisch-Technische Bundesanstalt, Braunschweig (2006).
[80] ANTON, M., KAPSCH, R.-P., KRYSTEK, M., RENNER, F., Response of the alanine/ESR dosimetry system to MV x-rays relative to ^{60}Co radiation, Phys. Med. Biol. **53** (2008) 2753–2770.
[81] KAWACHI, T., et al., Reference dosimetry condition and beam quality correction factor for CyberKnife beam, Med. Phys. **35** (2008) 4591–4598.

[82] PANTELIS, E., et al., “On the implementation of a recently proposed dosimetric formalism to a robotic radiosurgery system”, Standards, Applications and Quality Assurance in Medical Radiation Dosimetry (IDOS) (Proc. Int. Symp. Vienna, 2010), Book of Extended Synopses, IAEA, Vienna (2011) CD-ROM, 61–62.
[83] ANTYPAS, C., PANTELIS, E., Performance evaluation of a CyberKnife® G4 image-guided robotic stereotactic radiosurgery system, Phys. Med. Biol. **53** (2008) 4697–4718.
[84] DRZYMALA, R.E., WOOD, R.C., LEVY, J., Calibration of the Gamma Knife using a new phantom following the AAPM TG51 and TG21 protocols, Med. Phys. **35** (2008) 514–521.
[85] GOETSCH, S.J, et al., Physics of rotating gamma systems for stereotactic radiosurgery, Int. J. Radiat. Oncol. Biol. Phys. **43** (1999) 689–696.
[86] SOMIGLIANA, A., et al., Dosimetry of Gamma Knife and linac-based radiosurgery using radiochromic and diode detectors, Phys. Med. Biol. **44** (1999) 887–897.
[87] MELTSNER, S.G., DEWERD, L.A., Air kerma based dosimetry calibration for the Leksell Gamma Knife, Med. Phys. **36** (2009) 339–350.
[88] PALMANS, H., “Small and composite field dosimetry: The problems and recent progress”, Standards, Applications and Quality Assurance in Medical Radiation Dosimetry (IDOS) (Proc. Int. Symp. Vienna, 2010), Vol. 1, IAEA, Vienna (2011) 161–180.
[89] DERREUMAUX, S., BOISSERIE, G., BRUNET, G., BUCHHEIT, I., SARRAZIN, T., “Concerns in France about the dose delivered to the patients in stereotactic radiation therapy”, Standards, Applications and Quality Assurance in Medical Radiation Dosimetry (IDOS) (Proc. Int. Symp. Vienna, 2010), Vol. 1, IAEA, Vienna (2011) 273–286.
[90] DIETERICH, S., SHEROUSE, G.W., Experimental comparison of seven commercial dosimetry diodes for measurement of stereotactic radiosurgery cone factors, Med. Phys. **38** (2011) 4166–4173.
[91] LAUB, W.U., WONG, T., The volume effect of detectors in the dosimetry of small fields used in IMRT, Med. Phys. **30** (2003) 341–347.
[92] GONZALEZ-CASTAÑO, D.M, et al., A convolution model for obtaining the response of an ionization chamber in static non standard fields, Med. Phys. **39** (2012) 482–491.
[93] LOOE, H.K., et al., The dose response functions of ionization chambers in photon dosimetry: Gaussian or non-Gaussian? Z. Med. Phys. **23** (2013) 129–143.
[94] LI, X.A., SOUBRA, M., SZANTO, J., GERIG, L.H., Lateral electron equilibrium and electron contamination in measurements of head-scatter factors using miniphantoms and brass caps, Med. Phys. 22 (1995) 1167–1170.
[95] KALACH, N.I., ROGERS, D.W., Which accelerator photon beams are ‘clinic-like’ for reference dosimetry purposes? Med. Phys. **30** (2003) 1546–1555.
[96] SIBATA, C.H., MOTA, H.C., BEDDER, A.S., HIGGINS, P.D., SHIN, K.H., Influence of detector size in photon beam profile measurements, Phys. Med. Biol. **36** (1991) 621–631.
[97] HIGGINS, P.D., SIBATA, C.H., SISKIND, L., SOHN, J.W., Deconvolution of detector size effect for small field measurement, Med. Phys. **22** (1995) 1663–1666.

[98] GARCIA-VICENTE, F., DELGADO, J.M, PERAZA, C., Experimental determination of the convolution kernel for the study of the spatial response of a detector, Med. Phys. **25** (1998) 202–207.
[99] PANTELIS, E., et al., Dosimetric characterization of CyberKnife radiosurgical photon beams using polymer gels, Med. Phys. **35** (2008) 2312–2320.
[100] AZANGWE, G., et al., Detector to detector corrections: A comprehensive experimental study of detector specific correction factors for beam output measurements for small radiotherapy beams, Med. Phys. **41** (2014) 072103-1–16.
[101] SEUNTJENS, J., OLIVARES, M., EVANS, M., PODGORSAK, E., Absorbed dose to water reference dosimetry using solid phantoms in the context of absorbed-dose protocols, Med. Phys. **32** (2005) 2945–2953.
[102] TELLO, V.M., TAILOR, R.C., HANSON, W.F., How water equivalent are water-equivalent solid materials for output calibration of photon and electron beams? Med. Phys. **22** (1995) 1177–1189.
[103] KHAN, F.M., The Physics of Radiation Therapy, 4th edn, Lippincott Williams & Wilkins, Philadelphia, PA (2010).
[104] PODGORSAK, E.B., "External photon beams: Physical aspects", Radiation Oncology Physics: A Handbook for Teachers and Students, Vienna, IAEA (2005) 161–217.
[105] SECO, J., CLASIE, B., PARTRIDGE, M., Review on the characteristics of radiation detectors for dosimetry and imaging, Phys. Med. Biol. **59** (2014) R303–R347.
[106] INTERNATIONAL ELECTROTECHNICAL COMMISSION, Medical Electrical Equipment: Dosimeters with Ionization Chambers as Used in Radiotherapy, IEC 60731:2011, IEC, Geneva (2011).
[107] McEWEN, M.R., Measurement of ionization chamber absorbed dose k_Q factors in megavoltage photon beams, Med. Phys. **37** (2010) 2179–2193.
[108] GEORG, D., KNÖÖS, T., McCLEAN, B., Current status and future perspective of flattening filter free photon beams, Med. Phys. **38** (2011) 1280–1293.
[109] LE ROY, M., et al., Assessment of small volume ionization chambers as reference dosimeters in high-energy photon beams, Phys. Med. Biol. **56** (2011) 5637–5650.
[110] JOHANSSON, J., et al., "Monte Carlo calculated and experimentally verified correction factors for clinical reference dosimetry for the Leksell Gamma Knife®: Application of a new IAEA dosimetry formalism", paper presented at the 16th Int. Mtg of the Leksell Gamma Knife Society, Sydney, 2012.
[111] ANDREO, P., PALMANS, H., MARTEINSDÓTTIR, M., BENMAKHLOUF, H., CARLSSON-TEDGREN, Å., On the Monte Carlo simulation of small-field micro-diamond detectors for megavoltage photon dosimetry, Phys. Med. Biol. **61** (2016) L1–L10.
[112] AGOSTINELLI, S., GARELLI, S., PIERGENTILI, M., FOPPIANO, F., Response to high-energy photons of PTW31014 PinPoint ion chamber with a central aluminum electrode, Med. Phys. **35** (2008) 3293–3301.
[113] LEYBOVICH, L.B., SETHI, A., DOGAN, N., Comparison of ionization chambers of various volumes for IMRT absolute dose verification, Med. Phys. **30** (2003) 119–123.

[114] ANDERSSON, J., et al., A comparison of different experimental methods for general recombination correction for liquid ionization chambers, Phys. Med. Biol. **57** (2012) 7161–7175.
[115] TÖLLI, H., SJÖGREN, R., WENDELSTEN, M., A two-dose-rate method for general recombination correction for liquid ionization chambers in pulsed beams, Phys. Med. Biol. **55** (2010) 4247–4260.
[116] PARDO-MONTERO, J., GOMEZ, F., Determining charge collection efficiency in parallel-plate liquid ionization chambers, Phys. Med. Biol. **54** (2009) 3677–3689.
[117] CHUNG, E., DAVIS, S., SEUNTJENS, J., Experimental analysis of general ion recombination in a liquid-filled ionization chamber in high-energy photon beams, Med. Phys. **40** (2013) 062104-1–7.
[118] GOMEZ, F., GONZALEZ-CASTAÑO, D., DIAZ-BOTANA, P., PARDO-MONTERO, J., Study of the PTW microLion chamber temperature dependence, Phys. Med. Biol. **59** (2014) 2705–2712.
[119] WESTERMARK, M., ARNDT, J., NILSSON, B., BRAHME, A., Comparative dosimetry in narrow high-energy photon beams, Phys. Med. Biol. **45** (2000) 685–702.
[120] EKLUND, K., AHNESJÖ, A., Modeling silicon diode energy response factors for use in therapeutic photon beams, Phys. Med. Biol. **54** (2009) 6135–6150.
[121] EKLUND, K., Modeling Silicon Diode Dose Response in Radiotherapy Fields Using Fluence Pencil Kernels, PhD Thesis, Uppsala Univ. (2010).
[122] SCOTT, A.J., NAHUM, A.E., FENWICK, J.D., Monte Carlo modeling of small photon fields: Quantifying the impact of focal spot size on source occlusion and output factors, and exploring miniphantom design for small-field measurements, Med. Phys. **36** (2009) 3132–3144.
[123] YIN, Z., HUGTENBURG, R., BEDDOE, A.H., Response corrections for solid-state detectors in megavoltage photon dosimetry, Phys. Med. Biol. **49** (2004) 3691–3702.
[124] HEYDARIAN, M., HOBAN, P.W., BEDDOE, A.H., A comparison of dosimetry techniques in stereotactic radiosurgery, Phys. Med. Biol. **41** (1996) 93–110.
[125] McKERRACHER, C., THWAITES, D.I., Verification of the dose to the isocentre in stereotactic plans, Radiother. Oncol. **64** (2002) 97–107.
[126] BUCCIOLINI, M., et al., Diamond detector versus silicon diode and ion chamber in photon beams of different energy and field size, Med. Phys. **30** (2003) 2149–2154.
[127] DE ANGELIS, C., et al., An investigation of the operating characteristics of two PTW diamond detectors in photon and electron beams, Med. Phys. **29** (2002) 248–254.
[128] LAUB, W.U., KAULICH, T.W., NÜSSLIN, F., Energy and dose rate dependence of a diamond detector in the dosimetry of 4–25 MV photon beams, Med. Phys. **24** (1997) 535–536.
[129] LAUB, W.U., KAULICH, T.W., NÜSSLIN, F., A diamond detector in the dosimetry of high-energy electron and photon beams, Phys. Med. Biol. **44** (1999) 2183–2192.
[130] BETZEL, G.T., LANSLEY, S.P., BALUTI, F., REINISCH, L., MEYER, J., Clinical investigations of a CVD diamond detector for radiotherapy dosimetry, Phys. Med. **28** (2012) 144–152.

[131] CIANCAGLIONI, I., et al., Dosimetric characterization of a synthetic single crystal diamond detector in clinical radiation therapy small photon beams, Med. Phys. **39** (2012) 4493–4501.
[132] MARSOLAT, F., et al., A new single crystal diamond dosimeter for small beam: Comparison with different commercial active detectors, Phys. Med. Biol. **58** (2013) 7647–7660.
[133] RALSTON, A., TYLER, M., LIU, P., McKENZIE, D., SUCHOWERSKA, N., Over-response of synthetic microDiamond detectors in small radiation fields, Phys. Med. Biol. **59** (2014) 5873–5881.
[134] ARCHAMBAULT, L., BEDDAR, A.S., GINGRAS, L., ROY, R., BEAULIEU, L., Measurement accuracy and Cerenkov removal for high performance, high spatial resolution scintillation dosimetry, Med. Phys. **33** (2006) 128–135.
[135] GAGNON, J.-C., et al., Dosimetric performance and array assessment of plastic scintillation detectors for stereotactic radiosurgery quality assurance, Med. Phys. **39** (2012) 429–436.
[136] MORIN, J., et al., A comparative study of small field total scatter factors and dose profiles using plastic scintillation detectors and other stereotactic dosimeters: The case of the CyberKnife, Med. Phys. **40** (2013) 011719-1–11.
[137] LIU, P.Z.Y., SUCHOWERSKA, N., LAMBERT, J., ABOLFATHI, P., McKENZIE, D.R., Plastic scintillation dosimetry: Comparison of three solutions for the Cerenkov challenge, Phys. Med. Biol. **56** (2011) 5805–5821.
[138] PAI, S., et al., TG-69: Radiographic film for megavoltage beam dosimetry, Med. Phys. **34** (2007) 2228–2258.
[139] DEVIC, S., Radiochromic film dosimetry: Past, present, and future, Phys. Med. **27** (2011) 122–134.
[140] NIROOMAND-RAD, A., et al., Radiochromic film dosimetry: Recommendations of AAPM Radiation Therapy Committee Task Group 55, Med. Phys. **25** (1998) 2093–2115.
[141] BEKERAT, H., et al., Improving the energy response of external beam therapy (EBT) GafChromic™ dosimetry films at low energies (≤100 keV), Med. Phys. **41** (2014) 022101-1–14.
[142] ALNAWAF, H., BUTSON, M.J., CHEUNG, T., YU, P.K.N., Scanning orientation and polarization effects for XRQA radiochromic film, Phys. Med. **26** (2010) 216–219.
[143] RAMANI, R., RUSSELL, S., O'BRIEN, P., Clinical dosimetry using MOSFETs, Int. J. Radiat. Oncol. Biol. Phys. **37** (1997) 959–964.
[144] FRANCESCON, P., et al., Use of a new type of radiochromic film, a new parallel-plate micro-chamber, MOSFETs, and TLD 800 microcubes in the dosimetry of small beams, Med. Phys. **25** (1998) 503–511.
[145] MARINELLO, G., "Radiothermoluminescent dosimeters and diodes", Handbook of Radiotherapy Physics: Theory and Practice (MAYLES, P., NAHUM, A., ROSENWALD, J.C., Eds), Taylor & Francis, Boca Raton, FL (2007) 303–320.
[146] IZEWSKA, J., HULTQVIST, M., BERA, P., Analysis of uncertainties in the IAEA/WHO TLD postal dose audit system, Radiat. Meas. **43** (2008) 959–963.

[147] AGUIRRE, J.F., ALVAREZ, P., IBBOTT, G.S., FOLLOWILL, D.S., "Testing, commissioning and validating an optically stimulated luminescence (OSL) dosimetry system for mailed dosimetry at the Radiological Physics Center", Standards, Applications and Quality Assurance in Medical Radiation Dosimetry (IDOS) (Proc. Int. Symp. Vienna, 2010), Vol. 2, IAEA, Vienna (2011) 411–421.
[148] ARAKI, F., MORIBE, N., SHIMONOBOU, T., YAMASHITA, Y., Dosimetric properties of radiophotoluminescent glass rod detector in high-energy photon beams from a linear accelerator and Cyber-Knife, Med. Phys. **31** (2004) 1980–1986.
[149] PERKS, J., GAO, M., SMITH, V., SKUBIC, S., GOETSCH, S., Glass rod detectors for small field, stereotactic radiosurgery dosimetric audit, Med. Phys. **32** (2005) 726–732.
[150] ABREGO, F.C., CALCINA, C.S., DE ALMEIDA, A., DE ALMEIDA, C.E., BAFFA, O., Relative output factor and beam profile measurements of small radiation fields with an L-alanine/K-band EPR minidosimeter, Med. Phys. **34** (2007) 1573–1582.
[151] MELLENBERG, D.E., DAHL, R.A., BLACKWELL, C.R., Acceptance testing of an automated scanning water phantom, Med. Phys. **17** (1990) 311–314.
[152] BUTSON, M.J., CHEUNG, T., YU, P.K., Solid water phantom heat conduction: Heating and cooling rates, J. Med. Phys. **33** (2008) 24–28.
[153] ANDREO, P., BENMAKHLOUF, H., Improved Reference and Relative Dosimetry of Small Radiation Therapy Photon Beams, SSM Rep. 2014:26, Strålsäkerhetsmyndigheten, Stockholm (2014).
[154] INTERNATIONAL COMMISSION ON RADIATION UNITS AND MEASUREMENTS, Stopping Powers for Electrons and Positrons, ICRU Rep. 37, ICRU, Bethesda, MD (1984).
[155] INTERNATIONAL COMMISSION ON RADIATION UNITS AND MEASUREMENTS, Tissue Substitutes in Radiation Dosimetry and Measurement, ICRU Rep. 44, ICRU, Bethesda, MD (1989).
[156] INTERNATIONAL COMMISSION ON RADIATION UNITS AND MEASUREMENTS, Key Data for Ionizing-Radiation Dosimetry: Measurement Standards and Applications, ICRU Rep. 90, ICRU, Bethesda, MD (2014).
[157] INTERNATIONAL COMMISSION ON RADIATION UNITS AND MEASUREMENTS, Radiation Dosimetry: Electron Beams with Energies Between 1 and 50 MeV, ICRU Rep. 35, ICRU, Bethesda, MD (1984).
[158] INTERNATIONAL ATOMIC ENERGY AGENCY, The Use of Plane Parallel Ionization Chambers in High Energy Electron and Photon Beams: An International Code of Practice for Dosimetry, Technical Reports Series No. 381, IAEA, Vienna (1997).
[159] NIATEL, M.-T., Rayons X et γ: Influence de la vapeur d'eau sur l'ionisation de l'air dans le cas d'une chamber à cavité, C. R. Hebd. Séances Acad. Sci. **B268** (1975) 361–363.
[160] BOAG, J.W., CURRANT, J., Current collection and ionic recombination in small cylindrical ionization chambers exposed to pulsed radiation, Br. J. Radiol. **53** (1980) 471–478.
[161] WEINHOUS, M.S., MELI, J.A., Determining P_{ion}, the correction factor for recombination losses in an ionization chamber, Med. Phys. **11** (1984) 846–849.

[162] PALMANS, H., THOMAS, R.A., DUANE, S., STERPIN, E., VYNCKIER, S., Ion recombination for ionization chamber dosimetry in a helical tomotherapy unit, Med. Phys. **37** (2010) 2876–2889.
[163] WANG, Y., EASTERLING, S.B., TING, J.Y., Ion recombination corrections of ionization chambers in flattening filter-free photon radiation, J. Appl. Clin. Med. Phys. **13** (2012) 3758.
[164] KRY, S.F., POPPLE, R., MOLINEU, A., FOLLOWILL, D.S., Ion recombination correction factors (P_{ion}) for Varian TrueBeam high-dose-rate therapy beams, J. Appl. Clin. Med. Phys. **13** (2012) 3803.
[165] LANG, S., HRBACEK, J., LEONG, A., KLÖCK, S., Ion-recombination correction for different ionization chambers in high dose rate flattening-filter-free photon beams, Phys. Med. Biol. **57** (2012) 2819–2827.
[166] DAS, I.J., et al., Accelerator beam data commissioning equipment and procedures: Report of the TG-106 of the Therapy Physics Committee of the AAPM, Med. Phys. **35** (2008) 4186–4215.
[167] LOW, D.A., MORAN, J.M., DEMPSEY, J.F., DONG, L., OLDHAM, M., Dosimetry tools and techniques for IMRT, Med. Phys. **38** (2011) 1313–1338.
[168] DAS, I.J., et al., Small fields and non-equilibrium condition photon beam dosimetry: AAPM Task Group Report 155, Med. Phys. (in preparation).
[169] SAITOH, H., FUJISAKI, T., SAKAI, R., KUNIEDA, E., Dose distribution of narrow beam irradiation for small lung tumor, Int. J. Radiat. Oncol. Biol. Phys. **53** (2002) 1380–1387.
[170] JONES, A.O., DAS, I.J., JONES, F.L., Jr., A Monte Carlo study of IMRT beamlets in inhomogeneous media, Med. Phys. **30** (2003) 296–300.
[171] CHEUNG, J.Y., NG, B.K., YU, K.N., Dose enhancement close to platinum implants for the 4, 6, and 10 MV stereotactic radiosurgery, Med. Phys. **31** (2004) 2787–2791.
[172] JONES, A.O., DAS, I.J., Comparison of inhomogeneity correction algorithms in small photon fields, Med. Phys. **32** (2005) 766–776.
[173] INSTITUTE OF PHYSICS AND ENGINEERING IN MEDICINE, Physics Aspects of Quality Control in Radiotherapy, IPEM Rep. 81, IPEM, York (1999).
[174] THWAITES, D.I., MIJNHEER, B., MILLS, J.A., "Quality assurance of external beam radiotherapy", Radiation Oncology Physics, IAEA, Vienna (2005) 407–450.
[175] KLEIN, E.E., et al., Task Group 142 report: Quality assurance of medical accelerators, Med. Phys. **36** (2009) 4197–4212.
[176] BEDDAR, A.S., MASON, D.J., O'BRIEN, P.F., Absorbed dose perturbation caused by diodes for small field photon dosimetry, Med. Phys. **21** (1994) 1075–1079.
[177] BASSINET, C., et al., Small fields output factors measurements and correction factors determination for several detectors for a CyberKnife® and linear accelerators equipped with microMLC and circular cones, Med. Phys. **40** (2013) 071725-1–13.
[178] ZHU, T.C., et al., Report of AAPM Therapy Physics Committee Task Group 74: In-air output ratio, S_c, for megavoltage photon beams, Med. Phys. **36** (2009) 5261–5291.

[179] BENMAKHLOUF, H., JOHANSSON, J., PADDICK, I., ANDREO, P., Monte Carlo calculated and experimentally determined output correction factors for small field detectors in Leksell Gamma Knife Perfexion beams, Phys. Med. Biol. **60** (2015) 3959–3973.
[180] ANDREO, P., WULFF, J., BURNS, D.T., PALMANS, H., Consistency in reference radiotherapy dosimetry: Resolution of an apparent conundrum when ^{60}Co is the reference quality for charged-particle and photon beams, Phys. Med. Biol. **58** (2013) 6593–6621.
[181] KOSUNEN, A., ROGERS, D.W.O., Beam quality specification for photon beam dosimetry, Med. Phys. **20** (1993) 1181–1188.
[182] ROSS, C., SHORTT, K., ROGERS, D., DELAUNAY, F., "A test of TPR 20 10 as a beam quality specifier for high energy photon beams", Measurement Assurance in Dosimetry (Proc. Int. Symp. Vienna, 1993), IAEA, Vienna (1994) 309–321.
[183] ROSSER, K., et al., "The NPL absorbed dose to water calibration service for high energy photons", Measurement Assurance in Dosimetry (Proc. Int. Symp. Vienna, 1993), IAEA,Vienna (1994) 73–81.
[184] CEBERG, C., JOHNSSON, S., LIND, M., KNÖÖS, T., Prediction of stopping-power ratios in flattening-filter free beams, Med. Phys. **37** (2010) 1164–1168.
[185] DZIERMA, Y., LICHT, N., NUESKEN, F., RUEBE, C., Beam properties and stability of a flattening-filter free 7 MV beam: An overview, Med. Phys. **39** (2012) 2595–2602.
[186] STERPIN, E., MACKIE, T.R., VYNCKIER, S., Monte Carlo computed machine-specific correction factors for reference dosimetry of TomoTherapy static beam for several ion chambers, Med. Phys. **39** (2012) 4066–4072.
[187] ARAKI, F., Monte Carlo study of a Cyberknife stereotactic radiosurgery system, Med. Phys. **33** (2006) 2955–2963.
[188] FRANCESCON, P., CORA, S., CAVEDON, C., SCALCHI, P., STANCANELLO, J., CyberKnife dosimetric beam characteristics: Comparison between experimental results and Monte Carlo simulation, Robotic Radiosurgery **1** (2005) 71–80.
[189] DUANE, S., et al., SU-FF-T-195: Dosimetry audit for tomotherapy using alanine/EPR, Med. Phys. **33** (2006) 2093–2094.
[190] BAILAT, C.J., BUCHILLIER, T., PACHOUD, M., MOECKLI, R., BOCHUD, F.O., An absolute dose determination of helical tomotherapy accelerator, TomoTherapy High-Art II, Med. Phys. **36** (2009) 3891–3896.
[191] GAGO-ARIAS, A., et al., Correction factors for A1SL ionization chamber dosimetry in TomoTherapy: Machine-specific, plan-class, and clinical fields, Med. Phys. **39** (2012) 1964–1970.
[192] JERAJ, R., MACKIE, T.R., BALOG, J., OLIVERA, G., Dose calibration of nonconventional treatment systems applied to helical tomotherapy, Med. Phys. **32** (2005) 570–577.
[193] MARTENS, C., DE WAGTER, C., DE NEVE, W., The value of the PinPoint ion chamber for characterization of small field segments used in intensity-modulated radiotherapy, Phys. Med. Biol. **45** (2000) 2519–2530.

[194] SCHWEDAS, M., SCHEITHAUER, M., WIEZOREK, T., WENDT, T.G., Strahlenphysikalische Einflussgrößen bei der Dosimetrie mit verschiedenen Detektortypen, Z. Med. Phys. **17** (2007) 172–179.
[195] STASI, M., BAIOTTO, B., BARBONI, G., SCIELZO, G., The behavior of several microionization chambers in small intensity modulated radiotherapy fields, Med. Phys. **31** (2004) 2792–2795.
[196] TANNY, S., SPERLING, N., PARSAI, E.I., Correction factor measurements for multiple detectors used in small field dosimetry on the Varian Edge radiosurgery system, Med. Phys. **42** (2015) 5370–5376.
[197] UNDERWOOD, T.S., ROWLAND, B.C., FERRAND, R., VIEILLEVIGNE, L., Application of the Exradin W1 scintillator to determine Ediode 60017 and microDiamond 60019 correction factors for relative dosimetry within small MV and FFF fields, Phys. Med. Biol. **60** (2015) 6669–6683.
[198] ARCHAMBAULT, L., et al., Water-equivalent dosimeter array for small-field external beam radiotherapy, Med. Phys. **34** (2007) 1583–1592.
[199] BUCCIOLINI, M., RUSSO, S., BANCI BUONAMICI, F., PINI, S., SILLI, P., Dosimetric characterization of a bi-directional micromultileaf collimator for stereotactic applications, Med. Phys. **29** (2002) 1456–1463.
[200] CRANMER-SARGISON, G., WESTON, S., EVANS, J.A., SIDHU, N.P., THWAITES, D.I., Implementing a newly proposed Monte Carlo based small field dosimetry formalism for a comprehensive set of diode detectors, Med. Phys. **38** (2011) 6592–6602.
[201] CROP, F., et al., Monte Carlo modeling of the ModuLeaf miniature MLC for small field dosimetry and quality assurance of the clinical treatment planning system, Phys. Med. Biol. **52** (2007) 3275–3290.
[202] EATON, D., TWYMAN, N., THOMAS, S., Commissioning a miniature multileaf collimator for small field radiotherapy, Med. Dosim. **35** (2010) 1–6.
[203] FIPPEL, M., HARYANTO, F., DOHM, O., NÜSSLIN, F., KRIESEN, S., A virtual photon energy fluence model for Monte Carlo dose calculation, Med. Phys. **30** (2003) 301–311.
[204] GODWIN, G.A., SIMPSON, J.B., MUGABE, K.V., Characterization of a dynamic multi-leaf collimator for stereotactic radiotherapy applications, Phys. Med. Biol. **57** (2012) 4643–4654.
[205] GRIESSBACH, I., LAPP, M., BOHSUNG, J., GADEMANN, G., HARDER, D., Dosimetric characteristics of a new unshielded silicon diode and its application in clinical photon and electron beams, Med. Phys. **32** (2005) 3750–3754.
[206] HARYANTO, F., FIPPEL, M., LAUB, W., DOHM, O., NÜSSLIN, F., Investigation of photon beam output factors for conformal radiation therapy: Monte Carlo simulations and measurements, Phys. Med. Biol. **47** (2002) N133–N143.
[207] KRAUSS, H., The Quest for the Ideal Detector (2016), http://www.wienkav.at/kav/kfj/91033454/physik/PTW/liquid.htm
[208] LAMBERT, J., et al., A prototype scintillation dosimeter customized for small and dynamic megavoltage radiation fields, Phys. Med. Biol. **55** (2010) 1115–1126.

[209] BENMAKHLOUF, H., Key Data for the Reference and Relative Dosimetry of Radiotherapy and Diagnostic and Interventional Radiology Beams, PhD Thesis, Stockholm Univ. (2015).
[210] BENMAKHLOUF, H., SEMPAU, J., ANDREO, P., Output correction factors for nine small field detectors in 6 MV radiation therapy photon beams: A PENELOPE Monte Carlo study, Med. Phys. **41** (2014) 041711-1–12.
[211] CRANMER-SARGISON, G., WESTON, S., EVANS, J.A., SIDHU, N.P., THWAITES, D.I., Monte Carlo modelling of diode detectors for small field MV photon dosimetry: Detector model simplification and the sensitivity of correction factors to source parameterization, Phys. Med. Biol. **57** (2012) 5141–5133.
[212] KAMIO, Y., BOUCHARD, H., Correction-less dosimetry of nonstandard photon fields: A new criterion to determine the usability of radiation detectors, Phys. Med. Biol. **59** (2014) 4973–5002.
[213] PAPACONSTADOPOULOS, P., TESSIER, F., SEUNTJENS, J., On the correction, perturbation and modification of small field detectors in relative dosimetry, Phys. Med. Biol. **59** (2014) 5937–5952.
[214] UNDERWOOD, T.S., WINTER, H.C., HILL, M.A., FENWICK, J.D., Mass-density compensation can improve the performance of a range of different detectors under non-equilibrium conditions, Phys. Med. Biol. **58** (2013) 8295–8310.
[215] WANG, L.L., BEDDAR, S., Study of the response of plastic scintillation detectors in small-field 6 MV photon beams by Monte Carlo simulations, Med. Phys. **38** (2011) 1596–1599.
[216] LARRAGA-GUTIERREZ, J.M., BALLESTEROS-ZEBADUA, P., RODRIGUEZ-PONCE, M., GARCIA-GARDUNO, O.A., DE LA CRUZ, O.O., Properties of a commercial PTW-60019 synthetic diamond detector for the dosimetry of small radiotherapy beams, Phys. Med. Biol. **60** (2015) 905–924.
[217] FRANCESCON, P., KILBY, W., SATARIANO, N., Monte Carlo simulated correction factors for output factor measurement with the CyberKnife system: Results for new detectors and correction factor dependence on measurement distance and detector orientation, Phys. Med. Biol. **59** (2014) N11–N17.
[218] WILCOX, E.E., DASKALOV, G.M., Evaluation of GAFCHROMIC® EBT film for CyberKnife® dosimetry, Med. Phys. **34** (2007) 1967–1974.
[219] CHALKLEY, A., HEYES, G., Evaluation of a synthetic single-crystal diamond detector for relative dosimetry measurements on a CyberKnife™, Br. J. Radiol. **87** (2014).

ABBREVIATIONS

AAPM	American Association of Physicists in Medicine
ABS	acrylonitrile butadiene styrene
COP	Code of Practice
CPE	charged particle equilibrium
DAP	dose–area product
FFF	flattening filter free (beam)
FWHM	full width at half maximum (dimension of the lateral beam profile at 50% of its maximum value)
IAEA	International Atomic Energy Agency
ICRU	International Commission on Radiation Units and Measurements
IMRT	intensity modulated radiotherapy
IPEM	Institute of Physics and Engineering in Medicine
IPSM	Institute of Physical Sciences in Medicine
LAC	large area parallel plane ionization chamber
LCPE	lateral charged particle equilibrium
MLC	multileaf collimator
MOSFET	metal oxide semiconductor field-effect transistor
msr	machine specific reference
NPL	National Physical Laboratory
NPSF	normalized peak scatter factor
PDD	percentage depth dose
PMMA	polymethylmethacrylate
PSDL	primary standards dosimetry laboratory
PTB	Physikalisch-Technische Bundesanstalt
SAD	source-to-axis distance
SDD	source-to-detector distance (in the case of an ionization chamber this is commonly referred to as source-to-chamber distance or SCD)
SFPM	Société Française de Physique Médicale
SRS	stereotactic radiosurgery
SSD	source-to-surface distance
SSDL	secondary standards dosimetry laboratory
TCPE	transient charged particle equilibrium
TMR	tissue maximum ratio
TPR	tissue phantom ratio
VSL	Van Swinden Laboratory (Dutch Primary Standards Laboratory)
WFF	with flattening filter (beam)

CONTRIBUTORS TO DRAFTING AND REVIEW

Alfonso, R.	Instituto Nacional de Oncologia y Radiobiologia, Cuba
Andreo, P.	Karolinska University Hospital, Sweden
Capote, R.	International Atomic Energy Agency
Christaki, K.	International Atomic Energy Agency
Huq, M. Saiful	University of Pittsburgh Cancer Institute and UPMC CancerCenter, United States of America
Izewska, J.	International Atomic Energy Agency
Johansson, J.	Elekta Instrument AB, Sweden
Kilby, W.	Accuray Inc., United States of America
Mackie, T.R.	University of Wisconsin, United States of America
Meghzifene, A.	International Atomic Energy Agency
Palmans, H.	National Physical Laboratory, United Kingdom, and EBG MedAustron GmbH, Austria
Seuntjens, J.	McGill University, Canada
Ullrich, W.	Brainlab AG, Germany
Vatnitsky, S.	EBG MedAustron GmbH, Austria

IAEA
International Atomic Energy Agency

No. 25

ORDERING LOCALLY

In the following countries, IAEA priced publications may be purchased from the sources listed below or from major local booksellers.

Orders for unpriced publications should be made directly to the IAEA. The contact details are given at the end of this list.

CANADA

Renouf Publishing Co. Ltd
22-1010 Polytek Street, Ottawa, ON K1J 9J1, CANADA
Telephone: +1 613 745 2665 • Fax: +1 643 745 7660
Email: order@renoufbooks.com • Web site: www.renoufbooks.com

Bernan / Rowman & Littlefield
15200 NBN Way, Blue Ridge Summit, PA 17214, USA
Tel: +1 800 462 6420 • Fax: +1 800 338 4550
Email: orders@rowman.com Web site: www.rowman.com/bernan

CZECH REPUBLIC

Suweco CZ, s.r.o.
Sestupná 153/11, 162 00 Prague 6, CZECH REPUBLIC
Telephone: +420 242 459 205 • Fax: +420 284 821 646
Email: nakup@suweco.cz • Web site: www.suweco.cz

FRANCE

Form-Edit
5 rue Janssen, PO Box 25, 75921 Paris CEDEX, FRANCE
Telephone: +33 1 42 01 49 49 • Fax: +33 1 42 01 90 90
Email: formedit@formedit.fr • Web site: www.form-edit.com

GERMANY

Goethe Buchhandlung Teubig GmbH
Schweitzer Fachinformationen
Willstätterstrasse 15, 40549 Düsseldorf, GERMANY
Telephone: +49 (0) 211 49 874 015 • Fax: +49 (0) 211 49 874 28
Email: kundenbetreuung.goethe@schweitzer-online.de • Web site: www.goethebuch.de

INDIA

Allied Publishers
1st Floor, Dubash House, 15, J.N. Heredi Marg, Ballard Estate, Mumbai 400001, INDIA
Telephone: +91 22 4212 6930/31/69 • Fax: +91 22 2261 7928
Email: alliedpl@vsnl.com • Web site: www.alliedpublishers.com

Bookwell
3/79 Nirankari, Delhi 110009, INDIA
Telephone: +91 11 2760 1283/4536
Email: bkwell@nde.vsnl.net.in • Web site: www.bookwellindia.com

ITALY

Libreria Scientifica "AEIOU"
Via Vincenzo Maria Coronelli 6, 20146 Milan, ITALY
Telephone: +39 02 48 95 45 52 • Fax: +39 02 48 95 45 48
Email: info@libreriaaeiou.eu • Web site: www.libreriaaeiou.eu

JAPAN

Maruzen-Yushodo Co., Ltd
10-10 Yotsuyasakamachi, Shinjuku-ku, Tokyo 160-0002, JAPAN
Telephone: +81 3 4335 9312 • Fax: +81 3 4335 9364
Email: bookimport@maruzen.co.jp • Web site: www.maruzen.co.jp

RUSSIAN FEDERATION

Scientific and Engineering Centre for Nuclear and Radiation Safety
107140, Moscow, Malaya Krasnoselskaya st. 2/8, bld. 5, RUSSIAN FEDERATION
Telephone: +7 499 264 00 03 • Fax: +7 499 264 28 59
Email: secnrs@secnrs.ru • Web site: www.secnrs.ru

UNITED STATES OF AMERICA

Bernan / Rowman & Littlefield
15200 NBN Way, Blue Ridge Summit, PA 17214, USA
Tel: +1 800 462 6420 • Fax: +1 800 338 4550
Email: orders@rowman.com • Web site: www.rowman.com/bernan

Renouf Publishing Co. Ltd
812 Proctor Avenue, Ogdensburg, NY 13669-2205, USA
Telephone: +1 888 551 7470 • Fax: +1 888 551 7471
Email: orders@renoufbooks.com • Web site: www.renoufbooks.com

Orders for both priced and unpriced publications may be addressed directly to:

Marketing and Sales Unit
International Atomic Energy Agency
Vienna International Centre, PO Box 100, 1400 Vienna, Austria
Telephone: +43 1 2600 22529 or 22530 • Fax: +43 1 2600 29302 or +43 1 26007 22529
Email: sales.publications@iaea.org • Web site: www.iaea.org/books

16-37201

ABSORBED DOSE DETERMINATION IN EXTERNAL BEAM RADIOTHERAPY
Technical Reports Series No. 398
STI/DOC/010/398 (229 pp.; 2000)
ISBN: 92-0-102200-X Price: €51.00

IMPLEMENTATION OF THE INTERNATIONAL CODE OF PRACTICE ON DOSIMETRY IN RADIOTHERAPY (TRS 398): REVIEW OF TESTING RESULTS
IAEA-TECDOC-CD-1455 (2010)
ISBN: 978-92-0-100610-3 Price: €15.00

DOSIMETRY IN DIAGNOSTIC RADIOLOGY: AN INTERNATIONAL CODE OF PRACTICE
Technical Reports Series No. 457
STI/DOC/010/457 (359 pp.; 2007)
ISBN: 92-0-115406-2 Price: €75.00

IMPLEMENTATION OF THE INTERNATIONAL CODE OF PRACTICE ON DOSIMETRY IN DIAGNOSTIC RADIOLOGY (TRS 457): REVIEW OF TEST RESULTS
IAEA Human Health Reports No. 4
STI/PUB/1498 (129 pp.; 2011)
ISBN: 978-92-0-114010-4 Price: €58.00

CALIBRATION OF REFERENCE DOSIMETERS FOR EXTERNAL BEAM RADIOTHERAPY
Technical Reports Series No. 469
STI/DOC/010/469 (73 pp.; 2009)
ISBN: 978-92-0-110708-4 Price: €23.00

ACCURACY REQUIREMENTS AND UNCERTAINTIES IN RADIOTHERAPY
IAEA Human Health Series No. 31
STI/PUB/1679 (297 pp.; 2016)
ISBN: 978-92-0-100815-2 Price: €76.00

QUALITY ASSURANCE PROGRAMME FOR COMPUTED TOMOGRAPHY: DIAGNOSTIC AND THERAPY APPLICATIONS
IAEA Human Health Series No. 19
STI/PUB/1557 (171 pp.; 2012)
ISBN: 978-92-0-128910-0 Price: €48.00

This is the first International Code of Practice dedicated to the dosimetry of small static fields used in radiotherapy. It is addressed to clinical medical physicists using small static photon fields with energies less than 10 MV, provided with ionization chambers calibrated in terms of absorbed dose to water traceable to a primary standards dosimetry laboratory. It provides consistent reference dosimetry traceable to metrological primary standards and enables common procedures for small field dosimetry to be followed within a country. An overview of the physics of small field dosimetry is presented, followed by a general formalism for reference dosimetry in small fields. Guidelines for its practical implementation using suitable detectors and methods for the determination of field output factors are given for specific clinical machines that use small static fields.

INTERNATIONAL ATOMIC ENERGY AGENCY
VIENNA
ISBN 978–92–0–105916–1
ISSN 0074–1914